University of Szczecin

Institute of Physics

Dominik Böhm

Nuclear fuel recycling by distillation-based separation

PhD Thesis
written under supervision of
prof dr hab Zbigniew Konrad Czerski

Szczecin 2023

OŚWIADCZENIE DOKTORANTA

Oświadczam, że moja praca pt.: **Nuclear fuel recycling by distillation-based separation**

a. została napisana przeze mnie samodzielnie,
b. nie narusza praw autorskich w rozumieniu ustawy z dnia 14 lutego 1994 roku o prawie autorskim i prawach pokrewnych (Dz.U. 2019 r. poz. 1231) oraz dóbr osobistych chronionych prawem,
c. nie zawiera danych i informacji, które uzyskałem / uzyskałam w sposób niedozwolony,
d. nie była podstawą nadania tytułu naukowego lub zawodowego ani mnie ani innej osobie.

Ponadto oświadczam, że treść pracy przedstawionej przeze mnie do obrony, zawarta na przekazanym nośniku elektronicznym jest identyczna z jej wersją drukowaną.

Szczecin, dn. 21.06.23 ..... Dominik Bolm .....

podpis doktoranta

OŚWIADCZENIE

Wyrażam / nie wyrażam zgodę / zgody na udostępnienie mojej pracy doktorskiej pt.: **Nuclear fuel recycling by distillation-based separation**

Szczecin, dn. 21.06.23 ..... Dominik Bolm .....

podpis doktoranta

Abstract

Since the beginning of the commercial use of nuclear energy, the issue of disposal of nuclear waste has remained largely unsolved. Currently proposed recycling methods, such as hydrometallurgical liquid-liquid extraction processes or pyrometallurgical salt-mediated separation and subsequent electrorefining, use numerous solvents or are still ineffective and environmentally unfriendly.

In this thesis, a separation concept has been developed for a distillation-based reprocessing of spent nuclear fuel using chlorination and subsequent distillation operations. This approach also includes downstream waste gas treatment and recycling of zirconium cladding material.

Validation of the distillation model and relevant separation units was performed on representative simplified test mixtures using self-written Octave code, which does not require any critical mixture component dat. Instead, simulations were based on Raoult's law applying partial vapor pressures. The numerical results of the distillation operation were compared with those obtained from ChemSep models, a common software for simulation of distillation columns. Both the results of the Octave code and the ChemSep model showed good agreement. Similarly, a simulation of Kroll's distillation-based process for extracting titanium from titanium ores by chlorination and distillation yielded positive results.

Due to the lack of important material data of spent nuclear fuel chlorides, in particular those needed to describe the behaviour of the vapor-liquid phase equilibrium as realistically as possible (the so-called VLE data), the conceptual design of the distillation process could be simulated under ideal phase equilibrium conditions using the Octave code.

For the distillation columns, a completely different design to that commonly used in the chemical industry was proposed, in the form of a specially designed closed system based on a total reflux column in this thesis, with subsequent cyclic product withdrawals. This solution also enables safe operation with high separation accuracy, which, however, requires significantly longer separation times.

The results of the simulation of the entire process scheme showed very good separability of the used nuclear fuel consisting of at least 95 mol% uranium tetrachloride, but also many other components, such as plutonium trichloride and lighter fission products. The proposed recycling method can be used at the nuclear power plant site as well as in external plants. In contrast to the chemical industry, the nuclear recycling of the spent fuel accumulated over the past decades can be completely processed within 65 years with six separation plants designed in this way. The concept presented is particularly suitable for liquid fuel reactors, such as the Dual Fluid Reactor or potentially a suitable type of Molten Salt Reactor, for which on-line reprocessing is envisaged. Furthermore, the method can also be used to recover valuable rare earth elements.

Streszczenie

Od początku komercyjnego wykorzystania energii jądrowej kwestia składowania odpadów promieniotwórczych pozostaje w dużej mierze nierozwiązana. Obecnie proponowane metody recyklingu, takie jak procesy hydrometalurgicznej ekstrakcji wodnej lub pirometalurgicznej separacji za pośrednictwem soli, a następnie elektrorafinacji, wykorzystują wiele rozpuszczalników lub są nadal nieskuteczne i nieprzyjazne dla środowiska. W niniejszej dysertacji opracowano koncepcję separacji opartą na destylacji ponownego przetwarzania wypalonego paliwa jądrowego za pomocą chlorowania i destylacji. Podejście to obejmuje również dalsze oczyszczanie gazów odlotowych i recykling cyrkonowego materiału okładzinowego.

Walidacja modelu destylacji i odpowiednich jednostek separacyjnych została przeprowadzona na reprezentatywnych uproszczonych mieszaninach testowych przy użyciu samodzielnie napisanego kodu przy w ramach platformy Octave, który nie wymaga żadnych krytycznych danych dotyczących składników mieszaniny. Zamiast tego symulacje oparto na prawie Raoulta, stosując cząstkowe prężności par. Wyniki numeryczne procesu destylacji porównano z wynikami uzyskanymi z modeli ChemSep, popularnego oprogramowania do symulacji kolumn destylacyjnych. Zarówno wyniki samodzielnie napisanego kodu Octave, jak i model ChemSep wykazały dobrą zgodność między sobą. Podobnie symulacja procesu Krolla oddzielania tytanu od rud tytanu przez chlorowanie i destylację dała pozytywne wyniki.

Ze względu na brak ważnych danych materiałowych chlorków wypalonego paliwa jądrowego, w szczególności potrzebnych do możliwie realistycznego opisania zachowania się stanu równowagi fazy para-ciecz (tzw. dane VLE), projekt koncepcyjny procesu destylacji był symulowany w idealnych warunkach równowagi fazowej przy użyciu kodu Octave.

Dla kolumn destylacyjnych zaproponowano zupełnie inną konstrukcję niż powszechnie stosowana w przemyśle chemicznym: w postaci układu zamkniętego opartego na ustawieniu całkowitych warunków zwrotnych kolumny z późniejszymi cyklicznymi poborami produktu. Rozwiązanie to umożliwia również bezpieczną pracę z dużą dokładnością separacji, co jednak wymaga znacznie dłuższych czasów separacji. To ostatnie nie stanowi problemu dla przemysłu chemicznego w obliczu ilości nagromadzonego w ostatnich dziesięcioleciach wypalonego paliwa jądrowego i możliwości jego ponownego przerobu.

Wyniki symulacji całego schematu procesu wykazały bardzo dobrą separowalność zużytego paliwa jądrowego składającego się z co najmniej 95% molowych tetrachlorku uranu, ale także wielu innych składników, takich jak trichlorek plutonu i lżejsze produkty rozszczepienia. Proponowana metoda recyklingu może być stosowana zarówno na terenie elektrowni jądrowej, jak również w specjalnych zakładach zewnętrznych. Całkowita separacja odpadów wypalonego paliwa jądrowego jest możliwe w ciągu 65 lat przy wykorzystaniu zaledwie sześciu zakładów segregacji zaplanowanych zgodnie z proponowaną koncepcją. Koncepcja ta jest szczególnie odpowiednia dla reaktorów na paliwo ciekłe, takich jak reaktor dwupłynowy (Dual Fluid Reactor), dla których możliwa jest utylizacja odpadów promieniotwórczych on-line. Ponadto metoda ta może być również wykorzystana do odzyskiwania bardzo cennych pierwiastków ziem rzadkich.

Contents

List of Figures

List of Tables

Symbols and abbreviations

Latin Symbols	
A	Area/cross-sectional area/parameter in correlation equations
a, b	Van Der Waals (equation of state) parameters
C	Constants in correlation equations for temperature-dependent material data
C_F	Inlet parameter in separation apparatus: Can also be understood as the ratio of the valve opening to the maximum inflow quantity.
c	Substance concentration (general)
D	Diffusion coefficient/ parameters in UNIQUAC model
E	Murphree efficiency/ energy term (general)
e	Thermal feed state in distillation column (related to molar vapour fraction)
F	Degree of freedom in thermodynamics for phase equilibria/ gas loading factor for distillation column design/ characteristic area fraction in the design of distillation columns and in various extended distillation models (e.g. for post-distillation heat estimation in total-reflux distillation columns).
f	Fugacity(thermodynamics/physics) / defined mathematical function related to functional sub-areas to equations of state (thermodynamics)
G, g	Gibbs energy as thermodynamic state variable (elementary in corresponding fundamental equations of thermodynamics), (molar specific Gibbs energy)/ gravitational constant of the Earth
H, h	Enthalpy, (molar specific enthalpy)
H	Column height
J	Diffusion flow
K	Separation factor for distillation
k	Material transfer coefficient (general)
k	Mass transfer exponent (correlation equation specific)
m, M_W	Mass, molar mass (general)
$\dot{m}$	Mass flow (general)
m'	mass flow rate
N	Number (taken in general terms as the total number in this work)
$\dot{N}$	Substance flow (general)
n	Molar Quantity (general)/ Number of Stages / Degree of Chlorination
$\dot{n}$	Mole flow (general)

p	Pressure (system pressure)
Q	Heat (general)
$\dot{Q}$	Heat flow (general)
q	Specific molar energy/ Van der Waals surface area
R	Total radius (general)
r	Radius (generally as a variable, e.g. related to ionic radius)
R	General gas constant
S, s	Entropy, molar specific entropy/ correction term in equation of state
T	Temperature (general)
t	Time (general)
u	Molar specific internal energy/ model parameters in UNIQUAC/LIQUAC
V	Volume (general)
$\dot{V}$	Volume flow (general)
V_R	Boil-up evaporation rate
v	Reflux ratio/ molar specific volume
w	Velocity (general)
x, y, z	Molar fraction: liquid, vapour, variable for solid, liquid or vapour (general)
y-error	Absolute deviation value to the mole fraction to the vapour phase (only used in linear error calculation, not generally defined)

Greek Symbols	
α	Relative volatility/ α solid phase/ geometric angle/ heat transfer coefficient
β	Mass transfer coefficient (general)
Γ	Interaction parameters (general)
γ	Activity coefficient (general)
δ	Termination value in iteration (general)
ε	Porosity (general)
ϵ	Lennard-Jones Potential Parameter (general)
η	Dynamic viscosity (general)
θ	Fraction to temperature of a separation stage in distillation/correction parameter
Λ	Interaction parameters in liquid (general)
λ	Mean free path length (general)
μ	Physical equilibrium
ν	Stoichiometric coefficient in chemical reaction network/ kinematic viscosity (general)
Π	Poynting Factor in the Description of Vapour-Liquid Equilibria at Higher Pressures in the $\gamma - \varphi$ Concept
ρ	Density (mass specific)
σ	Surface tension/ Cross section
τ	Parameters in NRTL model
φ	Fugacity coefficient/ ionic proportion factor
ϕ	Degree of ions specifically in an extended GE model for dissociation behaviour in molten salts/ proportion of liquid volume (general)
Φ	Ion potential ratio between two different ion components
Ψ	Parameters in Fenske-Underwood-Gilliland method
Ω	Collision integral related to the kinetic theory of gases

Indexes

Simple indexes	
0	Standard condition (thermodynamics): 25 °C and 1 bar
A, B	Exemplary substance component
az	Azeotropic, Referring to the azeotrope (example azeotropic composition).
col	Column(s) related
comp	Related to substance component
corr	Correction value
cond	Related to condenser area or condensation product
conv	Convective fraction
crit	Related to critical data of the pure substances
B	Bottom area in distillation column/ related to bottom product in distillation column
D	Condensation product
dist	Related to distillation product
E	Excess fraction (related to (thermodynamic) excess quantities)
eq	Thermal phase equilibrium
err	Error values/Parameter deviating from the mean values
evap	Related to evaporator range or evaporation product
F	Related to feed in thermal separator/ product feed in separator
G,g	Related to gaseous phase
i, k	Substance component (or run variable in sum)
id	Ideal state/thermal equilibrium state
in l	Considered within the liquid phase
inter	Related to intersection line in Fenske-Underwood-Gilliland method
ion	Related to ion fraction
j	Separation stage (running variable)
L	Related to liquid phase
l	Related to unit of length/relative column height
max	Maximum related size
min	Minimum related size

mix	Size related to the mixing state in the thermal separation process
mol	Molecular size
op	Optimisation variable within an optimisation process
Ph, Phase(s)	Related to separation phase within a thermal separation process
q	Geometrically cross-section-related
R	Related to the reflux in distillation column
res	Related to residence time behaviour
S	Size related to side stream draw-off in continuous distillation column
s,s,S	Related to solid phase
th	Current thermal state/ related to theoretical number of separation stages
Top	(Top) Condensation/distillation product in distillation column
tot	total
V	Related to vapour phase
VdW	(State) variable in Van Der Waals equation

Generalized indexes	
change	Related to any phase change
Phase	Related to separation phase within a thermal separation process in general
shaft	Size related to outlet shaft or tray in distillation column
spherical	Related to spherical objects/solid particles
stage	Related to theoretical separation stage

Acronyms and abbreviations

Energy and reactors		
CCU	Closed Chamber Unit	Experimental separation apparatus of a single-stage high-temperature distillation/evaporation unit for the thermal separation of metal chlorides
CSTE	Continuous-stirred tank evaporator	Continuous stirred tank evaporator as single-stage distillation/evaporation unit
CSTR	Continuous-stirred tank reactor	Continuous (chemical) stirred tank model reactor
DFR	Dual Fluid Reactor	Fast neutron, high-temperature reactor operating with two liquid circuits with a fuel circuit and a molten lead for indirect cooling
DFRm	metallic Dual Fluid Reactor type	Dual Fluid Reactor with a metallic-eutectic U-Cr or U-Cr-Pu mixture as fuel base mixture
DFRs	molten salt Dual Fluid Reactor type	Dual Fluid Reactor with molten salt as fuel
EROI	Energy Return On Investment factor	Ratio of usable energy to the total energy input of an energy power plant
GCP	Global Cycle Problem	The Global Cycle Problem in this thesis is defined as the generalised problem of the overall recycling of production, end-of-life products (neglecting littering effects) in closed-loop material systems (worldwide).
HLW	High-level (radioactive) waste	Compared to the literature, this refers to the amount of waste produced to date during the reprocessing of spent fuel elements (including extraction processes)
HLW-M	High-level waste management	Management for HLW handling and recycling, and possible storage or final disposal
LCFR	Lead-Cooled Fast Reactor	Lead-cooled fast reactors are fast fission reactors that use a fast neutron spectrum and a combination of a molten lead and a lead-bismuth eutectic coolant loop.

LFR	Liquid Fuel Reactors	Defined in this thesis as a group of nuclear reactors of the fourth generation or higher, based on molten liquid fuel, but without simple aqueous solution systems.
LWR	Light Water Reactor	Generally the most commonly used thermal neutron nuclear reactor with light water as cooling medium and solid fuels in fuel elements
MSR	Molten Salt Reactor	Liquid salt reactor with molten salt as fuel, diluted with other molten salts if necessary.
PCD/Pcd (file)	Pure Component data(base) file	This Pure Component Data(base) file of the ChemSep Lite software contains all relevant required property data as well as the selectable pure components that can be used for simulations with the ChemSep distillation models. It is the basic database of pure components and their pure component property data relating to thermodynamic, physical, molecular, conventional, critical, temperature dependent and a few more possible pure component related data.
PPC	Progressing process cycles of total reflux column operations	A continuous process cycle of the total reflux column operation chosen here, in which a distillate product is discontinuously enriched in a distillation column until the steady-state operation of a total reflux column is established, and then the distillate product is withdrawn, is referred to as PPC. All composition data that also refer to PPC of the total reflux column are the distillation compositions obtained in the separation stages of the column that are constant in the total reflux operation of a process cycle. In each PPC, product is removed until the limits of product purity are reached. Then the next PPC is performed.
PPU	Pyroprocessing Unit/ Pyrochemical Processing Unit	Process separation unit with high-temperature operations for substance and material separation, such as the separation of metal chlorides by distillation-based separation techniques.

PUREX	Plutonium-Uranium Recovery by Extraction	The PUREX process is a liquid-liquid extraction process for separating uranium and plutonium from spent nuclear fuel (SNF).
PWR	Pressurized Water Reactor	High pressure variant of the LWR reactor type
REE, (LREE, HREE)	Rare Earths Elements	Rare Earths (or Rare-Earth Elements) are chemical elements in the third subgroup of the periodic table, and the lanthanides are divided into light rare earths (LREEs), such as neodymium, praseodymium or samarium, and heavy rare earths (HREEs), such as dysprosium, erbium or holmium.
SEP/Sep (file)	SEParation file for ChemSep	The SEP file is the basic script file for simulating (and running) a thermal separation process (mainly distillation) of a given mixture with the ChemSep Lite software.
SFR	Sodium-cooled Fast Reactor	A fast neutron reactor with liquid sodium as coolant
SMR	Small Modular Reactor	Special reactors that tend to be mass producible and are smaller than ordinary reactors
SNF/UNF	Spent/Used Nuclear Fuel	This is the common waste material from thermal fission reactors defined as spent/used nuclear fuel.

Modelling and simulation of separation units and (thermal) phase changes	
BP	Boiling-Point method
CFD	Computational Fluid Dynamics
EQ,eq	Thermal equilibrium
FUG	Fenske Underwood Gilliland method
GE	GE-model
H	Enthalpy-term equation
HETP	Height equivalent to theoretical plate
LV	Phase change related to liquid-vapour equilibrium system: Often difference to the phase change is meant (example: enthalpy of evaporation).
LLE	Liquid-liquid phase equilibrium
M	Mass-term equation
MB	Mass balance
MESH	Mass equilibrium sum- rates enthalpy
MOD,model	see: Tab. (10), section (4)
S	Sum-rates-term equation
SL	Phase change related to solid-liquid equilibrium system: Often difference to the phase change is meant (example: enthalpy of fusion).
SR	Sum-rates
SV	Related to solid-vapour equilibrium system: Often difference to the phase change is meant (example: enthalpy of sublimation)
SLE	Solid-liquid phase equilibrium
VLE	Vapour-liquid phase equilibrium

Part I
Introduction

Throughout the history of human development, the availability of energy has been the driving force behind productivity, progress and prosperity. Ensuring lasting progress requires finding cost-effective, environmentally friendly and sustainable solutions in the areas of energy production, chemical and industrial production, and recycling of end products and waste streams. In the following, this global recycling problem is defined as the Global Cycle Problem (GCP). Similar to many natural material cycles on earth, all waste streams and end products should be recycled with minimum effort and minimal use of chemical additives.

The primary requirement for the fulfilment of chemical and industrial production and recycling of end products is cost-effective and cheap supply of energy, which should be as steadily and stable as possible in terms of power grid stability. This energy supply should also be generated with minimal amounts of materials usage and emission emission, including carbon dioxide. The cost-effective provision of energy depends on the one hand on the level of expenditures to build and run power plants and on the other hand on the recycling of waste streams.

The usability of different energy sources can be defined by the value of EROI or Energy Return On Investment. This is the ratio of the total usable energy produced to the total energy input over the entire period, including construction, operation and maintenance of the power plant. In [30], the various modern energy production methods were evaluated in terms of EROI values from 2013. In [30], pump storage for solar and wind was included in the EROI and referred to as the "unbuffered scenario", thus providing a range of EROI values. Solar was found to have a value in the range of 1.6-3.9 (buffered/unbuffered), wind 3.9-16 (buffered/unbuffered) and coal around 30. Hydropower has higher values in the range of 35-49 (buffered/unbuffered), but is severely constrained by limited water availability and is now close to full capacity. Conventional renewable energy sources, such as wind and solar, have the limitations of low EROI values and of non-base load electricity generation with strongly changing energy supply: They are far away from generating constant utilization frequency electricity. Achieving this would require energy storage with low energy conversion efficiency and high consumption of raw materials such as lithium and its extraction. In addition, wind turbines require large amounts of rare earths for the wind generators, and many materials are not recyclable after a long period of operation [31]. Nuclear energy, on the other hand, is a relatively cheap and stable energy production option [29].

Nuclear energy also shows a very high theoretically achievable maximum EROI value of 10,000 [1]. Indeed, compared to the chemical energy content of crude oil of about 45.5 MJ/kg , the usual fissile uranium-235 in Light Water Reactors (LWR) has an energy content greater by a factor of $1.1 \cdot 10^4$ [32] (p.338). However, today's thermal reactors based on solid fuel only achieve an EROI of 75 because only around 1 wt% of the fuel in the fuel matrix can be used, in addition to other factors that limit nuclear technology efficiency (see: [30]). The reason for the low usability is that only a small proportion of uranium, a few per cent of the thermally fissile U-235 isotope, is usable [33]. The much larger proportion of U-238 cannot be fissioned by the slow neutrons in today's solid fuel reactors. Only a tiny fraction of the U-238 is converted to thermally fissionable isotopes, as indicated by the fission cross sections of U-235 and Pu-239

presented in [33, 34].

In addition, also major disatvantage of solid fuels is no online refuelling and reprocessing is possible. Therefore, spent fuel still contains a large amount of potentially fissionable materials. This illustrates the very inefficient use of solid fuel reactors. The problem for long-term storage is the formation of long-lived transuranium and plutonium isotopes as well as active fission products in the fission yield composition. In fact, two types of fission products are generally produced in the U-235 of solid fuel thermal reactors: the short-lived, highly active, but rapidly decaying fission products exist at most for a few decades to hundreds of years, but others live much longer (compare the fission yields in e.g. [35]).

In order to solve the SNF waste problem and to avoid further waste, it would be conceptually feasible to process and reuse SNF on site in fast fluid or Liquid Fuel Reactors (LFR), such as the Molten Salt Reactor (MSR) or the Dual Fluid Reactor [1]. The Molten Salt Reactor uses liquid molten salts, in which the fissionable material is bound in these salt compounds. Other variants of reactor types are the lead-cooled fast reactor (LCFR), which uses a relatively thermally well-conducting liquid metallic with relatively high thermal conductivity. The Dual Fluid Reactor (DFR) combines the advantages of a lead cooling circuit and a liquid fuel reactor [1, 36]. This reactor type is capable of using long-lived fission products as fuel, as well as fuel material from SNF [1, 37] . However, significant use of SNF and long-lived fission products requires on-site material separation and cycling of the material flows at time intervals, as also reported by [1, 36, 37].

There are two variants of the Dual Fluid Reactor, a metallic variant (DFRm) using a basic fuel mixture of eutectic uranium-chromium or uranium-chromium-plutonium composition, or a salt variant using undiluted metal chlorides (DFRs). In the older molten salt variant of the Dual Fluid Reactor, the calculated EROI value aisto 2,000 [38, 39] (Tab. 1), already much closer to the theoretical maximum value of 10,000 than the common used nuclear solid fuel reactors. The innovation of the Dual Fluid principle rests on using separate fuel and cooling cycles, as shown schematically in Fig. (1). The corresponding idea of fuel cycle management for a Dual Fluid Reactor provides for the use of two separate liquid cycles with a reactor core designed as a kind of heat exchanger, in which the molten fuel flows through the tube system, while a lead cooling melt flows in the same direction for pure heat transfer similarly to a heat exchanger with indirect cooling. To realise the fuel cycle, a pyroprocessing separation unit is required, capable of returning fissile material to the Dual Fluid Reactor [29, 1, 37]. All the concepts and publications relating to the Dual Fluid Reactor can be found in [40, 41, 1, 36, 37] and [38, 39, 42, 43, 44, 45, 46, 47].

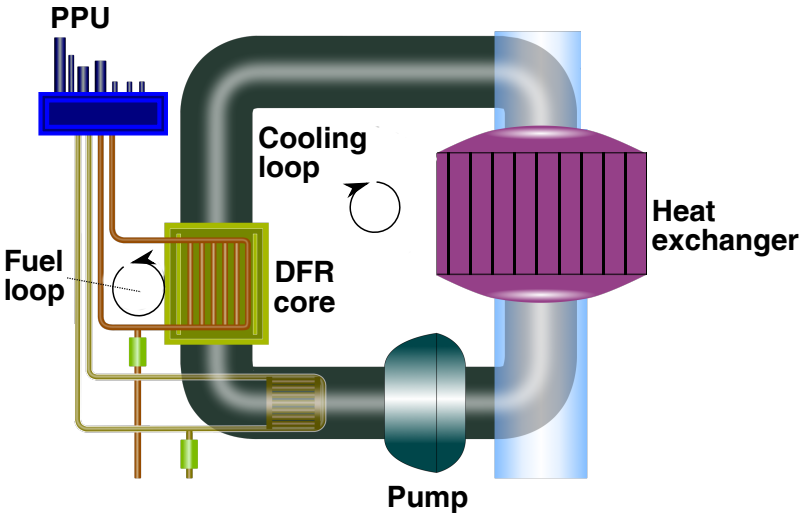

Figure 1: The Dual Fluid principle, Ref. [1]

Common modern thermal separation processes, mainly described in the literature, are based on liquid-liquid extraction processes [48], using numerous and considerably large amounts of solvents under moderate process conditions. The most important process is the PUREX (Plutonium-Uranium Recovery by Extraction) process, which deals with the separation of uranium and plutonium components, as summarised in [48], together with many other processes shown for the separation of other actinides and fissile materials. This results in large process waste streams that require expensive post-separation processes and lots of secondary sepatation effort (see [49, 48]). The main disadvantage of such liquid-liquid extraction processes is the use of large process streams with significant amounts of environmentally harmful solvents and extractants. They are also contaminated with the radioactive fuel material, which results in a significant increase of waste volume. This explains the numerous secondary separation efforts to clean solvents, extractants and fuel material. In addition, the extraction agents can only separate a few elements as active components per separation stage, with each stage separating each separable component into a single settler tank.

Another possible thermal and dry separation technique that does not generate such large extractant-fuel mixture streams is distillation via halogenation of the fuel to volatilise the fuel elements to be separated. The halogenation for distillation serves as an idea of the volatilisation of the fuel components in the fuel with different volatilities of the substance components, so that they can then be easily separated from each other. The main advantage over liquid-liquid extraction processes, where the fuel still has to be transferred to solution systems in a process-intensive manner, is that undiluted molten salts are directly usable for distillation. The idea of using distillation as a dry separation method without the use of solvents is a completely revolutionary idea which, despite its high potential, has not yet been explored for spent fuel recycling. Only a few initial studies in the 1960s and 1970s on the separation of uranium hexafluoride from fuels by distillation are known, see e.g. [50], although at that time the technical progress was not sufficient to allow the full potential of this technology to be utilised, in particular with regard to the lack of suitable structural materials.

Other general advantages of distillation include the use of a much more compact distillation column design at atmospheric pressure [51] compared to extraction methods where each separa-

tion stage is a separate separation apparatus. The distillation column corresponds to a compact countercurrent flow combination of single-stage distillation steps, as described in detail in [51] (Chapter 13). The separation stages are compactly integrated in a single separation column instead of individual separation stages. The separation is based on the volatility differences of the halogenated components, so that the separation is not component-specific, but has a separating effect on all material components via separation fractions. This is particularly useful in the reprocessing of fuel containing a wide range of components. Apart from halogenation, no other additives are added, one of the major advantages over liquid-liquid extraction. This results in a better recirculation and reuse of the fuel to solve the problem of final storage without secondary separation processes. Even the halides can be recovered in this process.

The only serious disadvantages of the distillation process are the higher process temperatures of 1,070 K on average, in the range of 500 K-2000 K and the formation of corrosive substances and halides. However, there are now materials able to tackle the corrosion problem, such as SiC or ZrC: highly performant, they can resist corrosion even at high temperatures above 2000 K [29]. Distillation as a separation technique for metal chlorides is not a new separation technique, is well understood and is already widely used in the extraction of raw materials in ores, particularly titanium in titanium ores. The most important process is the Kroll process developed in the 1940s for the distillation of titanium tetrachloride by chlorination of titanium ores, including the recovery of chlorine as a chlorinating agent. The pilot plant was built in the late 1940s, as the report in [12] shows, with good separation results. Further experience and applications of distillation in the nuclear field additionally to fluorination and distillation-based recovery of MSR fuels regarding to [50] can be found in the experimental investigation of the distillative processing of LiCl-KCl eutectics with separation of fission products and actinide chlorides, the results of which are shown in various studies, e.g. in [52, 53, 54, 55, 56, 57, 58, 59] with good separation results. This highlights the know-how about the application of such separation processes for the separation through distillation of actinides and fission products as well as about nuclear recycling problems in general. In [60, 61] detailed experimental explanations of single-stage distillation with Closed Chamber Units (CCU) are presented specifically in this context of practical application. This is a closed distillation system, similar to a glove box in the experimental setup, where a crucible is placed on a higher level where the molten salt is evaporated and condensed away from the crucible to a lower level melting pot. This device is often used for evaporation of molten salt and simple dilution as a single stage operation. This idea is also used as an idea for a single stage operation to implement a more complex total reflux column design in this thesis.

If distillation could be implemented today as a separation method for the processing of SNF material, this would not only solve the final storage problem, but also the scalability of circularity of fuel for LFRs. This would be an enormous technological advance for mankind, with circularity of the fuel ensuring sustainability and solving the disposal problem. The low-cost, carbon dioxide-free energy production can be used for further energy-intensive technical production, as explained in the Global Cycle Problem (GCP). Distillation can also be used to recycle Rare Earths Elements (REEs), e.g. compare [62, 63, 64], and metallic raw materials in the same way as nuclear fuel processing. Despite the high energy intensity of such separation processes, the provision of low-cost nuclear energy makes the use of distillation processes possible

and contributes significantly to the recycling of metallic resources. A large number of studies on recycling by chlorination and selective evaporation and distillation of REEs and other metallic raw materials have already been carried out in [62, 65] and show good separation results. Even the use of carbon dioxide chemistry would be conceivable in this case of low-cost energy production.

The main focus of this thesis is on the technical feasibility of distillation via chlorination for the reprocessing of spent fuel from today's nuclear reactors, including the recycling of cladding material also via chlorination and distillation. Chlorination is preferred as a volatilisation agent to ensure large liquid ranges of the components to be separated and to obtain the preferred thermally stable uranium tetrachloride, the boiling point of which is far from that of the other chloride components, so that very large proportions of SNF material containing mainly uranium can potentially be separated as high purity separation components. Secondly, the relative volatility between the chlorides is also very large compared to each other and the triple points are low to prevent sublimation of few components compared to other halogenides such as fluorides, iodides or bromides (compare boiling points from [24, 66, 18, 67]). During the development of the separation process, a novel distillation design is proposed in this thesis for the reprocessing of nuclear fuel: this leads to a closed system via total reflux column states. This column design would not be economically suitable for industrial use but can be used to solve nuclear fuel reprocessing problems by distillation, given the absence of valuable product to keep for sale and the magnitude of the waste problem . Numerous process simulations are carried out on simplified test mixtures and on more complex fuel composition examples of SNF and DFRm feed materials using my own custom codes for the overall flow diagram simulation (including the distillation column design developed here).

Simulation codes written by the author of this thesis were compared with ChemSep, a software for simulation of thermal separation processes in the chemical industry (see [68]), for simple test mixtures. It shows good agreement, thus validation the simulation codes written here. The distillation column for the pilot and laboratory column of the Kroll titanium recovery process of the technical report is also simulated and shows excellent results, largely consistent with the experimental measurement results in [12].

In the appendix of the thesis, different waste compositions are simulated up to the so-called HLW (High Level Waste) (see [69]). In addition, the simulation for the processing of metallic fuel melts from the Dual Fluid Reactor with the same flow diagram can be found in the appendix, in order to be able to demonstrate the (re-)cyclability of the fuel with the PPU on the basis of such an example liquid fuel reactor. The simulation results also impressively demonstrate the applicability of processing such separation mixtures by distillation, so that it can be concluded that distillation is a robust separation technology for SNF processing and that the generation of fuel cycles between this distillation-based pyroprocessing separation plant and the liquid fuel reactor potentially works excellently.

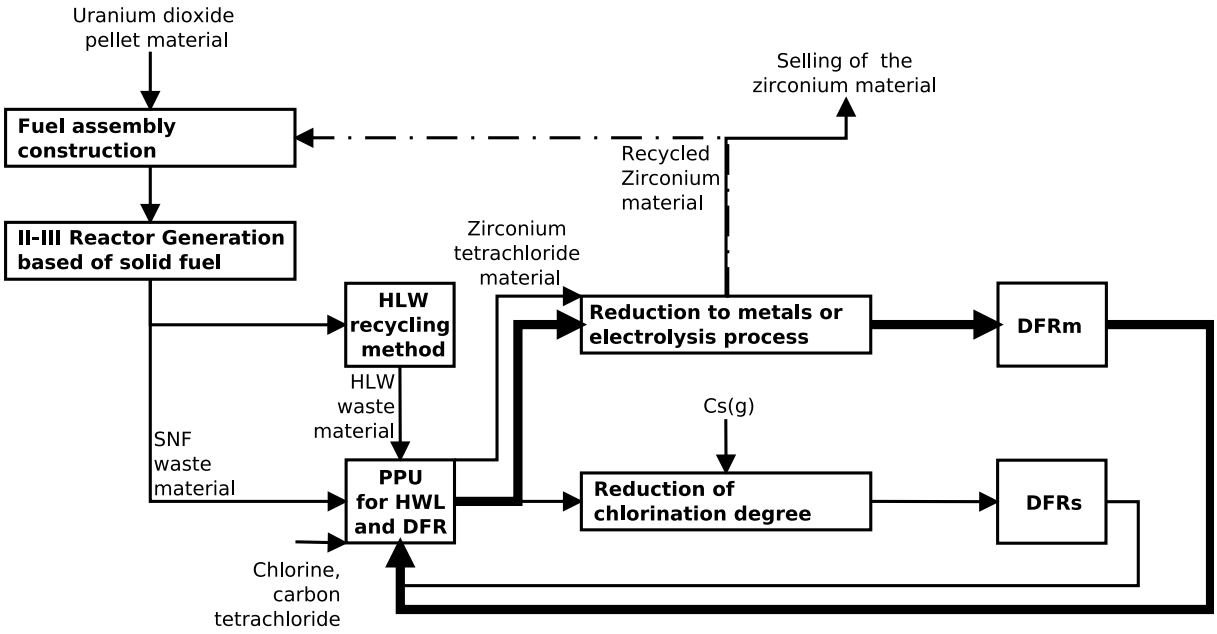

Figure 2: The main DFR cycle

Fig. (2) illustrates the overall main proposed DFR cycle process of the interconnection between the PPU unit and the DFRm, taking into account the SNF, HLW and dual-fluid feed recycling of the DFRm. The completion of the process cycle is shown schematically in bold in Fig. (2). Here, the SNF, HLW and DFR feed materials can be separated or reprocessed in certain mixing ratios as a mixed feed stream in the PPU unit shown in the centre of Fig. (2). After material separation in the PPU, complete reduction by electrolysis is required to be able to use the separated materials for the metallic DFRm reactor variant. At the same time, zirconium tetrachloride can also be electrochemically reduced to usable zirconium in an electrolysis process, and then zirconium alloy material can be produced again, which can be sold or reused in smaller quantities for other possible fuel rod cladding material applications. In the much less efficient salt variant of a Dual Fluid Reactor, a reduction of the degree of chlorination to lower-value chlorides is required, e.g. from uranium tetrachloride to trichloride, so that the vapour pressure of the salts in the DFR core is not too high and evaporates there. The degree of chlorination can be reduced, for example, by adding gaseous cesium.

In the last part of the thesis, a global analysis of the SNF inventories to be processed worldwide is carried out on the basis of the simulation results of a distillation separation plant. This analysis shows thst the complete distillation of all SNF inventories would take 65 years with only six worldwide assumed separation plants. Thus this thesis shows evidence that a complete solution to the problem of final disposal is possible through the application of the Dual Fluid Technology and the distillation-based separation technology combination. This paves the way towards the entry into a new, further advanced industrial age. It would allow the general worldwide increase in productivity, progress and prosperity of mankind together with fulfilling to a large extent the points mentioned above of energy production, industrial production and recycling regarding the GCP.

The separation concept developed in this thesis is also used in a modified form by the author of this thesis for the processing of NdFeB magnets (see [70]), using chlorination and distillation.

This publication shows that with this method, which is fundamental for the production of nuclear fuels, it is also possible to recycle and recover common metallic valuable raw materials in order to solve the recycling problem. NdFeB magnets are still indispensable in the automotive industry, in electronics such as mobile phones and PCs, and in industry in general [48, 71] and the Rare Earth component are also involved in the nuclear fuel. Thus, the study of rare earth separation for non-radioactive materials would also help to study the separation problem of nuclear waste, also taking into account the very similar boiling points of cerium trichloride and plutonium trichloride (e.g. compare: [24, 66, 18, 67]). Even from the perspective of the non-radioactive industrial chemical industry, the potential use of SNF distillation and the use of nuclear liquid fuel reactors, such as the Dual Fluid Reactor with the implementation of liquid fuel loops, significantly reduces the need for such raw materials.

Part II
Theoretical background

First, the chosen process development methodology (in section (1)) is followed as it is required for SNF reprocessing. Simulations were used to iteratively develop such a separation process, including pre-processing, defined in this work as the separation of non-volatile components and the separation of volatile gases from the almost completely assumed chlorinated molten SNF salt. Subsequently, the fundamentals of the simulation of distillation and crystallisation are discussed in this chapter in the section (2). Theoretical fundamentals refers to the modelling of distillation and crystallisation, where the theoretical background is also covered. Other necessary theoretical foundations for the calculations in the appendix are given in section (A). The basic theoretical background of separation process development as a conceptual design method is now described.

1 Separation process development

In the application case of (optimal) conceptual separation process development, the primary and secondary conditions have to be explored and sorted according to their importance, and separation criteria and separation specifications (e.g. separation accuracies) have to be defined. Subsequently, a heuristic prioritisation of these conditions and criteria is required, as described in [72, 73], among others.

The prioritised criteria, boundary conditions and constraints often already provide exclusion criteria for the selection of possible separation operation per separation task and per iteration step. In a heuristic way, this already significantly reduces the scope of the selection of possible separation options. The aim is to iteratively carry out the process design starting from the initial composition (feed) until the separation is fulfilled with regard to defined separation specifications and conditions or comes closest to these. These conditions include:

- Minimise the area required and the height of separation units, due to radiation protection reasons regarding the minimisation of shielding enclosure area of the operating rooms.
- Add as few or no chemicals as possible, avoiding solvents and extraction agents as much as possible to avoid further contamination with the additives and secondary separation efforts.
- The maintenance effort of each separation apparatus should be as low as possible.
- The separation process should, if possible, take place at normal pressure. For licensing reasons of the nuclear device, there should be no low pressures during the entire separation process.
- Due to the construction material, maximum temperatures of 2225 K at normal pressure of 1 atm are applicable under stationary conditions.
- Large temperature gradients within a separation unit should be avoided if possible or suitable for the process.

- The choice of the fundamentally selected separation operation per separation step should also be oriented practically to the generally available know-how in process engineering, whereby experimental and industrial experience in the handling of this separation operation with similar material components should be available. [1]

Permissible basic operations on the separation problem include:

- Chemical reaction,
- Distillation,
- Crystallisation & solids separation,
- Absorption,
- Adsorption,
- Extraction,
- Electrolysis,
- Chromatography,
- Electrochemical separation processes,
- Metal separation processes.

Criteria such as investment costs or the sale of separation products, as is usual in chemical process engineering, play a practically minor role in the development of the separation process for the separation problem of this thesis. This is because, in this case of nuclear processing, there are no products to be sold and the time limit must therefore be assessed as being significantly higher than for all industrial and chemical products in chemical process technology.

After validating all the simulation models by simulating test mixtures and comparing the results with other already validated simulation software, process development is carried out in this thesis. The subsequent selection for the separation operations of the process development in this thesis is initially directed towards the separation of the most critical impurities, such as solids and highly volatile substances, which are difficult to separate. A further condition is that the component with the highest proportion should be separated as early as possible, such as uranium for the SNF material of nearly 95 mol% contained in the fuel material. This is also the basis for selecting the permissible basic operations for the partial separation problem defined in this way. The simulation results then show the feasibility of the separation operation. This is followed by an evaluation of the reduced mixture after separation of the previous components. Thus, the separation concept is developed iteratively with the help of these heuristic rules (other possible heuristics are listed in [73, 72]). Only then is a possible combination of several separation operations considered. Examples of such considerations could be the performance of crystallisations in a subsequent distillation. An innovative idea could be to use the evaporator of the distillation

[1] The Kroll process for the distillation of titanium tetrachloride mentioned in the introduction serves here as an example of a comparable possibility for the distillative separation of chlorides from tetrachlorides, such as uranium tetrachloride.

column simultaneously as a crystalliser by inducing supersaturation of the dissolved solids and to design the evaporator also as a separator. In this case, the evaporator could perform the three functions of evaporator, crystalliser and separator.

More complex process development methods with detailed numerical or semi-numerical optimisation procedures, such as those described in [74, 75], are not used in this work. However, complex numerical optimisation methods for the selection and synthesis of separation operations are not used in this thesis.

The process development results in a flow sheet with all process conditions and simulation results, which can be evaluated as a process flow sheet, only the detailed design of the separation units contained therein is missing in the optimisation task of this thesis for process synthesis.

2 Modelling of distillation and crystallization units

The most commonly used models for the simulation of distillation are the equilibrium stage model and the rate-based approach as a non-equilibrium stage model (see: [51]). The stage model divides the separation column into discrete separation stages as equilibrium regions. In the equilibrium stage model, the mass and energy flows entering and leaving each separation stage are assumed to be always in thermodynamic equilibrium. In the non-equilibrium stage model, the vapour and liquid phases are balanced separately as balance region, using appropriate mass transport equations with a rate-based approach via mass transfer and mass transfer conditions instead of the equilibrium relationship. Mass transport plays an important role in the separation of substances. For the simulation of distillation and crystallisation, however, only equilibrium stage models are used in this thesis.

2.1 Definitions and correlations of reference quantities for mass transfer

The necessary mass transport in a vapour-liquid or solid-liquid system, as described in detail in [76] and [77], can basically take place by two mechanisms. First, matter is transported through a macroscopic flowing medium by convection, where forced convection is defined by external mechanical action. Convection also depends on the type of flow, e.g. whether a laminar or turbulent flow profile is formed [78]. On the other hand, mass transport can also occur by diffusion, which is caused by microscopic random movements of molecules and is also known as Brownian molecular motion. Convection is understood as spatially directed mass transport, whereas diffusion occurs in all spatial directions, a kind of equilibrium depending on the diffusion potential. The mass flux $\dot{N}_A$ of the substance A to be transported is defined here as the sum of convection and diffusion

$$\dot{N}_A = x_A \dot{N}_{A,\text{conv}} + J_A. \tag{1}$$

In this thesis, the following important variables are defined:

- The molar fractionx_A is defined as the molar quantity n_A (or molar quantity flow $\dot{n}_A$) involved in relation to the substance component A per total gas molar amount (or total

molar amount flow). This mole fraction is defined as follows:

$$x_A = \frac{n_A}{\sum_i n_i}, \tag{2}$$

$$= \frac{\dot{n}_A}{\sum_i \dot{n}_i}. \tag{3}$$

- The molar amount n_A and the molar flow $\dot{n}_A$ of component A is determined via the molar mass $M_{w,A}$

$$n_A = \frac{m_A}{M_{w,A}}, \tag{4}$$

$$\dot{n}_A = \frac{\dot{m}_A}{M_{w,A}}. \tag{5}$$

- The present concentration of a substance is defined as the molar amount (or molar flow) of A per total volume V (or total volumetric flow $\dot{V}$)

$$c_A = \frac{n_A}{V}, \tag{6}$$

$$= \frac{\dot{n}_A}{\dot{V}}. \tag{7}$$

- The mass-specific density belongs to the pure substance data and is defined as the mass of substance A that the substance occupies per volume

$$\rho_A = \frac{m_A}{V}$$

$$\equiv \frac{\dot{m}_A}{\dot{V}}$$

For the convection part with the convection velocity w_{conv} the following continuity condition applies

$$\dot{N}_{A,\text{conv}} = c_A \cdot w_{\text{conv}}. \tag{8}$$

The transport fraction J_A in equation (1) is defined as the diffusive mass flux of component A flowing perpendicularly through a cross-sectional area A due to the time-varying mass particle number of A with

$$J_A = \mathrm{A}^{-1} \frac{dN_A}{dt}. \tag{9}$$

In the case of single-substance systems, this is defined as self-diffusion of the substance component. In the diffusion of two involved substance components A and B, component A diffuses through a solvent system of substance component B with J_{AB}. In the ideally mixed N-component substance system, the combination possibilities of the diffusion of the substances are to be considered with $(\mathrm{N}-1)^2$ combinations in each case to each other [76] (p.185f). The theory of multicomponent diffusion is discussed in more detail in (A.1).

2.2 Modelling of basic separation units

For all thermal separation processes, in addition to the setting up of thermodynamic phase equilibria and the determination of mass and heat transport, it is the consideration of the required modelling depth for the equilibrium stage modelling that plays a significant role in the appearance of the simulation results. Within a defined balance area, the mass and energy balance as well as the detailed equations for mass transport, thermodynamic equations of state and phase equilibrium relationships are part of the main model equation system for each individual separation step. The depth of modelling, as a parameter of model complexity, depends on the target parameters to be investigated in order to represent the separation problem as realistically as possible. In general, numerous simplifications and assumptions are required to set up the model equations, which leads to an increasing idealisation of the separation problem and an increasing deviation from the realistically representable separation case.

In this thesis, for example, a high degree of idealisation is used for the simulations due to the lack of substance property data for pure components (elements or compounds) and mixtures of the components as well as the measurement of sufficiently representative, usable phase equilibria. In terms of phase equilibria, the simplest assumption is to consider ideal phase equilibria, neglecting the activity of the liquid phase. The simplified modelling is used in this thesis to show the separability and applicability at all, as a kind of lower bound for a feasibility assessment of the applicability of this distillation-based separation method. This also applies to the subsequent conceptual design development of the entire separation process in this thesis. For more realistic simulations, however, it is always necessary to measure the phase equilibria of representative mixtures of substance systems, which is not the aim of this thesis.

2.2.1 Overview of industrial distillation processes and modeling

Simple single distillation steps are rarely used on an industrial scale compared to distillation columns because the separation accuracy is often not high enough. Known single stage distillation processes are only used for very large vapour pressure differences of certain components. These include pressure expansion processes such as flash evaporators, in which the liquid is expanded by means of a throttle and the highly volatile components pass into the vapour phase. These separation processes are simulated as isothermal or adiabatic evaporators, taking into account the change in pressure. This requires the numerical solution of an algebraic non-linear equation in combination with thermodynamic equilibrium conditions, mass and energy balances, as described in [51] (chapter 13: One-step equilibrium flash operations). By analogy with evaporation, it is also possible to carry out condensation of certain components present in a residual vapour stream. The use of flash evaporation followed by condensation also allows the separation of the non-volatile components remaining in the vapour stream. An important aspect here is to increase the so-called defined volume-specific contact area, which should be large enough to allow the components to pass into the corresponding phase and diffuse into the other phase.

In industrial distillation technology, higher separation accuracies are often required, requiring multi-stage distillation processes. The distillation stages are integrated in a distillation column. The distillation principle in such an industrial distillation column is shown schematically in Figure 3 . A feed stream, in this example a so-called zeotropic (non-azeotropic) mixture consisting of

three material/substance components, is fed to one separation stage of the column. In the countercurrent flow principle of the distillation column, vapour and liquid are then in active contact with as large a volume-specific contact area as possible, so that the mass transfer between the two phases is as large as possible. Reaction columns[2] allow a countercurrent process of liquid and vapour, where the liquid flows downwards and the vapour rises upwards due to the buoyancy principle inside the distillation or rectification column [51] (chapter 13), [78] (pp. 291 - 340). The liquid from each separation stage flows through an outlet shaft into the separation stage below. In the separating stage, vapour and liquid are in active contact when vapour enters the separating stage from below. The light-boiling component, shown in red in fig. 3, accumulates in the upper part of the column and increasingly in the condenser, while the heavy-boiling component (shown in blue) accumulates mainly in the lower part of the column. The medium boiling component tends to remain in the middle of the column. This illustration of the distillation column in general with such theoretical column stages can also have a more abstract realisation of the column stage with column trays, structured packing material or fluidically optimized random packing devices (see: [79, 80]). The distillation column in general has a monotonic temperature profile with the coldest temperature in the condenser and the hottest temperature in the evaporator. For the medium boiling component this means that it only circulates in the middle part of the column due to its real volatility, as this component condenses in the direction of the condenser before reaching the condenser and also evaporates in the direction of the evaporator before reaching the evaporator. Therefore, with this continuous distillation column principle shown in Fig. 3, this medium boiling component can only be removed in a more contaminated state as a side stream product via a side stream removal.

At the top of the column, the distillate is condensed in a condenser and then a certain fraction is removed as the valuable distillation product. The other part is fed to the distillation column (usually the first column stage after the condensation stage) to maintain the countercurrent principle and to enable the operating principle between the operating and equilibrium states per equilibrium column stage. For this purpose, a minimum amount of distillation product must be returned to the column to ensure and enable the distillation column principle. The ratio of the specific molar amount of distillation product fed back to the specific molar amount of distillation product at the top is defined as the reflux ratio v. The ratio to the minimum specific molar amount of distillation product fed back required to enable the distillation column principle is defined as the minimum reflux ratio $v_{\min}$. The value of the corresponding reflux ratio v is always greater than the thermodynamically determined minimum reflux ratio $v_{\min}$, which is limited downwards by the achievement of thermodynamic equilibrium between vapour and liquid. It follows that a minimum reflux ratio is required for rectification. It is also clear that the design of a distillation apparatus (distillation column or rectification column) depends to a large extent on the reflux ratio v. This fact must be taken into account, especially in various distillation column simulations, which makes it necessary to clearly estimate the minimum reflux ratio as accurately as possible. Another possible adjustable column reflux concept is the principle of the so-called total reflux column as a technically not directly practical application of distillation separation,

[2]Despite the common definition in the literature as typical industrial multistage distillation columns, where the generalised term distillation column is also used to refer to a generalised column, the term distillation column is used in this thesis to refer to a generalised column.

in which the entire top distillation product is returned to the column, but no distillation product is removed.

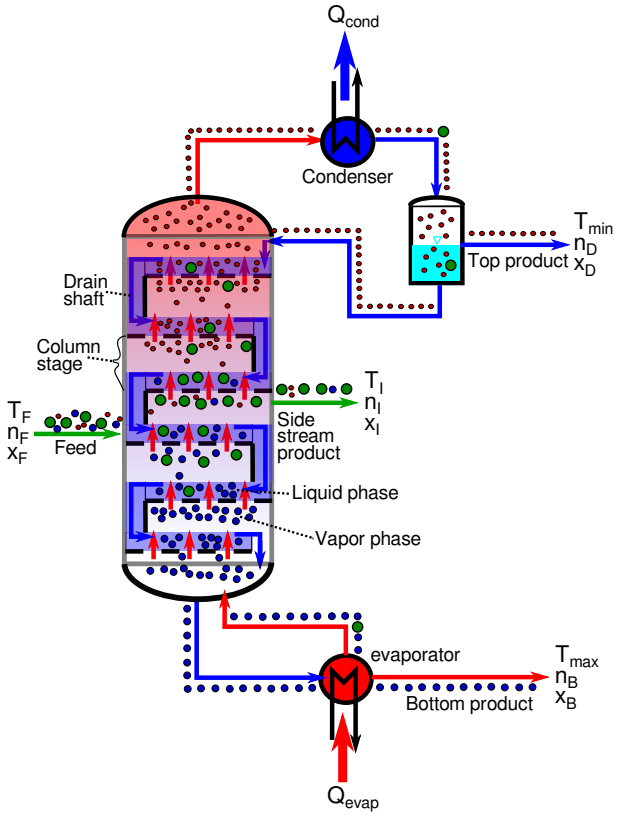

Figure 3: Operation principle of a continuous industrial distillation column

In the distillation column operation, the substance/material composition of both phases is either location-dependent average discretized expressible as separation stage according to the continuous mode of operation or, in the case of the total reflux process, after reaching equilibrium, or purely time-dependent as in the discontinuous mode of operation of a distillation column. While in continuous and total reflux column operation there are constant compositions per separation stage in steady-state operation, a discontinuously operating separation column works according to the 'boiling vessel principle' in a different mode of operation. Here, the mixture is fed once at the beginning of the column operation and evaporates discontinuously, whereby the substance components are distillated divided into fractions over time, which are drawn off by time at the condenser. This technically feasible variant of column operation also has a defined reflux ratio. As the volatility of the substance components at the condenser decreases in time, the proportion of heavy-boiling substance components increases, so that only medium-temperature mixed fractions can be recovered as fractions. Towards the end of distillation, a mixture of heavy-boiling components and other residues remains as a distillation residue, which can be removed as a bottom product. Various technical details of the product removal and the adjustment of the reflux ratio and the heat supply are described in more detail in [51]. Fig. 4 schematically summarises the differences between continuous and discontinuous process variants. With discontinuous separation columns, the product composition can often be better controlled. However, this technical variant is only used if the product streams are rather small in relation

to the usual separation quantities of the process technology.

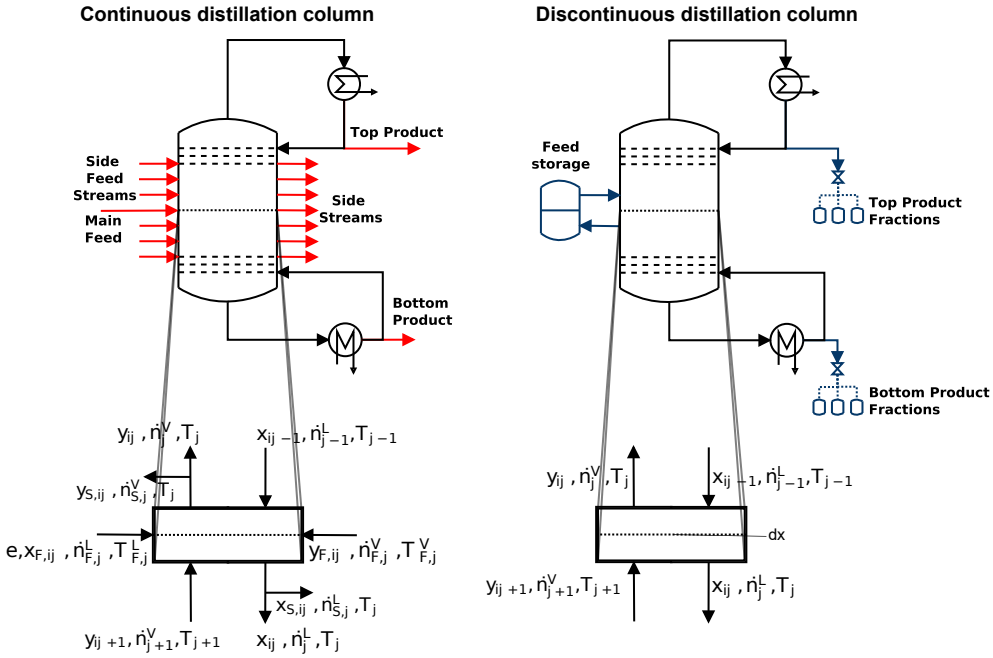

Figure 4: Illustration of the technical design and the modelling of the equilibrium stages of industrial distillation columns.

In distillation column operation, light-boiling substances tend to accumulate in the vapour phase on their way to the top of the distillation column, while heavy-boiling substances pass into the liquid and flow down the column. Only in the case of so-called azeotropic composition in special mixtures does the composition of liquid and vapour remain constant at the corresponding composition. Up to a certain composition limit at the azeotropic point, the mixture cannot be further separated. In addition, when the composition of a binary mixture is beyond the azeotropic point, the dominant distillation components are reversed as a heavy or light boiler distillation product component, otherwise the azeotropic composition previously summarised by composition values behaves as a single quasi-chemical opposite light or heavy boiler distillation product component. The condenser at the top of the column can be operated as a total condenser (everything is condensed) or as a partial condenser (part of the vapour stream is removed as vapour and not condensed). Also at the bottom of the column, a partial flow of the bottom distillation product must be fed back into the column in a similar way to the top of the distillation column in the form of vapour from the evaporator. The ratio to the amount of vapour returned is defined here as the boil-up rate V_R.

Internal separation-relevant static internals within the column, in the form of trays or any random or structured packing material column device, ensure intensive contact between the vapour and liquid phases. The greater the contact area between the phases, the better the kinetic approach to thermodynamic equilibrium.

In general, column trays in the form of bubble trays or sieve trays can be used very well as internals to realise the intensive contact of vapour and liquid (see: [79, 80]). In the tray column, the vapour enters each column stage through a hole opening and passes through the liquid in the form of a vapour bubble in its common optimised tray column operation state

(without flooding or too much gasification of the column). For all column types, there is no precisely definable and limited stationary surface contact area between liquid and vapour each column stage. Practically in the optimized tray column state care must be taken to ensure that the pressure of the vapor phase is optimized to prevent the liquid from raining through the hole openings each tray, but also not too high to allow the optimised liquid-vapor contact. In the real case, the (mean) residence times of vapour and liquid per separation stage are too short to achieve thermodynamic equilibrium per separation stage. Therefore, equilibrium stage models with bottom efficiency(s) per separation stage can be used to describe simulatively the deviation from thermodynamic equilibrium. This is important for further simulation of practical usable distillation column, where these bottom efficiency values must often be experimentally determined. Other internals that can be installed in rectification columns to allow an optimised contacting of liquid and vapour can be structured packings or various random tray packing devices with different geometries or structured material e.g. with pores and channels to optimise the flow behaviour . The design of distillation columns and other internals is discussed in detail in [51, 81] .

The theoretical separation stage is only a theoretical construct at the points in the column where the averaged composition is achieved according to the equilibrium stage model. Four modelling options are usually available for modelling and simulating distillation columns, although exact modelling is almost never used due to the high model complexity:

1. Simple estimates, calculations and graphical approximations as described in [51] provide initial guidance on the choice of separation design under the best possible conditions. This can provide a kind of lower bound on the feasibility of distillation as a first insight.

2. Equilibrium stage models, where the vapour and liquid streams are assumed to be in thermodynamic equilibrium at each separation stage, and from an operating kinetic point of view, deviations from equilibrium can be described in terms of bottom efficiencies. The bottom efficiency (the so-called Murphree efficiency) is defined as the ratio of the difference of the actually observed vapour composition difference between two separation stages to the vapour composition difference that would result in thermal equilibrium (see: [80] p.181 f) to

$$E_{j,j-1} = \frac{y_j - y_{j-1}}{y_j^{\mathrm{eq}} - y_{j-1}}. \tag{10}$$

   The basic equations of the equilibrium stage model are the so-called MESH equations (Mass, Equilibrium, Sum-rates, Enthalpy equations) for the simulation of distillation columns according to [51], where enthalpies and enthalpy differences are used to describe the energy balance. Mass transport equations do not appear in the equilibrium stage models. The activity of the components in the liquid phase mixture under thermodynamic equilibrium conditions physically describes the intermolecular interactions of the components in the mixture. It is only in the phase equilibrium relationship equations that the physically real separation behaviour is modelled, which differs from the idealized behaviour . The thermodynamic equilibrium equation must therefore be modelled as accurately as possible in order to achieve a physically realistic representation of the separation in the liquid phase mixture. The depth of modelling within the equilibrium stage models thus depends al-

most exclusively on the modelling of the activity of the components of the liquid phase by means of the equations of phase equilibrium relationships (or briefly defined as equilibrium conditions, which in this thesis are meant in connection with the modelling of distillation columns).

3. The rate-based oriented modelling of non-equilibrium stages according to [82, 51] also uses the principle of the separation stage, whereby the mass transfer equations with diffusion are additionally considered between separately considered liquid and vapour balance areas per separation stage. The mass transfer between the two phases is modelled between the phase transition region of the liquids, where the volume specific surface area depends on the surface tension, the viscosity of the liquid as well as many other mixing data, which are generally not really available for this thesis. Therefore, these modelling approaches will not be used in this thesis as this is the current state of development available in the literature.

4. Exact models are CFD simulations with additional required consideration of mass and energy transport equations through the phases and also a phase modelling method by tracking the boundary surface between liquid and vapour. The required model equations, separately for vapour and liquid, consist of mass balance, momentum conservation via the Navier-Stokes model with assumptions on fluid mechanics, energy transport as well as mass transport and transition conditions (material and energy balance) between vapour and liquid. The choice of column geometry and internal internals must also be well specified and known. Such models are extremely complex and are therefore rarely used in practice, including, of course, in this thesis. Therefore, these types of models will not be used in this thesis.

A detailed description of the first three modelling types can be found in [51]. Simulation with fluid dynamics is a specific CFD problem, so the CFD literature can be found on two-phase flow of free surface flows.

2.2.2 Overview of crystallization processes and remarks on equilibrium modeling

Crystallisation comprises those separation steps in which the components of a substance pass from a mobile phase, such as the liquid phase, into a structured crystal-solid matrix as the solid phase. In the case of crystallisation from solutions, as in the example of salt dissolved in water, the solution behaviour depends on concentration, temperature and pressure [83]. Similarly, a molten salt system with oxide or precious metal material involved can be simplified assumed to be a solution system and therefore roughly modelled as such. The aim is to obtain a supersaturated solution or melt solution, which can be achieved, for example, by cooling, precipitating or evaporating the solution. When crystallising from the melt or vapour phase using the position of the melting points of the components to be separated, the energy transport and the cooling rate (velocity) are of great importance. The crystallisation process from the melt has to be optimised by modelling the cooling rate [83].

The whole crystallisation process takes place in the following stages. Firstly, nucleation takes place in which the supersaturated system is somehow brought into a new thermodynamic equilibrium state of a solid phase by exceeding a critical nucleation size in primary nucleation.

Once the critical nucleation size is reached, crystal growth begins, with further agglomeration of solid particles with grain boundary formation in the advanced stage of crystallisation. As crystallisation usually occurs in a more ordered state in the solid from a uniformly distributed melt, a contribution of crystallisation energy is released. The nucleation growth process can often be understood as a kth order interfacial reaction (with a concentration difference Δc between the film and melt phases and a mass transfer kA)

$$\frac{dn}{dt} = kA \cdot \Delta c^{\mathrm{k}}. \tag{11}$$

Other aspects of crystallisation stages and progress, even Ostwald-Miers crystallisation diagram states, can be found in the secondary literature listed in [83], but the theoretical background here is not of great importance to this thesis and only part of the follow-up studies form this part of the work of the thesis. Absorption and agglomeration also play a secondary role in the formation of large solid particles. This part is also less relevant to the scope of this thesis and will be the subject of possible detailed future research. Nevertheless, chemical additives can sometimes be used to achieve or increase the crystallisation rate within the crystallisation phases. Details on mass transfer are described in [83]. Other technical processes and variants are also described in detail in [83]. For the present thesis, only the consideration of primary nucleation from a melt is essential and will be focused on.

According to [83], there are four main practical crystallisation methods described from the specific molten state rather than from solution, e.g. as aqueous solutions:

- Repeated solidification and/or melting: by slow solidification or melting, one component can preferentially pass into the other phase, with the melt itself acting as a kind of solvent.

- In layer crystallisation, the substance to be crystallised is deposited on the wall of a plate heat exchanger, with the temperature difference acting as the driving force. The advantage of this method of crystallisation is that it is simple in design, with no moving parts, but with a high degree of operational reliability.

- Suspension crystallisation, which uses the molten liquid as a kind of solvent, is a viable continuous separation process that works in two steps: Suspension formation by homogeneous crystallisation followed by concentration of the formed solids. Suspension crystallisation can also be operated in several separation stages, as already mentioned. Suspension formation can be simulated in the same way as distillation columns using the MESH equations, applying the solid-liquid equilibrium (SLE) phase equilibrium relationships instead of VLE vapor-liquid equilibrium in its distillation model and therefore as great importance of estimating the use of crystallisation of separation method of oxide and precious metal material from a molten salt.

- In particular, zone melting can be used to produce metal or chloride melts to separate some components down to the ppm range. The material to be melted is placed in a tube and a rod inside is moved so that the melting zone is also moved. The idea is that as long as the cooling rate is relatively low, the impurities are more abundant in the melt and virtually do not pass into the solid phase. This separation process can only be used

for very small quantities of material due to the small amount of material involved. It is important that the impurities have completely different melting and dissolving properties to the main melt. The Czochralski method is a well-known sub-method for the production of high-purity metal alloy components that are completely free of other components (see e.g. [84] for more information).

More detailed descriptions of crystallisation processes can be found in [83] and for the separation of metals and oxides from a molten salt from fission products in [85].

2.2.3 Evaluation of thermodynamic phase equilibrium relations

The knowledge of measured or well-estimated phase equilibria of representative mixtures, as well as the knowledge of the required substance property data, is the essential basis for the correct thermodynamic description of the phase equilibria by using specific GE models with respect to the estimation of the activity of each component in the mixture. In addition to the use or creation of appropriate GE models, inaccurate activity predictions are often the result of incorrect pure component substance and mixture data or incompatible equilibrium data used to describe the phase equilibria. These aspects would have to be considered for a realistic representation of a vapor fluid system. Although this thesis uses highly simplified phase equilibrium conditions according to Raoult and Dalton (see: [51]), the knowledge of the deviation due to the simplifications made depends on the understanding of realistic phase equilibrium conditions, which can be set up as generally as possible in this thesis.

The Gibbs phase change rule The so-called Gibbs phase rule indicates how many thermodynamic degrees of freedom F a thermodynamic substance system in the thermodynamic equilibrium in the mixed state has, depending on the components and phases involved. According to this rule, the degree of freedom F in which the system can move depending on the state variables is determined from the sum of the number of components minus the number of phases as follows

$$F = N_{\text{comp}} - N_{\text{phase}} + 2. \tag{12}$$

For example, a one-component substance system in which only one phase is involved has exactly 2 degrees of freedom. Through pressure and temperature, a two-dimensional area can be obtained within the phase area as a representable surface in a three-dimensional parameter space, in which each state point can be approached without having to leave the phase. This changes, for example, at the so-called triple point of the pure substance, where all three phases, solid, liquid and vapour, meet. Then there is no longer a degree of freedom and the surface corresponds to only one state point, which can be specified as a pure property data point parameter for substance components defined as a triple point with the triple temperature T_{tr} and pressure p_{tr} as pure characteristic substance property data. At the end of the vapour pressure as another characteristic point there is also a phase point with respect to the Gibbs rule, where the component becomes supercritical and no condensed liquid or vapour phase can be distinguished. This phase point is known as the critical point with its pure component property data point of critical temperature, pressure

and volume T_C, p_C, v_C. Other such example single points are the later discussed the eutectic point into a SLE phase equilibria visible in a change diagram for a two components system and azeotropic points in the VLE equilibrium. In addition, in a three-component system with only one single phase, there are basically four degrees of freedom available in one phase, but these are reduced in the presence of several phases. In the presence of three phases, in contrast to the pure substance, a two-dimensional phase surface diagram can still be obtained. With an increasing number of substance components, the total number of degrees of freedom in which the system can move increases.

Phase change equilibria For a thermodynamic equilibrium, the pressure p, temperature T and chemical potential μ must be the same for all phase equilibria in all phases. In the so-called Gibbs phase rule, the following conditions then apply in a system with $\mathrm{N_{phase}}$ coexisting phases[83, 86]:

- Thermal equilibrium: $T^{(1)} = T^{(2)} = \cdots = T^{(\mathrm{N_{Phase}})}$,
- Mechanical equilibrium: $p^{(1)} = p^{(2)} = \cdots = p^{(\mathrm{N_{Phase}})}$,
- Physical equilibrium: $\mu_i^{(1)} = \mu_i^{(2)} = \cdots = \mu_i^{(\mathrm{N_{Phase}})}$,
- Chemical reaction equilibrium of equilibrium reactions: $\sum_i^{\mathrm{N_{react}}} \nu_{ij}\mu_i^{(j)} = 0$ with ν_{ij} as stoichiometric constants.

The chemical potential μ describes a thermal state variable that characterises the changes in energies as the number of substances changes. For ideal pure substances, the following equation describes the change in $\Delta\mu$

$$\Delta\mu = RT \ln\left(\left(\frac{p}{p_0}\bigg|_i\right)\right) \approx RT \ln\left(\frac{c_i}{c_{i,0}}\right). \tag{13}$$

For real behaving substances, however, the following applies with the pressure correction via the fugacity

$$\Delta\mu = RT \ln\left(\frac{f_i}{p_0}\right). \tag{14}$$

The fugacity f_i represents a corrected quantity to the pressure of the corresponding phase in the description of the specific Gibbs energy and the chemical potential according to [83]. In phase equilibrium for both phases, according to the isofugacity criterion, the fugacity of the two phases must be equal, with

$$f_i^{\mathrm{Phase:1}} = f_i^{\mathrm{Phase:2}}. \tag{15}$$

In order to establish the concrete phase equilibria via the isofugacity criterion according to equation 15, the so-called $\varphi - \varphi$ concepts can be used for liquid-liquid equilibria (LLE) and sometimes also for vapour-liquid equilibria (VLE). Preferably, however, the $\gamma - \gamma$ concept is often used for solid-liquid equilibria (SLE). The $\gamma - \varphi$ concept is often only used for describing vapour-liquid equilibria. For the description of the activity coefficients γ_i, special models for the calculation of the Gibbs excess enthalpy, in particular so-called GE models, are used. Depending

on the phases involved in the equilibrium system (mainly VLEs), some of the most important GE models are explained in more detail in the appendix 2.2.3.3.

In the $\varphi - \varphi$ and $\gamma - \varphi$ concepts, φ is known as the fugacity coefficient and is defined as

$$\varphi_i = \frac{f_i}{z_i p} \tag{16}$$

Here z_i is the mole fraction of the corresponding phase.

2.2.3.1 Examples and calculation of solid-liquid phase equilibria from melts The crystallisation behaviour of a melt in the solid-liquid equilibrium system for the separation of several solid components is crucial for the type of crystallisate formed later in terms of structure and composition. For example, solid solutions or pure substances can be crystallised during crystallisation.

In the case of a two-component mixture, the temperature curve dependent on the amount of substance is called the liquidus line, above which the medium is completely liquid. The solidus line is the boundary in the phase diagram that separates the solid-liquid region from the fully solid crystallised state. In the case of a so-called non-eutectic mixture, monotonic functions appear which only touch in the pure substance component state. The other example of a different mixture is the so-called eutectic mixture with one or more eutectic composition points, where all components are soluble in the liquid but largely insoluble at this single solid phase change point. In this case, at a constant eutectic freezing temperature, all components crystallise to the eutectic composition and form a fine crystalline structure from the different solid modifications. Deviating from the eutectic composition, the liquidus line in a Tx diagram usually bends away from the eutectic composition point to higher temperatures on both sides. This means that at the eutectic composition there is a global temperature minimum of the melting temperature as a function of mole fractions. In a binary mixture of two substances, the eutectic point means that the solidus and liquidus lines at this composition point non-continuously touch each other under significant decreased melting point of the mixture compared to the pure two single component melting points. The solidus line as a dividing line in the T-x diagram is a constant solidification temperature as long as solid solution formation is neglected or not present for the two component system in the T-x diagram. According to [78], such systems with one or more eutectics are most common in 80% of industrial melts. Other systems, such as systems with a so-called peritectic, are presented in [83] as well as the so-called peritectic.

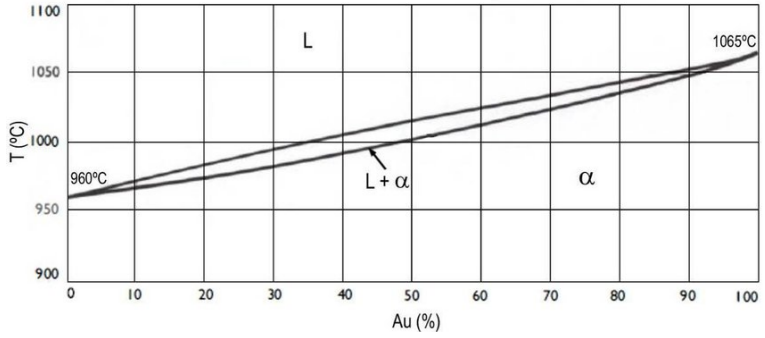

Figure 5: Ideal SLE phase diagram example: gold-silver system, Ref.:[2] p.127

The figures (5) and (6) show two examples of melts in the binary melt system. The first example in Fig. (5) is a binary solid-liquid system without eutectic composition of silver and gold. The region in which liquid and solid are in thermodynamic equilibrium together is delimited by the area enclosed by the lower solidus and upper liquidus lines in the Tx diagram. As pure substance components, the melting points of the two substance components are given for every substance component system where the solidus and liquidus lines touch. At any point in the liquid phase L, far from the compositions of the pure components, there will be mixed crystals of both components after the temperature is lowered above the sinking temperature below the liquidus line. When the temperature is below the solidus temperature, everything is crystallised in equilibrium. Compared to a higher compositional starting point of the melt, gold can only be enriched to a small mole fraction value by crystallisation due to the small separation area between the solidus and liquidus lines shown in Fig. (5).

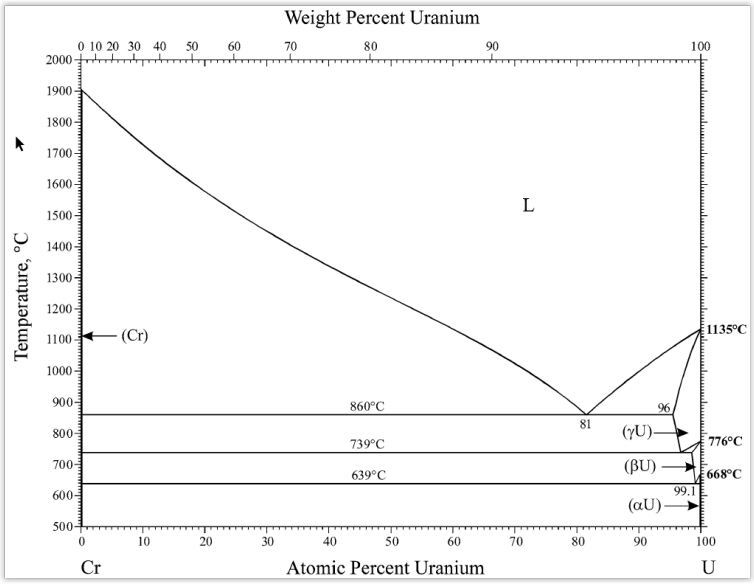

Figure 6: Eutectic SLE phase diagram: U-Cr system, Ref.:[3]

Fig. (6) shows a system of uranium and chromium as an example of an eutectic mixture with three solid phase transformations for uranium from the solidus modifications α to γ. The eutectic in this binary system has a mole fraction of$x_U = 0.81$. When the melt is cooled below the eutectic point, where the solidus and liquidus lines touch, it is assumed that a fine-grained structure of both uranium and chromium crystals is obtained at the minimum eutectic temperature of 860°C for this composition. Analogous to the definition of the triple point, according to the Gibbs phase rule in equation (12), the number of degrees of freedom is zero at the eutectic points and also at the end of the mixed solid phase transition points in Fig. (6). If the uranium composition is below the eutectic, pure chromium will crystallise from the melt. If the uranium composition is above the eutectic composition, uranium will crystallise accordingly. Depending on the composition and temperature, there are different modifications of the uranium-chromium mixtures. In an abstract way, for this binary system it can be assumed that on the left side of the eutectic, the uranium acts as a kind of solvent for the chromium, in which the pure chromium has a much higher melting point than in the mixture. On the other side of the eutectic composition, the

chromium can be seen as dissolved in the uranium, with an even lower melting temperature in the mixture than in the pure component.

Basic calculation of solid-liquid phase equilibria The description of solid-liquid equilibria according to [78, 83] is carried out via the $\gamma - \gamma$ concept, in which the fugacity applies to each phase (with "0" related to the pure substance components i):

$$f_i^{\text{Phase}} = x_i^{\text{Phase}} \gamma_i^{\text{Phase}} f_{0,i}^{\text{Phase}} \tag{17}$$

The isofugacity criterion provides a ratio of the fugacities of the pure substance components. It is

$$\frac{x_i^L \gamma_i^L}{x_i^S \gamma_i^S} = \frac{f_{0,i}^S}{f_{0,i}^L} \tag{18}$$

Then the free (Gibbs) enthalpy $g_{0,i}$ of the pure substance is calculated via equation (14) . Via the difference of the free enthalpy as free melting enthalpy under definition of the melting entropy $\Delta s_i^{\text{SL}} = \frac{\Delta h_i^{\text{SL}} T_{M,i}}{}$, melting enthalpy Δh_i^{SL} and melting temperature $T_{M,i}$ follows the corresponding calculation expression for the corresponding enthalpy change

$$\Delta g_i^{\text{SL}} = \Delta h_i^{\text{SL}} \left(1 - \frac{T}{T_{M,i}}\right). \tag{19}$$

Thus, after using the equations (17) and (19) in the isofugacity criterion for the solid and liquid phases, the following simple equation can be provided to determine the phase equilibrium relationship. Here is

$$\ln\left(\frac{x_i^L \gamma_i^L}{x_i^S \gamma_i^S}\right) = -\frac{\Delta h_i^{\text{LV}}}{RT}\left(1 - \frac{T}{T_{M,i}}\right). \tag{20}$$

The equation (20) refers only to the solid-liquid transformation. In the case of multiple solid-liquid transformations, the other phases must be added for all equations. In addition to equation (20) and analogous to $-\frac{\Delta h^{\text{LV}_i}}{RT}\left(1 - \frac{T}{T_{M,i}}\right)$, the sum of the other transformation points $-\sum_k \frac{\Delta h_i^{\text{change},k}}{RT}\left(1 - \frac{T}{T_{k,i}}\right)$ follows as another additional part in equation (20). Using the example of the uranium-chromium mixture shown in Fig. (6) the three solid modifications α, β, γ are present, so that for cooling to the α-U modification the following equation replaces equation (20) with the eutectic temperature of 860°C and phase transformation temperatures $T_{\gamma\beta,\text{U}} = 739°C$ and $T_{\beta\alpha,\text{U}} = 639°C$ C as follows

$$\ln\left(x_{\text{U}}^L \gamma_{\text{U}}^L\right) = -\frac{\Delta h_{\text{U}}^{\text{SL}}}{RT}\left(1 - \frac{T}{T_{M,\text{U}}}\right) - \sum_k \frac{\Delta h_{\text{U}}^{\gamma\beta}}{RT}\left(1 - \frac{T}{T_{\gamma\beta,\text{U}}}\right) - \sum_k \frac{\Delta h_{\text{U}}^{\beta\alpha}}{RT}\left(1 - \frac{T}{T_{\beta\alpha,\text{U}}}\right). \tag{21}$$

It should also be noted that according to Fig. (6) the areas on the right side of the diagram represent the pure uranium modifications αU, βU, γU. In the case that no solid solution is formed in the solid phase, the equation (20) can be replaced by the simplification $x_i^S \gamma_i^S = 1$. Then, according to equation (20), only the activity of the liquid phase is relevant for the description of the non-ideal crystallisation behaviour . The calculation of the activity of the liquid phase γ_{U}^L can be done with a suitable GE model approach in the SLE and LLE system, such as the

Non-Random-Two-Liquid model (NRTL) according to (2.2.3.3).

A further condition for crystallisation from a melt is the formation of stable nuclei above a critical nucleation radius of solid particles. The possibility of estimation is described in the appendix after the section (A.3) and is not included in this thesis for ideal phase equilibria because the calculations depend essentially on the activity of the phases to be able to estimate realistic values. Therefore, the calculation under ideal conditions cannot be usefully applied to this thesis. In addition, other important crystallisation processes are described in order to obtain high purity crystallisation products from the critical nucleation radius.

2.2.3.2 Calculation and examples of vapor-liquid equilibria (VLE) In the thermodynamic description of vapour-liquid equilibria, knowledge of the real behaviour of the liquid phase via the activity coefficients γ_i per component i is important in order to be able to describe the real phase equilibrium at all. With $\gamma_i = 1$ an ideal phase equilibrium exists. Furthermore, heuristics at low pressures below 10 bar indicate that other non-ideal influences on the phase equilibrium do not clearly emerge, but only the part due to interactions of the molecules and the real behaviour of the liquid flows into the non-ideal part via the description of the activity coefficients. This shows the importance of the determination of the activity coefficients by suitable GE models for the description of real phase equilibria.

The description of vapour-liquid equilibria can be done by applying the isofugacity criterion $f_i^V = f_i^L$ according to equation (15) for the liquid phase L and vapour phase V via two different calculation methods, the $\varphi - \varphi$ or the $\gamma - \varphi$ concept [87, 78]. In the φ approach, the following calculation condition applies separately for the description of the two different phases

$$f_i^{\text{Phase}} = x_i^{\text{Phase}} \varphi_i^{\text{Phase}} p. \tag{22}$$

In the γ approach, equation (17) can be used.

The $\varphi - \varphi$ calculation concept follows a model concept for determining the fugacity coefficients and is defined as a homogeneous calculation method according to [87]. According to [87], application of the $\varphi - \varphi$ concept and equation (22) yields the following calculation equation (22) depending on temperature T, pressure p, density ρ_i^{phase} and mass fraction x_i with regard to the fugacity coefficients φ_i per substance component i

$$x_i \varphi_i^L \left(p, T, \rho_i^L(x_i)\right) = x_i \varphi_i^V \left(p, T, \rho_i^V(y_i)\right). \tag{23}$$

As can be seen in equation (23), the calculation approach depends exclusively on the calculation method of the fugacity coefficients φ_i via suitable equations of state. However, according to [87] (p.161f), the equations of state are usually only known for non-polar, simple molecules. For molten salts, electrolytic solutions or polymer mixtures of organic substances, these are only simple approximations as well. The calculation methods via volume- and pressure-dependent equations of state and application of the virial equation is necessary for the estimation of the fugacity coefficients. However, this method is not applied in this thesis due to insufficient knowledge of suitable equations of state and model functions under insufficient knowledge of numerous material and substance property data. In addition, the results from the $\varphi - \varphi$ calculation ap-

proach concept are also strongly dependent on the concrete calculation of the mixture variables via the interaction parameters between the molecules of the vapour and liquid phases. It follows that for molten salts, electrolytic solutions or polymer mixtures, the $\varphi - \varphi$ concept is rather not applicable for the separation problem mentioned here.

A much better way is the calculation via the $\gamma - \varphi$ concept, in which only pure substance component fugacities and coefficients are required and the non-ideality of the liquid phase is largely determined via the activity coefficient. Several GE models are available for the determination of the activity coefficient, which must be suitably selected and adapted to the experimental phase equilibrium data (compare [51]). Typical examples of empirical GE models for the description of VLE equilibria are the Wilson model or the model according to UNIQUAC, which are explained in the following section (2.2.3.3). According to [87] (p.160f), the calculation approach of the $\gamma - \varphi$ concept is as follows

$$x_i \gamma_i^L f_{0,i}^L = y_i p \varphi_i^V. \tag{24}$$

The equation (24) applies in good approximation following [87] also for the solubility of solids with $S \rightarrow L$, as well as for sublimation processes in the vapour phase $S \rightarrow V$. For the determination of the fugacity of the pure substance the following calculation approach applies via the so-called Poynting pressure correction $\Pi_{0,i}$ and the fugacity coefficient of the pure substance in the VLE system $\varphi_{0,i}^{LV}$ (see also [88] (p.8 .11f))

$$f_{0,i}^L = \left(p_i^{LV} \varphi_{0,i}^{LV}\right) \cdot \Pi_{0,i}. \tag{25}$$

The pressure correction term $\Pi_{0,i}$ can be determined via the specific molar volume $v_{0,i}^L$ with $v_{0,i}^L \approx \frac{M_{w,i}}{\rho_i}$ via the following calculation approach and further the following approximation

$$\begin{aligned} \Pi_{0,i} &= \exp\left(\frac{\int_{p_i^{LV}}^{p} \frac{M_{w,i}}{\rho_i} dp}{RT}\right), \\ &\approx \exp\left(\frac{\frac{M_{w,i}}{\rho_i}\left(p - p_i^{LV}\right)}{RT}\right). \end{aligned} \tag{26}$$

For the predominant fraction of substance components in the liquid phase, as for example in [88] (p.8.11,8.12), the Poynting correction for the pressure difference $p - p_i^{LV} < 10\,\text{bar}$ in the calculations is in good approximation, so $\Pi_{0,i} \approx 1$ can be idealized assumed. Then, for low total pressures of $p < 10\,\text{bar}$, the ratios of the fugacities to $\varphi_{0,i}^{LV}/\varphi_i^V \approx 1$ can also be estimated, which simplifies the phase equilibrium relationship equation (26) as follows

$$x_i \gamma_i^L p_i^{LV} = y_i p. \tag{27}$$

The equation (27)now contains only the activity coefficient to describe the real substance in the mixture. For the ideal liquid phase, with $\gamma_i = 1$, the Raoult and Dalton law applies. In Dalton's law, the total pressure is the sum of the partial pressures in an ideal gas mixture with $p_i = y_i p$ and $p = \sum_i p_i$. According to Raoult's law, the partial pressure of the ideal liquid phase is defined

as $p_i = x_i p_i^{\mathrm{LV}}$ as a fraction of the vapour pressure p_i^{LV} with the mole fraction x_i of the pure substance component i. In this case, a highly simplified version of the equation (27) is obtained for the determination of the phase equilibria with $\gamma_i = 1$. Deviations from the ideal case can be understood as deviations from the ideal Rauolt behaviour of the liquid phase. Then, for ideal phase equilibrium conditions, the following equation for the phase equilibrium condition is valid for each component i as follows

$$x_i p_i^{\mathrm{LV}} = y_i p. \tag{28}$$

Equation (27) is the simplified phase equilibrium condition which is mainly used in the context of this thesis, since for almost all substance systems VLE data are missing as well as numerous substance data, as explained in the next chapter in section (3.1).

Graphical illustration of exemplary vapor-liquid equilibria In a binary system the following basic forms of phase equilibria are represented as shown in Fig (7). In the ideal case $\gamma_i = 1$, according to Raoult's law, it allows the description via the partial pressures as linear functions $p(x), p(y)$ in the multi-component mixture and linear equations $p(x_1), p(y_1)$ in the binary mixture. For $\gamma_i > 1$ there is a positive deviation and for $\gamma_i < 1$ a negative deviation from the ideal phase equilibrium behaviour as shown in Fig. (7). The deviations can be so large that may results in an azeotrope. In an azeotropic mixture with a positive deviation from Raoult's law, the intermolecular interactions in the mixture are weaker than would be expected between the pure components. This results in a temperature minimum below the boiling points of the pure components. In the case of a negative deviation, the interactions in the mixture are correspondingly stronger, resulting in a temperature maximum in the azeotropic composition above the boiling points of the pure components. The two cases $\gamma_i < 1$ and $\gamma_i > 1$ result in two different distillation ranges where the azeotropic composition represents the limiting case for both separation ranges during distillation, above which further purification by conventional distillation is not possible.

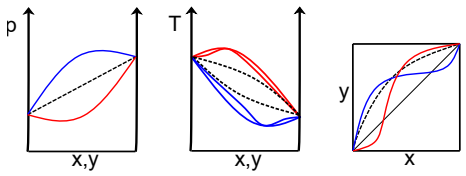

Figure 7: Binary phase equilibrium diagram

For the binary mixture, the three cases of phase equilibrium diagrams in Fig. (7) are shown together in the $p - xy, T - xy, xy$ diagram. The upper line in Fig. (7) of the Tx diagram represents the dew point curve, where the vapour condenses first when the temperature falls below it and two phases coexist as vapour and liquid. The lower line is called the bubble point curve, where the liquid starts to evaporate and two phases exist. In the ideal case of a binary mixture, a single separation region is obtained where the boiling point curve and the dew point curve only touch at the boundary compositions of the pure components. Such a separation region is defined by the VL boiling range as shown below. The dotted case represents the case

of a negative deviation from Raoult's law with a maximum at the temperature at which the azeotropic composition is reached, whereas in the case of a positive deviation from Raoult's law a minimum is reached at the temperature of the azeotropic composition. Consequently, due to the azeotropic composition condition, the dew point and bubble point curves must coincide. Thus, for the dashed case shown in Fig. (7) , two separate separation regions are obtained by distillation. It should also be noted that azeotropes are very often pressure dependent and the azeotropic composition can change with pressure changes. Incidentally, this property is often exploited in the so-called pressure swing process to separate mixtures of components at different pressures by shifting the equilibrium point to the other distillation region of the other phase separation region.

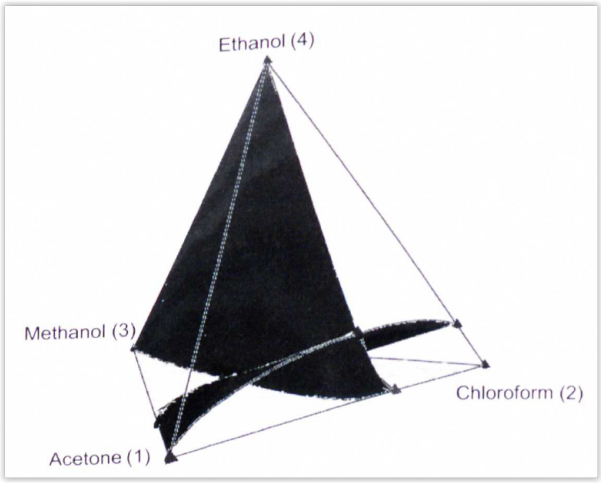

Figure 8: Multicomponent equilibrium diagram with azeotropes , Ref.: [4]

For multicomponent mixtures it follows that the azeotrope defines a space of dimension $N_{\mathrm{az}} < N_{\mathrm{comp}}$ as the limiting distillation region, analogous to the Gibbs phase rule, as shown in Fig. (8) for a four-component mixture. From the starting point of the feed to the end point of the distillation in the diagram of Fig. (8), either the pure composition or an azeotropic composition is approximately obtained as the separation product with many separation steps. The question of the dimension N_{az} depends on the number of types and the number of boundary azeotropic compositions. These boundary distillation regions can only be circumvented by two separations with different pressures in between, where the azeotrope is first separated on the binary mixture in order to obtain a pressure change on the other side of the separation region in the case of an azeotropic composition, if the azeotropic mixture is sufficiently significant pressure dependent. Iteratively, this also applies to multi-component substance systems with a maximum of $N_{\mathrm{az}} + 1$ required separation procedures for the respective azeotrope and pure substance separation. Other possibilities include the use of solvents, the use of combined-simultaneous further separation operations such as extraction or the exploitation of pre-existing mixing gaps in the liquid phase. Mixtures that do not exhibit an azeotrope are called zeotropic mixtures. For further examples, various ternary mixtures and four component mixtures are shown in appropriate residual curve diagrams according to [4].

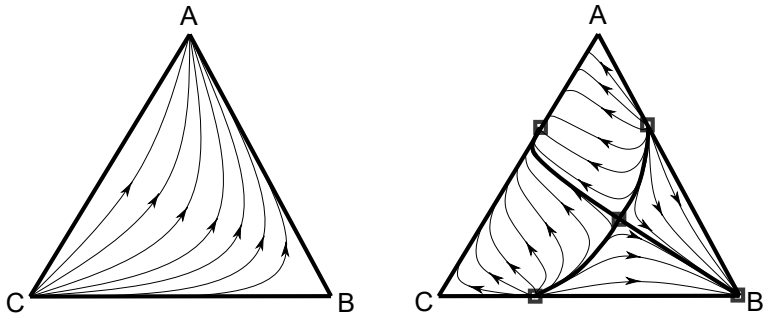

Figure 9: Residual plot of zeotropic and azeotropic mixture

Fig. (9) shows an example of a ternary mixture consisting of a zeotropic mixture (shown on the left) and an azeotropic mixture with five azeotropic composition points of different types, which shows a boundary distillation region (shown on the right), indicated as bold boundary distillation lines. On the left the distillation lines of a zeotropic mixture are shown as trajectories starting at the high boiling point C and ending at the low boiling point A. The distillation lines can be determined directly from the phase equilibrium equation (27) with the function $y_i = K_i x_i$ and the separation factor K_i. According to the phase equilibrium equation (27), the following common calculation approach should generally be used to calculate the K-factors

$$K_i = \frac{\gamma_i p_{0,i}^{LV}}{p}. \tag{29}$$

In the ideal case of ideal phase equilibrium conditions, the K-factor as an important separation factor is exclusively the ratio of the vapour pressure of component i to the total pressure. Another important key factor is the relative volatility α_{ij}, as a dimensionless value of the characteristic ratio of the volatility of the ideal binary separability of component i to component$j$ at a given pressure and temperature. The following applies to the relative volatility in the idealized case with $\gamma_i = 1$

$$\alpha_{ij} = \frac{p_i^{LV}}{p_j^{LV}}. \tag{30}$$

Here, the heavy boiler component is often used for the substance component j. According to this, the following equation applies for the evaluation of the distillation line for ideal mixtures after applying equation (28) (equation (27) with $\gamma_i = 1$)

$$y_i = \frac{\alpha_{ij} x_i}{1 + \sum_{j=1}^{N_{\text{comp}}} (\alpha_{ij} - 1)\, x_j}. \tag{31}$$

If the initial and target compositions are given for the use of distillation steps, the composition-dependent serial sequence of separation steps can be evaluated iteratively via the equation (28) by multiple successive equilibrium step evaluations with vapour phase condensation followed by vapour phase distillation purification steps. For this purpose the following analytically derivable iteration equation with feed composition x_0 for all substance components can be used for ideal mixtures

$$x_{i,n_{\mathrm{th}}} = \frac{\alpha_{ij}^{n_{\mathrm{th}}} x_{i,0}}{1 + \sum_{k=1}^{j-1} (\left(\alpha_{ij}^{n_{\mathrm{th}}} - 1\right) x_{j,0})}. \tag{32}$$

The following equations can also be extended for $\gamma_i \neq 1$.

The right hand figure in Fig. (8) shows the differences that can form when azeotropes are present. The boundary distillation lines formed between the five azeotropic composition points move from the more volatile, less stable azeotropes to the more stable azeotropes. The two binary minimum and maximum boundary azeotropes shown are connected by a ternary saddle point azeotrope. The distillation lines of the real mixture lie within the boundary regions. Distillation beyond the boundaries of the separation regions is only possible with the separation methods already mentioned, such as the pressure swing method, if the system is significantly pressure dependent.

Further examples of azeotropic ternary mixtures are given in [4]. According to [4], two azeotropic points can be assumed for the ternary mixtures $AlCl_3 - TaCl_5 - NbCl_5$ and $MgCl_2 - NaCl - KCl$, since the combinatorically representative binary mixtures each contain two azeotropes.

2.2.3.3 Thermodynamic equilibrium behaviour of real mixtures Applications of the fundamental equations to determine the Gibbs free enthalpy are necessary to understand the evaluation of real mixtures. The fundamental equations can also be used to determine the enthalpies/energies. The real proportion deviating from the pure substance proportion and the proportion of the ideal mixture, the so-called excess part, can then be determined with suitable correlative GE model approaches up to more complex GE models (G for Gibbs enthalpy and E for excess fraction).

Fundamentals for the characterization of real mixtures The basis for the determination of GE models and the enthalpy determination is the thermodynamic fundamental equation, which describes the change of the system in the state variables and the molar number change. In the (thermodynamically considered) open system with $h = h\left(S, p, n_1, \ldots, n_{N_{\mathrm{Comp}}}\right)$ and the definition of the chemical potential change $\sum_{i=1}^{N_{\mathrm{Comp}}} \mu_i dn_i = \sum_{i=1}^{N_{\mathrm{Comp}}} \frac{\partial u}{\partial n_i} dn_i$, as well as the use of the simplification $\sum_{i=1}^{N_{\mathrm{Comp}}} \frac{\partial h}{\partial n_i} dn_i \approx \sum_{i=1}^{N_{\mathrm{Comp}}} \frac{\partial u}{\partial n_i} dn_i$, follows from [89] (p. 10), depending on the other constant system variables for the total differential enthalpy, the following basic calculation expression follows

$$dh = \frac{\partial h}{\partial S} dS + \frac{\partial h}{\partial p} dp + \sum_{i=1}^{N_{\mathrm{Comp}}} \mu_i dn_i, \tag{33}$$

$$= TdS + Vdp + \sum_{i=1}^{N_{\mathrm{Comp}}} \mu_i dn_i. \tag{34}$$

The enthalpy of the mixture is given by the enthalpy of the ideal mixture with the sum fractions of the pure substance enthalpies $h^{\mathrm{id}} = \sum_i x_i h_{i,0}$ and the deviating excess fraction to

$$h = h^{\mathrm{id}} + h^{\mathrm{E}}. \tag{35}$$

The following fundamental equation also applies analogously to the Gibbs energy

$$dG = -SdT + Vdp + \sum_{i=1}^{N_{\mathrm{Comp}}} \mu_i dn_i. \tag{36}$$

To determine the chemical potential, the following applies via the derivation

$$\mu_i = \frac{\partial G}{\partial n_i}. \tag{37}$$

Since for the ideal mixture the condition $\Delta\mu = \int_{p_0}^{p} vdp$ applies approximately and the ideal gas law $v = \frac{RT}{p}$ can be used, the following expression for the chemical potential of the real mixture follows via the definition of the fugacity and the activity coefficient composed of ideal and excess fraction with $\Delta\mu = \int_{p_0}^{f} vdp$ to

$$\Delta\mu = RT \ln x_i + RT \ln \gamma_i. \tag{38}$$

Analogously, following from [89], then applies to the Gibbs (free) energy summed over its proportions of the pure substance Gibbs energy ($(G_0 = \sum_{i=1}^{N_{\mathrm{comp}}} x_i \mu_{i,0})$, the ideal mixture Gibbs energy ($G^{\mathrm{id}} = RT \sum_{i=1}^{N_{\mathrm{comp}}} x_i \ln x_i$) and the Gibbs excess (free) energy part ($G^E = RT \sum_{i=1}^{N_{\mathrm{comp}}} x_i \ln \gamma_i$) as the following linear combination

$$G = \sum_{i=1}^{N_{\mathrm{comp}}} x_i \mu_{i,0} + RT \sum_{i=1}^{N_{\mathrm{comp}}} x_i \ln x_i + RT \sum_{i=1}^{N_{\mathrm{comp}}} x_i \ln \gamma_i. \tag{39}$$

The calculation relation to the Gibbs energy proportions is then, using the above equation and referring to [89, 83, 88], as follows

$$\frac{g^E}{RT} = \sum_{i=1}^{N_{\mathrm{comp}}} x_i \ln \gamma_i, \tag{40}$$

$$\ln \gamma_i = \frac{\partial \left(\frac{G^E}{RT} \right)}{\partial n_i}. \tag{41}$$

These calculation approaches in equation (40) and (41) are carried out via empirical calculation approaches or via suitable, more complex thermochemical-correlative GE models as described in the following section. To determine the parameters of simple calculation approaches, the experimental measurement of $\ln \gamma_i^{\infty}$ in infinite dilution of the substance component i to be measured by evaluating the equation (41) is suitable. Alternatively, the activity coefficients can be measured by measuring the equilibrium composition and evaluating the equation (24). Knowing the fugacity and an approach for the calculation, the determination can also be done via the determination of the state functions, as it is done for the enthalpy determination. The determination follows via the fugacity coefficients with the application of a suitable equation of state [89, 87]

$$\frac{G^E}{RT} = \ln \varphi_{\mathrm{mix}} - \sum_{i=1}^{N_{\mathrm{comp}}} x_i \ln \varphi_i. \tag{42}$$

Excerpt of important GE-models for the calculation of activity coefficients This section briefly introduces the most important GE models. Detailed information on the GE models can be found in [89] (Ch. 3 - 4), [88] (Ch. 8f), [83] (p.52f).

Simple empirical calculation approaches according to [88, 89] are e.g. simple mathematical product approaches such as the Porter approximation for binary mixtures, the Margules approach or the Redlich-Kister model. Empirical models derived from equations of state according to [89, 90, 91] include van Laar's approach. More complex models for the description of molecular interaction parameters under consideration of the principle of local composition are, among others, models according to Wilson, NRTL (Non-Random-Two-Liquid), Flory&Huggins, UNIQUAC (Universal Quasichemical) (see also [89] (chap. 3 - 4), [88] (chap. 8 et seq.), [83] (p.52f)). A further application to substance systems with dissolved salts is the so-called LIQUAC model according to [92], which can also be applied in the special case of molten salts, where the model can be described in a dissociative-ionic part with an ionic portion ϕ_{ion} of the dissolved substance components in the same medium (mainly liquid medium) with a molecular part ϕ_{cov} with respect to undissociated molecules. The equations and the application of the GE models are described in more detail in the subchapter (A.2).

The Wilson or UNIQUAC models are particularly suitable for describing real phase equilibria in VLE systems. The van-Laar approach is also suitable for VLE systems, but with the restriction of similar properties and molecular sizes of the components involved. The NRTL model is only suitable for VLE systems if the determined parameters are within a certain permissible physical range of validity (see e.g. [89] pp. 111). Examples of suitable models for the description of LLE systems (liquid-liquid systems as they occur in liquid-liquid extraction) are the NRTL model or the Flory&Huggins model, whereby the model of Flory and Huggins is mainly used for the description of liquid polymer solutions [89] (pp. 62). It should also be noted that Wilson's model is not well suited for describing LLE systems. According to [89], the NRTL model is even well suited for describing SLE systems and supercooled LLE systems.

The simplest approach for a binary substance system is the one-parameter Porter approach with the parameter A_{12} of the form

$$\frac{g^E}{RT} = A_{12} \cdot x_1 \left(1 - x_1\right), \tag{43}$$

$$\ln \gamma_i = \left(1 - x_i\right)^2 \cdot A_{12}. \tag{44}$$

Due to the strong symmetric simplification of the activity coefficient description, van Laar's approach is practically never applicable and simplifies the activity in a substance system too much. Instead, according to Margules, a polynomial is used for the approximation, which is shifted from symmetry by the proportion $\Delta_1 \tilde{A}(x_1) = A_{12} \cdot (1 - x_1) + A_{21} x_1$ with the parameters A_{12} and A_{21}. For binary substance systems of the n-th order, the series expansion approach with the k-th order shift terms $\Delta_k \tilde{A}(x_1) = A_{k,12} \cdot (1 - x_1) + A_{k,21} x_1$ is then as follows

$$\frac{g^E}{RT} = \sum_{k=1}^{N} \Delta_k \tilde{A}(x_1) \cdot (x_1 x_2)^k . \tag{45}$$

For example, for $N = 1$ the approach for the activity coefficient is then as follows

$$\ln \gamma_1 = A_{12} (1 - x_1)^2 + 2x_1 (1 - x_1)^2 (A_{21} - A_{12}), \tag{46}$$
$$\ln \gamma_2 = A_{21} x_1^2 + 2 (1 - x_1) x_1^2 (A_{12} - A_{21}).$$

Van Laar's approach takes into account the parameter equation originally derived from the Van der Waals equation of state for the determination of the enthalpy of excess h^E according to [90] for real mixtures of the form

$$h^E = \frac{x_1 (1 - x_1) b_1 b_2}{x_1 b_1 + (1 - x_1) b_2} \left(\frac{\sqrt{a_1}}{b_1} - \frac{\sqrt{a_2}}{b} \right)^2. \tag{47}$$

The parameters a_1, a_2, b_1, b_2 are the parameters of the Van der Waals equation of state per substance component. Here the van der Waals equation is as follows

$$\left(p + \frac{a}{v^2} \right) (v - b) = RT. \tag{48}$$

The Van-der-Waals equation (equation (48)) is an extension of the ideal gas equation by the internal pressure: The pressure component $\frac{a}{v^2}$ caused by the attractive forces of the liquid molecules and b the component of the geometric expansion of the molecules. Correlatively modified for the GE approach, according to [90], the GE model with the parameters A_{12}, A_{21} are thus as follows described

$$\frac{G^E}{RT} = \frac{A_{12} A_{21} \cdot x_1 (1 - x_1)}{A_{12} x_1 + A_{21} (1 - x_1)}, \tag{49}$$
$$\ln \gamma_1 = \frac{A_{12}}{\left(1 + \frac{A_{12} x_1}{A_{21} (1 - x_1)} \right)^2}, \tag{50}$$
$$\ln \gamma_2 = \frac{A_{21}}{\left(1 + \frac{A_{22} (1 - x_1)}{A_{12} x_1} \right)^2}. \tag{51}$$

It should be noted that more complex GE models can only be usefully applied after measuring phase equilibria or, moreover, after measuring infinite dilution (determination of $\ln \gamma_i^\infty$) by fitting the model parameters to a multidimensional fitting function for multi-component mixtures and temperature dependence as parameters.

2.2.4 Modelling of distillation units and separation columns with equilibrium stage models

The modelling of distillation based separation units by means of equilibrium stage models is carried out in Octave/MATLAB, a software for the numerical solution of mathematical problems. Software for comparison and validation of simulation results is performed with validated and ready-implemented equilibrium stage models or rate-based solution approaches from ChemSep[3].

[3]Suitable software with validated simulation codes and graphical user interface are simulation models from the freely available ChemSep Lite version (see documentation and manual in [68]). The advantage over common commercial software such as Aspen is not only the royalty-free access, but also the use of simpler models with more accessible simulation code, which is better suited for simulations with highly simplified phase equilibria.

In the following, single-stage separation processes are first described, from which a multi-stage separation process can be created by combining modified single-stage separation units. On the basis of the theoretical principles and the necessary MESH basic equations, simulation models are developed which can easily be supplemented with non-ideal phase equilibrium behaviour for later tasks and simulation work (e.g. after knowledge of suitable VLE data).

2.2.4.1 Continuous single-stage distillation operations Technically applicable single-stage separation processes are mainly understood to mean the separation of components from a liquid-vapour boiling mixture or from the vapour phase, defined as vapour transport, by volatilisation of a primary element or component to be separated. The transition of the components from the liquid phase is referred to as evaporation of the components to be separated, while the transition from the vapour phase to the liquid phase is referred to as condensation of the components to be separated. A precondition for the technical applicability of single-stage separation is therefore that the volatility and the position of the boiling points of the pure substances to be separated are clearly different from each other, i.e. with a relatively high relative volatility value and, for technically applicable reasons, with suitable absolute volatility values for each component. In the most common industrial and other technical separation processes, multi-stage separation using distillation columns must be used.

Basic model approach for first approximations The following simple distillation model estimates are applicable to the technical single stage distillation processes. The model equations consist of the mass and energy balance with coupling of phase equilibrium relationships per component, which characterise the separation performance of each component. The solution of a simulation of the separation stage must satisfy the sum condition that in each phase the sum of all components involved is 100%, in the validity range 0 - 100% per component mole fraction.

Fig. (10) (left) schematically shows the separation process of a single-stage industrial distillation unit. A single continuous saturated liquid feed stream $\dot{n}_F$ enters the separation unit with feed composition x_F, y_F and a vapour and liquid stream $\dot{n}^V$ and $\dot{n}^L$ leave the separation stage with different compositions x and y (as liquid and vapour mole fractions) respectively. With constant energy input $\dot{Q}_{\text{evap}}$ the mixture is evaporated and the vapour is condensed at the condenser with constant cooling power $\dot{Q}_{\text{cond}}$ and removed. Either before or after condensation of the top distillation product, its composition remains the same with $y = x^V$, since the condenser does not act as a separator. In this case, the exiting vapour and liquid streams are in thermal equilibrium in the model, so that the operating temperature of the separation process of the separation stage can be determined as a constant temperature. For idealized phase equilibrium estimates, the equation (28) with the validity of Dalton's and Raoult's law is used, for example, in this thesis mainly for the simulation of single stage distillation units. For real mixtures, the iterative determination of the temperature via the activity coefficients can be done as follows

$$p = \sum \gamma_i \cdot x_i \cdot p_i^{LV}(T). \tag{52}$$

The equation (52) is to be understood as an additional condition for the thermal equilibrium to be fulfilled under saturated liquid thermal conditions with constant operating temperature T.

In contrast, the mass and energy balance of the single-stage separation unit only relates to the selected column operation itself, e.g. if there is a flash evaporator or another single-stage distillation step. If the operating temperature is known, the system of equations can be simplified into an operating range and an equilibrium range. Using a binary mixture as an example, the following linear operating function can be set up directly in a very simplified way under idealized VLE (with equation (28)) conditions:

$$y_i^{\text{operative}}(x_i) = \frac{\dot{n}_F}{\dot{n}_F - \dot{n}^L} x_F - \frac{\dot{n}_L}{\dot{n}_F} x_i. \tag{53}$$

In the binary system, the equilibrium line must be set equal to the operating line to obtain the solution for a given operating temperature. This is illustrated in Fig. (10) (on the right of the xy-diagram) where, for a feed composition x_F with slope $-\frac{\dot{n}_L}{\dot{n}_F}$ of the operating line, the operating line intersects the equilibrium line. The composition of the liquid can then be read graphically at this point on the x-axis, while projected onto the diagonal with $x^V = y$, the composition of the condensed distillate can be found. This graphical construct in Fig. (10) thus fully illustrates the most simplified single stage separation unit of a binary mixture.

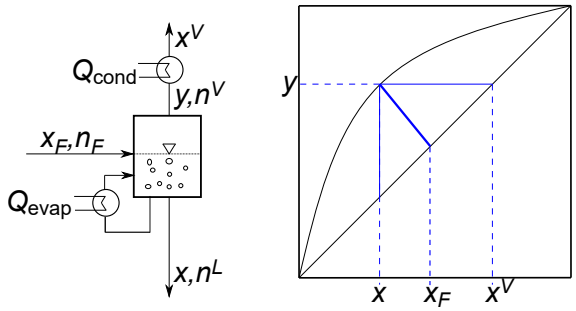

Figure 10: Continuous single-stage distillation

The single-stage separation process discussed refers to a constant pressure with no pressure change. However, for the application of a technically relevant separation unit, pressure relief is usually performed as a pressure change, in which the liquid is brought from a high pressure to a lower pressure by means of a throttle or spray nozzle in order to achieve a reasonably high separation efficiency. Such a single stage process is called flash evaporation. In simple terms, they are usually calculated and designed as adiabatic or isothermal evaporators. For the isothermal flash evaporator, for example, according to [51] with $x_i = \frac{x_{F,i}}{1+\frac{\dot{n}^V}{\dot{n}_F}(K_i-1)}$ and $y_i = K_i x_i$, the following balance equation applies

$$\sum_i \frac{x_F\,(1-K_i)}{1-\frac{\dot{n}^V}{\dot{n}_F}\,(1-K_i)} = 0. \tag{54}$$

The equation (54) depends only on the vapour flow $\dot{n}^V$ as the quantity to be determined. From the determination of the vapour flow $\dot{n}^V$, the composition of the liquid x_i and the vapour y_i per substance component i can be determined directly analytically. For the solution of equation (54) the one-dimensional Newton-Raphson method or the interval bisection method are suitable (see [93]). Further explanation of the calculation of these evaporators can be found in [51].

2.2.4.2 Modelling and simulation of continuous multistage distillation columns The equations for single stage separation can be used to derive the system of non-linear equations for the connected stage in the multi-stage separation process for continuous or total operating distillation columns. For batch and discontinuous distillation column operation, the equations are given as differential-algebraic balance equations in time, according to [51]. The continuous operation of a distillation column gives a non-linear system of equations, which in most cases must also be solved numerically. To apply equilibrium stage models for the simulation of a continuous distillation column at constant pressure as shown in Fig. (4), the stages are connected as shown in Fig. (4) below. For each separation stage, the feed and side stream withdrawals, as well as the incoming and outgoing material flows, must be balanced in terms of mass and energy and connected with a suitable equilibrium condition. For the energy balance, enthalpies are used instead of internal energies for each separation stage. As already discussed in the section (2.2.1), the so-called MESH equations are used for modelling. Considering separation stage j as shown in fig. (4), the MESH equations according to [51] for this continuous distillation column (per component i and theoretical separation stage j) are as follows

$$\text{M:}\; e_j x_{F,ij} \dot{n}^L_{F,j} + (1-e_j) y_{F,ij} \dot{n}^V_{F,j} + x_{ij-1} \dot{n}^L_{j-1} + y_{i,j+1} \dot{n}^V_{j+1} = x_{ij} \dot{n}^L_j + x_{S,ij} \dot{n}^L_{S,j} + y_{ij} \dot{n}^V_j + y_{S,ij} \dot{n}^V_{S,j}, \tag{55}$$

$$\text{E:}\; y_{ij} = K_{ij} x_{ij}, \tag{56}$$

$$\text{S:}\; \sum_{i=1}^{N_{\text{comp}}} x_{ij} = 1, \; \sum_{i=1}^{N_{\text{comp}}} y_{ij} = 1, \tag{57}$$

$$\text{H:}\; e_j h^L_{F,ij} \dot{n}^L_{F,j} + (1-e_j) h^V_{F,ij} \dot{n}^V_{F,j} + h^L_{ij-1} \dot{n}^L_{j-1} + h^V_{i,j+1} \dot{n}^V_{j+1} = h^L_{ij} \dot{n}^L_j + h^L_{S,ij} \dot{n}^L_{S,j} + h^V_{ij} \dot{n}^V_j + h^V_{S,ij} \dot{n}^V_{S,j}. \tag{58}$$

The dependencies $h^L_{ij} = h^L_{ij}(x_{ij,}T_j)$,$h^L_{ij} = h^L_{ij}(x_{ij,}T_j)$ and $K_{ij} = K_{ij}(x_{ij}, y_{ij}, T_j)$ apply to the equations (55)-(58). The thermal feed condition of the fed mixture e_j is used to specify the thermal state of the feed as a dimensionless number and refers to the saturated liquid with a value of 1. The general expression of the thermal feed condition follows from the energy balance calculated with enthalpies around the feed stage position

$$e_j = 1 + \frac{h_{j,\text{mix}}(T = T') - h^L_{F,j,\text{mix}}(T_j)}{\Delta h^{LV}_{\text{mix}}}. \tag{59}$$

$e = 1$ defines the thermally saturated liquid state, $e = 0$ the saturated vapour and $0 < e < 1$ the region where liquid and vapour are present and is following defined as liquid-vapour region especially in this thesis. For $e > 1$ the feed at stage j is in the subcooled liquid state and for $e < 0$ the feed is classified as superheated vapour. The $2N_{\text{comp}} + 3$ MESH equations (55)-(58) contain the $2N_{\text{comp}} + 3$ unknown quantity variables$\dot{n}^L_j, \dot{n}^V_{j+1}, x_{ij}, y_{ij+1}, T_j$, which are very often obtained only by numerical solution. In order to solve the MESH equation system, it is usually necessary to have product specifications or specifications for each stage of the column. Usually the temperature and composition for the top and bottom products are assigned in a meaningful way. The iterative calculation of the stages at the condenser at the top of the column can

then be started to solve the equation system numerically. Here, the reflux ratio v, as always defined, determines how much liquid must be returned to the column to fulfil the required basic countercurrent flow principle of the column (even without having inactive column areas). With the calculation of the condenser performance, the upper distillation streams can be calculated by mass and energy balance of the first separation stage. This is followed by the calculation of the subsequent stages. At the end of the iterative calculation of the column stages, the evaporator performance results from the external energy balance of the entire column and the evaporation rate (boil-up rate) can then be determined, for example, from the external mass balance and the balance of the last stage. However, for the initial determination of the reflux ratio v, various calculation and estimation approaches are available in the literature, such as the Fenske-Underwood-Gilliland (FUG) method.

Equally relevant to the numerical solution is the initial definition of the separation product specifications as boundary conditions for the total mass and energy balance of the entire distillation column. Often the product compositions at the top and bottom of the column are specified as product specifications, in order to be able to determine the mass balance of the entire column from all incoming and outgoing material flows as a linear system of equations. For example, in the case of a simple column with only a single feed inlet and a top and a bottom product stream ($\dot{n}_B$ and $\dot{n}_T$), the following simple linear system of equations has to be solved

$$\begin{pmatrix} 1 & 1 \\ x_{T,i} & x_{B,i} \end{pmatrix} \cdot \begin{pmatrix} \dot{n}_T \\ \dot{n}_B \end{pmatrix} = \begin{pmatrix} \dot{n}_F \\ x_F \dot{n}_F \end{pmatrix}. \tag{60}$$

However, as an alternative to specifying the composition according to equation (60), numerous other specifications can be made, such as the temperature at the condenser including the thermal state, from which the composition at the condenser can be calculated. As constraints, the reflux ratio v, the evaporation rate (or boil-up rate) V_R and the thermal conditions e_{ij} must be determined, so that the equations (55)-(60) become an optimisation problem to be solved with respect to the best separation accuracy or other aspects of the specification. These quantities can also be estimated as initial values using shortcut approximation methods before running the simulation. The number of stages required, on the other hand, results from the criteria of the specified separation accuracy, the subsequent optimisation problem or is simply specified as a fixed quantity.

To solve the system of equations (55)-(58), these are usually simplified or special determination methods are chosen. A simplification of the system of equations can be done, for example, by specifying the initial temperature or by choosing tears streams[4]. With interval bisection for the temperature and the use of the energy balance as a criterion for approximation by inserting the selected temperature into equation (58), the system of equations can already be greatly simplified. The solution methods that are often used are triagonal matrix methods, such as the boiling point method or the sum rates method, which are discussed in detail in [51]. In these methods, the system of equations is decomposed into individual equations to be solved succes-

[4]Tears streams are provisionally assumed to be zero currents, which are later determined numerically by the prediction-correction method according to a suitable algorithm, such as the algorithm described in [94].

sively, which, with the exception of the energy balance, are then corrected primarily analytically by the initial specification in this type of simulative optimisation procedure and numerically by correction through the energy balance or perhaps other defined central equation part. According to [51], this also includes measures to reduce the order of the equation system and the application of the so-called Naphtali-Sandholm method, which works with material component-related material flows (e.g.$n_{ij}^{L} = x_{ij}\dot{n}^{L}$) and thus requires only $2N_{\text{comp}} + 1$ equations to determine the unknown quantity variables. The Newton-Raphson method can then be used for the solution. The advantage is that unstable normalisation equations such as the sum-rates from equation (57) are not needed. Sum rates are summation conditions for the compositions per phase, where the sum of all substances involved per substance component must be 100%. Further summarised solution methods can be found in [51].

2.2.4.3 Approximate solution methods for distillation The application of simplified solution approaches serves to determine initial values for the reflux ratio v, the possible evaporation rate V_R (boil-up rate) and the total number of separation stages n_{th}. The above variables are then used as initial values in a formulated optimisation problem for the distillation column, as mentioned in the previous section. The graphical solution methods can be used to determine the solution for binary and ternary systems. For binary systems, the McCabe-Thiele method according to [51, 78] is suitable under the assumption of small differences in enthalpy changes or, if the enthalpies can be determined well, the Poinchon-Savarit method, e.g. according to [95], analogous to the procedure of the principle of single-stage distillation for estimating the stage construction of a distillation column. The reflux ratio v can be determined by the practically minimum possible reflux ratio v_{min} (to enable the distillation countercurrent flow) if the operating line in the multistage process touches the equilibrium line. For the estimation of the stage construction of a rectification or other multistage distillation column operation, this means an infinite number of theoretically required separation stages, as graphically illustrated in more detail in the graphical solution methods of the following section on a binary system. From the practical cost estimation between separation effort and required back feeding of parts or the distillation products, a permissible range for the correction value S with $v = S \cdot v_{\text{min}}$ as the real reflux ratio is often determined. According to [78, 72, 73] the value $S = 1.3$ is often used, as the range for industrial purposes very often varies between values of 1.1 and 1.5. The McCabe-Thiele and Poinchon-Savarit methods are suitable approximation methods for binary mixtures. For ternary mixtures the analysis can be carried out graphically in the triangular diagram of a total reflux distillation column (with $v \to \infty$) as shown in the sections (2.2.3.2) and (2.2.4.1).

The McCabe-Thiele method For binary systems the McCabe-Thiele method is often used, which is explained in every distillation and process engineering handbook, e.g. [51, 78, 72]. It allows direct transfer to the xy diagram of binary VLE systems. However, this method neglects pressure losses and evaporation enthalpy changes. Heat effects and heat losses are also neglected. For the sake of clarity, this also applies to the temperature dependence, which can only be considered very roughly by creating a new equilibrium line after each stage construction step. This has the further consequence that the relative volatility α in the separation range to be investigated must not be too large and with negligibly small temperature dependence in order

to obtain meaningful results.

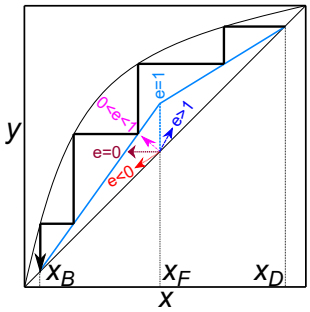

Figure 11: Principle sketch for the application of the McCabe-Thiele method using the example of a simple continuous distillation column, within five important thermal feed condition cases

To illustrate the operating principle of the McCabe-Thiele method, which is described in [51, 78, 77] among others, the stage construction is shown schematically in an xy diagram according to figure (11). In this, assuming the same mole flow ratios $m' := \frac{\dot{n}_k^V}{\dot{n}_k^L} = \text{const.}, k = 1, \cdots, j, \cdots, n_{\text{th}}$, an analytically derivable equation for the kth feed stage for the operating line is obtained

$$y_j = m'(x_{j-1} - x_j) + y_{j+1}. \tag{61}$$

The operating lines are straight line equations $y^{\text{operating}} = m \cdot x + b$, which are determined by mass balance by balancing the material flows from the balance area of the current separation stage to the top of the column. The unknown variables are contained by the simplifications that the approximate vapour-liquid molar flow ratio per separation stage must remain the same [78]. To eliminate the unknown variables of each equation, a single balance equation between top and feed flow can be established from the balance equations of the mass balance per separation stage including the definition of the reflux ratio $v = \frac{\dot{n}_R}{\dot{n}_D}$. In this way the operating line can be determined as a correlation equation, which is shown schematically in Fig. (11) as a straight line equation in light blue. Between $x_F < x < x_D$ and for saturated liquid feed condition with $e = 1$ the following determining equation is available

$$y_{\text{rect}}^{\text{operative}}(x) = \frac{v}{v+1} \cdot x + \frac{x_F}{v+1}. \tag{62}$$

For a total reflux column without feed and withdrawal streams, where all the distillate is fed back to the column with $v \to \infty$, the diagonal equation $y_{\text{rect}}^{\text{operating}}(x) = x$ follows from the equation (62) for the operating line. According to the definition of [51] for $e = 1$, the upper part of the distillation column is called the rectifying section, while the lower part of the column is called the stripping section, as the separation process is more similar to that of a stripping column for the purification of gases and vapours by a scrubbing liquid. There are usually two operating lines passing through the feed stream. The point of intersection is determined by the thermal condition state of the feed e. By combining the mass and energy balances for the feed, a line of intersection point of the two operating lines can be obtained. Using the energy balance, the thermal condition of the feed can be expressed by the equation (59). The mathematically derived

line of intersection is now as follows

$$y^{\text{inter}}(x) = \frac{e}{e-1} \cdot x - \frac{1}{e-1} x_F. \tag{63}$$

To determine the reflux ratio from the equation (62) with $v = v_{\min}$, the value of $v_{\min}$ can be obtained by finding the point of intersection which lies on the equilibrium line under minimum reflux ratio. For this purpose, for $x = 0$, the expression for the minimum reflux ratio $v_{\min}$ can be obtained graphically by $v_{\min} = \frac{x_F}{y_0} - 1$. To calculate $v_{\min}$ for $e = 1$, the intercept at x_F is on the equilibrium line. For example, for an ideal mixture, the minimum reflux ratio at the equilibrium line can be determined as follows

$$v_{\min} = \frac{1}{\alpha - 1} \cdot \left(\frac{x_D}{x_F} - \alpha \cdot \frac{1 - x_D}{1 - x_F} \right). \tag{64}$$

The slope of the intersection line is shown by the dashed line in Fig. (11) for the five different thermal feed states of subcooled liquid with $e > 1$, saturated liquid feed state with $e = 1$, liquid-vapour region state with $0 < e < 1$, saturated vapour with $e = 0$ and superheated vapour condition with $e < 0$. For $e = 1$ the intersection is at $x^{\text{inter}} = x_F$ and for $e = 0$ at $y^{\text{inter}} = x_F$.

From the intersection and another operating point $y(x_B) = x_B$, the straight line equation between x_B and x_F shown in Fig. (11)can easily be determined as a light blue straight line. Starting from the composition at the top of the column, the column stage construction, shown as black steps in Fig. (11), can now be carried out iteratively. Assuming a finite number of stages, the vapour and liquid phase compositions of the stage construction are obtained up to the product specifications. If a basic efficiency of $\eta < 1$ is present, the real ratio is to be deviated in percentage from the intersection point of the horizontal construction line of the stage and drawn further in the direction of the diagonals, so that the separation stage becomes correspondingly smaller by the factor $1 - \eta$.

The slope of the operating straight line depends on the respective mass balance between the column sections at which feed or side streams are supplied. Iteratively, all operating lines must be determined from the top to the bottom of the column, so that for a column with N_F feed streams and N_S side streams, $N_F + N_S + 1$ operating lines exist and must be determined one after the other. The stage construction is then completely analogous between equilibrium and operating line construction, as shown in Fig. (11) for a single inlet flow. The entire stage construction method for this and other types of distillation columns and operations is described in detail in [51].

Short-cut methods Shortcut methods are often used for the rough design of distillation columns and for the estimation of reflux ratios. The estimation of the reflux ratio is carried out for the multi-component mixture according to Underwood's method, where key components have to be defined according to [72] from representative components. Estimation of the minimum number of stages required is carried out according to the Fenske method. According to Fenske's method, the minimum number of required separation stages of a binary mixture is estimated for an infinite reflux ratio, in which, after defining and inserting the equilibrium relationship for phase equilibrium according to [51] of the relative volatilities of the components of light and

heavy boilers of all separation stages, the elimination of the other components in the estimation approach takes place, so as a reduction of the complex problem. For $n_{\mathrm{th,min}}$ stages including the evaporator, the evaluation equation is as follows

$$\prod_{j=1}^{n_{\mathrm{th,min}}+1} \alpha_{1N_{\mathrm{comp}},j} = \frac{x_{D,1}}{x_{D_{N_{\mathrm{comp}}}}} / \frac{x_{B,1}}{x_{B_{N_{\mathrm{comp}}}}}. \tag{65}$$

With suitable simple averaging to calculate the mean $\bar{\alpha}$-value, such as geometric averaging between top, feed and bottom composition or further averaging methods according to for example [77, 51], a simple approximation equation to the theoretically-minimum required number of stages can be determined, which is as follows

$$n_{\mathrm{th,min}} = \frac{\ln\left(\frac{x_{D,1}}{x_{D_{N_{\mathrm{comp}}}}} / \frac{x_{B,1}}{x_{B_{N_{\mathrm{comp}}}}}\right)}{\ln\left(\bar{\alpha}\right)} - 1. \tag{66}$$

The empirical calculation method according to Gilliland [51] is suitable for determining the real number of stages, where a correlative fit function is plotted over the experimental data in $\frac{n_{\mathrm{th}}-n_{\mathrm{th,min}}}{n_{\mathrm{th}}+1}, \frac{v-v_{\mathrm{min}}}{v+1}$-diagrams. For a mixture without too large a boiling range of all the components involved, the following correlation approach applies as a rule of thumb as a good approximation for a simple distillation column according to [51] with $\Psi = \frac{v-v_{\mathrm{min}}}{v+1}$ and the parameters $C_1 = 54.4, C_2 = 11$ and $C_3 = 117.2$

$$\frac{n_{\mathrm{th}} - n_{\mathrm{th,min}}}{n_{\mathrm{th}} + 1} = 1 - \exp\left[\left(\frac{1 + C_1\Psi}{C_2 + C_3\Psi}\right)\left(\frac{\Psi - 1}{\sqrt{\Psi}}\right)\right]. \tag{67}$$

In the Underwood method for determining the required minimum reflux ratio v_{min} for the distillation column, a constant correction value θ (corresponding to the relative volatility averaged over the column stages) averaged over the column is assumed, which ranges between the values of the relative volatility of the low boiling component to the high boiling component. At the thermal feed state, the following relationship equation to be numerically solved is then to be evaluated according to [51, 72]

$$\sum_{i=1}^{N_{\mathrm{comp}}} \frac{x_{F,i}\bar{\alpha}_i}{\bar{\alpha}_i - \theta} = 1 - e. \tag{68}$$

From equation (68), assuming $\theta = \mathrm{const}$, the minimum reflux ratio can be calculated numerically, which is obtained by substituting θ into the following equation for the column head according to the following equation

$$\sum_{i=1}^{N_{\mathrm{comp}}} \frac{x_{D,i}\bar{\alpha}_i}{\bar{\alpha}_i - \theta} = v_{\mathrm{min}} + 1. \tag{69}$$

The right-hand side of equations (68) and (69) follows directly from the mass balance. The determination of the minimum reflux ratio according to equation (68) and (69) can be calculated numerically according to the Underwood method, e.g. by using the interval bisection method. The complete combined calculation procedure which is presented here is also known as the Fenske-Underwood-Gilliland method. It can be used for substance mixtures that do not boil too

broadly, especially for substance components whose boiling points have similarly large intervals and are relatively close to each other.

Estimated column design of distillation columns on low information and data basis This section explains the estimation for estimating the column height and diameter. The column cross-sectional area can be calculated using the so-called gas loading factors, called F-factors, and the continuity condition $A_{\mathrm{col},D} = \frac{\dot{m}^V}{\rho^g_{\mathrm{mix}} w^g}$ with the empty pipe gas velocity $w_g = f(\mathrm{F}^V, \cdots)$. In this case, the F-factors can be interpreted from a physical point of view from the balance of the forces of the fluid acting on the upper cross-sectional area, with a fluid-side and a vapour-side loading factor with F^L and F^V in the detailed design for the top of the column [81, 72] and as simplification of the column stages as well assuming a mean column diameter. Thus, the simplified functional approach $f(\mathrm{F}^V)$ at the top of the column is essentially dependent on the column type, vapour flow characteristics and column operation, and thus a function of the gas loading factor. Methods for calculating the F-factors for packed columns can be taken e.g. from [81] (chapter 2). The simplest calculation approach of the empty tube gas velocity can be made via a simple kinetic force $F = \rho^g/2w^g$ estimation, so that the approach via the gas loading factor F is as follows

$$w^g \approx \frac{\mathrm{F}}{\sqrt{\rho^g_{\mathrm{mix}}}}. \tag{70}$$

Common values for F-factors can be found in [96, 73], where for an atmospheric pressure of 1 atm a value of 2.0 is to be taken as a first estimate, but may deviate to 1.5 at overpressure. According to equation (70), the cross-sectional area $A_{\mathrm{col},D} = \frac{\dot{V}}{w^g}$ is determined by the volumetric flow rate of the vapour stream at the top of the column, where for a circular column cross-section the column diameter is given by $d_{\mathrm{col},D} = \sqrt{\frac{A_{\mathrm{col},D}}{\pi}}$. The height of the column can be determined in two ways:

1. Determination by experimentally determined height equivalent values of a separation stage, the so-called HETP values.

2. Determination by mass transfer units according to the HTU-NTU principle.

Often the column height equivalent value is also used for column packings. Experimentally determined HETP values can then also be used for other similar substance systems. The column height is determined via the theoretical separation stage number nth of this separation column as follows

$$H = n_{\mathrm{th}} \cdot \mathrm{HETP}. \tag{71}$$

In the HTU-NTU concept (HTU: Height of Transfer Unit, NTU: Number of Transfer Units), the height of a transfer unit is characterised by the mass transfer and can be used for absorption and packed columns. In contrast to the principle of the theoretical separation HETP value, the HTU-NTU includes the mass transfer across the phase interface in a discretised way. It is therefore the preferred method for calculating column height when modelling non-equilibrium stages. Using the differential mass balance between the vapour and liquid phases, the mass

balance equation can be established where, for an equilibrium composition y^{eq} and a differential height dh on the vapour side, the following applies

$$\frac{dy}{y - y^{\mathrm{eq}}} = \frac{k^V c^g A_{\mathrm{col}} \frac{A_{\mathrm{phase}}}{V_{\mathrm{phase}}}}{\dot{n}^g} dh. \tag{72}$$

Here, the unit NTU is a dimensionless index for the speed of mass transfer between the phases liquid and vapour. The NTU unit is defined by the mass transfer β, the contact time Δt in the volume of the separation stage $\dot{V} \approx \frac{V}{\Delta t}$ under which there is a change in the molar composition $y^{\mathrm{eq}\cdot} - y$ of the vapour phase. The expression for the NTU unit is

$$\mathrm{NTU} = \int_{y_{\mathrm{in}}}^{y_{\mathrm{out}}} \frac{dy}{y - y^{\mathrm{eq}}}, \tag{73}$$

$$= \frac{\beta^V A_{\mathrm{col}}}{\dot{V}^V}. \tag{74}$$

For the HTU unit, the expression $\frac{k^V c^g A_{\mathrm{col}} \frac{A_{\mathrm{phase}}}{V_{\mathrm{phase}}}}{\dot{n}^g}$ follows, so that for the HTU-NTU method for calculating the column height, the following applies

$$\int_{y_{\mathrm{in}}}^{y_{\mathrm{out}}} \frac{dy}{y - y^{\mathrm{eq}}} = \frac{k^V c^g A_{\mathrm{col}} \frac{A_{\mathrm{phase}}}{V_{\mathrm{phase}}}}{\dot{n}^g} \cdot \mathrm{H}. \tag{75}$$

Similarly, the mass transfer can also be determined from the liquid side.

Part III

Modelling of Distillation Units and simulation results with representative Test mixtures

The modelling of distillative separation processes in this thesis relates to the study of the separation of metal chlorides from molten salts produced during the reprocessing of nuclear fuels. In such fuels, uranium, Caesium and plutonium are among the most common representatives, for which, however, hardly any data on vapour-liquid equilibria are available from the literature for the chlorinated species in order to be able to simulate a distillation process adequately. Therefore, the process conceptualisation in this thesis mainly follows the simulation of ideal phase equilibrium data as a most optimistic case calculation. For the conceptual design, suitable representative mixtures are simulated by self-developed Octave/Matlab models. The simulation results of these representative mixtures will be used for the simulation of distillation and thermal separation processes using validated program codes of the ChemSep. In addition to the ideal phase equilibrium calculations, exemplary chloride molten salt mixtures will be simulated with real measured data of real vapour-liquid behaviour from the literature in order to obtain qualitative statements on the non-ideal behaviour for the relevant mixtures for the current fuel processing task. This will be followed by calculations to estimate the separation of particularly volatile components and, conversely, particularly low to non-volatile components, such as non-chlorinated oxide material or non-chlorinated precious or refractory metals, which occur in the separation process. This knowledge can then be qualitatively included for subsequent process simulations with complex material mixture systems in the next chapter (IV) to evaluate the waste problem under ideal phase equilibrium behaviour . The following results and elaborations of these work items have been carried out and are available in this thesis

- Extensive material data research from publicly available sources, including the development of a proprietary material database of pure and mixed component systems required or usable for the study of material component separation in the general case, covering conventional pure material data, temperature-dependent material data and mixture properties.
- Simplified simulative estimations using self-developed models for separability testing have been done exemplarily on selected binary and ternary substance systems, including validation and evaluation of the performance of the simulation models with ChemSep and experimental data from comparative systems to the Kroll method.
- Initial estimates and simulations with non-ideal phase equilibrium relationships based on binary test mixtures have been carried out.
- Estimation of the decay heat in distillation columns is used to estimate the heat effect limits in spent fuel reprocessing and nuclear distillation-based fuel recovery.
- The development of the distillation-based separation process design and the flowsheet development in chapter (IV) have been carried out under ideal phase equilibrium conditions in order to present an overview of the nuclear relevant separation process under the most

optimistic conditions, where the separation in the real mixture can be further developed from the simplified process. The necessary steps include

- Pre-study of chlorinability for molten salt recovery and subsequent post-treatment required for distillation-based component separation study.
- Simulative determination of the minimum separation efficiency and estimation of the number of column stages required for the use of distillation to determine the minimum separation efficiency required for the subsequent conceptual design.
- Based on the simulations, a semi-numerical development and creation of an overall separation technology concept has been carried out, followed by an evaluation of the realisation of a separation process on an industrial scale.
- Analysis for spent nuclear fuel reprocessing, but also high active waste material (HWL) recycling and DFRm fuel recovery with the same evaluated distillation-based conceptual design in this thesis.
- An evaluation of possible working strategies for future follow-up work and projects has been undertaken in this thesis study.

In the appendix of this thesis, the availability of mainly pure substance property data from the generally available literature according to section (B) has been discussed, as well as the elaboration of a conceptual design of additional recycling tasks to be simulated (see (IV)).

3 Vapor-liquid equilibrium estimation approach

Inorganic molten salts of simple monochlorides as the pure substance component are very often characterised by broad, thermally stable liquid regions with higher boiling points compared to higher chlorinated chlorides (see e.g. melting and boiling points of monochlorides from [14, 24, 67, 18, 97]). As can be concluded from studies of molecular dynamics simulations on liquid uranium trichloride by [98], from a modelling point of view, part of the pure molten salt compound can be assumed to be fully ionic, another part to be partially ionic, and another part to be covalency-bound salt molecules. So the pure component system itself generates a multi-component system, which has to be modelled somehow in a VLE system. Thus, even for a single pure salt component system, a very large complexity of possible interactions can be assumed for modelling as a kind of complex multi-component system depending on the dissociation behaviour depending on a possible estimable dissociation constant. Molecular dynamics studies of uranium trichloride in the eutectic chloride mixture LiCl-KCl are available in and show the complex dissociation mixing behaviour in [99, 100, 101]. It is not possible to simulate such a complex interaction behaviour in a meaningful way in this thesis, because the interaction behaviour is mostly still unknown, but qualitative approaches to the analysis of the most important relationships follow in this section. With the help of simulations of ideal phase equilibria and the acquired qualitative deviation behaviour to such VLE chloride-based subsystems, an optimistic capture of the separation can be made as an upper bound of the feasibility of a distillation and subsequently a conceptual design of a spent fuel recovery in the most optimistic separation case. However, complex simulations on simplified mixtures need to be performed in the future. In order to qualitatively identify the

most important relationships, the dependence of the attractive, repulsive intermolecular forces in the fully dissociated and fully undissociated state of a salt mixture on the degree of chlorination of the component involved must be qualitatively clarified.

In the following, the degree of chlorination n is defined as the number of chlorine atoms bound to a single metal component M in a specific salt compound MCl_n. From [102] it can be concluded that as the degree of chlorination increases for the pure chloride component, the attractive force component decreases due to the effects of the predominantly surrounding chloride anions as a kind of force-shielding effect on the interacting molecular attractive forces, so that the boiling point of the higher chlorinated chloride decreases compared to the monochloride. This effect broadens the observed differences in the boiling points of chlorides depending on the degree of chlorination, as can be seen in the comparison of the melting and boiling points of the different uranium chlorides in [97] (e.g. p. 172) and the other chlorides with different degrees of chlorination.

For chloride mixtures with the same or different degrees of chlorination, an even wider range of possible interaction behaviour can be assumed than for the pure salt component system. In addition to the dissociated fraction of chlorides, the intermolecular interaction behaviour in the molten salt is also more significant depending on the ionic potential and the volume expansion of the dissociated cationic component as mentioned in [11]) mentioned. The formula for the ionic potential is

$$\phi_{\mathrm{M(diss)}} = \frac{Z_{\mathrm{M}^{n+}}}{r_{\mathrm{M}^{n+}}}. \tag{76}$$

In the equation (76), the volumetric expansion expressed by the expansion radius $r_{\mathrm{M}^{n+}}$ of each charge $Z_{\mathrm{M}^{n+}}$ influences the repulsion of similarly charged cations and the attraction of chlorides or chloride ions, even to another chloride component in a molten salt mixture. It can be further concluded that the analysis of the dominant fully ionic effects significantly influences the partial pressures of the species involved. In addition to these effects, the formation of predominantly uncharged chlorides must also be considered when the chloride components are transferred from the liquid to the vapour phase.

The delimitation of all important effects for a rough qualitative assessment of the extent to which such a VLE system is non-ideal and whether it tends to azeotrope formation or not is done in the following by the simplifying assumption of two possible states, coupled via the mixture-dependent dissociation constant or indirectly indicated via the net ionic degree depending on all degree of chlorination s of all chloride components:

- Fully dissociated fraction: influence of the ionic radii of the ionic components of the melt in combination with the ionic potential ratios between the cations (see e.g. [11]) for a simplified description of the repulsion and attraction behaviour of the ions in the melt in molar fraction ratios (depending on the chlorination degree ratios) of the occurring ion species.

- Completely undissociated fraction (covalency fraction): Description of intermolecular interactions with mainly covalency binding character and simplified assumption of similar Van Der Waals interaction behaviour between the undissociated salt molecules.

The classification of the possible behaviour of VLE molten salt chloride systems is based on

the following model, which is illustrated in Fig. (12). In a binary mixture XY with the pure components X and Y, which are not assumed to be dissociated, in general not only the interactions of the pure substances exist, but also those of the components X and Y among each other for each type of intermolecular interaction, as shown in the first case of Fig. (12). If the intermolecular interactions of the components among themselves are of the same magnitude as those of the pure substance components, an ideal phase equilibrium behaviour with $\gamma_i = 1$ would occur according to equation (28). In this case the interactions between the components X-X, Y-Y and X-Y would energetically compensate each other and the VLE system would only depend on the vapour pressures of the pure substances. Substance systems that exhibit a behaviour close to this property then behave in an ideal manner according to the validity of Raoult's law. Such a VLE behaviour is probably not expected for the mixtures with chlorides in general, as mentioned above, so for the chloride mixtures three possible intermolecular interaction types for the formation of VLEs are predicted to be classified as follows, for the sake of simplicity, according to the molten salt mixtures of Fig. (12) (Type I and II).

The first example concerns a binary chloride system in which one chloride component has a much higher degree of chlorination than the other chloride component, so that the attractive forces between the chloride group in bound or dissociated form as ions of the higher chlorinated component interact more strongly with the cation of the lower chlorinated component. Such a case is illustrated in Fig. (12) as type I of chloride VLE systems. In both the covalently bonded and the fully ionised states, these attractive forces clearly dominate over the repulsive forces. Secondly, the interaction forces between the pure components are much weaker. In the fully dissociated state, the cation of the less chlorinated component is surrounded on average by chloride ions of the counterpart, also with a higher ratio of surrounding chloride anions of the more chlorinated counterpart species. Thus, the intermolecular interactions of the pure substances are on average significantly weaker, instead of the attractive dominating interaction behaviour between the substance components. It can therefore be qualitatively concluded that the intermolecular attractive fractions in the sum of X-Y in the defined substance system XY dominate or even strongly dominate in contrast to the remaining net intermolecular pure substance interaction fractions X-X and Y-Y considered. A possible example of such a system could be uranium tetrachloride and any monochloride such as caesium chloride, which is shown as type I in Fig (12). For the alkali element cations of the monochloride, a very dominant attractive interaction behaviour in the network between the components uranium tetrachloride and cesium chloride can be predicted, which can be so strong that it can lead to a temperature maximum azeotrope, which can be described with a negative deviation from Raoult's law. But also for other systems where the degree of chlorination is very high, while the degree of chlorination of the counter current chloride is much lower, with $n \leq 3$. Because of these attractive-dominant intermolecular forces, the assumed more volatile chloride component is strongly prevented from phase transition from the liquid phase to the vapour phase, so that the boiling temperature of the mixture is rising above the boiling points of the pure substances. There is then a point at which the number of attractive intermolecular forces is equal to the ability of the two chloride components to leave the liquid phase, resulting in equal mole fraction values of vapour and liquid. This point is known as the azeotropic point. If the liquid molar fraction of the higher chloride component is

smaller than that of the azeotropic composition, the lower chloride component will preferentially pass into the vapour phase compared to the higher chloride component. In this case of application of distillation, the corresponding distillation behaviour is then reversed and the actually higher chlorinated component with higher degree of chlorination is obtained as a light boiling component and the corresponding other component with lower degree of chlorination as a heavy boiling component. An example of such a conceivable binary system relevant to this thesis could be the mixture of uranium tetrachloride with monochlorides such as caesium chloride, as shown in Fig. (12).

In another conceivable second case with a higher but also approximately equivalent degree of chlorination with $n_A, n_B > 3$, a repulsive-dominant intermolecular repulsion behaviour in the net between the substance components can also be assumed to be just as predictable. In this case, the chloride groups between the same and different components tend to have a dominant-effect repulsive interaction between the components, leading to a greater volatilisation of the chloride compounds within the mixture. For this purpose, a degree of chlorination of at least four should be available for each substance component for the spatial structure formation in the undissociated molecular state, in order to have a spatially distributed model of the distributed chloride ions starting from tetrahedral in the VESPR model (explained in [20]) for the original undissociated state, which preferably also does not change the spatially distributed state during the partially dissociating melting process with assumed distribution of chlorine anions and a resulting shielding effect of the positive charges. Such an example could be the case shown in Fig. (12) as type II. Under very dominant repulsive interaction behaviour of the chlorides, a moderate minimum azeotrope is then obtained with a strong positive deviation from Raoult's law in an analogous inverse manner to the Type I chloride mixture.

In a further definable type III chloride VLE mixture, various such combinations of the above-mentioned interaction VLE type behaviour an other intermediating molecular interaction effects can be observed, up to indifferent azeotropic behaviour , as well as saddle point azeotropic behaviour , if such a pseudo-chloride component system is present by assuming partly dissociation or complete dissociation behaviour of the liquid molten salt. Examples could be present in this thesis for the binary substance systems $AlCl_3$-$FeCl_3$ from [5] as a zeotropic real mixture and $TiCl_4$-$AlCl_3$ from [6] with indifferent multi-azeotropic behaviour of several additional dissociated assumed chloride components in a more complex VLE substance system.

However, there is a significant lack of available experimentally determined vapour-liquid property data for all nuclear-relevant mixtures to be investigated in this thesis in order to be able to use validatable GE models with parameter fitting, even in simple or advanced UNIQUAC or any modified LIQUAC models for molten salts (e.g. the originally developed model for dissolved salts according to [103, 92]). Therefore, for optimistic design with process simulations in this thesis, only ideal phase equilibrium behaviour is usually considered to show that distillation is usable as a possible separation method.

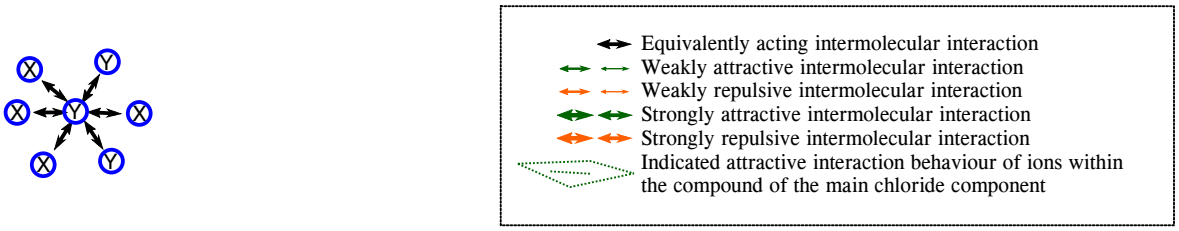

(a) (left): Intermolecular interactions between non-dissociating and thermally stable components X,Y in an idealized vapour-liquid phase equilibrium with validity of Raoult's law.
(right): Legend for possible interaction intensity

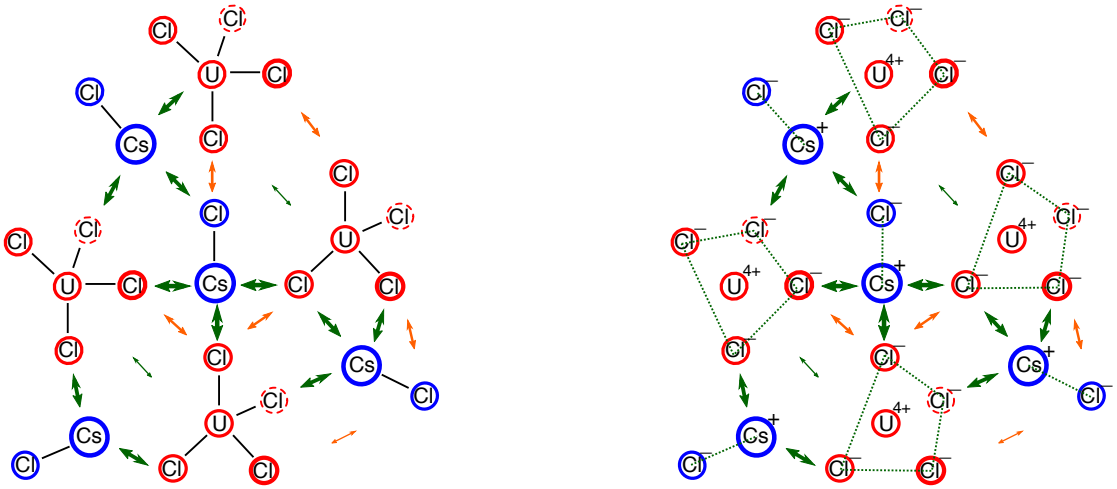

(b) Intermolecular interactions of assumed type I with assumed formation of a temperature maximum azeotrope with a negative deviation from Raoult's law for the exemplary substance system UCl_4-CsCl under covalent undissociated and completely dissociated ionic model conception.

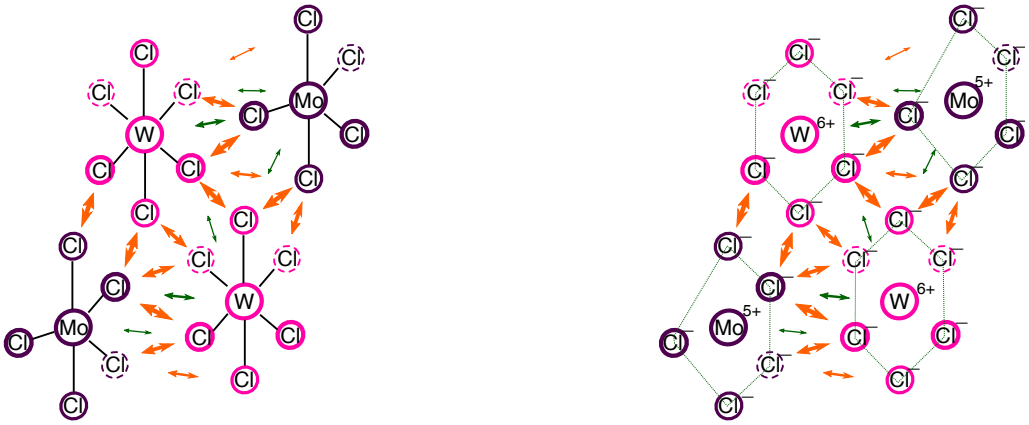

(c) Intermolecular interactions of assumed type II with assumed formation of a temperature minimum azeotrope with positive deviation from Raoult's law for the exemplary substance system WCl_6-$MoCl_5$ under covalent undissociated and completely dissociated ionic model conception.

Figure 12: Illustrative presentation of the intermolecular interaction behaviour of molten salts in vapour-liquid equilibrium with the most important liquid mixture types: Idealized, I and II. The circularly depicted area per element does not illustrate the specific volumetric size, but only the geometric-spatial indication over the depicted thickness.

3.1 Availability of vapor-liquid equilibrium data for molten salt systems

Completely experimentally measured VLE data from the literature are only known for fluoride systems and some chloride systems. Examples of measured VLE data for fluoride and mixed halide systems include the following substance systems:

- LiF-NaF-BeF_2 and LiF-BeF_2,: see: [104] and [8],
- UF_6-MF_6 or MF_5 with M=W, Ta, Sb, V, Te, see: [105, 106],
- UF_6-UF_5Br and other uranium fluorides, see: [107, 108].

For pure chloride-based salt mixtures, VLE data are mainly known as binary systems with aluminium trichloride, such as the zeotropic mixture$AlCl_3$-$FeCl_3$ according to [5] or the azeotropic mixture $TiCl_4$-$AlCl_3$ according to [6]. These mixtures with aluminium trichloride will be discussed in more detail in the following section as they are relevant to the Kroll process for the purification of titanium ores after chlorination to chloride salts and distillation to titanium tetrachloride.

Furthermore, experimental literature data on molten salt distillation, preferably for single-stage operations, can also be used to estimate the real phase equilibrium behaviour of these mixtures in order to evaluate an applicable GE model for activity estimation. Secondary, even qualitative statements on the distillability of such real molten salt mixtures are possible. Further experimental investigations on the distillability of such substance systems have been carried out in [109, 110] using a closed chamber unit or have been described in more detail in other distillation apparatuses, e.g. in [111, 50] on the basis of fluoride or in [112] on the basis of chloride. In [113, 114, 115], experimental investigations on the distillation of uranium hexafluoride are carried out, among other things, as follow-up studies to the experimentally measured VLE systems of uranium hexafluoride mixtures according to [107]. From some experimental results on the composition of the distillation product, the activity could also be estimated for a single stage distillation unit from the equilibrium condition of the $\gamma - \varphi$ concept according to equation (27) with p $<$ 10 bar

$$\ln \gamma_i = \exp\left(\frac{y_i p}{x_i p_i^{LV}}\right). \tag{77}$$

However, as in [112, 114], it is often not sufficient to recognise whether the measured value for the distillation product composition refers to the usable value in which a VLE equilibrium system can be approximately assumed in order to be able to evaluate the activity coefficient according to equation (77). Therefore, this approximation method will not be used for VLE determination in this thesis. However, it can be used in the future for later validation of activity data in general, after a higher state of knowledge. On the other hand, molecular dynamics simulations and Lennard-Johnes potential data are of particular importance, because with the knowledge of these data the simulation of the mixing behaviour of the liquid phase according to the UNIQUAC and LIQUAC model is physically feasible. In addition, Density Functional Theory (DFT) work from the literature could also be helpful in the investigation as it provides information on the potential used in the literature. However, these MDS and DFT data on the interaction parameters are only given for the substance system UCl_3-LiCl-KCl in [99, 116], where

the interactions of the ion pairs and components have been measured by Molecular Dynamics Simulations (MDS). More information on modelling for other matter systems can be found in [117, 103, 98, 118].. GE models for the description of the behaviour of actinides in LiCl-KCl mixtures are described in [119], but can also be used theoretically only as a rough approximation for the description of the salt mixtures investigated in this thesis. However, the simulation effort would be large and the results difficult to validate. In addition, the simulations are only limited in their ability to describe these mixtures, so even no literature data on molecular dynamics simulations and density functional theory will be used in this thesis for simulations and other estimations.

Further information on the real VLE behaviour and the description of the type of VLE for chloride systems is given in [4]. From these data in [4, 5, 6] the following classification of vapour-liquid volatiles can be made for the following substance systems:

- Binary zeotropic VLE systems of chloride mixtures:
  AgCl-$PbCl_2$, $AlCl_3$-$FeCl_3$, $AsCl_3$-$SbCl_3$, $AsCl_3$-$GeCl_4$, $AsCl_3$-$SnCl_4$, $BaCl_2$-$MnCl_2$, $CaCl_2$-KCl, $CaCl_2$-$MnCl_2$, KCl-$SmCl_2$, KCl-$SrCl_2$, KCl-$YbCl_2$, MgCl-$MnCl_2$, $MnCl_2$-$SrCl_2$, $PbCl_2$-$ZnCl_2$, $SbCl_3$-$GeCl_4$, $GeCl_4$-$SiCl_4$, $HfCl_4$-$ZrCl_4$, $SiCl_4$-$SnCl_4$, $SiCl_4$-$TiCl_4$, $SiCl_4$-VCl_4, $SnCl_4$-$TiCl_4$, $SnCl_4$-VCl_4, $TiCl_4$-VCl_4, $TiCl_4$-$NbCl_5$, $TiCl_4$-$TaCl_5$, $NbCl_5$-$TaCl_5$.

- Binary azeotropic VLE systems of chloride mixtures with temperature maximum azeotropes (expected Type I mixture):

  - Low pressure measurement of AgCl-$MgCl_2$ without apparent pressure dependence of the azeotrope with azeotropic composition measured at $y_1 = 0.6799$ for 0.002-0.018 bar.
  - $AlCl_3$-$NbCl_5$ with observable pressure dependence of the azeotrope and the azeotropic compositions at $y_1 = 0.2050$ für 1-0133 bar and $y_1 = 0.1820$ measured for 5.0663 bar.
  - $AlCl_3$-$TaCl_5$ with azeotropic composition at $y_1 = 0.1250$ measured for 1.0133 bar.

- Mixtures of binary chloride VLE systems with tendency to form a temperature minimum azeotrope (expected Type II mixture): or other types of azeotropes (expected Type III mixture):

  - $MoCl_5$-WCl_6 with azeotropic/zeotropic composition between $0.9750 < y_1 \leq 1$ (with $y_1 = 1$ as zeotropic mixture) measured for 1.0133 bar.
  - $TiCl_4$-$AlCl_3$ with two indifferent azeotropic composition points at $0 < y_1' < 0.05686$ and $y_1'' = 0.7685$ with uncertainties of +10.494-mol% and -4.332.mol% for slightly higher pressures than 1.0133 bar measured in [6].

This exemplary list of zeotropic versus azeotropic behaviour of various molten chloride salt systems shows wide range of possible interaction behavour. But type II mixtures with strong net attractive-dominating intercomponent interactions in the liquid can be expected for mixtures of aluminium trichloride and a pentachloride with niobium or molybdenum as counterchlorde component the a significant higher degree of chlorination of five. This supports the hypothesis that possibly net dominating attractive interaction effects for the mixture of type II are present,

if one of the chloride components have a significant higher degree on chlorination and the other chloride component with a lower degree of chlorination of $n \leq 3$. In this case, for the azeotropic mixtures, the attractive-dominant intermolecular interactions would lead to a significant reduction in the partial pressure of the chloride component within such a mixture, when considered as an average of all intermolecular interactions, which alone could explain the formation of a temperature maximum azeotrope in such a VLE system. This explanatory approach is purely theoretically applicable to all the above-mentioned mixtures of substances with temperature maximum azeotrope formation of the type I chloride mixture, regardless of whether the components would be present in the molten salt in dissociated-ionic or undissociated molecular form from a modelling point of view, since the higher degree of chlorination of the opposite chloride component would always predominate and thus, even in fully dissociated form, the attractive interactions between cation and anion of the opposite component would predominate in a purely proportional manner with attractive interaction forces due to the chloride ions present in the mixture in the higher stochiometric molar number.

Furthermore, it can be observed from the three given azeotropic mixtures with a temperature maximum, such as the mixtures $AlCl_3$-$NbCl_5$, partly show significant pressure-dependent azeotropes. Therefore, pressure swing methods are suitable for using distillation as a separation application as explained in detail in [79] (p. 247f (Chapter 7)). For example, with two continuously operating distillation columns, the composition in a second column could easily be shifted to the other side of the azeotropic composition in these examples using these higher pressures in a second column.

The mixture $MoCl_5$-WCl_6, which according to [4] has the opposite tendency to the potential formation of a temperature minimum azeotrope, follows the theoretically suggested explanation of the Type II interaction behaviour from Fig. (12). In this case it can be assumed that the net repulsive interactions between the chloride components are present as strong dominating intermolecular interactions between the two different chloride compounds. Consequently, azeotrope formation would result in a decrease in the boiling temperature of the mixture due to the increase in vapour pressure of the components in the mixture.

A comparison of similar binary mixtures based on fluoride salts also shows exceptions to the above approach to explaining the formation of such forms of azeotropic mixtures. According to [4], the mixture AlF_3-NaF is a zeotropic mixture instead of a forecast azeotrope with a temperature maximum. Another exception that contradicts the predicted expectation of azeotrope formation is the mixture LiF-HfF_4 with a pressure independent temperature minimum azeotrope at $y_1 = 0.8800$ instead of a qualitatively expected temperature maximum azeotrope. The binary mixtures of uranium hexachloride with molybdenum or tungsten hexafluoride instead show a zeotropic mixture behaviour . For the qualitative prediction and estimation of the equilibrium behaviour of a binary molten salt vapour-liquid system, the above primary qualitative approach to the behaviour of intermolecular interactions is therefore not always really sufficient.

Another way to roughly estimate the vapour-liquid equilibrium behaviour of mixtures with uranium or other actinide chlorides is to look at tabulated data at lower temperatures of the melt, where the melt cannot evaporate. Furthermore, solid-liquid equilibria (SLE) can also be considered for this purpose as a very rough first approximation to obtain possible purely

hypothetical conclusions about the vapour-liquid system. However, two important simplifying assumptions have to be made for this consideration. The first simplification is the assumption that the activity data change only slightly from SLE to VLE system behaviour . The second simplifying assumption is that the azeotrope is pressure independent. In this case, the activity as a function of composition can be used as an approximation to estimate the temperature from the $\gamma-\varphi$ concept for the VLE system according to equation (27). Such estimates are made for binary VLE systems with uranium tetrachloride and partly even with thorium tetrachloride according to [10, 9, 11, 120, 121] in the following section. For other actinide mixtures, only some activity data are available for measurements with low concentrations of the actinide chlorides or measurements related to the infinite dilution determination, such as those from [122, 123, 124, 125, 126, 127]. Activity measurements at infinite dilution in the LiCl-KCl system with a eutectic composition of LiCl and KCl or molten cadmium are of less interest in this thesis, since only the case of the actinide at dilution is considered for this particular system, and not the other cases of measuring low concentrations of the other components in the actinide chloride. However, these data can be used in future studies after this thesis. The activities and ionic activities in some electrochemical studies of the behaviour of the species in LiCl-KCl eutectics at infinite dilution are americium di- and trichlorides listed in [128, 129, 130, 131]. References to neptunium chlorides can be found in [130, 131, 122], among others, as well as to numerous uranium and plutonium chlorides, and to thorium tetrachloride in [132, 130, 131, 133, 116]. Theoretical and qualitative data on the behaviour of the melt with curium trichloride can be found, for example, in [134, 135, 136].

3.2 Estimation of VLE data and evaluation of the influence of real equilibrium behaviour

When defining the problem for the investigation of important representative mixtures for the reprocessing of spent nuclear fuel from fuel elements, it already became clear that mixtures with uranium tetrachloride and fission product chlorides, e.g. with cesium chloride as monochloride, as well as mixtures with actinide chlorides, e.g. plutonium trichloride, neptunium tetra- or trichloride, are missing for this thesis. For the estimation of the possible real deviation behaviour , as already mentioned in the previous section on the availability of such data from the literature, further substance systems are available for other non-nuclear relevant VLE molten salt systems. These include the following mixtures with particularly large deviations from the ideal vapour-liquid equilibrium behaviour with $\gamma_i = 1$ representing $AlCl_3$-$FeCl_3$ as a zeotropic classified mixture and $TiCl_4$-$AlCl_3$ as an azeotropic classified mixture. These mixtures are intended to illustrate the complexity of possible relevant binary VLE systems that may occur for relevant binary sub-systems in the study of nuclear fuel reprocessing.

Calculations of activity in the BeF_2-LiF system for the range of melting points of the pure substances and the range of boiling points are intended to show qualitatively that statements about the possible real phase equilibrium behaviour in the VLE system may be possible if the activity coefficients between the range of melting points of the pure substances and the range of the corresponding boiling points are of similar magnitude. This comparison is important in that approximate values for VLE data can be derived from SLE and activity data in the temperature range of non-evaporating molten salts with uranium tetrachloride from the literature, but only

and exclusively to clarify a possible simple non-ideal phase equilibrium behaviour . The extrapolated data, however, have no relation to the real VLE, but only illustrate a possible real deviation behaviour as well as the tendency to form azeotropic mixtures due to the above mentioned model conception of activity by attractive dominating forces between cation and opposing component depending on the degree of chlorination n and the ionic potentials of the cations simplified as completely dissociative ($\Phi_{r^{n+}}$).

3.2.1 Examples of VLE data for molten salt mixtures from the literature

For the $AlCl_3$-$FeCl_3$ mixture, classified as a zeotropic mixture, the VLE data have been measured from the literature at pressures slightly above 1 atm in [5]. In Fig. (13) the tabulated x_1, y_1, T data are plotted together with the $y_1(x_1)$ and $T(x_1, y_1)$ correlation functions approximated here from the literature data. The thin blue marked curve in Fig. (13) shows the graphically expected course for an ideal-zeotropic expected mixture adjusted to the temperature range as a function of pressure, where the highest measured values touch the maximum limit range of the ideal VLE curve compared to the real case and the ideal VLE curve ends in the temperature minima and maxima of the real VLE diagram. It shows the deviation behaviour for the real mixture in xy-diagram representation.

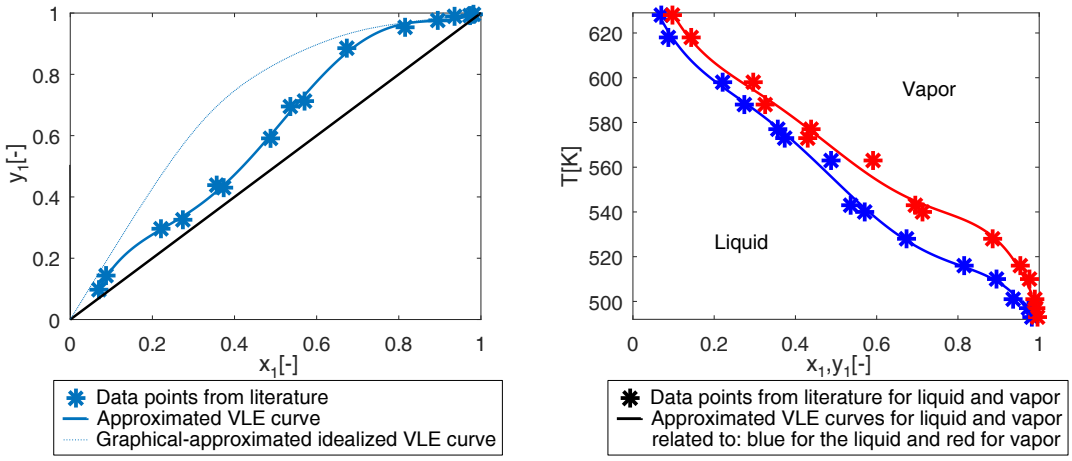

(a) xy-data (b) Txy-data:

Figure 13: The VLE system to the zeotropic mixture $AlCl_3$-$FeCl_3$ according to experimental measurement points from [5], with x_1/y_1 liquid/vapor mole fraction value of aluminium trichloride and T the temperature in K:
Fig. (a) shows the experimental measuring points, the fitted correlation function of the measurement points and the graphical-estimated idealized VLE curve, in which optimized just all measuring points are still below the ideal phase equilibrium curve, matching the temperature and pressure range.
Fig. (b). shows the experimental measuring points together with the fitted correlation function.

As the xy-diagram in Fig. (13) shows for the mixture $AlCl_3$-$FeCl_3$, the zeotropic VLE behaviour for $0.1 < x_1 < 0.6$ deviates visibly from the ideal case for $\gamma_i = 1$. The boiling range is significantly narrowed in this composition range. This narrowing of the distillation liquid-vapour region is also clearly visible in the Txy diagram of Fig. (13) . The Margules approach is not

sufficient to approximate these literature equilibrium data. This would require modelling with more complex models to implement the complex VLE data profile. To approximate the data points in the xy plot and Txy plot, 5th order polynomials are required. $T(x_1) = C_0 + C_1x_1 + C_2x_1^2 + C_3x_1^3 + C_4x_1^4 + C_5x_1^5$ with all necessary details in tab (7) to describe the VLE data.

Fig. (14) shows the literature-given azeotropic mixture example $TiCl_4$-$AlCl_3$ with analogous convention as for the $AlCl_3$-$FeCl_3$ except for the choice of approximation functions. Here, separate non-linear functions are defined piecewise for each xy, Tx and Ty correlations, as mentioned in the description in Fig. (14). The details of the correlation functions for the approximation of the$y_1(x_1), T'(x_1)$ and $T''(x_1)$ curves of both mixtures are given in Tab. (7). To fit correlation functions to the xy-diagram of the $TiCl_4$-$AlCl_3$ mixture, among others, the first region can be well approximated with an exponential approach up to the mole fraction of 0.077455. For larger composition values, a logarithmic approach is used for fitting. With respect to the determination of the correlation functions for the Txy diagram, the functional relationship of the form $T(x_1) = C_0(C_1 + C_2x_1^{-1} + C_3x_1^{-2} + C_4x_1 + C_5x_1^2)$ has been chosen. $T(x_1) = C_0(C_1 + C_2x_1^{-1} + C_3x_1^{-2} + C_4x_1 + C_5x_1^2)$ gewählt worden.

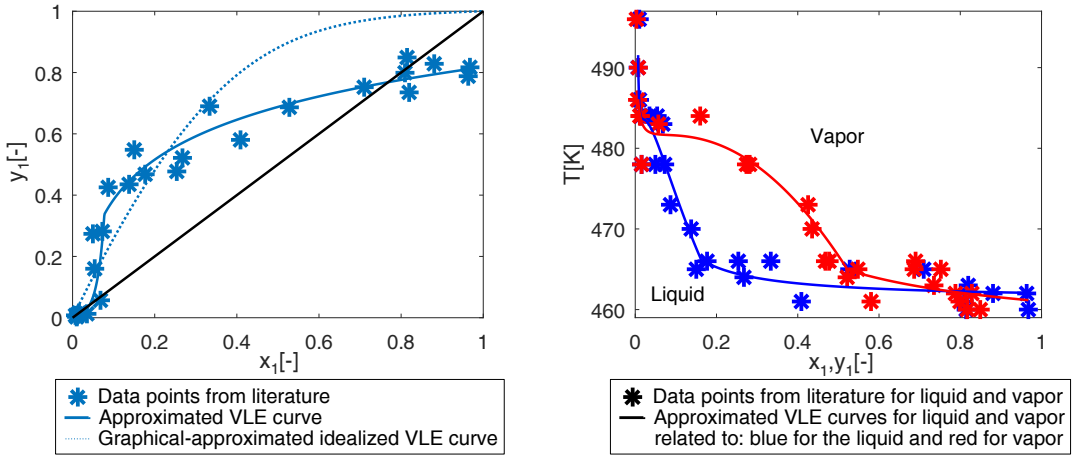

(a) xy-data (b) Txy-data

Figure 14: The VLE system to the double-azeotropic mixture $TiCl_4$-$AlCl_3$ according to experimental measurement points from [6, 7], with x_1/y_1 liquid/vapor mole fraction value of titanium tetrachloride and T the temperature in K.
Fig. (a) The xy-data are presented from the data points [6], fitted correlation function of the measurement points and the graphical-estimated idealized VLE curve matching the temperature and pressure range. A single approximation function is not sufficient to describe the complex azeotropic VLE behaviour , especially at low titanium tetrachloride concentrations.
Fig. (b) The Txy-data are presented as data points [6] and fitted correlation function of the measurement points. A single approximation function for each phase is not sufficient to describe the complex azeotropic VLE behaviour , especially at low titanium tetrachloride composition values.

The system $TiCl_4$-$AlCl_3$ in [6] has two azeotropic points at $y_1^{az,I} = 0.045 \pm 0.01$ and $y_1^{az,II} = 0.7722 \pm 0.0474$, which cannot be clearly classified as a type III azeotropic mixture. It can also be clearly seen that the VLE curve for the ideal phase equilibrium behaviour intersects the curve (hereafter referred to as the ideal VLE curve) for the real phase equilibrium behaviour . For the

azeotrope at $y_1^{az,I}$ there is no temperature minimum or maximum.

Table 7: Parameters to the approximation functions for fitting experimental data for the VLE systems with AlCl3 according to [5, 6].

(a) $AlCl_3$-$FeCl_3$

Approximation function	$f(x_1) = C_0 + C_1x_1 + C_2x_1^2 + C_3x_1^3 + C_4x_1^4 + C_5x_1^5$		
Constants, boundaries & Functions	$y_1(x_1)$	$T(x_1)$	$T(y_1)$
C_0	-0.13115	657.75552	677.04116
C_1	4.55508	-601.6701	-725.01278
C_2	-20.8824	2498.2712	2963.6095
C_3	51.5518	-6030.699	-6801.0288
C_4	-53.8858	6468.8022	7210.434
C_5	19.8054	-2504.9317	-2830.2461
Lower limit	0.069801	0.069801	0.097309
Upper limit	0.981846	0.981845	0.995886
Standard deviation value of approximation	0.011570	2.74 K	3.39 K

(b) $TiCl_4$-$AlCl_3$ part I

Approximation function	$f(x_1) = C_0 \exp(C_1x_1)$	$f(x_1) = C_0 + C_1 \ln(x_1)$
Constants, boundaries & Functions	$y_1(x_1)$, $x_1 < 0.077455$	$y_1(x_1) \geq 0.077455$
C_0	0.0038531	0.8180015
C_1	57.7475069	0.1878156
Lower limit		
Upper limit		
Standard deviation value of approximation	0.087091	0.052939

(c) $TiCl_4$-$AlCl_3$ part II

Approximation function part II	$f(x_1) = C_0(C_1 + C_2x_1^{-1} + C_3x_1^{-2} + C_4x_1 + C_5x_1^2)$	
Constants, boundaries & Functions	$T(x_1)$, $x_1 < 0.162$	$T(x_1) \geq\ x_1 = 0.162$
C_0	1.00	1.00
C_1	4.9517e+02	461.2477
C_2	-2.1813e-01	0.8008
C_3	1.4334e-03	0.0
C_4	-2.1836e+02	0.0
C_5	2.9348e+02	0.0
Lower limit	0.007049	0.162000
Upper limit	0.162000	0.967592
Standard deviation value of approximation	3.01 K	1.74 K

(d) $TiCl_4$-$AlCl_3$ part III

Approximation function part III	$f(x_1) = C_0(C_1 + C_2x_1^{-1} + C_3x_1^{-2} + C_4x_1 + C_5x_1^2)$	
Constants, boundaries & Functions	$T(y_1)$, $y_1 < 0.520$	$T(y_1)\ y_1 \geq 0.520$
C_0	1.00	1.00
C_1	4.7999e+02	456.7698
C_2	5.1113e-02	4.2585
C_3	-6.4196e-05	0.0
C_4	2.0463e+01	0.0
C_5	-9.4584e+01	0.0
Lower limit	0.009880	0.0028145
Upper limit	0.967600	0.849153
Standard deviation value of approximation	2.39 K	1.98 K

For the azeotrope at $y_1^{az,II}$, however, there are not enough data points to classify the azeotrope, although a temperature minimum azeotrope can be assumed from the course in the xy diagram. While the ideal VLE curve for larger composition values near $y_1^{az,II}$ is significantly higher than the real literature VLE curve, the xx-diagonal in the xy-diagram intersects with the result of the azeotrope formation as a presumed temperature minimum azeotrope. For small $y_1^{az,I}$ values there should also be an intersection with the xx-diagonal. All further peculiarities in the course of the VLE in the Txy diagram with respect to the mixture of $TiCl_4$-$AlCl_3$ can be seen in Fig. (14) .

In the context of this thesis (for both mixtures $AlCl_3$-$FeCl_3$ und $TiCl_4$-$AlCl_3$), the theoretical explanations are still to be understood as purely hypothetical, without practical proof, as experimental investigations of further chloride mixtures in dependence on different degrees of chlorination and metal components. Firstly, a comparison of the mixtures shows a clear dependence of the degree of chlorination with iron(III) chloride at the same degree of chlorination on aluminium trichloride and titanium tetrachloride at a higher degree of chlorination of four. In addition, the nature of the metal component of the chloride compound also seems to play a significant role, as shown by the comparison of other binary mixtures of a trichloride and a tetrachloride component according to the data in [4], as well as numerous examples given in the previous section. Assuming a high degree of dissociation, a complex interaction behaviour would be expected in addition to the degree of chlorination assumed in the effective range of the cations (see ion potential and ion radii). For the mixture $AlCl_3$-$FeCl_3$ a narrowing of the boiling range is observed in the xy diagram with a reduction of the boiling temperature, especially for aluminium trichloride components which are not too large according to Fig. (13). However, due to the associated reduction in the attractive forces between cation and chlorine ion in the dissociated partial state, the same number of dissociated chlorine ions would be spatially available for both chloride compounds to form the vaporous compound for evaporation due to the same degree of chlorination of three. Thus, in the dissociated state, the same number of chloride ions would always be available for each composition value for the new formation of the undissociated trichloride component during the transition to the vapour state due to the same degree of chlorination, which makes azeotrope formation unlikely from the previously theoretically assumed interaction behaviour . This mixture behaviour in the VLE system then changes for the $TiClTiCl_4$-$AlCl_3$ mixture, in which fewer chloride atoms would be available at low titanium tetrachloride contents, but theoretically the charge shielding effect with the consequence of a temperature minimum azeotrope formation would still be effective due to the dominating strongly pronounced assumed repulsive intermolecular interactions between the two component participants. Whether a temperature minimum azeotrope really exists for the mixture $TiCl_4$-$AlCl_3$, as mentioned in [6] for the range of low titanium tetrachloride contents, cannot be sufficiently clarified, since there are too few data points behind the azeotropic composition in the direction of the pure substance. For the other azeotrope it cannot be excluded that the measured azeotrope is not caused by measurement errors, e.g. impurities or decomposition of the aluminium trichloride component. It should be emphasised that aluminium trichloride in the vapour phase becomes thermally unstable at high temperatures (see e.g. the indirect information on the thermal stability behaviour of $AlCl_3$ in [67, 14] at 1 atm for the liquid and vapour phases).

In summary, the VLE examples presented here with aluminium trichloride according to [5, 6] on the VLE behaviour as well as the considerations of the different VLE forms of binary chloride systems according to [4] also mentioned in the previous section generally show a broad possible interaction behaviour for any chloride mixture system. Qualitative assessments of the VLE behaviour of representative binary mixtures for nuclear fuel processing are therefore only possible to a very limited extent within the framework of the qualitative theoretical-physical interpretation carried out here. One possibility for a rough estimate is to approximate the VLE from SLE data or activity data for representative chloride melts at lower temperatures where the chlorides do not yet evaporate. These very rough activity estimates for the relevant VLE system are made in the following section for binary chloride mixtures with uranium tetrachloride as the main component in the task of distillative treatment of nuclear waste.

3.2.2 Hypothetical estimated influence of real vapor-liquid phase equilibrium behaviour for $UCl_4 - MCl_n$ mixtures

With regard to a possible simple estimation of the VLE behaviour with uranium tetrachloride, only a few SLE data are available, as well as data in the temperature range of non-evaporating binary chloride mixtures with uranium tetrachloride, e.g. according to [10, 9] for lanthanum trichloride or manganese dichloride. Furthermore, it is to be estimated whether a mixture with uranium tetrachloride can tend to azeotrope formation and how such a separation system could look qualitatively. Fig. (15) shows that the activities between the melting points and the boiling points of the pure substance components are always in the whole order of magnitude between the minimum and the maximum of the activity values compared to the activity data in [8] on the basis of the two original sources mentioned there with Ref.1 and Ref.2. Only the activity curve as a function of the amount of beryllium dichloride changes significantly. With the exception of γ_{LiF} according to Ref.2 at 1942 K, larger deviations of the activity values result at high material component fraction values of beryllium difluoride. In addition, the differences between the two partial sources Ref.1 and Ref. 2 are also very large and in some cases even larger than for the different temperatures. Thus, it can be concluded that a rough estimation of the azeotropic tendency of a mixture based on extrapolation of the activity data for VLE data is potentially possible, but is not suitable to realistically represent the activity behaviour as a function of the composition of the components. However, a first estimate of the potential azeotropic tendency of a mixture with uranium tetrachloride is sufficient for discussion purposes, even though the actual VLE behaviour may be quite different.

To estimate binary VLE data for $UCl_4 - MCl_n$ mixtures from SLE or low-temperature activity data of non-evaporating melts at low melting temperatures, the activity functions $\gamma_i(x_1), i = 1, 2$ must first be determined neglecting the temperature dependence. Then the sizes of $T'(x_1), y_1(x_1)$ and $T''(y_1(x_1))$ can be determined.

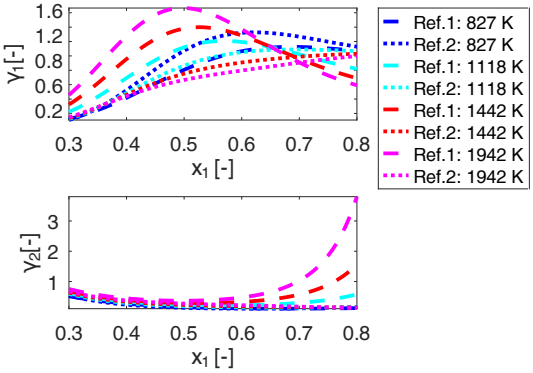

Figure 15: Example of some reference data given in [8] for the mixture BeF_2-LiF for the calculation of the activities (γ_1 for BeF_2,γ_2 for LiF) as a function of the liquid mole fraction value of beryllium dichloride (x_1) at melting and boiling temperatures as representative temperatures of the pure substances according to two different sources Ref.1 and Ref.2 from [8].

3.2.2.1 Used VLE estimation procedure Due to the lack of VLE data for binary systems containing uranium tetrachloride, estimates of $\gamma_i(x_1), i = 1, 2$ are simplified for non-evaporating tabulated activity data. For example, tabulated x_i, γ_i value pairs for the substance systems UCl_4-$MnCl_2$ and UCl_4-$LaCl_3$ are given in [10, 9] . Furthermore, for some $UCl_4 - MCl_n$ substance mixtures, two values are given from the literature for the partial molar Gibbs excess energy of the second substance component at $x_1 = 0,9$ (i.e. $G_2^E(x_1 = 0,9)$) and the molar Gibbs excess energy of the mixture at $x_1 = 0.5$ (i.e. $G^E(x_1 = 0,5)$). From these values, the activity can be determined in a very simplified way using the Margules approximation according to the equations (45) with $N = 1$. For this, the equation (46) for $G_2^E(x_1 = 0.9)$ is used only for the γ_2-equation part and the equation(45) with $N = 1$ is used for the determination of $G^E(x_1 = 0.5)$ in order to obtain a linear system of equations of the parameters A_{12}, A_{21} to be determined. The solution finally gives the two activity functions $\gamma_1(x_1), \gamma_2(x_1)$ according to equation (46) of the correlative Margules model approach. The approximation of such activity functions is possible for the determination of the VLEs of the following substance mixtures UCl_4-$ThCl_4$, UCl_4-$LaCl_3$, UCl_4-$CdCl_2$ and UCl_4-MCl, M=Li,Na,Cu,Ag from corresponding G^E data according to [11] using the presented approximation scheme. It should be noted that the approximation of the activity functions $\gamma_i(x_1), i = 1, 2$ at only two composition points is by no means a sufficiently representative representation of the activity of such a real binary system as a function of composition. However, the approximation at the same two composition points can roughly show the potential possibility of the azeotropic tendency, where simulations can predict possible deviations from the ideal case as illustrative qualitative case studies. On the other hand, in order to evaluate the approximability of the Margules approach for the substance systems UCl_4-$MnCl_2$ and partially UCl_4-LaCl, the Margules function can be approximated on the basis of several tabulated data.

From the determined activity functions $\gamma_i(x_1), i = 1, 2$, the VLE is now determined via the functional relations $T'(x_1), y_1(x_1)$ and $T''(y_1)$. These functions can be determined using the equilibrium conditions and the partial pressures related to the real mixture to be approximated. The numerical determination of T' from known x_i and the determined activity functions$\gamma_1(x_1), \gamma_2(x_1)$

is done by the following determination equation

$$p = x_1\gamma_1(x_1)p_1^{\mathrm{LV}}(T') + (1-x_1)\gamma_2(x_1)p_2^{\mathrm{LV}}(T'). \tag{78}$$

The composition of the vapour $y_i(x_1), i = 1,2$ is then determined directly analytically by evaluating equation (95). Since from the graphical observation of the general Txy-VLE diagram the corresponding value pair y_1, T'' also belongs to each value pair x_1, y_1, the relation $T'' = T''(y_1(x_1))$ follows directly, with which T'' is also derived directly from equation (95) for already calculated or known $\gamma_i(x_1), y_i(x_1), i = 1,2$.

3.2.2.2 Results of the estimation of VLEs from exemplary literature data Tab. (8) shows for the substance systems UCl_4-$MnCl_2$ and UCl_4-$LaCl_3$ the evaluated γ_1, x_1, x_1, y_1 and T, x_1, y_1 data with UCl_4 as substance component 1 from the literature activities $a_i = x_i \cdot \gamma_i$ tabulated in [10, 9]. Between the evaluated points, the linear interpolation of the required VLE data values is performed for simulation purposes by the interpolation formula

$$f_i(x_{i,\mathrm{val}}) = \frac{f_{ik+1} - f_{ik}}{x_{ik+1} - x_{ik}}\,(x_{ik+1} - x_{i,\mathrm{val}}) + f_{i,\mathrm{val}},\ f_{i,\mathrm{val}}\epsilon(f_{ik}, f_{ik+1})\,, \tag{79}$$

with nearest tabulated interval boundaries f_{ik},f_{ik+1} and $f = \gamma, y, T$.

The determined Margules parameters of all substance systems are listed in Tab. (9). Even when considering the absolute $|A_{12}|$ values, very high values are observed for mixtures of uranium tetrachloride and monochlorides in comparison to the other mixture examples listed. These Margules values are even significantly higher than for other known mixtures of e.g. organic substances or known from the literature from the chemical industry (see e.g.[51] (p.13-20f)). Considering the absolute values $|A_{21}|$ according to Tab. (9), there is no particular correlation of the dependence on ionic radii, degree of chlorination or ionic potential ratios, nor are there any significantly high absolute values in comparison to the $|A_{12}|$ values.

Fig. (16) shows the VLE data for binary mixtures with uranium tetrachloride evaluated for ideal phase equilibrium conditions with $\gamma_i = 1$ according to the equation (27) for monochlorides (lower part of sub-figure (a)) and chlorides with a higher degree of chlorination (upper part of sub-figure (a)). Since only the vapour pressure of the pure components plays a role in the idealized phase equilibrium, only idealized zeotropic mixtures can exist for the mixtures of the monochlorides, in which uranium tetrachloride is the most volatile. In such a mixture with ideal phase equilibrium behaviour , the intermolecular interactions between the two components, uranium tetrachloride and the other chloride component, are on average equal to the average interactions of the corresponding pure substances. In the pure substance, as [97] also emphasises, a chloride component is particularly volatile at a high degree of chlorination due to the charge-shielding effect of the chlorine atoms or chloride anions. Due to this charge shielding effect, the order of volatility and boiling point of the pure substance component is tetrachloride, dichloride, trichloride, monochloride, with decreasing volatility and increasing boiling point. Compared to the use of the uranium tetrachloride component with a degree of chlorination of four under high shielding chlorine content in the mixture, the difference in boiling points and volatilities

is therefore particularly high for the components with decreasing degree of chlorination, i.e. according to figure (a) of (16) for the order of monochlorides (NaCl, LiCl and AgCl which possibly form type I azeotropic mixtures as suggested in Fig. (12)), cadmium dichloride, manganese dichloride, lanthanum trichloride and thorium tetrachloride. Below the idealized VLE shown in Fig. (16) are the characteristic VLE properties of zeotropic and azeotropic Margules estimated mixtures compared to the idealized phase equilibrium conditions (see: equation (28) for idealized VLE expression), shown as partial figures in the upper figures (a) and (b) for the lower real course. For the Margules estimated VLE properties, the equation (27) for the VLE expression is used. In the idealized vapour-liquid equilibrium according to the validity of Raoult's law, where only the vapour pressures in the mixture play a role for the VLE of this mixture, no deviations are generally to be expected.

Table 8: Estimated VLE data excerpt examples from tabulated activity literature data ($a_1 = x_1\gamma_1$) from [10, 9] for the molten salt (a) UCl_4-$MnCl_2$ and (b) UCl_4-$LaCl_3$ mixtures

(a) UCl_4-$MnCl_2$

x_1	$\gamma_1(x_1)$	$y_1(x_1)$	$T'(x_1), T''(y_1)$
0.00000	–	0.00000	1510.7
0.05400	0.72222	0.72536	1367.2
0.09000	0.71111	0.83449	1319.4
0.13700	0.70803	0.90032	1277.6
0.24200	0.70661	0.95636	1221.3
0.31900	0.70219	0.97174	1195.4
0.39800	0.69849	0.98091	1175.3
0.48200	0.68050	0.98640	1160.4
0.54800	0.67153	0.98966	1150.2
0.60600	0.67162	0.99212	1141.4
0.65100	0.72197	0.99495	1129.2
0.71000	0.80563	0.99660	1112.7
0.77500	0.84129	0.99785	1102.1
0.85300	1.00470	0.99911	1080.6
0.92800	1.01510	0.99967	1073.5
0.97500	1.00620	0.99988	1070.4
1.00000	1.00000	1.00000	1069.0

(b) UCl_4-$LaCl_3$

x_1	$\gamma_1(x_1)$	$y_1(x_1)$	$T'(x_1), T''(y_1)$
0.00000	–	0.00000	2047.5
0.05200	0.46154	0.98979	1493.9
0.12700	0.45669	0.99895	1356.5
0.21800	0.44954	0.99955	1288.9
0.35600	0.42416	0.99983	1239.4
0.52300	0.37094	0.99993	1212.8
0.63000	0.30794	0.99993	1212.8
0.71800	0.24652	0.99993	1222.4
0.77500	0.22839	1.00000	1222.4
0.83200	0.25120	1.00000	1205.2
0.90400	0.85619	1.00000	1088.7
0.91500	0.88087	1.00000	1085.5
0.94700	0.93242	1.00000	1078.4
0.97300	0.97533	1.00000	1072.9
1.00000	1.00000	1.00000	1069.0

Table 9: Estimated Margules parameters for exemplary selected binary substance systems from [11] for determination of activity coefficients with (1) approximated from tabulated actvitiy data, (2) form given $G_2^E(x_1 = 0,9)$,$G^E(x_1 = 0,5)$ data.
r_2^{n+}: Ionic radius of cation component of the second MCl_n substance component)
$\Phi_{r_2^{n+},r_1}$: Ionic potential ratios between the cation of component 2 and the uranium cation (component 1)
*Marked absolute Margules parameter values might be unrealistically high for a successful VLE approximation with the Margules model.

Substance system	r_2^{n+}[nm] from [11]	$\Phi_{r_2^{n+}}$ from [11]	A_{12}	A_{21}	Ref. & method
UCl_4-$MnCl_2$	–	–	-1.4428	-0.1434	(1) [9]
UCl_4-$LaCl_3$	0.110	0.66	-4.8563	0.1485	(1) [10]
UCl_4-$ThCl_4$	0.102	0.95	-1.2464	-1.3568	(2) [11]
UCl_4-$LaCl_3$	0.110	0.66	-4.3970	1.9916	(2) [11]
UCl_4-$CdCl_2$	0.095	0.51	-1.50149	0.24374	(2) [11]
UCl_4-LiCl	0.072	0.34	-15.6824*	-2.8624	(2) [11]
UCl_4-CuCl	0.093	0.26	-20.6511*	1.0309	(2) [11]
UCl_4-NaCl	0.100	0.24	-29.8082*	-3.1351	(2) [11]
UCl_4-AgCl	0.118	0.21	-29.9198*	-1.0610*	(2) [11]

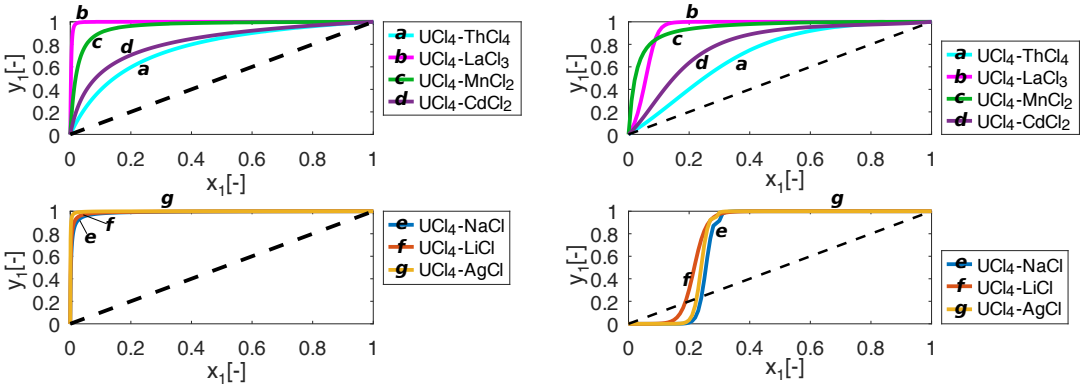

(a) Estimated VLE data under idealized equilibrium conditions at 1 atm

(b) Margules approximated VLE data at 1 atm

Figure 16: Plot of the idealized versus roughly approximated xy-VLE data* (with x_1/y_1 liquid and vapor mole fraction value of uranium tetrachloride) at 1 atm for zeotropic (top figure part) and the corresponding azeotropic classified mixtures (bottom figure part).
* xy-VLE data obtained from the Margules fit for the mixtures UCl_4-$MnCl_2$ & UCl_4-$LaCl_3$ from [9, 10] and use of the two G^E-data from [11] for Margules approximation using (45) and (46) for the other binary uranium tetrachloride-based mixtures.

Compared to the estimates of the VLE according to the pressure-independent Margules approach at the same composition points, the deviations from the ideal VLE behaviour according to the partial picture (b) in Fig. (16) seem to result essentially from the differences in the intermolecular attractive forces between the metal component or the cation and the opposing

substance component, which become particularly large when a substance component has a particularly low degree of chlorination. In addition to the assumed charge shielding effect, the effect of chloride ion reduction theoretically occurs particularly in mixtures with monochlorides and uranium tetrachloride in the dissociated state with decreasing uranium tetrachloride mole fraction. Up to a certain azeotropic temperature maximum, theoretically assumed dominant attractive forces between the uranium tetrachloride and monochloride components are still present around the uranium tetrachloride component. According to this VLE behaviour , this separation behaviour of the components will be reversed if a lower composition of uranium tetrachloride than the azeotropic composition is used for distillation, since then, compared to the distillation of uranium tetrachloride as a light boiler in the vapour phase, the original monochloride component will act as a light boiler and the azeotropic composition as a pseudo component as a heavy boiler. From the physical point of view, by decreasing the uranium tetrachloride azeotropic composition, the attractive force to leave uranium tetrachloride inside the liquid is higher then the volatility behaviour to escape from the mixture, due to its dominant attractive interaction force. Fig. (16) (lower part of subfigure (b)) shows such an estimated temperature maximum at the composition points 18.6415-mol% for UCl_4-LiCl, 22.4196-mol% for UCl_4-AgCl and 24.0753-mol% for UCl_4-NaCl. Since the Margules approach is pressure independent, the composition point of the azeotrope does not change in this model. Furthermore, strictly speaking, the VLE data estimated from [11] are only valid for the moderate process pressures of about 1 atm used here. For mixtures of uranium tetrachloride with other chlorides of higher chlorination, a zeotropic VLE behaviour is present below the Margules approximation made according to figure (a) and upper part of figure (b) in (16). However, the mixtures of uranium tetrachloride with the monochlorides show strong azeotropic behaviour as shown in the upper part of figure (b). As zeotropic mixtures, the large deviations between the Margules approximation and the ideal VLE are observed for the mixture of uranium tetrachloride with lanthanum trichloride as the trichloride species. In addition, the thorium tetrachoride, manganese dichloride and cadmium dichloride also show a deviation from the idealized VLE, but comparatively much smaller as shown for the trichloride component (see Fig. (16) ((a) and (b))).

The presentation of the real estimated VLE data in Txy plots below shows in detail the corresponding VLE behaviour for the mixture examples mentioned. For mixtures of uranium tetrachloride with manganese dichloride or lanthanum trichloride several possibilities of Margules approximation are available, which are shown in Fig. (17) as an example for both mixture examples.

For the mixture UCl_4-$MnCl_2$, there are only small deviations between the tabulated data according to Tab. (8) (case A) and the Margules approximation from the tabulated data (case B) are shown. As Fig. (17) (a) shows, the chosen approach of the Margules approximation (B) from the tabulated data is able to reproduce the approximation via the tabulated values alone very well. For the description of the vapour phase in approach (A) of the tabulated data, practically no data points are available for small composition values $x_1 \leq 0.6$ in order to be able to represent the data range well (physically sensible), so that the vapour phase has only been approximated by a straight line approximation. The approximation according to case (B) from the two data points manages with a suitable slope value at the last composition point of the

vapour phase to be able to represent the VLE curve physically-realistically up to $x_1 = 0$.

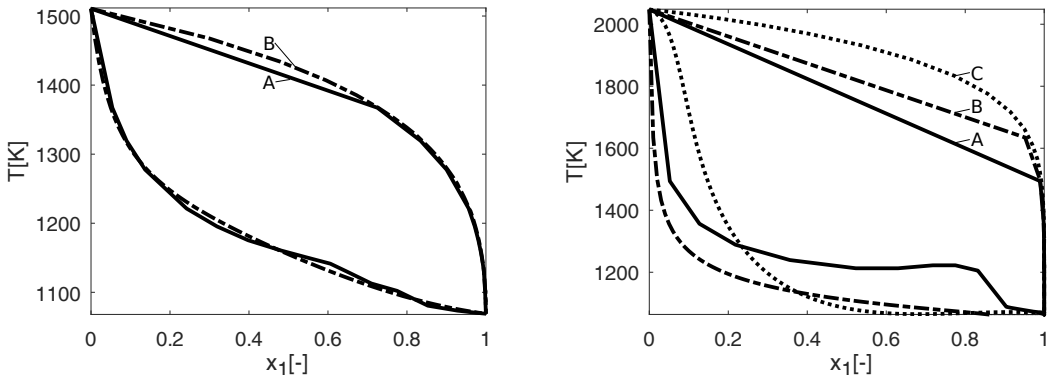

(a) UCl_4-$MnCl_2$ at 1 atm (b) UCl_4-$LaCl_3$ at 1 atm

Figure 17: Comparison of approximated VLEs (with x_1/y_1 liquid and vapor mole fraction value of uranium tetrachloride and T temperature in K) depending on the selected approximation method and the different literature data ([11, 9, 10]) for the mixtures at 1 atm (a) UCl_4-$MnCl_2$ and (b) UCl_4-$LaCl_3$ with estimated zeotropic equilibrium behaviour .
Different estimation methods are used:
A – Direct linear interpolated from the experimental given data with equation (79)
B – Approximated Margules functions by fitting the $x_1\gamma_1$ data from Tab. (8)
C – Approximated Margules functions from the G^E-data given in [11]
Note: The melting point of lanthanum trichloride as a pure component is 1131-1133 K > boiling point of pure uranium tetrachloride at 1064-1068 K (1 atm).

In the case of the substance system UCl_4-$LaCl_3$ according to Fig. (17) (b), the deviations between the approximation variants (A to C) are greater compared to the system with manganese dichloride, since the temperature in the VLE system of $LaCl_3$ falls below the melting temperature of pure lanthanum trichloride at high proportions of uranium tetrachloride in this substance system. The uranium tetrachloride-lanthanum trichloride system is a more complex system of VLE and possible SLE behaviour . A simple Margules approximation is not able to represent the phase equilibrium VLE behaviour here in a physically meaningful way. The tabulated data (case (A)) shows a unusual curvature of the vapour composition curve between $x_1 = 0.3$ and $x_1 = 0.85$. For this substance system, the Margules approximation from the tabulated values according to Tab. (8) only provides meaningful values for representing the VLE behaviour for high contents of uranium tetrachloride in the vapour phase. The Margules approximation from two points at $x_1 = 0.5$ and $x_1 = 0.9$ shows the slightly different VLE behaviour of the liquid and vapour composition with higher values in the vapour phase as well as in the liquid phase between $x_1 = 0.02$ and $x_1 = 0.218$. Accordingly, the deviations of the approximation variants show that the Margules approximation according to case (C) is certainly applicable for a very rough and qualitative VLE approximation.

Fig. (18) shows the curve progression of the VLEs for the substance systems UCl_4-$CdCl_2$ (subfigure (a)) and UCl_4-$ThCl_4$ (subfigure (b)), which were determined according to the Margules approximation in case (C). For the substance system UCl_4-$ThCl_4$, the retraction-bending curve of the said liquid composition can be seen very clearly between $x_1 = 0.0$ and $x_1 = 0.3$, while between $x_1 = 0.0$ and $x_1 = 0.1$ there is only a deviation from the ideal zeotropic liquid-vapour

region.

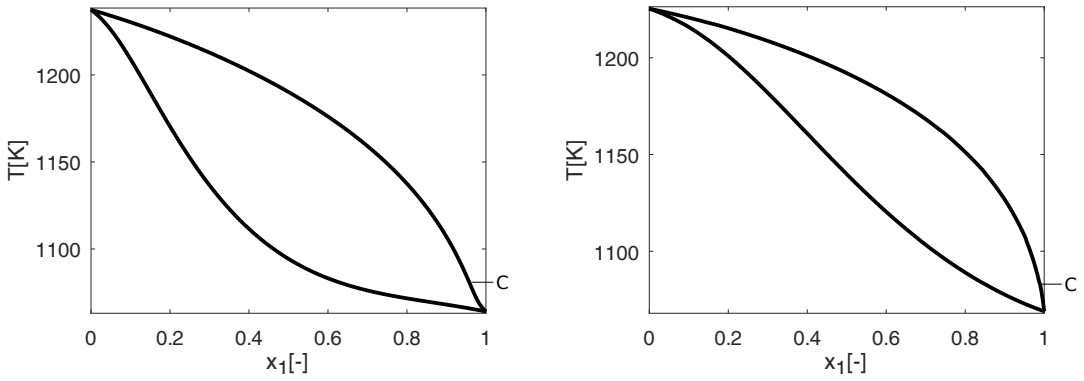

(a) UCl_4-$CdCl_2$ at 1 atm (b) UCl_4-$ThCl_4$ at 1 atm

Figure 18: Roughly approximated VLEs (with x_1/y_1 liquid and vapor mole fraction value of uranium tetrachloride and T temperature in K) from G^E data of [11] for the mixtures at 1 atm (a) UCl_4-$CdCl_2$ and (b) UCl_4-$ThCl_4$ with estimated significant zeotropic equilibrium behaviour .

Fig. (19) shows the Txy data according to the Margules approximation approach for case (C) for binary systems of uranium tetrachloride with the monochlorides lithium and silver chloride at a pressure of 0.1 bar. The results show a clear temperature maximum near the composition point of $x_1 = 0.2$. According to the Margules approximation approach, the Margules functions can only be approximated from two given composition points at $x_1 = 0.5$ and $x_1 = 0.9$ for the Gibbs excess energy from [11]. Unfortunately there are no data from [11] for $x_1 < 0.5$ and therefore it is only a very rough approximation, especially for monochlorides, in determining the height of the temperature maximum and the imageability of the azeotropic point location, especially for the very large temperature height. At pressures of 1 atm, the temperatures for sodium chloride at 2200 K are already well above 2000 K, so that distillation using this approximation by Margeules would not be technically feasible. For the mixtures with the monochlorides, this approach according to Margules is not suitable to physically adequately represent the representability of the temperature maximum of the azeotrope in composition point and temperature height. This Margules approach can therefore only be used to approximate from the SLE data to describe zeotropic VLE systems. The Margules approximation therefore only gives an indication of whether and how such a mixture behaves azeotropically.

Due to the lack of validity of the VLE data for mixtures of uranium tetrachloride with the other chlorides and, in particular, due to the lack of representability for the VLE behaviour of corresponding binary mixtures with monochlorides, the subsequent simulations in this thesis in the following chapters, including the conceptual design of the separation plant for the reprocessing of nuclear fuel, can only be carried out with the ideal phase equilibrium relations according to Raoult's and Dalton's law for $\gamma_i = 1$ according to equation (28). However, it allows the investigation of the best possible separability, where the deviating separation behaviour does not lead to a fundamental change in the process design. Thus, for zeotropic mixtures, only more separation stages would be required, whereas for mixtures with azeotropic separation, in the presence of distillation barriers due to azeotropic compositions, more separation columns are

required depending on the separation regions separated by the azeotropes.

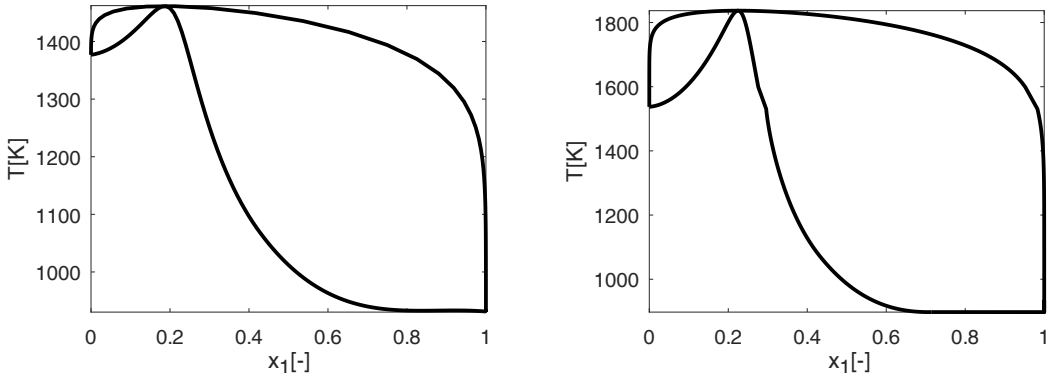

(a) UCl_4-LiCl at 0.1 bar (b) UCl_4-AgCl at 0.1 bar

Figure 19: Comparison of roughly approximated VLEs (with x_1/y_1 liquid and vapor mole fraction value of uranium tetrachloride and T temperature in K) for the mixtures (a) UCl_4-LiCl and (b) UCl_4-AgCl with estimated significant azeotropic equilibrium behaviour at reduced pressure of 0.1 bar and neglecting the positions of melting points of sodium chloride which is 1073.8 K > boiling point of pure uranium tetrachloride at 1064-1068 K.

Nevertheless, the knowledge obtained here for estimating the possible VLE behaviour can be used qualitatively to show possible qualitative deviations in the simulation results due to non-ideal VLE behaviour from the binary VLEs estimated here according to Margules for zeotropic and azeotropic mixtures with uranium tetrachloride in dependence on the degree of chlorination of the opposite choride component. For example, the increased number of separation stages for the distillation of various tetrachlorides with uranium tetrachloride can be predicted for small proportions of light boilers such as neptunium tetrachloride (as a light boiler in a binary system with uranium tetrachloride). Furthermore, it can be shown by examples that the separation behaviour of uranium tetrachloride from a mixture UCl_4-$CdCl_2$ is clearly approaching the ideal VLE behaviour , and thus simulation results generally show similar results the more the real behaviour of the VLE approaches the ideal one. For mixtures of uranium tetrachloride with monochlorides such as cesium chloride or silver chloride, azeotropic behaviour is clearly to be assumed on the basis of the behaviour approximated here with sodium, lithium and silver chloride from the activity approximation data according to [11]. Simulations of the distillation of such mixtures with these exemplary approximated VLE data are given as examples in the appendix of the section (D.1) despite the poor approximability from the data of [11], but do not have a sufficient physical basis in relation to the corresponding realistic separation problem. In the case of an azeotrope behaviour that is not necessarily pressure dependent, as shown in Fig. (19) of the (right) distillation range shown for mixtures of uranium tetrachloride with the monochlorides (e.g. For mixtures of uranium tetrachloride with the monochlorides (e.g. lithium chloride or silver chloride), it can be seen that up to an azeotropic composition of around $x_1 = 0.2$ (depending on the monochloride component) a normal distillation column can be used to separate the azeotrope as a pseudo-substance component in the heavy boiler component and high purity uranium tetrachloride as the light boiler component distillation product. A small addition of pure monochloride to the azeotrope is then sufficient to obtain the composition to the left of

the azeotrope shown in Fig. (19). In a further separation column, the monochloride can then be recovered as the light-boiler component and the azeotrope as the heavy-boiler component at the same pressure. In this way, the azeotrope can be separated repeatedly in a cycle analogous to the azeotrope separation methods of the pressure swing process according to [51], and both substances can be obtained by high purity distillation. In the case of a significant pressure dependence, the pressure swing method can also be used directly for the separation of substances, as generally described in [51].

4 Developed models for the simulation of distillation units

For the simulation, and for better comparability of the subsequent simulation results, two types of models have been used for each separation unit:

- A self-implemented model per separation unit, which requires little substance data and has been implemented in Octave/MATLAB (a simulation tool for solving mathematical problems).
- An external model with validated code from the software tool ChemSep Lite for the simulation of distillation and other thermal separations, as also explained in the tutorial [68].

The ChemSep models require more pure substance property data and have been used to estimate and illustrate the operation of the simulation codes implemented in this thesis and the following simulation results in the next sections and in the conceptual design. For an overview, there are four different self-implemented models in Octave/Matlab and the ChemSep Lite software on distillation units, which are listed in (10). For this purpose the self-implemented models with O/M (Octave/Matlab) and the ChemSep comparison models with C/S are listed in the table, which are only used in this thesis.

Distillation models	Octave/Matlab	ChemSep
Single stage distillation	SSD-O/M	SSD-C/S
Flash operation	Isothermal flash: IF-O/M	Simple Flash F-C/S
Continuous distillation column	Finite reflux column FRC-O/M	Simple distillation SD-C/S
Total reflux column	Total reflux TRC-O/M	Total reflux TRC-C/S

Table 10: Octave and ChemSep models for the simulation of various distillation units

The MESH equations (of the equations (55), (56), (57), (58)) are usually used for single and multi-stage separations in distillation processes with simulation of multi-component mixtures. For the isothermal flash (model IF-O/M) the reduced equation (54) has to be solved, which only depends on the vapour flow as a variable to be solved.

After modelling the single stage distillation units, the multi-stage distillation column is discussed below based on the model equations for the single stage distillation process. Compared to the simple continuous distillation column modelling, the modelling of the total reflux column operation is of much greater importance for this work, since the concept proposes a separation column concept for nuclear distillation that differs from the industrial column operation.

4.1 Flash evaporation

For flash evaporation, the IF-O/M model simulates an isothermal single stage continuous flash evaporator (in steady state) with a single feed and the outgoing vapour and liquid streams. The pressure difference is not considered. Therefore only the simplified equation 54 for the isothermal flash has to be solved numerically to determine the vapour flow $\dot{n}^V$. These equations can be seen in the section on the basics of simplified model approximations for distillation in section (2.2.4.1). Other flash model operations are described in [51] (p.13-25 – p.13-26). For comparability of this octave flash model with ChemSep in the F-C/S model, as can be seen in [68], such an isothermal flash evaporator could be simulated by assigning the same temperature as feed and operating temperature. Similarly, the same pressure should be used to simulate the isothermal flash evaporator in ChemSep as in the IF-O/M octave model.

4.2 Single stage distillation unit

For the solution procedure, the model SSD-O/M of a single-stage column is considered first. Instead of using the Newton-Raphson method to solve the MESH equation system in this thesis, the interval bisection method with a reduced system of equations will be used to avoid invalid solutions or convergence problems. A better handling of the possible solution range is also easy to handle. In a reduced system of equations, a variable can be chosen in the interval bisection procedure that is strongly coupled to the equations in the entire MESH system of equations in order to simplify the system of equations. By reducing the number of variables, a corrector equation must be defined. So, by the idea of interval bisection, the value closest to the solution is chosen and a new interval is created, similar to the one-equation interval bisection method described in [93]. It is also an order reduction method to solve the system of equations separately. The sub-systems of equations can be solved by simple numerical methods such as interval bisection for one variable or the Newton-Raphson method. The selected variables into which the initial values are inserted are defined as reduced variables only in this thesis. The mass or energy balance as an equation can be used as a corrector solution by selecting the range in the interval bisection whose solution value is closest to the equation solution in terms of the interval bisection idea. Thus, the entire solution process is based on the implementation of only two iteration loops to solve the reduced system of equations and to apply the interval bisection procedure. An outer loop is for the main predictor corrector bisection procedure, while reducing the equation system and the inner loop is for solving the sub-equations.

In the following, the vapour flow is chosen as the reduced variable of the system of equations, as it was also defined as a variable in the IF-O/M model. Unlike the IF-O/M, the reduced system of equations cannot necessarily be converted directly into a simple analytical equation. For this purpose, the two vapour flow values from the left and right interval of the interval bisection procedure are used in the mass balance to determine the liquid flows. For a single stage distillation unit with feed $x_F, \dot{n}_F$, distillate product $y, \dot{n}^V$ and remaining liquid $x, \dot{n}^L$, the molar flow of liquid $\dot{n}^L$ can be determined as follows

$$\dot{n}^L = \dot{n}_F - \dot{n}^V. \tag{80}$$

The solution is inserted into the equations of the component-specific mass balance equation part of the MEST equations (equation (55)) and the equilibrium relation (equation (56)) with $y_i = x_i K_i$. For the K-factors the expressions $K_i = \frac{p_i^{LV}}{p}$ (for ideal phase equilibria) and $K_i = \frac{p_i^{LV}\gamma_i}{p}$ (for real phase equilibria) apply. Thus the following reduced equation is to be evaluated here

$$\tilde{x}_i = \frac{x_{F,i}}{\dot{n}^L + K_i \cdot \dot{n}^V} \cdot \dot{n}_F. \tag{81}$$

Here $\tilde{x}_i$ does not correspond to the liquid mole fraction, because the liquid mole fraction is not yet normalised and contradicts the criterion of the sum rates in the MESH equations, because for values outside 0 and 100 mol% for the mole fractions no (useful) solution for the sum rate equation of the MESH equations is available. Accordingly,$\tilde{x}_i$ is normalised by $\frac{\tilde{x}_i}{\sum_i |\tilde{x}_i|}$ and inserted into the reduced system of equations until the mass balance (55) is satisfied. Within this reduced system of equations, the system pressure must be equal to the sum of all corrected partial pressures with

$$p = \sum_{i=1}^{N_{\text{comp}}} x_i p_i^{LV}(T)\gamma_i(x_i, T). \tag{82}$$

For ideal phase equilibrium conditions the solution of the temperature T from the previous equation lies between $T_{B,\min} = \min\left\{T_{B,1}, \ldots, T_{B,N_{\text{comp}}}\right\}$ and $T_{B,\max} = \max\left\{T_{B,1}, \ldots, T_{B,N_{\text{comp}}}\right\}$. So the interval bisection method is also suitable as a solution method for the sub-equation system. The energy balance is the correction equation in which the solution for the vapour flow is chosen which is closer to the solutions of the following equation using enthalpies in the energy expression terms as the following equation

$$f_{\text{corr}}(x, y, \dot{n}^L, \dot{n}^V, T) = h_F(x_F, T_F)\dot{n}_F - \left(h^L(x,T)\dot{n}^L + h^V(y,T)\dot{n}^V\right), \tag{83}$$

$$f_{\text{corr}}(x, y, \dot{n}^L, \dot{n}^V, T) \to 0. \tag{84}$$

The iteration procedure continues until a predefined termination value is reached, such as $\delta = 1E-06$ in

$$\Delta\dot{n}^V_{\text{err}} = \delta \cdot \dot{n}_F. \tag{85}$$

In the case of an evaporator, the thermal feed state is defined as liquid-boiling. As a second possibility, saturated vapour can be condensed out. Thus, a single-stage evaporator or condenser can be simulated via the single-stage distillation, which is still of decisive importance for the flow formation development. Those inputs to the flash evaporation model F-C/S are also to be used under isobaric conditions to simulate such a single-stage evaporator or condenser as close as possible to the corresponding IF-O/M Octave model.

In ChemSep Lite the compatible single stage distillation model SSD-C/S can be selected. By setting the same conditions as for the Octave model, the simulation results of both models can be usefully compared. For more information on modelling and simulation procedure see [68].

4.3 Total-reflux distillation column

Typically, total reflux column models are used only to validate the GE models and to be able to apply these GE models to continuous distillation columns with physically meaningful phase

equilibrium descriptions. As mentioned earlier, the continuous operation of this total reflux column principle is of interest because a liquid to be distilled is presented to maintain such steady-state continuous conditions during operation. When the steady-state column operation is switched off, the distillation product and, if possible, the bottom product or by-products are removed. Since there are no valuable products to be sold, i.e. the economic factor is missing for the nuclear relevant reprocessing problem, the total reflux column operation is of great technical importance for the nuclear separation problem. Moreover, the main distillation can be carried out in a closed system, which is clearly preferable from the point of view of safety and emission prevention. In addition, the total reflux principle requires fewer separation stages to achieve the same separation result than the continuous or discontinuous modes of operation commonly used in chemical industry. This is why the simulation of the total reflux column is so important for this thesis. The conceptual design of the distillation column is described in section (5.2). In this section, the important point is to explain the simulation of steady-state total reflux column operation, which requires the column design described in section (5.2).

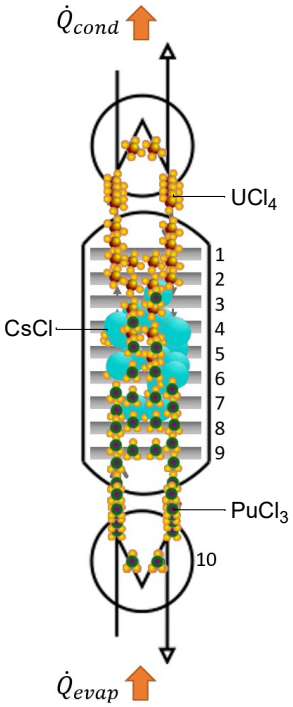

Figure 20: Illustration of the steady-state total-reflux-column principle:
The simplified illustration of UCl_4-CsCl-$PuCl_3$ distillation with ten stages (including evaporator as column stage) and under simplified non-dissociating behaviour of the chloride compounds

Fig. (20) clearly exemplary illustrates the scheme of a distillation column according to the stationary total-reflux principle using the separation example of the substance system UCl_4-CsCl-$PuCl_3$ under the simplifying condition that the compounds are molecular, do not dissociate and that ideal phase equilibrium conditions exist. Volatile uranium tetrachloride accumulates in the condenser and plutonium trichloride can be recovered in the evaporator. Caesium chloride remains as an intermediate boiling component between the third and seventh separation stages because it is too cold to remain further up in the vapour phase and too hot to remain further down

in the column towards the column evaporator. The cesium chloride is then contaminated with uranium tetrachloride or plutonium trichloride in these intermediate separation stages. After separation of the light and heavy boilers (uranium tetrachloride and plutonium trichloride), the process can be repeated to separate the two material components from the cesium chloride.

The simulation of the total reflux column is based on the specification of the mole fraction in a selected separation stage and the specification of the liquid or vapour mole flow in the first separation stage. The choice of the first separation stage is crucial for an adequate possible comparison of the simulation results with the ChemSep model TRC-C/S, since the specification of the material flow of the first separation stage is required in the TRC-C/S model. In the k-th separation stage, either the composition of the liquid phase or the vapour phase must be specified. The peculiarity of the simulation of a total reflux column is that no flows are added or removed and therefore, in terms of mass balance, the fraction of liquid of the previous stage must be equal to the vapour phase of the next stage in equilibrium and therefore fulfil the following equations

$$y_{ij+1} = x_{ij}, \tag{86}$$

$$\dot{n}^V_{j+1} = \dot{n}^L_j. \tag{87}$$

Since in the steady-state total reflux column principle no external flows are added to or removed from the column, the evaporator performance must also be equal to the condenser performance. For the energy balance, the heat loss from each column is neglected, so that the main column is in an adiabatic condition.

Due to the sum of the above conditions for the operation of the total reflux column, the entire modelling is extremely simple by applying the equilibrium condition according to equation (27). The mass balance and composition equations can be evaluated separately as well as the energy balance. The composition of the liquid and vapour phases is evaluated with subsequent calculation of the material flows via the energy balance between the condenser and the column stage. The calculation scheme for the simulation of the whole reflux column on the equilibrium stage model is therefore carried out in the following simple steps:

1. Request the substance components, the total number of stages, the mole flow for the first separation stage and the mole composition at a separation stage k per phase.

2. Internal stage iteration: Simultaneous evaluation of the stage temperature according to equation (82) and evaluation of the equilibrium relation according to equation (27) with the help of the application of the interval bisection method via the temperature as variable. Starting from the iteration of the composition specification at the kth separation stage, the following calculation scheme follows:

   (a) Upper section of the column with separation stage j, $j \leq k$: Calculation of the vapour fraction y_{ij} and the temperature T_{j} of stage j with subsequent application of the equation (86) for the total reflux column.

   (b) Lower part of the column with separation stage j, $j > k$: calculation of the liquid

fraction x_{ij} and the temperature T_j of stage j with subsequent application of the equation (86) for the total reflux column.

3. Calculation of the condenser performance and the evaporator Performance with

$$\dot{Q}_{\text{evap}} = \left|\dot{Q}_{\text{cond}}\right|, \tag{88}$$

$$\dot{Q}_{\text{cond}} = -\sum_{i=1}^{N_{\text{comp}}} \left(x_{D,i}\Delta h_i^{LV}(T_{\text{cond}})\right) \cdot \dot{n}_D. \tag{89}$$

4. Calculation of the mole flows via the energy balance between condenser and separation stage by evaluating the following analytical calculation equation after application of equation (87) for the liquid mole flow

$$\dot{n}_j^L = \frac{\left|\dot{Q}_{\text{cond}}\right|}{h_{j+1}^V + h_j^L}. \tag{90}$$

This very simple iteration scheme is used to simulate the stationary total-reflux column.

In relation to the ChemSep Lite software, the same model can be used for total reflux simulation with a slightly different solution methodology as described in [68]. For this purpose, the Total Reflux Column model, here abbreviated as TRC-C/S, is directly available in (any) ChemSep Lite version and the necessary specifications are congruent with the corresponding Octave model TRC-O/M.

4.4 Continuous distillation column for binary mixtures in Octave/MATLAB

For binary mixtures, the total reflux column (TRC) is simplified so that only the determination of the light boiling component is required for the binary composition itself. However, for the continuous distillation column with a realistic continuous reflux rate, the effect of simplifying the MESH equations (equations (55)–(58)) is more significant. As a result, the Sum-rate condition can be separated from the MESH equations for a binary system as follows.

The modelling and simulation of the finite reflux distillation column in Octave according to the FRC-O/M model (for binary mixtures only) can then be simplified for each thermal state feed condition. With the thermal feed condition e=1 (liquid boiling feed state) and with $x_2 = 1 - x_1$ from the sum rates criterion (equation (57), but for a binary mixture), the following system of equations is obtained, which is much easier to solve numerically:

$$p = x_{1j+1}\gamma_1(x_{1j+1}, T_{j+1})p_1^{\text{LV}}(T_{j+1}) + x_{2j+1}\gamma_1(x_{2j+1}, T_{j+1})p_2^{\text{LV}}(T_{j+1}), \tag{91}$$

$$\dot{n}_j^V + \dot{n}_j^L = \dot{n}_{j+1}^L + \dot{n}_{j-1}^V + C_F\dot{n}_F, \tag{92}$$

$$y_{1j}\dot{n}_j^V + x_{1j}\dot{n}_j^L = x_{1j+1}\dot{n}_{j+1}^L + y_{1j-1}\dot{n}_{j-1}^V + x_{F,1}C_F\dot{n}_F, \tag{93}$$

$$h^V(y_{1j}, T_j)\dot{n}_j^V + h^L(x_{1j}, T_j)\dot{n}_j^L = h^L(x_{1j+1}, T_{j+1})\dot{n}_{j+1}^L + h^V(y_{1j-1}, T_{j-1})\dot{n}_{j-1}^V + C_F h^L(x_{1F}, T_F)\dot{n}_F. \tag{94}$$

The composition of the vapour phase can be evaluated directly by equation (56) as an equilibrium condition, so that with the known quantities x_{1j}, T_j and the system pressure p follows directly:

$$y_{1j} = \frac{x_{1j}\gamma_1(x_{1j}, T_j)p_1^{\mathrm{LV}}(T_j)}{p}. \tag{95}$$

The determination of the unknown quantity variables to be calculated are $\dot{n}_j^V, \dot{n}_{j+1}^L, x_{j+1}$ and T_{j+1} from the equations (91) –(94) using the interval bisection method as explained in the main section above. This is done by initially specifying the vapour flow $\dot{n}_j^V$ (as in this thesis so called reduced variable) between the minimum and maximum specified mole flow values. This allows the molar flow $\dot{n}_{j+1}^L$ to be determined via the equation(92) and subsequently the composition of the liquid phase of the next stage with the molar fraction x_{j+1} by evaluating the equation (93). The temperature of the next stage T_{j+1} is determined by the equation (94), where a simple numerical method such as Newton's method with the variableT_{j+1} can be used. As a criterion for the interval bisection procedure to determine $\dot{n}_j^V, \dot{n}_{j+1}^L, x_{j+1}$ and T_{j+1}, the appropriate $\dot{n}_j^V$ is chosen whose solution still best satisfies equation (94). The appropriate interval is then readjusted with respect to the solution of $\dot{n}_j^V$ using the interval bisection method for the new range of the reduced variable $\dot{n}_j^V$.

Between the boil-up rate and the reflux ratio, the value of the boil-up rate at the end of the column iteration of the last separation stage (not to be confused with the bisection iteration, which is not meant here) can be determined in terms of mass balance without the need to determine the tears streams before.

5 Simulation results of representative selected test mixtures

The evaluation of feasibility and performance in the distillation application of nuclear fuel processing is carried out simulatively using representative preferred binary and ternary mixtures under ideal phase equilibrium behaviour . Simulation calculations under ideal phase equilibrium behaviour essentially represents the best possible separation effort. Deviations from ideal phase equilibrium behaviour is assumed in high separation accuracy, which results in more required number of separation stages for such a real zeotropic mixtures or, in the presence of azeotropes, additional separation columns become necessary, e.g. using pressure swing separation if the azeotropic composition points are significant pressure dependent. The evaluation of feasibility and performance in the distillation application of nuclear fuel processing is carried out simulatively using representative preferred binary and ternary test mixtures under ideal phase equilibrium behaviour . All calculations are simplified under ideal phase equilibrium conditions with $\gamma_i = 1$ of all possible separations required for the conceptual design according to chapter (IV). First a mixture with uranium tetrachloride cadmium dichloride and cesium chloride is simulated. Here, uranium tetrachloride is the main component of nuclear fuel, accounting for 95-98 mol%, with cesium chloride as the fission product chloride being the second most important component. Validation and comparisons are possible by simulation of the Kroll process. In [12] the experimental discontinuous distillative purification of titanium tetrachloride under high reflux ratio is carried out in a small laboratory test column, which comes closest to the

principle conditions of the total reflux column mainly used in this thesis, and in a pilot plant of a discontinuously operating five-stage distillation column.

5.1 First idealized approximation results

In order to obtain initial estimates and indications of distillability, simple calculations are made using the mixture UCl_4-$CdCl_2$ with the composition $[0.55, 0.45]^T$. This mixture is chosen because it is not expected to have as strong interactions as monochlorides compared to cesium chloride under real phase equilibrium conditions, as shown in the comparison between ideal and real phase equilibrium conditions in the previous section 3. Thus, azeotropes are not expected and the original calculations assuming ideal phase equilibrium are justified. The feed temperature is 1136 K and is based on the boiling temperature of the mixture determined at 1 atm.

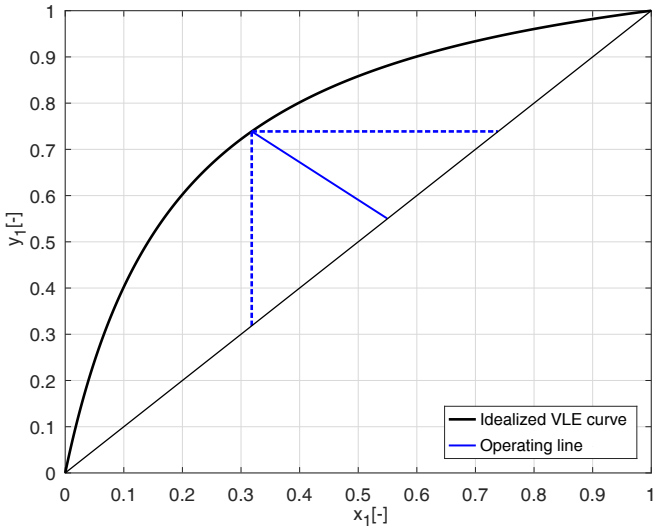

Figure 21: Graphical representation of the single-stage distillation of a UCl_4-$CdCl_2$ mixture at 1136 K and 1 atm (with x_1/y_1 liquid and vapor mole fraction value of uranium tetrachloride)

In a single stage distillation unit, the method of calculating the intersection of the operating and equilibrium lines is carried out as explained in section 2.2.4.1. The calculation result for the single stage distillation is shown in Fig. (21). In the vapour phase, the molar composition fraction of uranium tetrachloride is 0.73883 and in the liquid gas it is 0.31825. The distillation efficiency can be considered good with a relative volatility of $\alpha_{UCl_4,CdCl_2} = 6.06$. However, even with an impurity content of only 10 mol%, single-stage distillation is not sufficient to separate the chlorides roughly. Single stage distillation processes are therefore only suitable for separating gases dissolved in the melt or highly volatile chlorides. Examples of such separations would be the separation of boron trichloride with a boiling point of 285.8 K from a low volatility uranium tetrachloride-plutonium trichloride-cesium chloride melt.

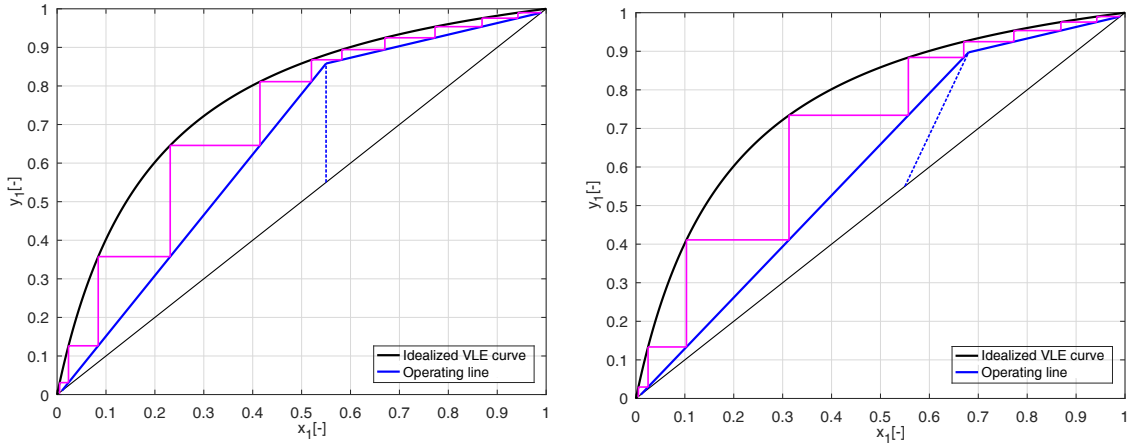

Figure 22: McCabe-Thiele diagram for the UCl_4-$CdCl_2$ (with x_1/y_1 liquid and vapor mole fraction value of uranium tetrachloride) distillation into a continuous distillation column of twelve separation stages:
left: under saturated liquid feed (thermal feed condition)
right: subcooled liquid feed (thermal feed condition)

Fig. (22) shows the evaluation of the distillation of the UCl_4-$CdCl_2$ mixture in a continuous distillation column according to the McCabe-Thiele method for $e = 1$ (saturated liquid feed) on the left and $e = 1.1$ (subcooled liquid feed) on the right. The separation accuracy has been assumed to be 1 mol% and the equilibrium line sketched for the feed temperature. The blue lines in Fig. (22) are the operating lines of the rectifying section of the distillation column and the yellow lines are those of the stripping section of the column. In the case of liquid boiling feed, the intersection is unfavourably high and ensures a large number of necessary separation stages in order to obtain as distillation products only uranium tetrachloride with an impurity level of 1 mol-% in the top of the column and cadmium dichloride in the bottom. According to Underwood's estimation method, the reflux ratio here is relatively small, with a value of $0.32 < v < 0.49$. The ratio of the separation stages is almost the same in both column sections (rectifying-section and stripping-section), which means that the feed in the column can be placed on the sixth separation stage. Since the equilibrium line has only been determined at the feed temperature, the degree of separation must be set lower than when evaluating the composition as a function of temperature. Due to the lower separation efficiency at high substance proportions for one of the two substance components, more stages are then required according to the McCabe-Thiele method.

For improving separation by reducing the number of separation stages required, the thermal feed condition for distillation can be modified by subcooling the liquid to reduce the rectifying part of the column. In this way, the separation process is preferably shifted to the stripping part of the column, which is more favourable for separation. For a value of $e = 1.1$ and higher, according to the results of Fig. (22) (right), only ten separation stages are required. The feed is then on the fourth separation stage, while the stripping section of the column has been enlarged.

Further detailed analyses of such and numerous other separation examples with such simplified graphical methods were carried out in [29] and will not be discussed in detail here in this thesis. Much more important is the presentation of the simulation of suitable distillation columns

with test mixtures with the self-implemented simulation models in the following sections.

5.2 Simulation results for the total reflux column

The use of the total reflux column to separate chlorides as accurately and selectively as possible is investigated theoretically. In the following, a new idea of column operation mode is presented, specially developed for this thesis, which involves successive total reflux column settings in a closed operating system and subsequently allows separate product removal without grossly interfering with the operation of the column. As shown in Fig. (20), the column is completely closed during the total reflux operating phase. Fig. (20) presents the column design in two column operating states shown in blue.

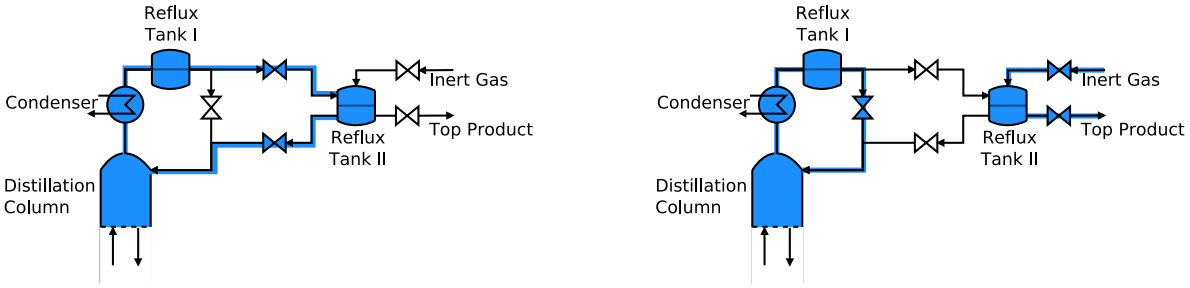

(a) First operating state:
Overall total reflux column operation

(b) Second operating state:
Distillation product removal and separate internal total reflux operation mode

Figure 23: Conceptual design of the main distillation column used in this nuclear fuel reprocessing with two separate column operation modes.

In the first step before use, the liquid feed to be distilled is fed into the column in a quantity n_F and with a homogeneous composition x_F. The column is then switched to operating mode and operated according to the total reflux principle until the column has reached a steady state. Once the steady state total reflux mode has been reached, the top distillation product and possibly the bottom product are concentrated in a first and second secondary distillation product reflux drum connected in series. At the top of the column, in total reflux mode, no distillate is removed from the first and second serially connected reflux drums and all of the distillate is completely returned to the distillation column. By closing the second reflux drum but switching the first reflux drum to total reflux mode by opening the reflux valve in the first drum while closing the second reflux drum, it is easy to remove distillate without affecting the total reflux principle. In the second reflux drum, the pressure must also be kept constant during the removal of the distillation product, which is achieved by inert gas injection, as shown in Fig. (20) (on the right second operating state) in the second operating mode. Similarly, the same could be done for bottom product removal if technically necessary. So the advantage is that a closed, safer distillation system is always available, and it comes very close to the more optimised total reflux column operation, with a lower number of stages required for distillation compared to the continuous or discontinuous column operation common in the industry. The only disadvantage is the lower amount of distilled product, so this column principle is not suitable for the chemical

industry when large amounts of product are sold in most cases, where this distillation concept would never be economical.

For the simulations in this thesis, the compositions are only evaluated in the discrete stationary column mode according to the total reflux principle. In order to be able to simulate the column in general, the summation or integration of the substance-specific molar flows must be determined as a function of the column height, which is equal to the batch quantity circulating in the column per active operating time in the running process cycle (PPC) Δt_{PPC}. A continuous process cycle of the total reflux column operation selected here, in which a distillate is enriched discontinuously in a distillation column until the steady-state operation of a total reflux column is reached and then the distillate is withdrawn, is called PPC. For the batch volume per time

$$\dot{n}_F = \frac{n_F}{\Delta t_{\mathrm{PPC}}}. \tag{96}$$

To simulate the total reflux mode of each PPC, the simulations for the entire reflux column must be optimised so that the substance-specific molar flows of the liquid per separation stage with $\dot{n}_{ij}^L = x_{ij}\dot{n}_j^L$ are equal to the circulating molar flow $\dot{n}_F$. This can be done iteratively by setting the default molar composition as a variable iteration variable. Following a suitable non-gradient-based optimisation procedure, the composition is varied after each simulation until the circulating batch flow per total time is equal to twice the amount of substance-specific liquid phase molar flows per separation stage. Since for each separation stage the mole flows and mole fractions between the liquid phase and the next vapour phase must be equal according to the equations (86) and (87), the sum of the liquid flows must be equal to the vapour flows after applying the mass balance. Therefore, for the simulation in the steady-state mode of the total reflux column, the following applies

$$\dot{n}_F \approx 2 \sum_{i=1}^{N_{\mathrm{comp}}} \sum_{j=1}^{n_{\mathrm{th}}} x_{ij}\dot{n}_{ij}^L. \tag{97}$$

In the following simulations, only the stationary operation of the total reflux column is simulated in this thesis by first determining the composition, molar flows and temperatures for each separation stage to be able to start the total reflux simulation. This idea of distillation column operation, together with the simulation of its total reflux PCCs, is of great importance in the conceptual design.

5.2.1 Distillation of the UCl_4-$CdCl_2$-CsCl system

The first test mixture used is the substance system UCl_4-$CdCl_2$-CsCl with the corresponding composition $x = [0.96, 0.016, 0.024]^{\mathrm{T}}$ which is primarily fed to the column. A PPC total reflux column operation is then simulated and the simulation results are shown in Fig. (24).

The simulation results show that in stationary operation of the total reflux column, high purity uranium tetrachloride can be concentrated in the first separation stage and high purity cesium chloride in the last separation stage. As the number of stages increases towards the evaporator, the proportion of the light-boiling component uranium tetrachloride decreases and the

proportion of cesium chloride continuously increases. The separation curve of cadmium dichloride occurs in the middle section of the column with a global maximum of the separation curve as a typical medium boiling component. The maximum of the cadmium dichloride separation curve with respect to cadmium dichloride is located in the seventh separation stage with a stage temperature of 1237 K, close to the boiling point of cadmium dichloride. Further away from the sixth and seventh stages, cadmium dichloride is much more depleted because the temperatures there are too cold or too hot for this component to remain as an intermediate boiler in these column areas. As a result, this component tends to accumulate in the vicinity of the seventh and sixth column stages. In the first and last stages, the amount of cadmium dichloride involved is less than 1E-04 mol%.

With regard to the temperature profile, it is noticeable that there are essentially two temperature plateaus in the simulation results for the temperature, depending on the boiling point of the light and heavy boiling components of uranium and cadmium chloride. As the proportion of the medium boiling component cadmium dichloride is always lower than for the other two components, cadmium dichloride contributes little to the average setting of the stage temperature via the thermal equilibrium state. As the proportion of uranium tetrachloride clearly predominates in stages 1 to 6 and the proportion of cesium chloride clearly predominates in stages 8 to 12, the boiling temperature there is also in the direction of the corresponding pure components. Due to the requirement that the feed should contain 96 mol% uranium tetrachloride, the proportion of uranium tetrachloride in the liquid molar stream of separation stages 1-5 is correspondingly greater than in other separation stages. In the seventh stage, where the cadmium dichloride fraction is maximum and the cesium chloride fraction is already reduced compared to the eighth stage, the liquid molar flow becomes minimum. Therefore, a global minimum is reached in the mole flow profiles in the seventh stage. Consequently, the mole flow profiles in the temperature plateaus of the column between stages 1-5 with uranium tetrachloride as the dominant material component and between stages 8-11 with cesium chloride as the dominant material component assume constant values.

For real VLE behaviour , the possibility of azeotrope formation in the interaction behaviour between uranium tetrachloride and cesium chloride could be present here, as discussed in section (3.1) for similar mixtures of uranium tetrachloride and monochlorides of the alkali elements. As the azeotropy results have shown, mixtures of uranium tetrachloride with lithium or sodium chloride are estimated to be strongly azeotropic mixtures. This could also be the case for the uranium tetrachloride-cesium chloride system. In the ternary mixture UCl_4-$CdCl_2$-CsCl, the formation of a limiting distillation line in the form of a distillation barrier is conceivable, taking into account the function $f(x_1, x_3)$ of the composition of uranium tetrachloride (1) and cesium chloride (3). For this, the binary VLE substance system UCl_4-CsCl would first have to be measured to check if and where the azeotropic composition is present. The ternary system can then be tested experimentally in the future for the presence of such a distillation boundary line. If such a distillation boundary line exists, it would be possible to cross it by adding cesium chloride at certain composition points in the region of the distillation boundary line in order to enter the other distillation region. Alternatively, if the azeotrope shows a significant pressure dependence from the measurements, the usual pressure change method can be used as explained

in section (3.2.2).

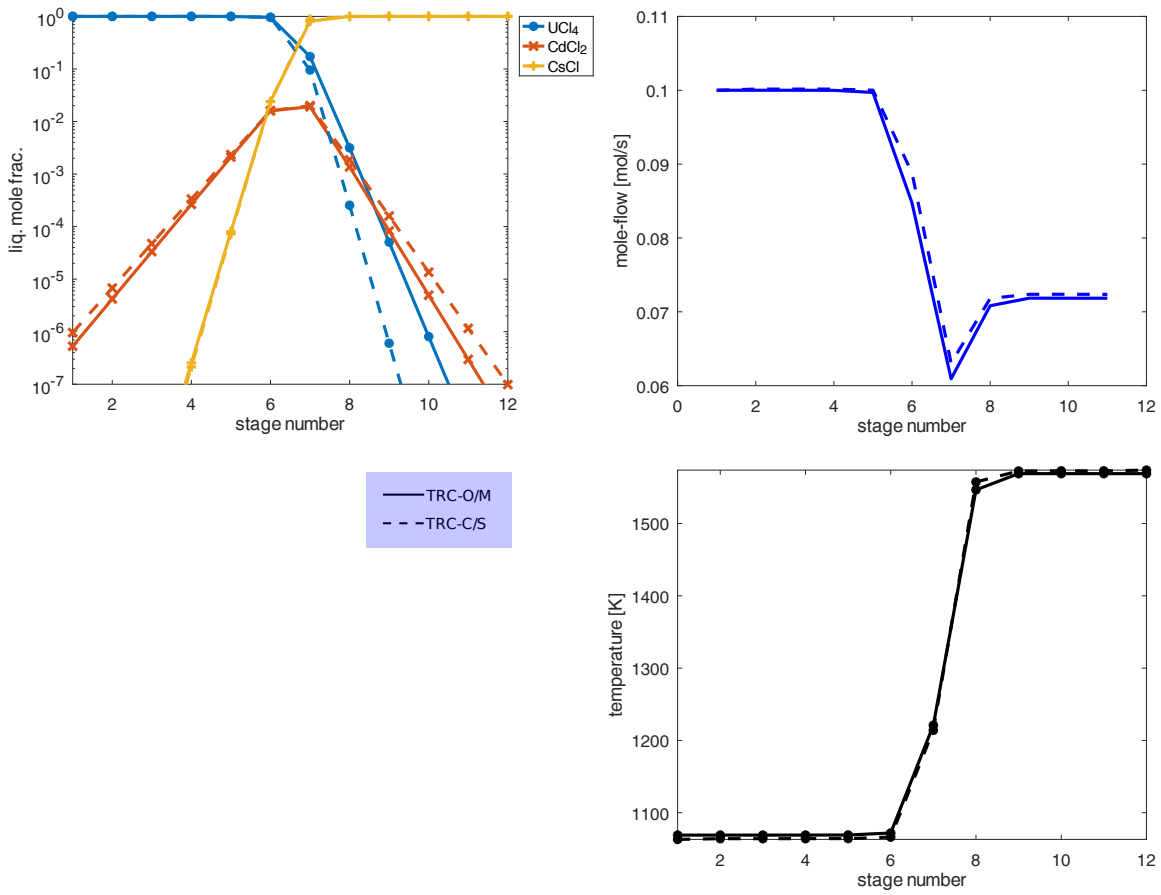

Figure 24: Simulation results for the total-reflux distillation of the UCl_4-$CdCl_2$-CsCl mixture with the assumption of ideal phase conditions
(boiling points of UCl_4: 1064 K, $CdCl_2$: 1237 K, CsCl: 1570 K)

The final comparison of the simulation results of Octave Matlab and the ChemSep Lite model in Fig. (24) under ideal phase equilibrium behaviour shows a very good agreement between the results. Both models are able to describe the separation problem in the same qualitatively and quantitatively correct way. This underlines the applicability of the Octave/Matlab model to use it for the analysis of more complex substance systems of the conceptual design even with little known substance data. The largest logarithmic deviations of the simulation results are shown for the mole fraction of uranium tetrachloride with increasing number of stages and for cadmium dichloride for compositions, the further the separation stage is from the feed stream or the global maximum of the cadmium dichloride separation curve of the seventh separation stage. When determining the liquid mole flows, the mole flow curve of the ChemSep model used is slightly higher than that of the Octave/Matlab model. The presumed reason for this is probably the different determination of enthalpy via heat capacities in the total reflux Octave/Matlab model. The deviations in the temperature profile are quantitatively even smaller and only differ noticeably by a few degrees in the eighth separation stage.

5.2.2 Simulation of titanium purification from the Kroll distillation process in total reflux columns

A pilot plant for the chlorination of various titanium-containing ores and the distillation of titanium tetrachloride from the corresponding fully chlorinated volatile salt mixtures according to the Kroll process was technically realised as early as the 1940s. The experimental results for the distillation are given in the technical report in [12]. Two distillation examples for the simulation of a total reflux column are taken from this report. First, a total reflux distillation column is simulated according to the TRC-O/M and TRC-C/S models for a binary mixture of silicon tetrachloride and titanium tetrachloride.

The aim is to first re-simulate a five-stage laboratory column according to [12] under high reflux ratios, in which the separation of titanium tetrachloride with a purity of 99 mol% as a heavy boiler and more volatile silicon tetrachloride as a light boiler with an impurity of 6 mol% of titanium tetrachloride. Here total-reflux simulation is useful to nearly simulate the separation condition in [12] of special high reflux rate for the laboratory column. In this case, the simulation results (Fig. (25)) show that a separation with five separation stages is sufficient to obtain exactly these product specifications by total-reflux distillation column.

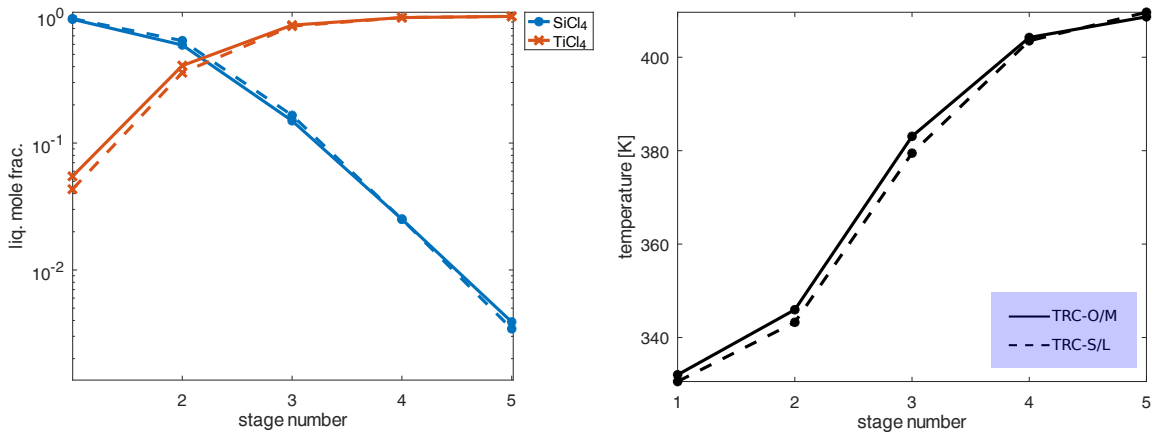

Figure 25: Comparison of the simulation results of the $SiCl_4$-$TiCl_4$ distillation

The comparison of the results in Fig. (25) shows almost the same simulated results as in the literature in [12]. The simulation results are therefore in remarkably good agreement with the experimental results. At the condenser the residual titanium tetrachloride content according to our own TRC-O/M model is 5.4 mol%, i.e. close to [12] values of an expected residual of 6 mol% at high reflux ratios. In the TRC-C/S model the value is slightly lower, as can be seen in Fig. (25). Further towards the evaporator the proportion of titanium tetrachloride increases according to the simulation results in Fig. (25) and the proportion of silicon tetrachloride as a low boiling substance decreases accordingly, as can be seen from the mole fraction values shown. From the third separation stage onwards, titanium tetrachloride dominates as the heavy-boiling component until titanium tetrachloride is obtained in the bottom distillation product with a separation accuracy below 99 mol-%, as also graphically mentioned in [12]. The separation accuracy is thus slightly better than that given in [12] (for the five-stage laboratory column at high reflux). In conclusion, both simulation models are able to reproduce the separation curves

and temperature profiles with good agreement between the results. Only the temperature curve differs by a few degrees between model and experimental results. All other deviations can be seen in Fig. (25). The results of the re-simulation of the distillation of the binary mixture in a five stage laboratory distillation column have shown that the results given in [12] are in full agreement. This demonstrates the applicability of the TRC-O/M model for simulations with ideal phase equilibria. This also indicates a very ideal zeotropic separation behaviour for such a binary VLE system.

As a further example, a more complex five-component mixture corresponding to the feed composition Lot1 according to [12] is now simulated in a total reflux column. A mixture of Cl_2-$SiCl_4$-$TiCl_4$-VCl_4-$FeCl_3$ with 97-5 mol% $TiCl_4$, 2 mol% $SiCl_4$ and small amounts of other specified components is used as the feed template for the total reflux column simulation. In contrast to the distillation column according to [12], chlorine is now to act as a light-boiling component and ferric chloride as a heavy-boiling component, so that the corresponding boiling temperatures (of the pure substances) must also occur in the column in order to maintain the pure substances. Secondly, a reflux ratio of 2 is assumed for the pilot plant and the same high reflux ratio for the laboratory column. According to the simulations, a column with fourteen separation stages is required to achieve this separation accuracy, with the simulation results shown in Fig. (25). However, it should be noted that in the experimental results chloride was not considered as a separation component within the distillation process, although its composition was measured in [12].

The molar flow according to the simulation results after total reflux column operation in fig. (26) of the first stage is about 0.85 mol/s. This flow consists only of circulating high purity volatile chlorine. The temperature profile shows that the chlorine content decreases rapidly from the fourth/fifth separation stage. The chlorine separation curve then follows a monotonically decreasing curve with increasing number of stages. Silicon tetrachloride is the next medium boiling component in this distillation column with a sharp global maximum in the fifth trap. This is followed by the intermediate components titanium tetrachloride and vanadium tetrachloride with a maximum in the eighth stage. The medium boiling component titanium tetrachloride dominates in the 6th to 8th stage. Matching the maximum of these two medium boiling components in the separation profiles, the maximum of the mole flow curve is also found at 0.43 mol/s. The temperature profile does not show a monotonous S-shape, as the temperature curve in the separation stage area of the column takes a different curve due to the medium boiling components. From the ninth separation stage onwards, the heavy-boiling iron(iii) chloride predominates. As a result, the temperature curve changes again from this separation stage onwards, as is typical of the heavy-boiling component. After the local maximum, the mole flow decreases and reaches a global minimum of 0.24 mol/s in the ninth stage. As the number of stages increases, the molar flux increases again to 0.3 mol/s in the fourteenth stage.

Comparing the models TRC-O/M and TRC-C/S it can be seen that the slope of the separation curve of the medium boiling components titanium tetrachloride and vanadium tetrachloride is almost the same for each separation stage (visible in the range of separation stages 5--12). This can be explained by the similar relative volatility values between 1.1 and 1.6 and similar boiling points of the pure substances of 409.5 K for titanium tetrachloride and 421.0 K for vanadium

tetrachloride. Here all the curves shown in Fig. X between the two models shown are in excellent agreement with each other. Both models reproduce almost exactly the same separation results, which shows that the Octave/Matlab models are able to simulate even complex mixtures very well compared to the professional software ChemSep Lite, which requires much more pure component data, since for the Octave/Matlab model nearly only vapour pressure data are necessary for a successful simulation of such a total reflux column with complex multi-component substance systems. Slightly larger deviations are only seen in the separation profiles of the medium boiling components with increasing number of stages due to the propagation of deviations between the two models. In the representation of the mole flow curve, the deviations are larger due to the different evaluation of the enthalpies for both models, as already indicated for the separation examples in the previous section. Apart from the ninth separation stage with a slightly larger deviation, the temperature profile is also correctly represented by the simulation results of both models.[5]

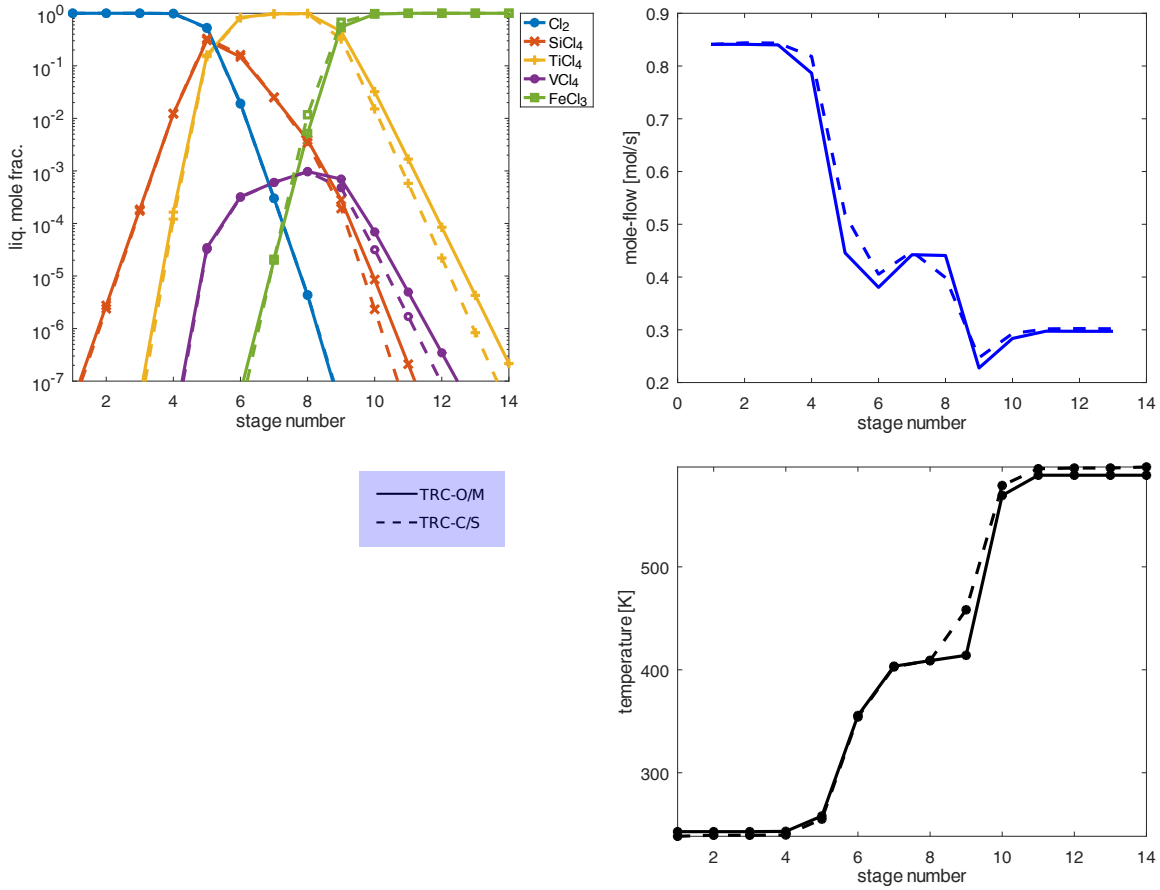

Figure 26: Comparison of the simulation results of the Kroll process

In order to compare the experimental results from[12] with the simulation results, it can be shown in the following on the basis of another simulation example that the VLE behaviour of the

[5]In summary for the comparison of Octave/Matlab and ChemSep Lite models, the comparison of the application of the simulation models shows the excellent applicability of the TRC-O/M model for the simulation of more complex substance mixtures under ideal phase equilibrium relationships. Although significantly less material data is required, the TRC-O/M model can be robustly applied to the development of separation processes in the distillation of spent fuels.

five-component mixture behaves very similarly to an ideal phase equilibrium behaviour without significant deviations from Raoult's and Dalton's law if chlorine is not considered as a substance component to be separated. As a substitute, a similar four-component mixture without chlorine is now simulated using the data on the feed state from [12] for "Lot-1" in Tab. (2) (of [12]) and the experimental distillation results for the laboratory column at very high reflux ratios in Tab. (5) (of [12]). The data are summarised in Tab. (11). This mixture is also excellently suited for simulation purposes as a substitute example for the representation of subsystems in nuclear fuel processing, in which a predominant tetrachloride component, namely uranium tetrachloride with 95-98 mass % (also known as weight %), is also present as a feed with further fission products (e.g. rare earths) or actinides (e.g. plutonium or neptunium) as tri- or tetrachlorides with preliminary neglect of di- and monochlorides. When considering a six-stage separation column (including the evaporator as an additional separation stage), as analogously used in [12] for the industrial column as a pilot plant, this column condition can be simulated very well with sufficient accuracy with a total reflux column at high reflux ratios. Deviations between experimental results and simulation results therefore only result from the differences in activity according to equation (27) for phase equilibrium behaviour between ideal and real phase equilibrium behaviour and from possible deviations caused by the numerical solution procedure compared to the distillation experiment according to [12] for laboratory column distillation.

The comparison of the simulation results with the experimental results according to [12] shows in Fig. (27) the good agreement of the simulation results between TRC-O/M and TRC-S/L also for this example. It can also be seen that for the main components silicon and titanium tetrachloride the separation behaviour is very similar to the experimental results. This shows that this zeotropic partial mixture must also behave very similarly to the ideal behaviour close to $\gamma_i \approx 1$, because almost exactly these separation limits are reached in the experimental case according to the presented results (experimental results according to [12], TRC-O/M and TRC-S/L). Only for ferric chloride and vanadium tetrachloride are there larger deviations, otherwise, according to the experimental results for vanadium tetrachloride, the distillation area should be concentrated in the opposite direction to the evaporator and there should be a measurable proportion of ferric chloride in the bottom product.

Thus, for this simulated mixture essentially for silicon and titanium tetrachloride, it is impressively shown that in both simulation models practically only the vapour pressures are sufficient with a simple model approach to be able to simulate complex mixtures under ideal phase equilibrium conditions. Compared to the very large deviation behaviour of the real measured equilibrium results of the $TiCl_4$-$AlCl_3$ mixture according to section (3.2.1), it is shown that for representative mixtures with uranium tetrachloride, the interaction behaviour does not necessarily have to show large deviations with respect to this similar comparable substance mixture with similar degree of chlorination of involved substances. This is also illustrated by the interaction behaviour with the mixtures of uranium tetrachloride and lanthanum trichloride, as they occur representatively in the case of the distillative treatment of spent fuel recovery in section (3.2.2) and the simulation results according to subsection (D.1), where the mixtures are zeotropic, but also not so far away from the ideal phase equilibrium behaviour condition of the VLE (if not too high separation accuracies are required, as conclusively shown in this example for the Kroll

process according to [12] and the re-simulation). Furthermore, according to [4], as also mentioned in section (3.2.1), the binary subsystems $SiCl_4$-$TiCl_4$, $SiCl_4$-VCl_4, $TiCl_4$-VCl_4 are known to be strictly zeotropic mixtures, except for iron(III) chloride. In this range of possible interaction behaviour s, such a separation behaviour can be expected for nuclear fuel processing when considering binary uranium tetrachloride systems.

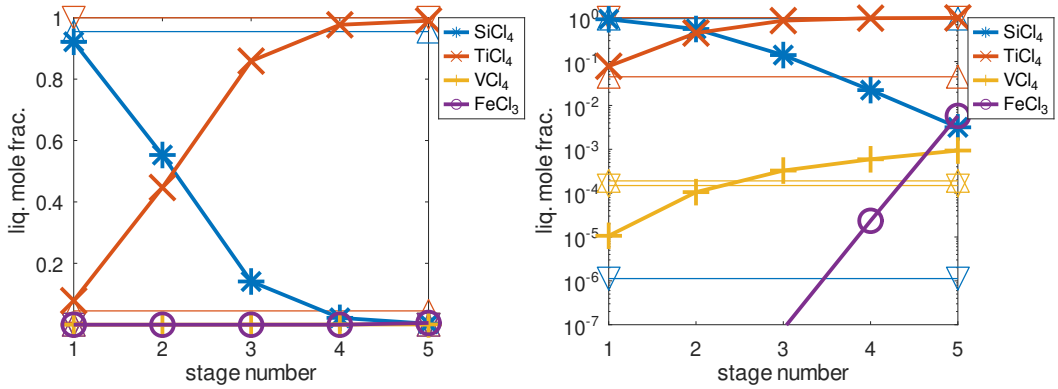

(a) Comparison between TRC-O/M and experimental results: (right in logarithmic scale)

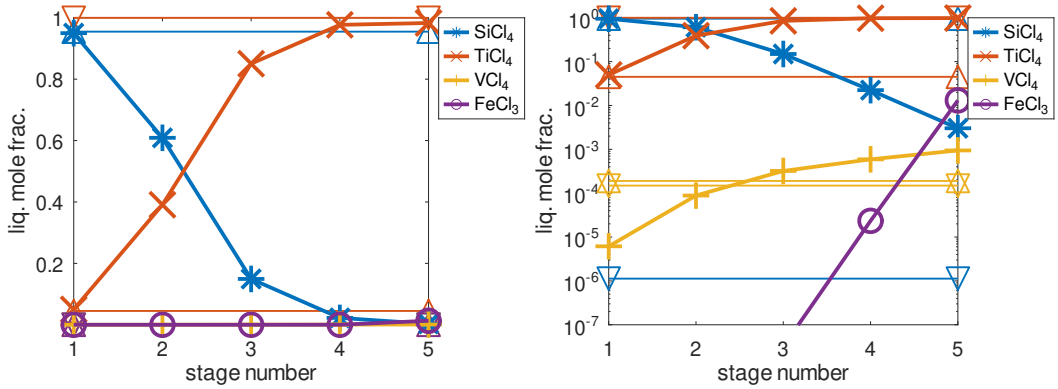

(b) Comparison between TRC-C/L and experimental results: (right in logarithmic scale)

Figure 27: Comparison between experimental and simulated results for a high reflux laboratory distillation column according to [12] for the composition "Lot-1" used in Tab. (11). The boundaries marked with an upward arrow in the thinner lines show the experimental results according to Tab. (11) as the top product composition and with a downward arrow as the bottom product.

Table 11: Experimental results in [12] in wt% for “Lot-1” of laboratory distillation column for fractionation of commercial titanium tetrachloride. Source of data: see [12].

Component	Feed	Top product (2-wt%)	Bottom product (93.4-wt%)	Residuals (3.3-wt%)
$TiCl_4$	97-98	5.0	99	99
$SiCl_4$	1.5-2.5	95.0	Negligibly small	Negligibly small
V as VCl_4	0.06	0.0215	0.015	0.015
$FeCl_3$	0.002	Negligible	Negligible	Not specified
Cl_2	0.03	Not specified	Not specified	Not specified

In conclusion, it can be said that for process development of distillation-based separation

processes, the calculation with ideal phase equilibrium behaviour using the Octave/Matlab models, as well as the simulation as simplified zeotropic mixtures, is reasonable as far as is known from the literature for representative mixture examples such as those used here. Therefore, in the next section and in the conceptual design part of this thesis, Octave/Matlab based models will be used, assuming ideal phase equilibrium.

5.3 Simulation of separation of non-chlorinated solids, gases and volatiles

This section deals with special situations for the separation of on the one hand highly volatile dissolved gases and volatiles and on the other hand non-volatile solids, such as non-chlorinated oxide or metal material of precious and refractory metals, which can occur during distillation under simplified ideal physical equilibrium conditions and a conceptual design of a separation plant. For the solids separation, the Octave/MATLAB distillation models were used, in which the otherwise usual phase equilibrium relationships according to equation (27) for the description of VLEs are replaced by SLE equilibrium conditions according to equation (20) for SLEs. In this way, concentration separation units for suspension melt solutions and crystallisers are simulated with these models.

In addition to the simulation results in the Appendix for the first section of the total reflux column, the decay heat effects in the distillation column are investigated in detail and the heat input per separation stage is determined. Simplified, it is assumed that, as in a continuous distillation column, the heat production is approximately in equilibrium when the continuous product is withdrawn, which is the case here. Sufficiently assured heat removal of decay heat is an important safety feature that should be mandatorily estimated for distillation based on the circulation of material components within the column on test mixtures with active elements contributing to the decay heat of each active isotope. Knowledge of the heat accumulation in the column also allows conclusions to be drawn about the cooling required and, where appropriate, the use of the active components as so-called active heat generating elements in the evaporator of a distillation column.

In this section, impurities are defined as dissolved gaseous or solid components that can be considered as suspended or dissolved in the molten salt after chlorination. These can be oxides, metals, precious metals or noble gases, but also highly volatile chloride components, some of which have boiling points well below 500 K. The highly volatile chlorides would cause practical problems in distillation, as many of the chlorides may be metastable in some phases, as in the example of selenium chlorides in the system $SeCl_4$(s)-Se_2Cl_2(l,g)-$SeCl_2$(g)-Se(s,l,g)-Cl_2(g). Other volatile chlorides may be formed, for example, by tellurium, antimony, niobium or tin chlorides in stable or metastable form. Therefore, after chlorination, such volatile chloride compounds should be separated at the lowest possible temperatures. Since uranium tetrachloride is often present in very high proportions in the salt mixture for most nuclear separation problems, the separation process of these volatile components should be carried out slightly above the melting point of uranium tetrachloride to prevent the melt from freezing. Unfortunately, the vapour pressure of uranium tetrachloride in the liquid phase is already relatively high and, under these conditions and circumstances, significant amounts of uranium tetrachloride are also present in the vapour phase. Therefore, the idea is to separate the volatile chlorides in two separation steps by

flash evaporation and subsequent condensation before using the main distillation if technically or theoretically feasible. In this process, the volatile components, including uranium tetrachloride, can first be removed via the vapour phase of flash evaporation at higher temperatures and then condensed out in the subsequent condensation unit at low temperatures (far) below the melting point of uranium tetrachloride. Only the volatile chlorides remain in the vapour phase in the second separation step. Therefore all volatile chlorides present in the original salt mixture are then completely separated.

Another issue is the earliest possible separation of solids. Non-chlorinated dissolved or suspended solids should not enter the distillation column stages to prevent crystallisation and mechanical blockage. Suspended salt melts can also increase the viscosity of the liquid phase. This also makes it necessary to separate such substances as early as possible before using distillation as the main separation step in this thesis. The advantage of these non-volatile materials is the different polarity compared to the chlorides, in which it should form miscibility gaps even the different polarity properties of these species compared to the chlorides. So the idea is to concentrate the melt step by step and possibly evaporate a little. This step can be combined with the previous separation step of volatile separation by phase change of the dissolved volatiles into the vapour phase. It can be assumed that the solids, as practically non-volatile components, cannot pass into the vapour phase, but only a few volatile chlorides and the volatile components themselves. In addition, the solubility of any dissolved solid components is significantly reduced by the evaporation of the chlorides and these components crystallise out of the melt. Since the melt contains only small amounts of solids, the amount of concentrated melt is much less than the original mixture. After concentration, these residual chlorides from the separated filtered solids can then be evaporated in a type of furnace unit at high temperatures of around 2000 K in the hot exhaust gas stream of a hot argon atmosphere stream. In this case there is even the possibility of a continuous operation variant using conveyor belt technology, where the melt is continuously fed into the furnace type and the remaining solids without chlorides are conveyed out after sieving and/or filtration. Other alternative methods for handling solids are described in detail in an experimental tech report in [85] regarding such solids in nuclear waste material, e.g. molten salts.

The above-mentioned preseparation processes prior to the actual main distillation of the molten salt are simulated in a simplified manner under ideal phase equilibrium conditions using the SSD-O/M and SSD-C/S models. For the separation of the highly volatile chlorides, the following test mixture $SbCl_3$-CsCl-$PuCl_3$ (boiling point of antimony trichloride 496.6 K compared to cesium chloride at 1573 K) with the composition vector $[0.083, 0.250, 0.667]^T$ is used for simulation. The feed mole flow here is 0.1 mol/s. The argon supply here allows the formation of a larger gas phase in which the antimony trichloride component can preferentially pass into the vapour phase. In addition, the argon supply is used to spray the liquid into the flash chamber to favour the exchange surface for mass transfer to the vapour phase.

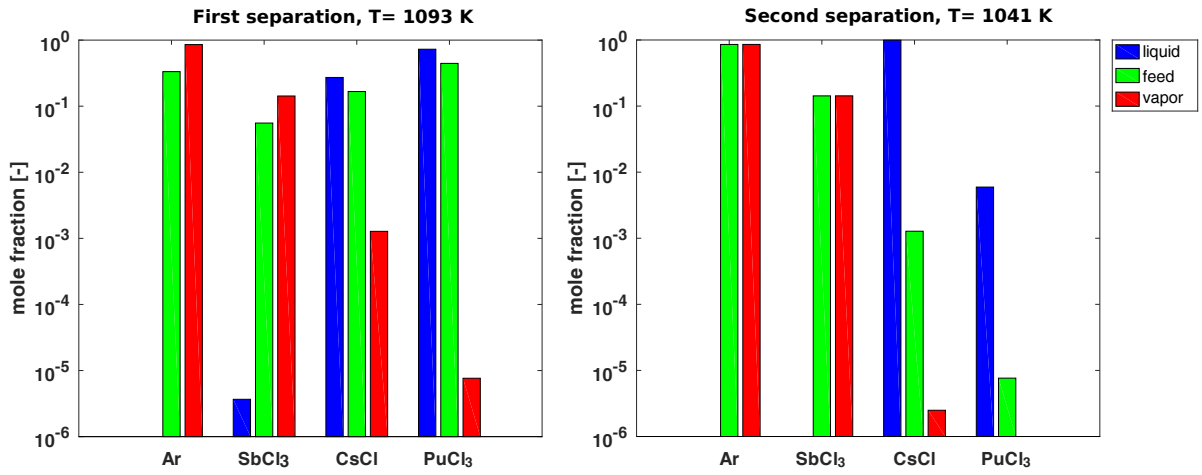

Figure 28: Simulation results for the separation of highly volatile $SbCl_3$ from the ternary mixture $SbCl_3$-CsCl-$PuCl_3$ at temperature T in the argon gas stream supplied at 1 atm.

The simulation results for flash evaporation and condensation are shown in Fig. (28) . At the optimal operating temperature of the first separation of 1093 K, the simulation results according to Fig. (28) (left figure) show that antimony trichloride occurs only in negligible amounts of 2E-04-mol% in the liquid phase (left partial bar shown in blue for $SbCl_3$). Thus, the majority of the antimony trichloride passes into the vapour phase (right green middle bar of $SbCl_3$ shown in red). Due to the higher operating temperature, some of the cesium chloride passes into the vapour phase, although the majority remains in the liquid phase (left blue bar for CsCl). The proportion of plutonium trichloride in the vapour phase is considered to be very low, passing through the vapour phase with a mole fraction value of 1E-03 mol%. Nevertheless, plutonium trichloride should be virtually completely separated from the volatile antimony trichloride component below the ppm separation range. The separation of cesium chloride and plutonium trichloride in the next separation step is simulated as pure condensation within the separation chamber with the simulation results in Fig. (28) (right figure). While antimony trichloride remains in the vapour phase, only a negligible amount of cesium chloride (of about 2E-04-mol%) is present in the vapour phase at 1041 K. Otherwise, cesium chloride and plutonium trichloride are condensed out of the vapour phase, as shown in the simulation results in Fig. (28) (right figure) (blue bar on the left for each component). The remaining argon-antimony trichloride gas flow is then only 0.038939 mol/s.

Fig. (29) shows the simulated separation result at 1093 K and 1 atm for flash evaporation when 10 mol% solids are added to the original mixture in the original antimony trichloride - cesium chloride - plutonium trichloride mixture. It is assumed that the melt contains 5 mol% rhodium, 4 mol% technetium and 1 mol% uranium dioxide. The vapour pressure of the solids is so low that no fractions are observed in the vapour phase, as can be seen in the plotted simulation results. In fact, all the solids remain in the liquid phase. The concentration of the solids rhodium, technetium and uranium dioxide in the melt is simulated via concentration and crystallisation with nine separation repetitions of crystallisation and sieving (at 1093 K and 1 atm). The separation results are shown in Fig. (30), with concentration starting in the first separation stage of the liquid feed and neglectable solid amount but available solid fraction.

From the simulation results it can be seen that all the solids are completely removed from the liquid phase in a few required separation steps (also further defined as separation stages) and the proportion of solids in the concentrated phase increases. The amount of solids will be different for each separation stage. The simulation shows that uranium dioxide is separated in the second stage, followed by technetium in the sixth stage and rhodium in the eighth stage. Since in the simulation model the solids are concentrated for each separation stage, the uranium dioxide component in the solid phase is virtually absent from the fifth separation stage onwards. As rhodium remains as the last component in the solid phase, the proportion of rhodium in the solid phase increases. From the ninth stage onwards, the separation of the solids can be considered to be complete, as there are virtually no solid components left in the liquid phase. The simulation results have thus successfully demonstrated the concentration and crystallisation of the solids. The separation of the volatile components has been shown in the previous analysed separation task in Fig. (28).

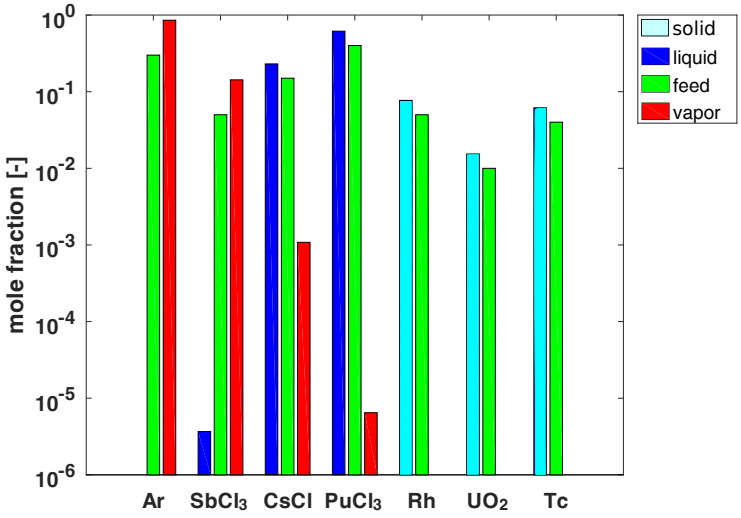

Figure 29: Simulation results for the separation of high volatile $SbCl_3$ from the $SbCl_3$-CsCl-$PuCl_3$-UO_2-Tc-Rh in the fed argon gas stream at 1093 K and 1 atm

The evaporation of the remaining chlorides from the solids separation can then be easily achieved by setting the temperature above 2000 K, although due to the very low vapour pressures of the solids, a transition to the vapour phase is practically impossible.

Another process idea is to carry out the concentration steps and solids removal discontinuously directly in the evaporator of a distillation column, where the solids are concentrated directly in the salt melt of the evaporator. However, the solids then have to be removed manually. Since everything should take place in the closed total reflux system discussed above, such a conversion in an evaporator of a distillation column is even more difficult to implement and integrate. Finally, the solids separation should be considered as a separate separation unit.

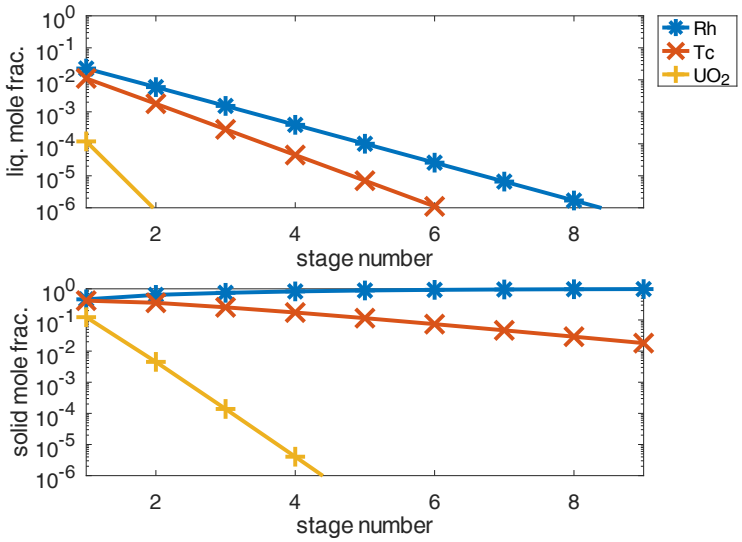

Figure 30: Simulation results of the concentration & crystallisation of solid impurities at an average temperature of 1093 K and at 1 atm.

Within the developed process of volatile and non-volatile separation in two single-stage separation units, all aspects for the basic conceptual design of spent fuel processing have been shown, so that the conceptual separation design can be developed. Since the distillation and preseparation can withstand some variability, at most a minor modification is required to also purify HWL and DFRm material by distillation, as shown in the Appendix after section (C.1.1). In fact, as the results in the appendix will show, no significant modification at all is required.

Part IV
Conceptual design of distillation-based processing for various nuclear waste materials

This section deals mainly with the reprocessing of spent nuclear fuel (SNF) from spent fuel elements, including all other additional separation units and steps required, such as the self-designed distillation-based cladding material recycling and waste gas treatment according to the Linde process (compare e.g. [137]). Using appropriate simulation models, a separation concept has been developed under ideal phase equilibrium conditions and ideal assumptions. The application of the developed separation process to other nuclear waste, such as high-level waste (HLW) from other reprocessing activities, is further investigated and discussed in the appendix in the section (C). The appendix also discusses the recovery of DFRm fuel with the same developed distillation-based conceptual distillation design shown, but under different process conditions. Furthermore, the applicability of distillation for the reprocessing of DFRm material is also simulated and its results are subsequently discussed in detail, including the point of integration and even possible mixing of different wastes, and it is shown that this is possible with the same conceptual separation design.

6 Process development of the main separation concept

Examples of nuclear distillation for SNF (re)processing, HLW recycling and DFRm fuel recovery can be applied to a single, independently developed separation concept in the context of the overall distillation-based SNF (re)processing concept. The section (C) with HLW and DFRm separation, while subsequent sections as central parts of this thesis deal with the basic SNF distillation-based separation processing concept. The simplified basic flow chart for this is shown in Fig. (31). With the exception of fuel chlorination, off-gas treatment and zirconium cladding material recycling, the separation process should operate at atmospheric pressure of about 1 atm.

The main flow chart The main focus in this chapter is on SNF processing. In the mechanical separation unit, the cladding material is separated from the SNF fuel under an argon atmosphere. In the conceptual design, the cladding material is crushed and the fuel is ground, e.g. in a ball mill, to a powder with a preferred mean particle size of 5 μm. The chlorination of the cladding material is carried out with chlorine as the oxidising agent, since the cladding material is based on metalloids and is therefore easier to chlorinate than the oxide SNF fuel. The oxide SNF fuel, which consists mainly of oxide material, essentially uranium oxide, is chlorinated over hydrogen-free chlorocarbons (fully chlorinated carbon compounds), preferably as a carbon tetrachloride-chlorine mixture. All chlorination steps are exothermic. A recommended chemical reaction concept with the use of a plasma flame is also theoretically conceivable for such oxide components in the SNF fuel in order to achieve high product yields. Concepts recommending chlorination-based burner concepts are recommended in [29, 127].

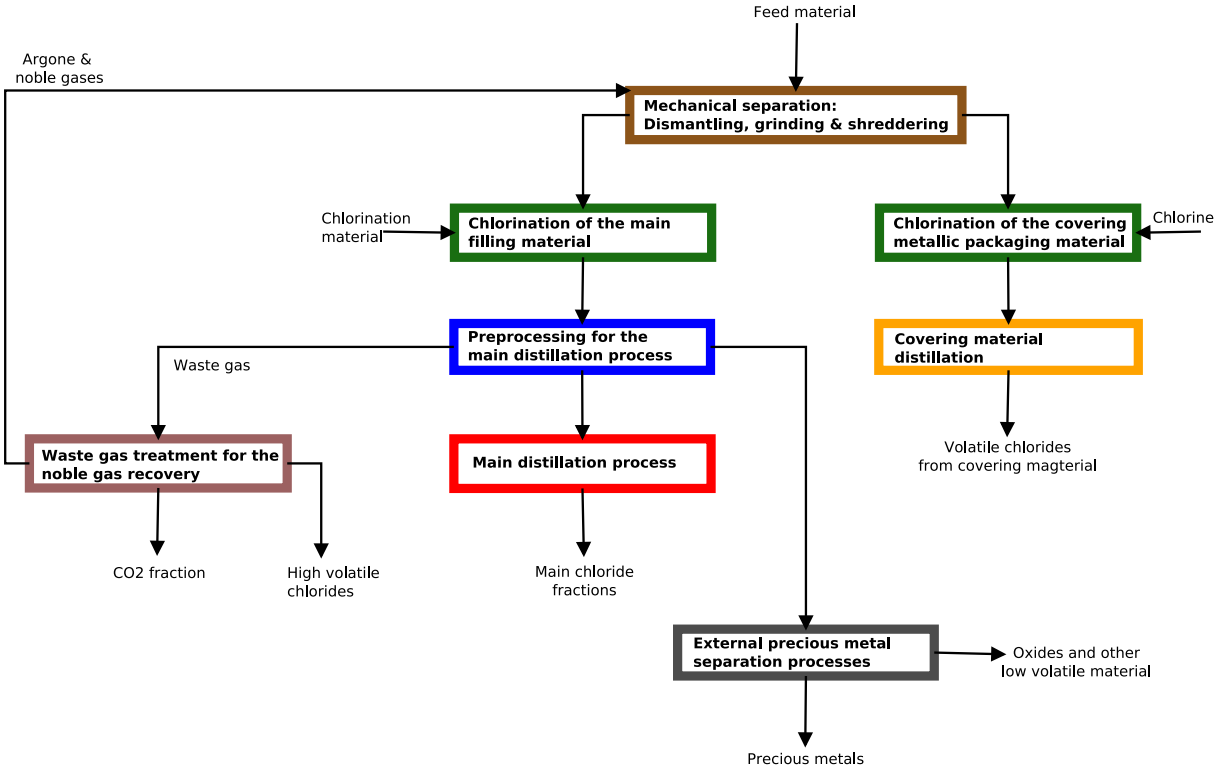

Figure 31: The generalized basic flow chart of distillation-based nuclear waste recycling

However, higher pressures are required for distillation-based cladding recycling. The material basis of the cladding material is based on zirconium of suitable zirconium alloys, in which zirconium tetrachloride is predominantly produced during chlorination for the distillation concept by chlorination for cladding material recycling. High pressure distillation separation processes are used to separate zirconium and the materially chlorinated cladding material zirconium alloy components by distillation. Higher pressures are required because zirconium tetrachloride as a pure substance does not have a liquid phase after chlorination below 1 atm. As the triple point of zirconium tetrachloride is 22.36 bar and 710 K, the pressures for distillation must be above the triple point in order for the zirconium tetrachloride to become liquid in the pure state required for separation.

For the chlorination of the SNF fuel, the process effort is increased not only for the chlorination of the oxide material, but also for the chlorination of some reaction components in order to achieve high chlorination product yields, whereby some residual precious metal components cannot be chlorinated, which is still conceptualised in this developed separation concept. Fortunately, however, the main component of the SNF fuel material is the potentially distillable uranium oxide, mainly present as uranium dioxide, which makes up on average at least 95 mol% of the SNF material (see [29]). The remaining 5 mol% are fission products in metallic or oxidised form. Therefore, chlorine is also required for the chlorination of the SNF material in the form of a carbon tetrachloride-chlorine mixture. In the calculation of the required chlorination step according to [29] for the volatilisation of the fuel material required for the application of distillation, the chlorination of uranium dioxide was assumed as the main focus, which could theoretically be realised in a type of plasma burner or a pulverised fuel combustion chamber. After chlorination, solid components of metals (refractory or noble metals) and oxides (mainly from the remaining

non-chlorinated feed material) remain in the chlorinated molten salt SNF material in dissolved or suspended form, as well as dissolved associated residual gases and volatile chlorides. Separation of these components should be carried out relatively early in the developed distillation process in a preseparation unit to obtain pure distillable molten salts, as described in detail in section (5.3) on the test mixture. This section also explains in detail the separation procedure for these components. In addition, volatile chlorides and volatile residual components (e.g. iodine, xenon and others) separated with the noble gas stream enter the off-gas treatment stage, where first the chlorides are condensed out and then the noble gas components are separated from each other by distillation in a noble gas treatment unit according to the Linde process (see among others [137]).

After the pre-treatment and preseparation steps required in the separation design for the use of the main distillation, the modified total-reflux distillation column principle proposed in section (31), as shown in red in Fig. (5.2), was used. In this part of the conceptual design, the chloride components are distillatively separated as sharply as possible. The column is operated in two process stages as a closed total reflux column, an idea from the previous chapter Conceptual Design Idea for Using SNF Distillation and Subsequent Safe and Even More Efficient Distillate Removal. The basic process idea without process simulation is still available in [47], but is slightly modified in this developed separation process by process simulations of each separation unit and within the designed total reflux column principle idea by cyclically repeating PPCs (Progressing Process Cycles). In a PPC, first the product feed and then the distillation takes place analogously to a discontinuous separation column, without influencing a favoured total reflux principle as the main column operating condition. In the final stage of a PPC, the distillate accumulated in the total reflux mode of a separation stage is then withdrawn without the need to change operation or shut down the entire separation column operation. In the discretely repeated operation of the respective designed distillation column process scheme, the fractionated distillation products are obtained with separation fractions that are as pure as possible, but also with transitional mixed fractions, whereby the mixed fractions can also be reused in the next batch of the column to be distilled. In this way, only a small amount remains in the column until the end of the entire lifetime of the column.

6.1 Conceptual design of a distillation-based SNF recovery

For simulations and calculations of complex SNF reprocessing mixtures, the detailed composition vector[6] is required. For the fission product composition in SNF material the thermal fission data of only U-235 in [35, 138] and in [139] have been used for the simulations required for the process development. Data from [139] for SNF waste have been specialized used for more precise estimation of the fission product vector of fuel material. Data for other actinide compositions involved are also taken from [139].

[6] The SNF material to be reprocessed is present in pellet form, mainly as oxide in fuel elements, as also described in [13]. The fuel consists mainly of uranium dioxide with a fraction of 95-98 mol%, depending on the fraction of fissile material. This fissile material fraction is limited to a maximum of 5 mol% as an upper limit for the accumulation of fission products in the solid fuel of today's solid fuel reactors [13].

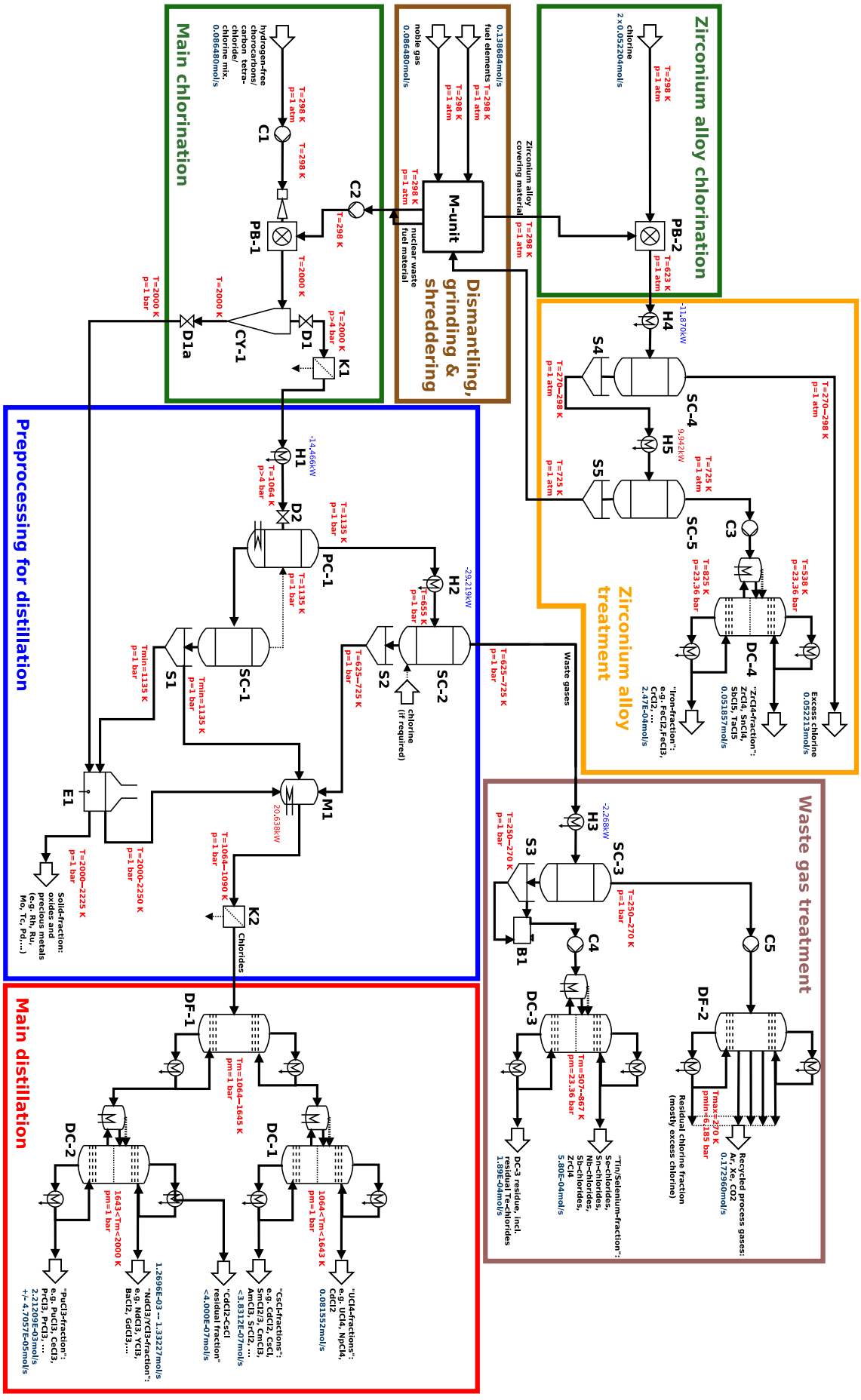

Figure 32: The main flow chart of the distillation-based SNF recovery

The separation process theoretically developed for this thesis is shown in Fig. (32), which is based on the flow chart separation idea of [47] and shows all relevant process conditions as well as all incoming and outgoing process flows. The separation plant should be capable of processing at least 1000 t/a with a maximum of 5 assumed maintenance days of plant downtime due to possible maintenance. The cladding material consists of a zirconium alloy with a clear predominance of metallic zirconium, as described in [15, 16]. So the mass fraction of zirconium cladding material relative to the amount of fuel material can be estimated from the geometric dimensions and shape of these fuel elements according to [16, 29] and is 0.37801. The total fuel input to the SNF reprocessing plant is estimated to be 0.138684 mol/s. In addition, the fuel mole flow feed is only 0.086480 mol/s and the zirconium mole flow is 0.052204 mol/s. The chlorination of the fuel is equimolar, with the same molar ratio of fuel to chlorinating agent. To ensure the exclusion of atmospheric oxygen, an argon inerting atmosphere is required for the fuel reprocessing, neglecting argon losses to the environment. The chlorination of the zirconium cladding material should also be equimolar, assuming pure zirconium and chlorine for chlorination. It is recognised that in practice the exact composition in the zirconium alloy may also vary. Given the defined recovery specification of 1E-04-mol%, the remaining molar fluxes can be determined by mass balance and all leaving process fluxes are shown in Fig. (32).

All other process conditions, process flows, heat supply and removal flows are also included in this flowchart. Note that the pressures pm in the flowchart refer to required minimum pressures, but are not set exactly to this value. Higher pressures would then be required for operation, such as for the separation of zirconium tetrachloride in the high-pressure columns DC-3 and DC-4 in which 23.36 bar as the minimum specified pressure corresponds exactly to the triple pressure of zirconium tetrachloride. The other explanations and following symbol labelling convention is chosen in the flow chart diagram of Fig (32):

- Separation-specific units:
  - DC-1–DC-4: Distillation column operating in the special total-reflux separation principle mode with PPCs as explained in section (5.2) of chapter (III),
  - DF-1–DF-2: Continuous fractionation column with possible side stream take-offs,
  - EV-1 or E1: Furnace with argon inerting (E1 simple design, EV-1 (not proposed as a variant in Fig. (32)) in continuous process in hot argon flow),
  - PB-1–PB-2: Chlorination units (PB=Plasma burner or fluidised bed),
  - PC-1: Single phase separator according to flash evaporation principle,
  - SC-1–SC5: Phase separator of a required condensation, crystallisation or concentration process step.
- Additionally necessary process units:
  - M-unit: Mechanical dismantling of the fuel elements to remove the fuel from the zirconium cladding, including grinding and crushing stages (see: [29, 37]),
  - SR-unit (For simplification of flow chart view, not explicitly shown in Fig. (32)): Electrolysis and chemical precious metal separation processes for separating precious metals from oxides, including recycling of the oxides to the renewed chlorination unit,

– PP-unit (For simplification of flow chart view, not explicitly shown in Fig. (32)): Possible necessary postprocessing steps.

- Necessary accessories:
  - B1–B2 (For simplification of flow chart view, not explicitly shown in Fig. (32)): Temporary storage in containers: in B2 this is theoretically replaceable by the system of M1 and K2,
  - C1–C5: Compressors and pumps,
  - D1,D1a,D2: Throttles and pressure relief valves,
  - H1–H5: Heat exchanger,
  - K1–K2: Retention device for solids, for example by means of retention sieves,
  - M1: Mixing unit as static mixer,
  - S1–S5: Concentration, enrichment or sedimentation tanks or vessels.

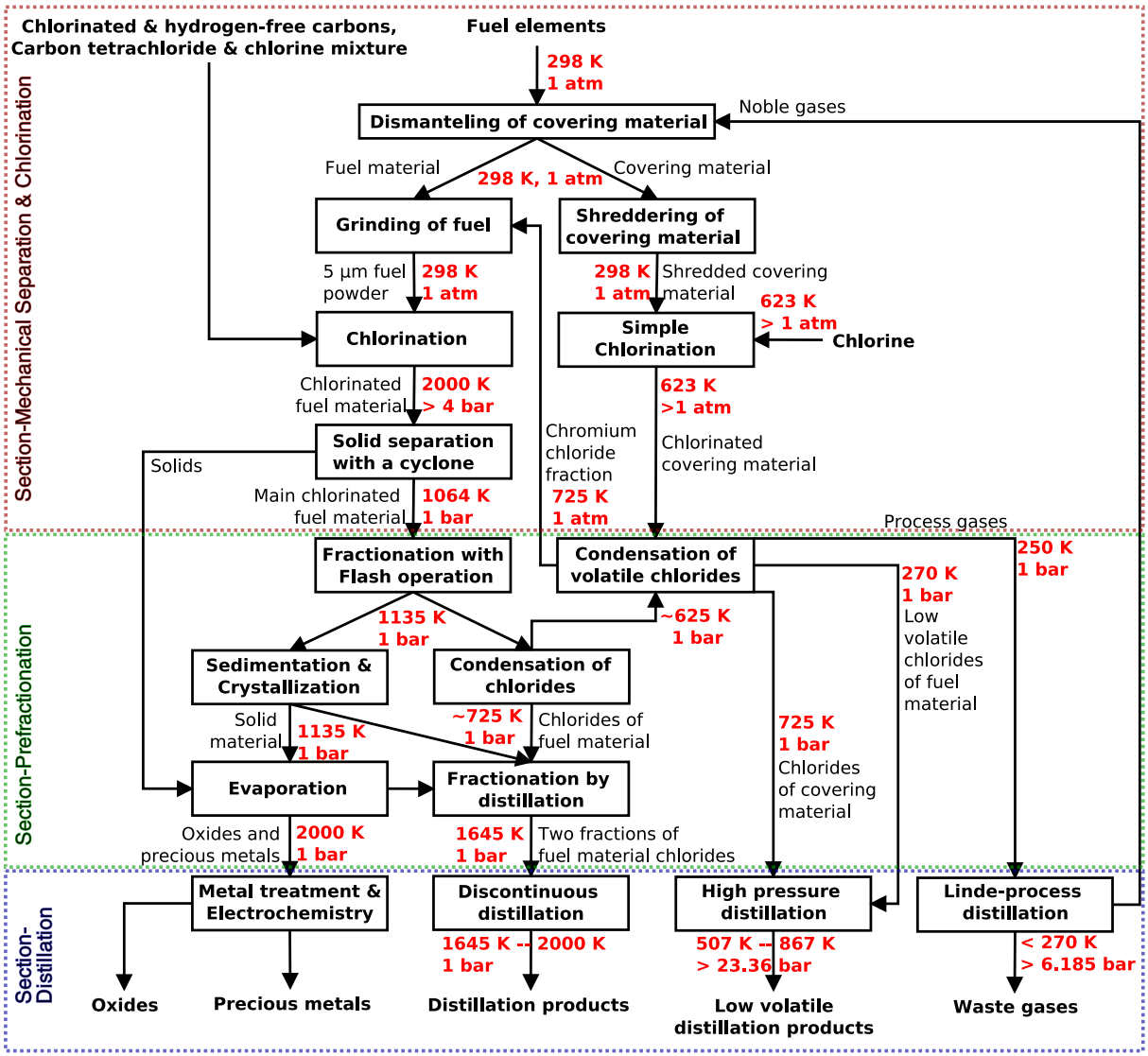

Figure 33: The detailed basic flow chart of distillation-based nuclear waste recycling, Ref.: [13]

In summary, the separation process developed comprises the necessary separation processes shown in Fig. (33), divided into three process areas:

1. Section mechanical separation and chlorination,
2. Section prefractionation,
3. Section distillation.

The condensation units are shown in Fig. (33) as a single separation unit.

In order to use a distillation-based separation process, the fuel and cladding material must first be mechanically separated. This involves removing the fuel material from the cladding material and further grinding it into powder. The cladding material is shredded. A concept for mechanical separation (preconditioning) is described in [29] (p.29 - 35) and includes the separation of the cladding material from the fuel. The fuel is ground in a ball mill to a mean solid particle size of $5\,\mu$m, corresponding to spherical solid particles of the same size. The cladding material, on the other hand, has to be coarsely crushed in the millimetre range. The particle size distribution is particularly important for the chlorination of the fuel material, since the rate of the macroscopic chlorination reaction in the selected chemical reactor is decisive, and the chlorination processes are strongly dependent on time and particle size in relation to the product yield. The particle size of $5\,\mu$m has been determined in the calculations to allow chlorination in PB-1 (as shown in Fig. 32) in continuous flow plasma burners or in discontinuous fluidised bed pulverised fuel combustion chambers. There, the oxide compounds are to be broken down in order to chlorinate the corresponding elements via a suitable chlorinated carbon-chlorine mixture, a preferable carbon tetrachloride-chlorine mixture, in order to obtain a fully chlorinated metal salt with high product yields. For the chlorination of uranium with carbon tetrachloride, the following reaction takes place

$$\mathrm{UO_2}(s) + \mathrm{CCl_4}(l/g) \rightarrow \mathrm{UCl_4}(V) + \mathrm{CO_2}(g). \tag{98}$$

First, it should be noted that under normal conditions in the range of 1000 K, despite a strongly negative enthalpy of reaction, chlorination to high product yields of uranium dioxide is still not possible according to (among others). The reason for this, according to [140], is that no diffusion and reaction to carbon dioxide can be assumed to take place due to the lack of desorption capacity of oxygen in the present crystal structure of uranium dioxide. This is the reason for choosing a type of plasma combustion with small particle sizes of about $5\,\mu$mand process ambient temperatures of 2000 K and higher process pressures or chlorination in fluidised beds.

Secondly, uranium tetrachloride should be obtained as the only uranium chloride component in the chlorination process, as this is the result of the process design presented here. It would be problematic to remove the volatile, simplified, thermally stable penta- or hexa-chloride uranium compounds together with the volatiles to be separated in the first preseparation step. Less volatile uranium trichloride would in addition accumulate in the heavy boiling fraction together with other actinide and lanthanide trichlorides and would significantly increase the separation flow for the distillation problem, since almost 95 mol% of the fuel is assumed to be uranium. In addition,

the separation of the uranium trichloride is between that of americium and plutonium trichloride, and also the relative volatility values show this, so the differences between the volatilities of the components would be much smaller compared to the quite optimal uranium tetrachloride with very high relative volatility compared to the trichloride component species.

In the chlorination of uranium dioxide, it should be noted that uranium chloride can exist in four possible chlorination states from tri- to hexachloride. Thus, the process temperature is chosen to obtain mainly the tetrachloride component in very high proportions of the total bound uranium after chlorination. However, this may include some oxochloride bonds as mixed oxychlorides of the form $\mathrm{UO}_n\mathrm{Cl}_m, n, m = 1, \ldots, 6$ (compare: [141]) as well as more complex $\mathrm{UO}_{n_1}Cl_{n_1 \cdot n_2}, k = 1 \ldots 3, n = 3 \ldots 6$ compounds possibly formed by chlorination with chlorine and carbon tetrachloride. However, the formation of thermally stable oxochlorides and $\mathrm{U}_{n_1}\mathrm{Cl}_{n_1 \cdot n_2}, k = 1 \ldots 3, n = 3 \ldots 6$ compounds at high temperatures up to 2000 K is still partly unclear. But it can be assumed that these compounds, especially the uranium chlorides $\mathrm{U}_{n_1}Cl_{n_1 \cdot n_2}$, cannot be thermally stable at these high process temperatures during chlorination. Indications for this can be obtained from the data of the standard reaction enthalpies and the temperature-dependent free molar enthalpies of formation and linearly extrapolated to 2000 K (cf. e.g. [14] pp. 1750-1751 for UOCl, UOCl_2, UOCl_3, $\mathrm{UO}_2\mathrm{Cl}_2$ for the oxochlorides and [18] (p. 404) for $\mathrm{U}_2\mathrm{Cl}_8$, $\mathrm{U}_2\mathrm{Cl}_10$).

In order to obtain particularly high yields of uranium tetrachloride only for the chlorination of uranium dioxide, an equimolar ratio of pure carbon tetrachloride to uranium dioxide is therefore recommended. Carbon tetrachloride does not necessarily have to be thermally stable for chlorination at high temperatures up to 2000 K for the reaction to occur, but the ratio of carbon for the formation of carbon dioxide and chlorine for the formation of uranium tetrachloride is important in the reaction. It is much more difficult to use carbon and chlorine in the correct proportions as explained in [127]. However, in addition to the chlorination of uranium dioxide with carbon tetrachloride, chlorine gas is also required as a chlorinating agent for the other components of spent fuel. In addition, chlorine is an important component as a process gas for chlorination in a type of burner or fluidised bed. Simplified calculations with chlorine on the reaction equilibrium network of the equilibrium system Cl_2(excess)-UCl_6-UCl_5-UCl_4-UCl_3 via the Gibbs free molar reaction enthalpy estimation $\Delta g_R(T) = \sum_{i=3}^{6} \nu_{\mathrm{UCl}_i} \Delta G_{f,\mathrm{UCl}_i}(T)$ from the tabulated temperature-dependent data of the free molar enthalpies of formation of the components $\Delta g_{f,\mathrm{UCl}_i}(T)$ according to [14] already show that at high temperatures up to 2000 K uranium tetrachloride is clearly preferentially formed (see Fig. (34)). In contrast, the corresponding Gibbs reaction enthalpies for uranium tri- and hexachloride are positive in Fig. (34) and are unlikely to be formed as expected in real experimental studies. As the temperature decreases, the negativity of the chlorine excess to the reaction enthalpy of the corresponding uranium tetrachloride component decreases. For uranium hexachloride, the positive value decreases significantly from 2000 K to the melting temperature of uranium tetrachloride (863 K). The tendency to form the pentachloride and hexachloride components thus increases at lower temperatures, and at the melting temperature of uranium tetrachloride these components are even preferentially formed. However, for a subsequent separation concept, the formation of uranium tetrachloride with larger fraction values is crucial in order to be able to separate the volatile components from

the uranium tetrachloride. Therefore, the gaseous chlorine component should be removed as a process gas as early as possible in the separation process and the proportion of chlorine required should be as low as possible. The non-chlorinated coarse material is then retained in the CY-1 cyclone. This includes inert precious metals and any residues of more complex carbon oxide compounds. A very coarse filter K1 retains particularly large residual solid particles from CY-1 down to the millimetre range, which are nevertheless initially carried along with the feed flow of the first preseparation stage for the separation of volatiles and dissolved solids.

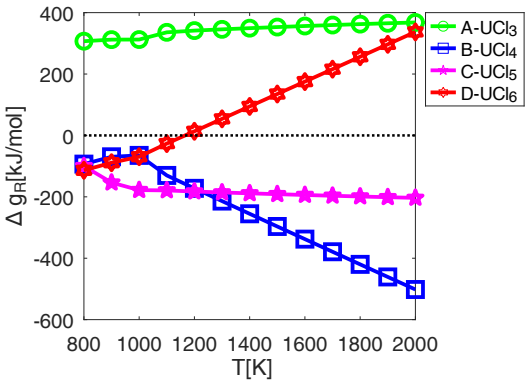

Figure 34: Plot of the temperature dependent Gibbs energy of reaction Δg_R for the molten chlorine-uranium chloride system from the temperature dependent molar specific Gibbs energy data $\Delta g_{f,i}(T)$ of pure substance components from [14].:
A-UCl_3 : $UCl_4 + UCl_5 + UCl_6 \leftrightarrow 3UCl_3 + 3Cl_2$,
B-UCl_4 : $UCl_3 + UCl_5 + UCl_6 \leftrightarrow 3UCl_4 + Cl_2$,
C-UCl_5 : $UCl_3 + UCl_4 + UCl_6 \leftrightarrow 3UCl_5 - Cl_2$,
D-UCl_6 : $UCl_3 + UCl_4 + UCl_5 \leftrightarrow 3UCl_6 - 3Cl_2$.

The chlorination to high product yields of the zirconium cladding material in PB-2, on the other hand, is comparatively simple according to [142] at 623 K under ambient pressure of 1 atm by chlorine as an oxidising agent (or as an electron acceptor) according to the following reaction

$$Zr(s) + 2Cl_2(g) \rightarrow ZrCl_4(g). \tag{99}$$

Such a reaction with high product yields is theoretically technically feasible, for example in a fluidised bed of the fuel by injecting chlorine, which would be technically extremely easy to implement in both continuous and discontinuous operation.

For all chlorination steps, it has been simplified that all other substance components involved are also co-chlorinated under high product yields and under these process conditions, as is also indicated in [29, 47].

After chlorination, the actual separation takes place in the pre-processing unit, the main distillation unit and the waste gas purification unit. In the pre-treatment stage, the mixture is pre-cleaned by removing solids and highly volatile components. The highly volatile components include more volatile chlorides that are difficult to separate, such as tin, antimony, niobium, tellurium, selenium or zirconium chlorides in the chlorinated fuel. Precious and refractory metals include technetium, molybdenum, but also rhodium or ruthenium. A separation concept of such solids and volatiles has already been discussed in principle in section (5.3). The separation of

the highly volatile components and the very volatile problematic chlorides takes place via a two to three stage separation process with isothermal flash evaporation and condensation of the less volatile, co-evaporated main chlorides in one or two condensation stages. In the flowchart shown in Fig. (32), the evaporation step consisting of the units H1, D2 and a flash evaporation PC-1 is carried out at temperatures of 1135 K, taking into account significant evaporation fractions of other chlorides such as uranium tetrachloride.

The subsequent condensation step then consists of the units H2, SC-2 and S2 as a continuous concentration step at 625 K to 725 K. If necessary, depending on the separation specification, a further separation stage of the same required units at a temperature of 625 K must also be selected in order to be able to separate the last chlorides, such as uranium tetrachoride, from the vapour phase. The remaining melt leaving PC-1 is thus practically free of volatile chlorides, but rich in solids in dissolved or suspended form, the insolubility of the solids being assumed on the basis of the different polarity between chlorides and non-chlorides. Similarly, section (5.3) explains how these impurities can be separated from the melt. Below PC-1, this requires multiple applications of concentration/crystallisation stages at 1135 K, followed by a sedimentation tank and removal of these solids by sieving, e.g. 10 mol% of exemplary assumed concentrated melt after each separation repetition for solids removal. In a furnace type at 2000 K to 2250 K, the chlorides remaining in the concentrated melt are evaporated from the solids under an argon atmosphere (see E1/EV1 in Fig. (32)). The chlorides are condensed out again after the argon flow has transported these salt impurities out of the main furnace. The main chlorides of the melt from S1, the thus evaporated chlorides from E1 and the condensed chlorides in S2 are collected and temporarily stored in M1. The solids retention K2 is shown in Fig. (32) to show that all solids must be retained at this point to prevent blockage or crystallisation in the continuous fractionation column DF-1. For this purpose, M1 can also be used as an intermediate storage in a first process step until enough material is available for distillation.

The chloride mixture from M1 consists of very large proportions of over 95 mol% uranium tetrachloride, in which the remaining chlorides almost all have significantly higher boiling points than uranium tetrachloride, with the exception of cadmium dichloride and the less volatile neptunium tetrachloride. Therefore, the separation of the smaller part of these less volatile chlorides is to be carried out continuously (as an exception not used in total reflux or discontinuous column operation) in the fractionation column DF-1 (with partial condenser) at temperatures of 1064 K - 1645 K (as an exception not used in total reflux or discontinuous column operation), in order to carry out the fine separation of the material components of both separated fractions separately in a distillation column close to the total-reflux principle, as explained before, in several PPCs (Progressing Process Cycles) (see also (5.2)). The chlorides of the uranium tetrachloride fraction are separated in DC-1, while the much smaller fraction in the range of about 5 mol% is separated in DC-2 distillation. In order to ensure the mass transfer of the D2 column due to the much smaller fraction and therefore a very small total fractional amount, it may be necessary to accumulate a sufficient amount in a receiver of the DC-2 before the column can be put into operation. The separation of uranium tetrachloride, which is purified as a material component in DC-1, also takes place in DF-1. Thus, already in DC-1, in the not too high temperature range of 1064 K - 1643 K at an ambient pressure of 1 atm, a very large part of the mixture to be

originally purified of at least 95 mol% can be easily separated to be reused as fuel in liquid fuel reactors such as the DFR. However, this is only the case if the neptunium tetrachloride does not have to be separated from the uranium tetrachloride. This is because, due to the similar volatilities of these tetrachlorides, separation by distillation of these components would require a large number of stages, but the separation is irrelevant for reprocessing if reused as fuel in the DFRm (see: [39]), so that separation of the chlorides has not been considered in the development of the separation process shown in Fig. (32). As a result, neptunium tetrachloride and uranium tetrachloride are recovered together as light-boiling products and used, among other things, as fuel in the DFRm.

In DC-2, the remaining 5 mol% of the original fuel is primarily processed, but only a coarser separation into different fractions is possible. Essentially, the substances accumulate in three to five fractions, as the simulation results in the following section will show under calculations with idealized phase equilibrium condition assumptions.

The separated waste gases (after leaving SC-2 and EV-1) still contain the volatile components whose pure components, such as zirconium tetrachloride or selenium tetrachloride, cannot form a liquid phase below 1 atm, some of which could form several metastable chlorides both separately and among themselves, which is undesirable in the separation, so fortunately these components are separated at the beginning of the developed separation concept. The separation of the chloride components involved from the waste gas is similarly achieved by a condensation step at low temperatures, but from 250 K to 270 K (0°C), as shown in Fig. (32) of the separation units of H3,SC-3,S3 and B1. In the cooled state, these chlorides are temporarily stored in B1 until a sufficient quantity is available for distillation to technically realise the mass transfer by contacting the two phases within the separation stages. In DC-3, at higher pressures above 23.36 bar in the temperature range of 507 K - 867 K, the chloride components are preferably separated from each other by distillation in a suitable column operating condition not specified here.

In DF-2, the noble gas components are also recycled by distillation at pressures above 6.185 bar using the Linde distillation process for air liquefaction, as described in [137] among others.

In the zirconium recycling unit, it is assumed that a very small residual amount of fuel will remain on the separated and crushed zirconium material and enter the zirconium processing plant. To ensure that this residual is not co-distilled in the DC-4, these materials are separated in the SC-5 evaporator (of the H5, SC-5 and S5 separation unit system). At temperatures of 725 K at 1 atm, the zirconium tetrachloride, together with the other volatile components of the chlorinated zirconium alloy, is evaporated from the residual material consisting of the small amounts of chromium and nickel and their chlorides and the remaining fuel material. These components can be fed to the fuel grinding step in the mechanical processing unit and then chlorinated in the PB-1 fuel chlorination unit. Similarly, non-chlorinatable material can then be separated in the same way as solids in E1/EV-1. The separation of most of the excess chlorine takes place in the condensation unit SC-4 (of the separation unit system H4, SC-4 and S4) at temperatures of 270 K - 298 K (preferably below the normal room temperature of 293 K (20°C)). The excess chlorine can be reused in the PB-2 chlorination unit.

Distillation in DC-4 takes place in almost complete analogy to distillation in DC-3 under similar process conditions at 538 K - 825 K and pressures above 23.36 bar. As the proportion of

volatile chlorides in the fuel is so small, the amounts collected in B1 are also relatively small, so that consideration can be given to feeding these chlorides to column DC-4 instead of column DC-3, thus eliminating the need for column DC-3. Another idea to simplify the process is to move the pre-treatment unit of all the separation units for solids separation to the evaporator unit of the distillation column DF-1, so that units SC-1, S1, E1 and K1 can be integrated compactly and easily. However, this requires manual product removal during column operation and increased maintenance, which is obviously more problematic for practical processing.

The following sections present and discuss the simulation results of the process simulation required to create and optimise the separation process design, including the process conditions mentioned. Each separation step is simulated or literature references are provided for its successful technical implementation. In addition, these simulation results prove that the developed separation process is valid if the ideal phase equilibrium behaviour used in the simulations and calculations is valid.

6.2 Simulation results of the SNF separation concept

For the flow sheet simulation, an appropriate calculation of the feed composition for the pre-processing unit and the distillation-based zirconium cladding material processing is required. According to the reaction of equation 98, the equimolar chlorination of the fuel produces the same molar amount of CO_2 as CCl_4 is stochiometrically required in relation to the molar flow of the fuel. The CO_2 molar flow is therefore equal to the fuel flow. The inerting ratio must be 1:1 in terms of argon:fuel. The supply of argon is necessary not only as an inert gas but also as a carrier gas (dissolving gas) so that the light boiling chlorides pass into this gas/vapour phase and can be removed from PC-1 in the vapour stream. Feeding or spraying in an argon atmosphere provides the contact surface for mass transfer after expansion. Otherwise, the mass flows are too small to form sufficiently large mass transfer contact surfaces. In order to obtain 1/3 of the vessel with melt in the molar ratio, the same molar amount of argon is stochiometrically required. Thus, the molar flow of argon is equal to the CO_2 flow.

Table 12: PC-1 Feed composition in mol-% of chlorinated SNF-material

Ar	CO_2	UCl_4	$PuCl_3$	$NpCl_4$
3.3333e+01	3.3333e+01	3.1413e+01	4.2285e-01	2.0097e-02
$AmCl_3$	$CmCl_3$	CsCl	$SrCl_2$	Tc
4.7145e-02	2.1413e-03	1.0617e-01	9.7788e-02	1.0465e-01
Ru	Rh	Mo	$BaCl_2$	$LaCl_3$
5.9953e-02	6.9970e-03	1.0466e-01	1.0775e-01	1.0777e-01
$CeCl_3$	$PrCl_3$	$NdCl_3$	$SmCl_3$	$EuCl_3$
1.9343e-01	9.3419e-02	1.3153e-01	9.6962e-03	7.7001e-03
$ZrCl_4$	$NbCl_5$	$SbCl_3$	$SbCl_5$	$TeCl_2$
1.1096e-01	1.1209e-01	2.2262e-04	2.2262e-04	7.2974e-02

For the uranium dioxide in the fuel, complete chlorination with 100% yield is assumed for simplicity. The feed composition for the PC-1 flash evaporation is given in the Tab. (12). The ratio of feed, CO_2 and argon is therefore about 1/3, based on the above data.

All other molar fractions combined are estimated to be only 1.9203 mol%, with plutonium trichloride in larger proportions, now including the gas phase as a major molar fraction. The fission product fraction is therefore no longer 5 mol% but less than 2 mol%, although the amount of fission product after chlorination has not changed. This is simply due to the fact that the argon gas is assumed to be ideal for the calculations and simplified homogeneously dissolved using a spray device. The proportions of the remaining 1.9203 mol-% are shown in Fig. (35) in percentages, related only to the fission fraction. The composition is derived from the fission product data in the SNF material according to [139, 35]. With the exception of higher proportions of lanthanide chlorides, in particular cerium trichloride and neodymium trichloride, the material components are quite evenly represented (in terms of molar percentages).

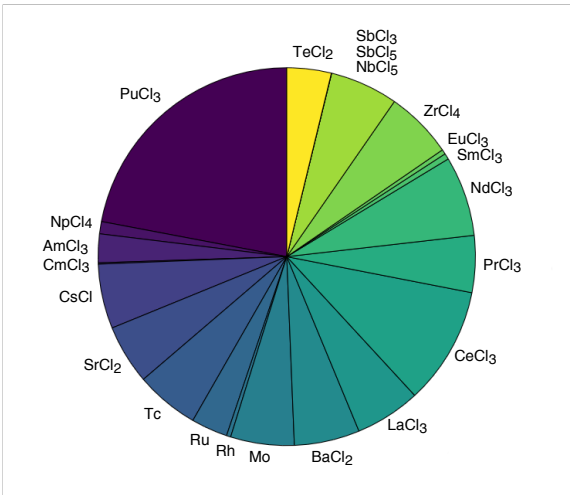

Figure 35: PC-1 Feed composition in mol% of residual SNF-Material without the components Ar, CO_2, and UCl_4

Exceptions with lower proportions are antimony chlorides, curium trichloride, samarium trichloride, europium trichloride and rhodium. Based on this composition of the feed material, the application of the flow scheme simulation with appropriate Octave/Matlab separation models from Tab. (10) of section (10) and the resulting separation simulation results are now discussed in detail.

6.2.1 The preprocessing unit

After chlorination of the fuel, flash evaporation is carried out in the preprocessing unit via the apparatus system H1,D2,PC-1 (of the flowchart in Fig. (32)), which is simulated as a single-stage isothermal flash evaporator according to the IF-O/M model (see Tab. (10)). The aim is to separate the light boiling chloride fraction from the molten fuel salt. The dissolved solid fraction of the precious metals without the chlorides also has to be sharply separated by concentration, crystallisation and sieving, where concentration and crystallisation are simulated simultaneously. However, the sieving is not simulated. The addition of argon has the effect of increasing the pro-

portion of volatile chlorides entering the vapour phase. Evaporation also has an oversaturation effect on concentration and crystallisation. The use of the flash inlet is proposed by spraying argon injectively, which simultaneously increases the contact exchange surface between liquid and gas/vapour phase. The simulation results in Fig. (36) (sorted according to the boiling points of the compounds) show the characteristic distribution of low and high boiling components, with the vapour fraction of the substance component increasing with increasing volatility. Barium dichloride, strontium dichloride and the solids rhodium, ruthenium, technetium and molybdenum are present only in the liquid or solid phase, while the gaseous components argon and carbon dioxide, including the antimony chlorides and niobium pentachloride, are not present as liquids. Approximately sorted by boiling point in the direction of decreasing volatility of the components, it can be observed that the proportion of the vapour phase decreases and the liquid proportion increases for each component. Since the process temperature of 1135 K is above the boiling temperature of pure uranium tetrachloride, it follows from the observation of ideal phase equilibria that in the ideal mixture the vapour fraction of uranium tetrachloride is significantly greater than in the liquid phase. Thus, in Fig. (36), the separation of light and heavy boilers is shown, with the middle boiler component being transition components, which are represented in both phases. The higher vapour content of uranium tetrachloride also means that the ratio of liquid to vapour in the separation option is not too large compared to, for example, assuming that no uranium tetrachloride evaporates.

The separation of the volatile compounds tends to follow a distribution with respect to the volatility of the compounds, sorted by their boiling points, as shown in Fig. (37). From this it can be seen that even when looking at the boiling points, there are four separation ranges in which larger boiling point differences to the next component can be seen (Fig. (37)). The noble gas fractions of argon and carbon dioxide, and the volatile chloride fractions of antimony pentachloride to zirconium tetrachloride are classified as light-boiling components, which are completely removed as vapour by flash evaporation. Neptunium tetrachloride and uranium tetrachloride are present separately as medium-boiling components, which should be easily distillable due to the high boiling point differences of at least 250 K from the other boiling points of the other components. The chlorides curium trichloride to lanthanum trichloride can be considered as heavy boiler components, whereas a larger boiling point difference of about 100 K can be observed between the chlorides europium trichloride and barium dichloride. In a distillation, a further division into light and heavy boiling components is therefore possible, starting from curium trichloride to barium dichloride as the light boiling component (according to the division of the substance components in Fig. (37). Finally, the metals rhodium to molybdenum follow as solids whose melting points are well above 2000 K, so that they can be separated by crystallisation and are not liquid as pure components.

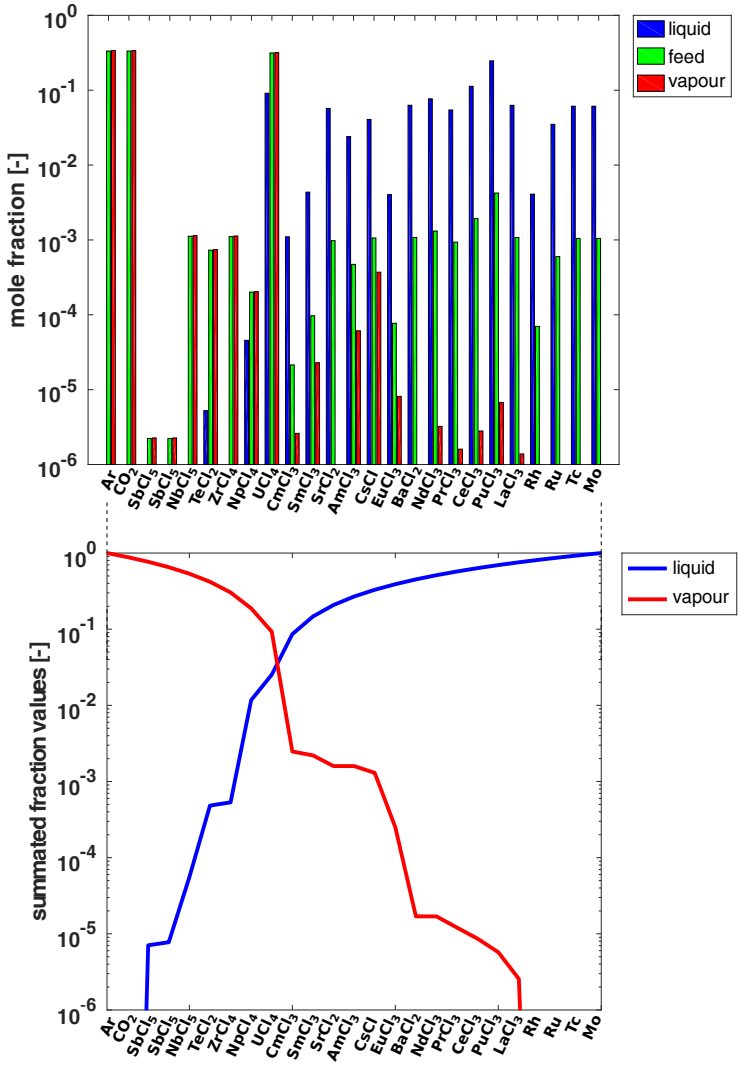

Figure 36: Flow-chart simulation of SNF distillation:
Upper figure: PC-1 results at 1135 K, 1 atm,
Lower figure: PC-1 summated and renormalised mole fraction curve

In the lower part of Fig. (36) the summed mole fractions are shown with a tendency from light-boiling components of the vapour phase to light-boiling components of the liquid phase. However, the summed consideration assumes the heavy-boiling component of the vapour phase and the heavy-boiling component of the liquid phase. The summed separation curves also illustrate the ratio of liquid to vapour to the component of interest. Above the volatility of uranium tetrachloride, the vapour phase predominates, with the red curve in Fig. (36) lying above the blue curve. At volatilities below uranium tetrachloride this relationship is reversed and the liquid component predominates. Ideally, a sharp separation of uranium tetrachloride with a sharp reversal of the peak fraction curve would be desirable. However, this one-step separation is not sharp and only allows separation into particularly light-boiling components, such as the gases argon and carbon dioxide, or heavy-boiling components, such as the practically non-evaporable metal components present. As already explained in section (5.3), a further condensation stage is required to separate the volatile components, in which the chlorides are completely condensed

out at lower temperatures below the volatility of neptunium tetrachloride.

Since the proportion of uranium tetrachloride in the vapour phase is so high according to Fig. (37), a condensation step in SC-2 at 725 K and 1 atm is not sufficient, especially for uranium tetrachloride, to completely separate uranium tetrachloride from the vapour stream, while all other less volatile chlorides of neptunium and uranium tetrachloride can be condensed out of this vapour phase within this single-stage separation step. This is shown by the simulation results (with model SSD-O/M) in Figure (38). To enable separation of uranium tetrachloride with a residual content of 1E-06, a second condensation step at 625 K below 1 atm is required. Temperatures lower than this cannot be set, otherwise the sublimation temperature for pure zirconium tetrachloride will be reached. In the first condensation stage, uranium tetrachloride is present with a vapour pressure of 1.6108E-04 bar, which is still relatively high at 1 atm. In the second condensation stage at 625 K, the vapour pressure of uranium tetrachloride is 8.1643e-07 bar, and the separation of uranium tetrachloride is just below a fraction value of 1E-04 mol% according to the simulation results, subject to the required separation target of having separated each volatile component with an impurity fraction value of 1E-04 mol%.

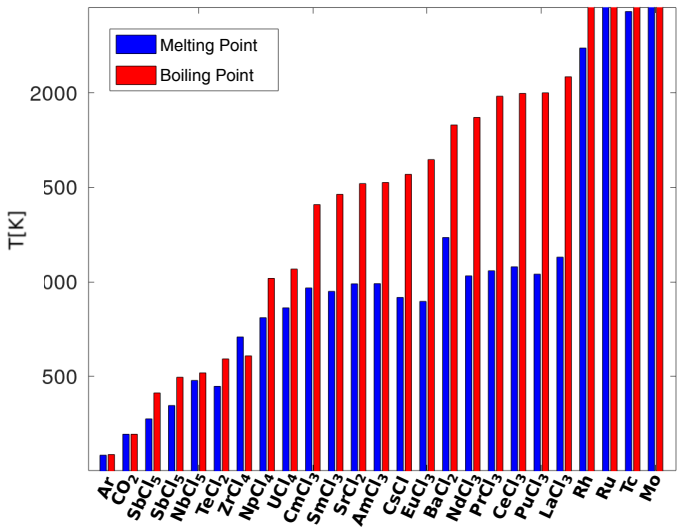

Figure 37: Melting and Boiling points of pure chlorides and high volatiles

Now follows the analysis of the solids separation according to section (5.3) by model SSD-O/M in series connection of the separation stages with SLE equilibria. The solid components rhodium, ruthenium, technetium and molybdenum have to be concentrated and separated in several steps in the concentration/crystallisation unit. This includes concentration to 10 mol% residual chlorides, which are then evaporated in E1/EV-1. The concentration could be operated discontinuously, with the downstream concentration and crystallisation stages simulated as single stage suspension crystallisers instead. The simulation results show that these solids can be removed from the molten salt under these conditions at 1135 K and 1 atm with a few separation repetitions under the separation specification of 1E-04 mol%. After each separation step, the concentrated solid is removed.

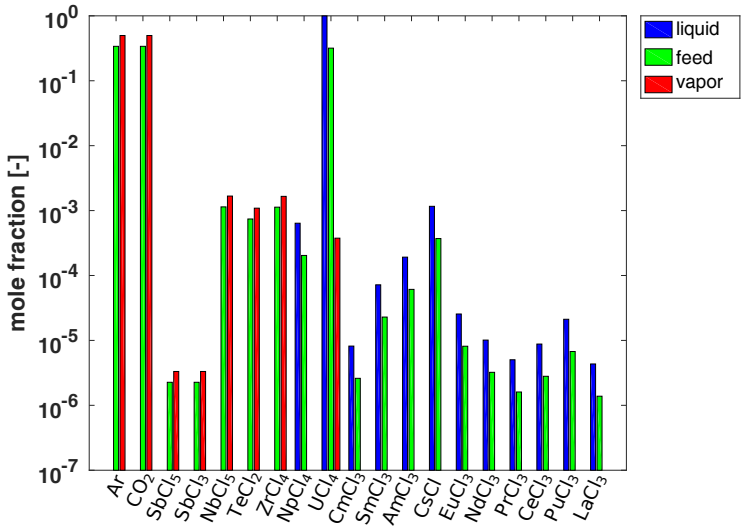

Figure 38: Flow-chart simulation of SNF distillation: SC-2,S2 results at 625-725 K, 1 atm

In (39) thirteen continuous separation stages have been simulated. Clearly visible in the liquid phase in (39) (right figure part) is the exponential depletion of solids per stage with logarithmic representation of the y-axis. Only the separation of rhodium is somewhat more complex, as the slope of the composition curve for each stage is lower than for technetium, ruthenium and molybdenum. For molybdenum and ruthenium, only six stages are required to separate from the liquid phase, whereas for technetium and rhodium eight stages are required to meet the separation specification of 1E-04 mol% impurity content with ideal phase equilibrium.

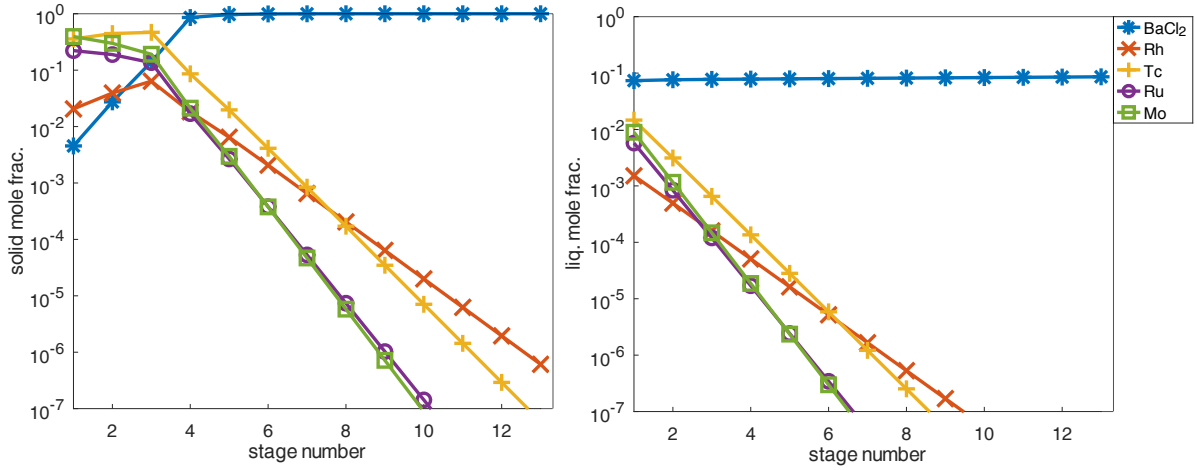

Figure 39: Flow-chart simulation of SNF distillation: SC-1,S1 results at 1135 K, 1 atm: left: solid mole fraction each separation stage, right: liquid mole fraction each separation stage

Barium dichloride also enters the solid phase as shown in Fig. (39)(left partial figure), which can hopefully evaporate from the suspension melt at temperatures of 2000 K if the chloride has crystallised on the surface. However, if it is dissolved deep in the crystallised solid matrix, it would be more difficult to separate this chloride component from the crystallisation product in E1/EV1. However, as the simulation results show, the barium dichloride content in the solid

phase unfortunately increases due to the solid separation as the metallic solid components are depleted in the liquid phase. While the barium dichloride content is still low at the beginning, it increases in the solid phase due to the solid separation, as the metallic solid components are much more depleted in the liquid phase with increasing crystallisation repetition. It should also be noted that as the number of separation stages increases, the amount of molar flux decreases significantly. As there are virtually no separable solved assumed solids left in the liquid at the last separation stages after the tenth stage, only a very small fraction of the molar flux enters the solid phase. As a result, the proportion of metals in the solid phase also decreases significantly from the third separation stage onwards, as most of the solids in the metals have already been separated. Since technetium and ruthenium are slightly more difficult to separate, the proportion of solids increases between stages 1-3 and the metals initially accumulate more in the solid due to the later separation. Although barium dichloride crystallises out, the separation effort of the simulation results shown has demonstrated the good separation of the solids. The partially removed barium dichloride component is not as being seen critical for the separation concept as for other components, such as more active isotopic elements (see form example in Tab. (18) of section (D.2) in the Appendix).

With a separation accuracy of 1E-02-mol%, the chlorides can be evaporated from the solid in the evaporator unit E1/EV-1, simulated in the SSD-O/M model with VLE properties, as shown in the simulation results as one-step evaporation in Fig. (40).

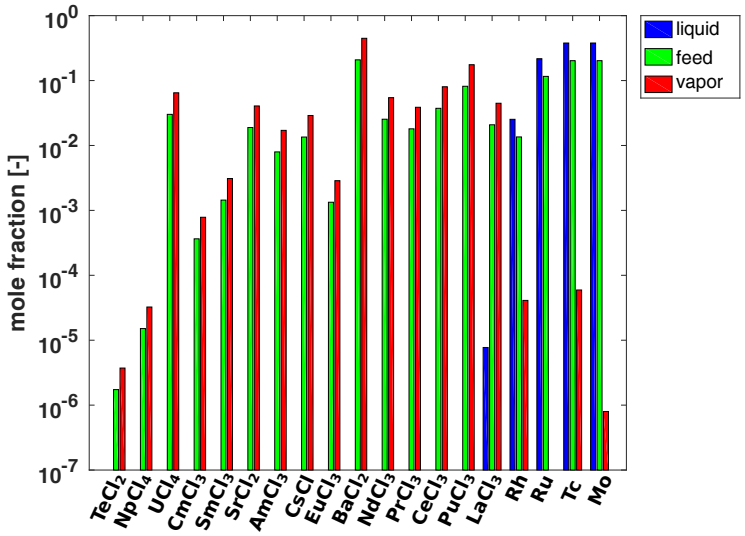

Figure 40: Flow-chart simulation of SNF distillation: EV-1 results, at 2000 K, 1 atm

Only in the case of lanthanum trichloride is the boiling point above 2000 K an exception here, so that complete evaporation from the liquid phase is not possible. However, the problem of solid separation is solved to such an extent that no active elements enter the vapour phase. Bit this should not be so problematic of these components. Looking at the metals, it is noticeable that a certain amount of vapour is present in the case of rhodium and technetium, since the molar flow is lower compared to the isothermal flash after PC-1 (Fig. (40)). Consequently, based on the simulation results, there is an increased vapour fraction. Since supersaturation, primary and secondary crystallisation have to be initiated in addition to crystallisation by evaporation, it can

be expected that the separation of already completely undissolved solids in a suspension melt without necessary crystallisation can be realised much more easily and with higher separation accuracy. Furthermore, the simulation results have shown that concentration is easier to implement than crystallisation (see: Fig. (40)). Therefore, the separation accuracies are expected to increase significantly and possibly fall below 1E-06 at an impurity level than would be expected from the simulation results for crystallisation. This means that the separation can be done better in this case with significantly higher separation accuracy.

This shows that the precious metals with possible impurities can be separated well from lanthanum trichloride so far, although a fine separation of the metallic components still has to be carried out in special precious metal separation processes. It is only important that the simulation results (see Fig. (40))) show that all other essential chlorides, especially all actinide chlorides in EV-1/E1, can be separated by evaporation in hot argon, neglecting a very small proportion of undesirable precious rhodium loss.

Table 13: Composition after mixing in M1 given in in mol-%

UCl_4	$PuCl_3$	$NpCl_4$	$AmCl_3$	$CmCl_3$	$CsCl$	$SrCl_2$
9.5887e+01	1.2907e+00	6.1345e-02	1.4391e-01	6.5362e-03	3.2407e-01	2.9849e-01
$BaCl_2$	$LaCl_3$	$CeCl_3$	$PrCl_3$	$NdCl_3$	$SmCl_3$	$EuCl_3$
3.2891e-01	3.2897e-01	5.9042e-01	2.8516e-01	4.0148e-01	2.9597e-02	2.3504e-02

As mentioned above, all chloride streams from S2, S1 and E1/EV-1 are collected and mixed in M1. In order to reach the temperature in DF-1, an external energy supply is required in addition to the mixing of the streams. Evaluating the mass and heat balance, a required heat flow with a remaining required heating value of 20.638 kW is calculated. The remaining mole flow is about 8.500E-02 mol/s and the temperature without heat input is estimated to be 678.6 K. The composition is given in Tab. (13). This composition is identical to the feed composition according to Tab. (12), only separately normalised for the substance components appearing in M1. Based on the simulation results so far, this must also be fulfilled, as the main chlorides are not present in the vapour phase of SC-2 or in the solid phase of the solids separation in E1/EV-1, with a few not more disturbing exceptions still to be discussed. This is then the pre-purified feed for the subsequent distillation unit which remains and has been collected in M1 as it enters the main distillation unit.

6.2.2 The main distillation

For the simulation of the distillation, the feed composition according to Tab. 13, where the mixed stream from the different chloride sub-streams is fed to the continuous distillation column DF-1 under liquid boiling conditions. Ideal phase equilibrium conditions without deviation from Raoult's law are further assumed for the simulations. The continuous fractionation column consists of three separation stages including the evaporator. The simulation results in Fig. (41) show the absolute separation results with condensate distillate liquid (left bar shown in blue in Fig. (41)) and the evaporator product in (right bar shown in red).

As can be seen from the simulation results considering ideal phase equilibrium behaviour in Fig. (41), the predominant fraction of uranium and neptunium tetrachloride is obtained from the initial mixture in the condenser. The remaining residual fraction is 2-3E-03-mol% as a bottom product of these components. Only a very small residual fraction of cesium chloride of about 1E-03-mol% remains in the distillation product of the condenser in the simulation results according to Fig. (41). This fraction would increase significantly if, according to the estimated VLE data between uranium tetrachloride and monochlorides such as lithium chloride, silver chloride or sodium chloride according to section (3.2.2), a similarly strong azeotropic separation behaviour analogous to that of cesium chloride would exist. However, under idealized phase equilibrium conditions, the results show the separation behaviour shown in Fig. (41). The consideration of other binary subsystems with a higher degree of chlorination according to section (3.2.2) with regard to the non-ideal phase equilibrium behaviour of the chlorides involved shows that they would form zeotropic mixtures. Only the number of separation steps would change slightly compared to the ideal phase equilibrium behaviour presented here, as can be observed in the extended simulation results according to section (D.1) for the corresponding estimated real VLEs. However, in the case of the monochloride cesium chloride, DF-1 would be extended by another column (e.g. DF-1-AZ) in which the azeotrope could be separated at higher pressure, if experimental results would show a strongly pronounced pressure-dependent behaviour of the limiting distillation barrier. On the other hand, it would be technically feasible to add cesium chloride close to the distillation limit of the complex mixture in order to reach the other side of the distillation range. A more precise interpretation would require experimental measurements on the binary subsystems, which tend to form azeotropes, which are not feasible and simulatable for the complex mixture conceptually required within the scope of this thesis. Therefore, only the rough qualitative assessment that would be observed when looking at the real VLE behaviour of the binary subsystems will suffice here and for the following simulative investigations for the main distillation unit. The main focus will be therefore on the simulation results under the first assumption of an idealized phase equilibrium.

In the following consideration of the simulation results with ideal phase equilibrium behaviour according to Fig. (41), the remaining chlorides are present exclusively in the melt phase of the evaporator product as heavy-boiling components. The mean operating temperature of the column is 1100 K, with the condenser temperature at the boiling point of uranium tetrachloride and the evaporator temperature at only 1645 K. Below these temperatures, practically no heavy-boiling components occur that could accumulate in the column.

In the condenser, practically only the mixture of neptunium tetrachloride and uranium tetrachloride with minor impurities of cesium chloride is obtained. The separation of the neptunium tetrachloride component from the uranium tetrachloride is not considered in detail in this thesis, as the separation is not necessary for use as fuel in many liquid fuel reactors, in particular for the DFR. In addition, due to the relatively close boiling points of neptunium tetrachloride and uranium tetrachloride, the separation effort in terms of the number of separation stages required would increase significantly. Column DC-1 is used for secondary fine separation to remove other chlorides, such as cesium chloride, from the corresponding mainly contaminated binary $NpCl_4$-UCl_4 mixture.

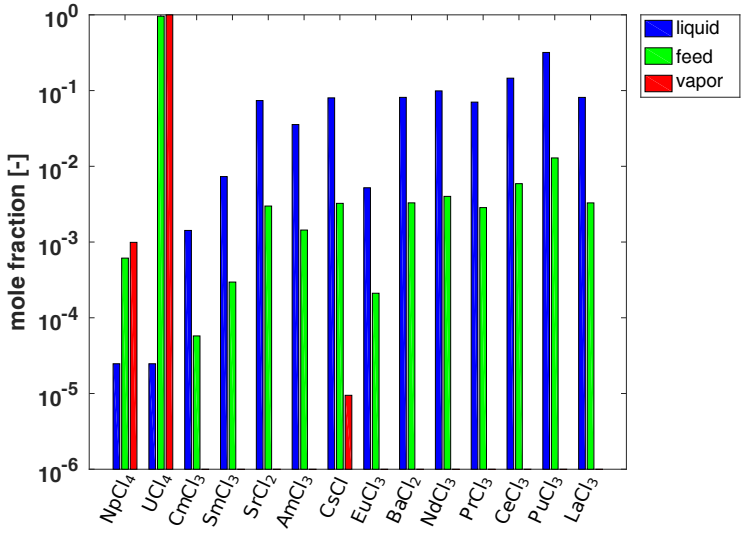

Figure 41: Flow-chart simulation of SNF distillation: DF-1 results at 1064-1645 K and at 1 atm

This separation is not shown further in the SNF preparation of this thesis using a total reflux column simulation.

The detailed separation of the remaining chlorides, neglecting the remaining neptunium and uranium tetrachloride fractions, is carried out in the total reflux column DC-2 with 25 separation stages. Due to the high complexity of all components involved, the simulation results for separable fractions with chlorides of similar boiling points are summarised in Fig. (42) in reasonable fractions instead of separation fractions in terms of mole fractions per separation stage for a single component. Detailed results can be found in the appendix in section (C.2).

The first application of the first distillation batch of the DC-2 column (as shown in Fig.(42) under total reflux PPC 1) corresponds to the simulation of the first steady-state total reflux column condition before the actual separation. The summarised separation curves of the light boiling, heavy boiling and the three medium boiling fractions are shown here.

The light-boiling fraction can be separated from the other fractions in the first separation stage with a separation specification of 1E-04-mol%, whereby only the $SmCl_3$-Fraktion fraction shown is present in the column in the first separation stage. Within the column, the fraction of the combined light-boiling fraction decreases and becomes significantly depleted from about the tenth stage onwards, as shown in the logarithmic representation in Fig. (42). From the seventeenth separation stage onwards, this fraction is practically no longer represented in the subsequent column stages. The heavy-boiling fraction (plutonium trichloride fraction with cerium, presodymium, plutonium and lanthanum trichloride) is also distillatively enrichable in the evaporator of the first stationary total-reflux column operating condition and later separable with high purities below 1E-04-mol%. The mole fraction value of this summarised heavy-boiling separation curve reduces in the direction of the condenser between the twenty-fifth and fifteenth separation stage only relevantly in terms of coarse separation accuracy to a fraction of about 60 mol% and then decreases significantly between the twelfth and fifteenth separation stage. A separation of plutonium trichloride with respect to cerium, presodymium or lanthanum trichloride is

technically not feasible within this distillation effort of assumed ideal phase equilibrium condition, as detailed simulation results is shown in the appendix in Fig. (73) of section (C.2). The same applies to the rare earths chloride components, where only neodymium trichloride is separable from cerium, presodymium and lanthanum trichloride exclusively for this purpose. Neodymium trichloride occurs together with barium trichloride in the neodymium trichloride fraction in an intermediate boiling summarized fraction of the simulation results. Here, the maximum molar fraction is reached for these components in the fifteenth separation stage with fraction values of 10 - 12-mol%. In the direction of the condenser, the proportion of the neodymium trichloride fraction decreases stronger than on the side of the evaporator. For the americium trichloride fraction, the maximum of the combined separation curve is in the fourteenth separation stage, from which it decreases more significantly with increasing number of stages towards the evaporator than towards the condenser. The europium trichloride fraction is in the middle between the two separation curves as intermediate boiler component. The temperature fraction, defined in the following as $\theta = \frac{T-T_{\min}}{T_{\max}-T_{\min}}$ (with $T_{\min}$ in the first separation stage and $T_{\max}$ in the last), shows the temperature distribution of the column depending on the represented boiling behaviour of the represented substance components. This temperature fraction curve shows a strictly monotonously increasing curve progression up to the accumulation of the heavy-boiling fraction and clearly approaches this fraction curve with increasing depletion of the other fractions.

The intermediate boiling fractions apart from the europium trichloride fraction are separately enriched in the next separation repetition of the next steady-state total reflux column operating condition PPC 2 according to Fig. (42) (lower figure). The active separation range of the column is here between stages 5-22. In each of the other stages, the americium trichloride light and neodymium trichloride heavy fractions are obtained with separation specifications well below 1E-04-mol%. In the range of the 5th-22nd separation stage, the europium trichloride medium-boiler fraction also accumulates with a maximum of about 1 mol% in the fifteenth separation stage. From the condenser to the fourteenth stage no clear fine separation of the light boiling component can be observed, but according to Fig. (42) (lower figure) it only runs visibly between stages 14-21. After stage 21, the medium and light fractions are no longer represented in the stages with significant impurities. In these stages the pure heavy fraction is obtained. The defined temperature fraction curve here is strongly dependent on the neodymium trichloride fraction, since the boiling points and temperature-dependent volatilities of the components in the other fractions are significantly lower than in the neodymium trichloride heavy-boiler fraction. The medium boiling component europium trichloride of the medium boiling fraction can only be separated in a mixture with strontium trichloride, as shown in another simulation of the next total reflux column operation in Fig. (43). It can be seen that cesium chloride as an intermediate boiling component can only be roughly separated from strontium in the first separation stage with a residual content of 8E-02-mol%. The same applies to the enrichment of europium trichloride with a residual cesium chloride content of just over 8 mol%. Further details on the simulation results of the separation curves can be found in Fig. (43).

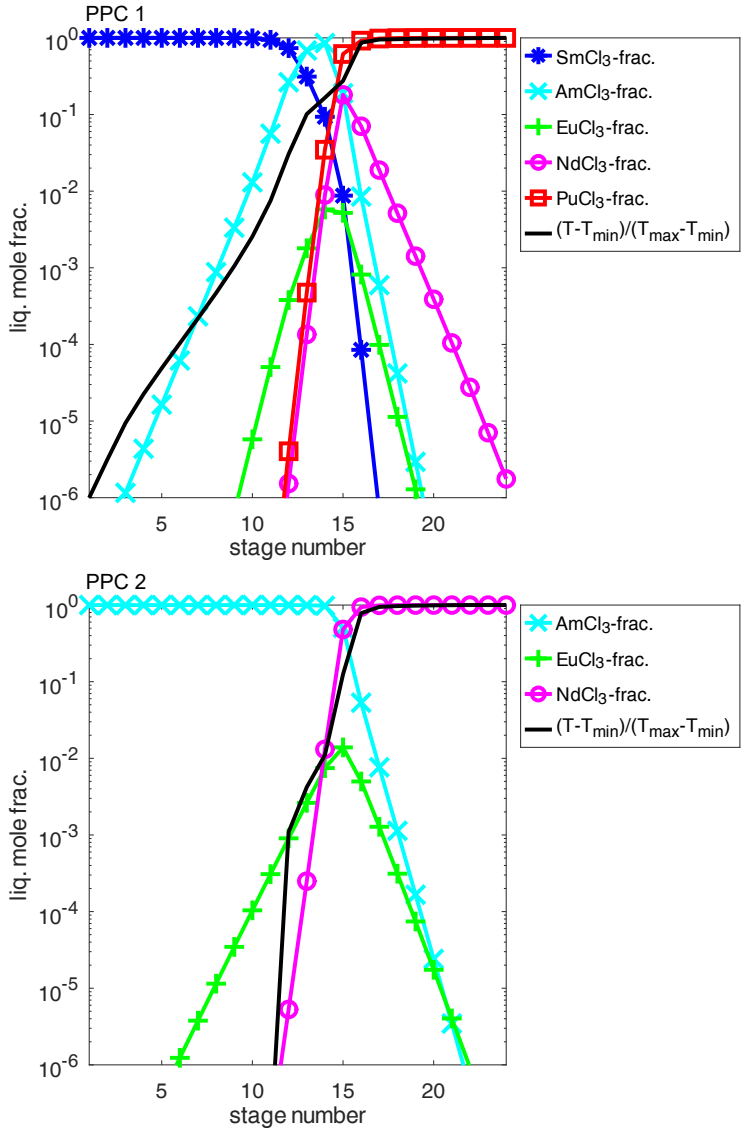

Figure 42: Flowchart simulation of SNF distillation: DC-2 Results PPC 1 & PPC 2 ***/**** at 1643-2000 K and at 1 atm **:
1*) $SmCl_3$-fraction/$CmCl_3$-fraction: $CmCl_3$, and traces of $SmCl_3$
2*) $AmCl_3$-fraction: $AmCl_3$, $SrCl_2$, CsCl, $SmCl_3$
3) $EuCl_3$-fraction: mainly $EuCl_3$, with impurities of CsCl and $SrCl_2$
4*) $NdCl_3$-fraction: $BaCl_2$, NdCl3
5) $PuCl_3$-fraction: $PrCl_3$, $CeCl_3$, $PuCl_3$, $LaCl_3$
*designated according to the largest proportion of the fraction present
**Separation accuracy: 1E-06
*** The choice of colors is intended to illustrate purely qualitatively the location of the respective substance component in relation to the temperature residence range of the component within the column: From dark blue with respect to cold temperatures in relation to the curium trichloride light-boiling fraction to red toward hot temperatures of the plutonium trichloride heavy-boiling fraction. Medium-boiling fractions are illustrated in mixed colors in relation to the temperatures.
**** Detailed results each chloride component are available in the comparison of SNF and HLW recovery in section (C.2) of the Appendix.

For a precise separation of europium trichloride and strontium dichloride, considerably more

separation stages would be required within the current distillation column operation. If only stable isotopes are present in this distillation repetition in the current PPC, the detailed separation of a simplified three-component mixture CsCl-$SrCl_2$-$PuCl_3$ is not mandatory. However, the third separation process is necessary if significant amounts of the active isotopes strontium-90 and cesium-137 are present, which contribute to the decay heat accumulation inside the distillation column, as shown by the results of the decay heat estimation in section (D.2),(D.2.2), (in the Appendix of this thesis), especially for the mixture of the substance system CsCl-$SrCl_2$-$PuCl_3$ investigated there (see also Fig. (88) and (89)).

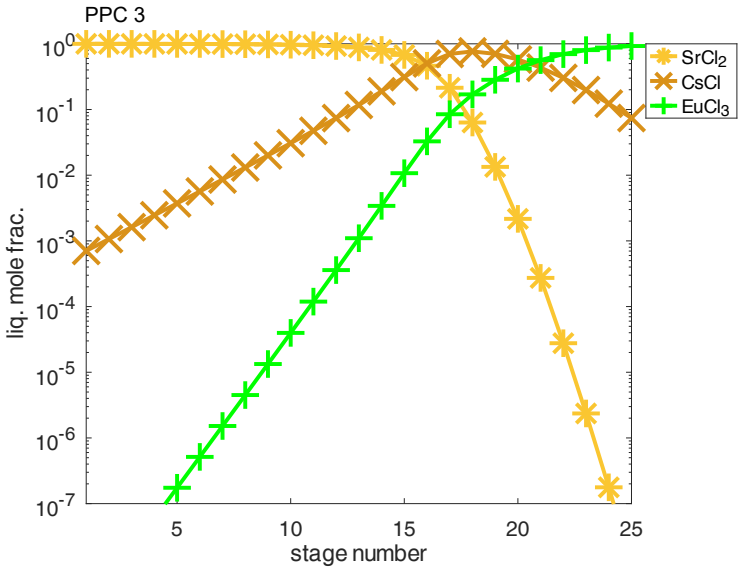

Figure 43: Flow-chart simulation of SNF distillation: DC-2 results PPC 3*** of a detailed third repetition of distillation following the total reflux principle at 1530-1645 K and at 1 atm**
**Separation accuracy: 1E-06
*** The choice of colors is intended to illustrate purely qualitatively the location of the respective substance component in relation to the temperature residence range of the component within the column: From dark blue with respect to cold temperatures in relation to the curium trichloride light-boiling fraction to red toward hot temperatures of the plutonium trichloride heavy-boiling fraction. Medium-boiling components are illustrated in mixed colors in relation to the temperatures

In conclusion, based on the simulation results of Fig.(42), it can be said that all actinides in fractions with other few chloride components are otherwise highly pure separable under separation specifications of 1E-04-mol% of the other chloride components involved. While already the largest represented fraction of SNF fuel with 95-96 mol% regarding uranium tetrachloride together with neptunium tetrachloride is separable under high-purity separation accuracy (1E-04 mol% of other chloride components), as shown in the DF-1 simulation results in Fig. (41), the transplutonium elemental chlorides can be obtained as only mediate pure or together in separable fractions of other chloride components. The transplutonium elemental chlorides can be separated as light-boiler components in the DC-2 column as fractions of only a few other chloride components, e.g. cesium chloride (see Fig. (42)). In the first separation of the DC-2 column, high purity enrichment and separation of curium trichloride with an impurity content of less than 1E-03 mol% of samarium trichloride is possible. Americium trichloride is recovered

together with samarium trichloride, cesium chloride and strontium dichloride in the next separation repetition of the PPC. Plutonium trichloride, on the other hand, can already be obtained in the first separation as a heavy-boiling component in the mixture of cerium trichloride, presodymium trichloride and lanthanum trichloride, but as a high-purity fraction without any other visible chloride components involved, as can be seen from the simulation results.

Concerning the separation of fission products, it can be concluded from the simulation results that the separation of neodymium trichloride with 1 mol% barium dichloride impurities as the only impurity component is feasible in the second stationary total reflux column operation. Unfortunately, the boiling points and also the volatilities of the lanthanide trichloride components are too similar, so that for many of these mixture fractions occurring in the distillative purification, even shown here in the simulation results as possible heavy-boiling distillation products, even a separation to medium purity is not possible. Furthermore, cesium chloride and strontium dichloride cannot be separated to high purity (in this DC-2 column), but are always present contaminated in other defined separation fractions. This is shown by the simulation results in Fig. (42) and Fig. (43), where the components are always present together in numerous fractions. Finally, especially with regard to the consideration of the post-decay heat accumulation of some isotopes, such as ^{137}Cs or ^{90}Sr according to Tab. (18), this has to be taken into account in general, especially during the distillation for the cesium chloride and strontium dichloride components. As the results of the third separation show, ^{90}Sr as a dichloride component could only be enriched together with cesium chloride among the possible ^{137}Cs present. However, since cesium chloride and strontium dichloride are also present in the americium trichloride and europium trichloride fractions, purified separation of these active components as separate components is not possible (see results for Fig. (42)). Detailed separation results for each component can be found in Figs. (72) and (75) of the (C.2) section in the Appendix. Nevertheless, the simulation results have shown the usefulness of the simulated designed flowchart as it always improves the separation problem even for difficult to separate components. For difficult to separate components, a much more intelligent fractionation of only a few components is possible, in which secondary distillation efforts can be used to separate these components, as simulation results have shown here and for test mixtures (from the simulation results in chapter (III)) even in this process by back-feeding as distillation feed.

6.2.3 Waste gas treatment and noble gas recovery

The waste gas treatment, consisting of volatile chloride separation and distillative purification and further waste gas purification for the separation of noble gases, mainly argon, can be operated externally, separate from the processing of nuclear fuels, since no actinides and other active fission products are involved in this separation part. Then, according to [29], the off-gas purification part is not subject to any legal requirements for handling radioactive materials, as long as the uranium tetrachloride content is well below the ppm range. A second SC-2 separator should be installed downstream at higher operating temperatures to ensure that all uranium tetrachloride impurities are completely separated in or quite below the ppm range.

Purification step of the volatile chlorides The simulation results of the condensation (or even crystallisation) unit SC-3 of the volatile chlorides at 270 K as presented in Fig. (38) show that all process and noble gases remain in the gas phase and all chloride compounds are completely condensed out of the vapour phase. The remaining red marked vapour fraction from the simulation results here only shows the components carbon dioxide and argon. In order to ensure that the uranium tetrachloride condensation product in SC-3 is completely below the separation specification of 1E-04 mol%, a second SC-2 condensation unit at 625 K (and 1 atm) is required. The impurification of uranium tetrachloride is followed directly from the simulation results of the SC-2 simulation results from Fig. (38).

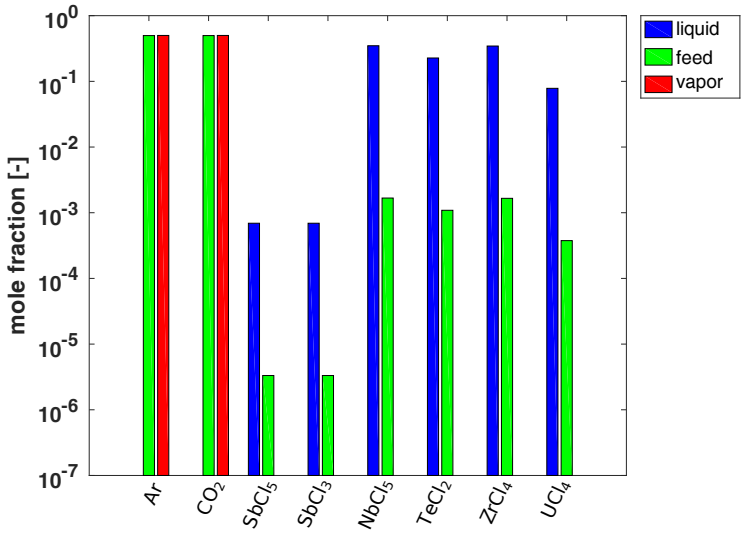

Figure 44: Flow-chart simulation of SNF distillation: SC-3 at 250-270 K and 1 atm

The separation simulation for the separation of zirconium tetrachloride and possible other components from the mixture of condensed or partly even possible crystallised volatile chlorides in the DC-3 distillation column follows. If no uranium tetrachloride is present, the separation specification of 1E-04-mol% is no longer necessary for all non-active elements in these chloride components (compare also [29]). This means that higher impurity levels are also permissible for zirconium tetrachloride separation. Since, unfortunately, zirconium tetrachloride only shows a liquid phase at pressures above 23.36 bar, the distillation must be operated and simulated at pressures above 23.36 bar. As an approximation to the pressure correction in equation (27) with $\gamma_i = 1$, only the Poynting correction according to equation (26) is considered for the following simulations. The simulation results are given in Fig. (45). A pressure of 25 bar is set for the simulations, but this is not specified in the flowchart as the pressure is not optimised and is only used here for simulation purposes. In the simulation results at higher pressure the separated pure chloride components have then significantly boiling points compared to normal pressure.

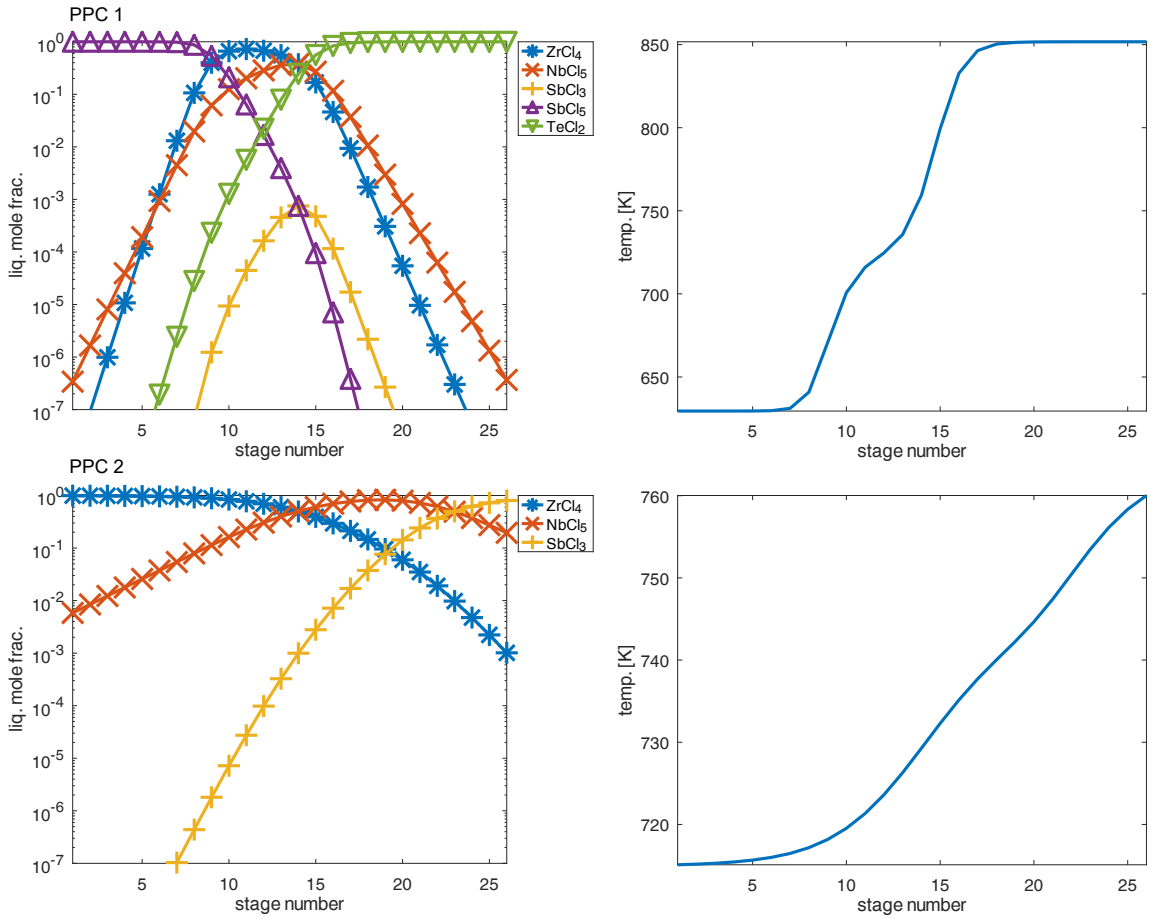

Figure 45: Flow-chart simulation of SNF distillation: DC-3 results of PPC 1 & PPC 2 at 25 bar

According to the simulation results in PPC 1, antimony pentachloride is distilled as a light-boiling component of high purity from the other components of the first separation stage using the usual total reflux column principle, despite the absence of radioactive components. Tellurium dichloride is also obtained as a high purity but high boiling distillation product in the final separation stage. In the separation stages 8-16, the proportion of the medium boiling components zirconium tetrachloride and niobium pentachloride increases significantly between separation stages 8-14, which leads to a bending of the temperature curve of the first separation process between separation stages 8-14, as shown in Fig. (45). The separation curve for niobium pentachloride has its highest composition value with a maximum of 26 mol% in the fourteenth separation stage. For zirconium tetrachloride the maximum is in the eleventh stage with a maximum mole fraction of 88 mol%. However, the medium boiling components of zirconium tetrachloride and niobium pentachloride dominate in these stages, with only about 10 mol% of other chlorides present, which is not sufficient for any separation accuracy. The temperature curve in PPC 1 is otherwise monotonically increasing from 629.5 K in the first separation stage to 851.7 K in the last separation stage, where the maximum proportion of the antimony trichloride separation curve is also obtained for the antimony trichloride component according to the thermochemical equilibrium conditions via [14]. The temperature curve in PPC 1 otherwise increases monotonically from 629.5 K in the first stage to 851.7 K in the last stage.

In PPC 2 the components zirconium tetrachloride and niobium pentachloride with impurities

up to a maximum of 1 mol% can be recovered by distillation in the simulation results (according to Fig. (45) (lower figure for total-reflux PPC 2). The tendency of the composition to change after the separation stages is significantly less pronounced in PPC 2 than in PPC 1 due to the significantly smaller temperature difference between the first and last separation stage in PCC 2 with 715 K to 760 K compared to PPC 1. The zirconium tetrachloride component is less depleted in the direction of the evaporator than in the previous separation, while the medium boiling component of at least 0.5 mol% is always present as an impurifying component in the mixture with zirconium tetrachloride. Only the antimony trichloride curve changes most significantly as a very weak medium boiling component with its maximum on the nineteenth stage. With respect to antimony trichloride, this component is enriched together with niobium pentachloride as a mixture in the heavy distillate product fraction of the boiler. Therefore, antimony trichloride is only recovered as a mixture with niobium pentachloride under these process conditions. It is possible to separate these components in the heavy boiler in order to select more separation stages for the whole column. In this case, higher purification accuracies can also be achieved for the other components in the PPC 2.

Alternatively, if additional chlorine is added to SC-2, which affects the presence of equilibrium reactions, the chemical equilibrium of the chlorides can be significantly shifted towards the more chlorinated volatile chlorides according to the Le'Chatelier principle. The reaction equation in SC-2 are then as follows (l defined as liquid and g as gaseous state)

$$\begin{aligned} \mathrm{SbCl_3}(l/g) + \mathrm{Cl_2}(g) &\leftrightarrow \mathrm{SbCl_5}(l/g), \\ \mathrm{NbCl_3}(l) + \mathrm{Cl_2}(g) &\leftrightarrow \mathrm{NbCl_5}(l/g), \\ \mathrm{TeCl_2}(l/g) + \mathrm{Cl_2}(g) &\leftrightarrow \mathrm{TeCl_4}(l/g), \\ \mathrm{ZrCl_2}(l/g) + \mathrm{Cl_2}(g) &\leftrightarrow \mathrm{ZrCl_4}(l/g), \\ \mathrm{SnCl_2}(g) + \mathrm{Cl_2}(g) &\leftrightarrow \mathrm{SnCl_4}(l). \end{aligned} \tag{100}$$

In this case, the antimony trichloride content would nearly disappear and niobium pentachloride could be obtained by distillation in the second separation process (total-reflux PPC 2) with significantly lower impurities well below 0.5 mol-% as the calculations have shown. This improves the separation accuracy even significantly compared to the simulation results from Fig. (45).

Off-gas purification For the recovery of argon from the equimolar carbon dioxide-argon gas mixture of the gas stream of SC-3, a modified Linde liquefaction process via cryogenic distillation at pressures above 6.2 bar can be applied in the separation operation of DF-2. The more detailed technical separation procedure is described in [137] and suitably modified to apply to the distillative separation of the equimolar Ar-CO_2 mixture. For this purpose, the corresponding DF-2 column is simulated in a simplified way as a total-reflux column and the simulation results are shown in Fig. (46) .

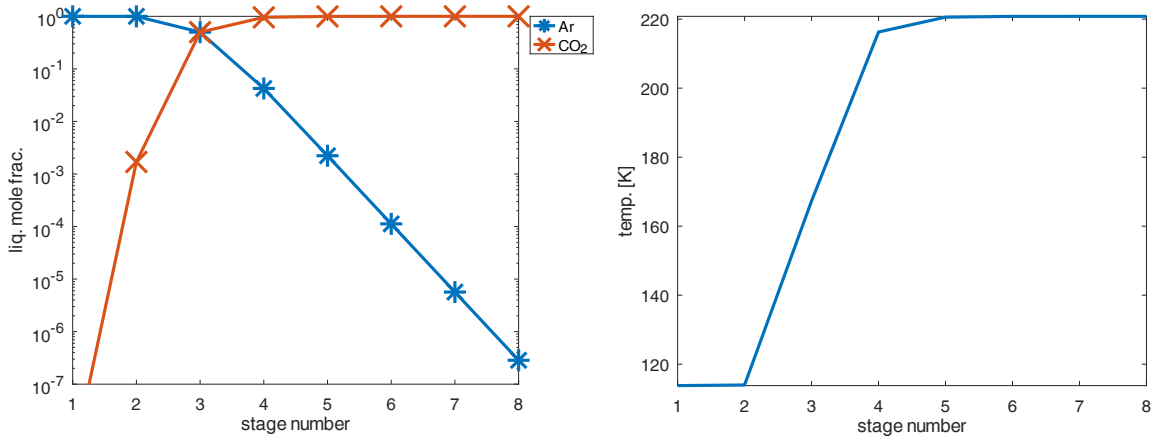

Figure 46: Flow-chart simulation of SNF distillation: DF-2 at 6.5 bar

These results show very good separation success with high separation accuracy. Within an eight stage distillation column it is therefore possible from 113.8 K to 220.0 K at 6.5 bar (and from 120 K to 270 K at about 8 bar) to recover argon with high purity in the condenser with separation accuracies well below 1E-04 mol%. Carbon dioxide is recovered with high purity in the evaporator. For the separation curves shown in Fig. (46), the argon content decreases steadily as the number of separation stages increases, while the carbon dioxide content correspondingly increases steadily. In the first two stages, where practically no carbon dioxide is present, the colder temperature of 113.8 K is reached, while from the fourth stage the carbon dioxide dominates and the temperature is close to 220 K. The challenge of this distillation is to achieve distillation at low temperatures, close to -160 °C. The required cooling energy can be obtained for the chosen liquid fuel reactor, preferably the metallic Dual Fluid Reactor version. Alternatively, this process step can be outsourced to other companies that have good technical solutions to the separation problem and can implement them.

6.2.4 Zirconium alloy treatment plant

The chlorination in PB-1 (see figure 31) of the shredded zirconium cladding alloy material takes place under relatively mild process conditions at 623 K and 1 atm. Fuel material entrained in the shredded zirconium cladding material and adhering to the walls, for example, cannot be chlorinated with pure chlorine under these process conditions, as explained in [142, 143, 16]. For the simulation calculations below, a maximum of 0.1 mol% of the original uranium dioxide molar content is assumed as entrained material in order to estimate that the separation of the uranium dioxide can then be easily and completely carried out in SC5, S5. According to [15, 142], the predominant molar fraction of the chlorinated cladding material is only 98.327 mol% zirconium tetrachloride. To obtain zirconium tetrachloride after reaction with chlorine gas via $Zr(s) + 2 \cdot Cl_2(g) \rightarrow ZrCl_4(s/g)$ with yields close to 100%, chlorine is used in excess. Since both the exact composition of the additional alloying elements can vary greatly and the excess amount of chlorine and the amount of entrained fuel material as uranium dioxide are unknown, only the composition from Fig. (47) is considered for illustrative purposes in the simulations. Fig. (47) shows the feed composition of all other components after chlorination as

additives to zirconium tetrachloride. These are mainly tin tetrachloride, niobium pentachloride, iron chloride, mainly as iron trichloride, in equal proportions and very small contribution of uranium dioxide inpurification from the fuel material. Furthermore, the small amounts of cobalt and rare earths are negligible according to data from [142, 15]. Nickel and nickel chlorides are also neglected as material components in the following calculations due to the lack of data on thermal properties at high temperatures. Most chlorides, such as chromium chlorides, are estimated to be thermally metastable based on ideal stability data according to [14, 24]. Therefore, in the following simulation calculations only chromium dichloride is assumed as the only chromium chloride. Other chlorides or even fission products are considered to be so small that they must be neglected here, since the exact composition value cannot be determined. Furthermore, variations in the zirconium alloy components are quite common, so only one example of such a composition is selected and simulated in these calculations.

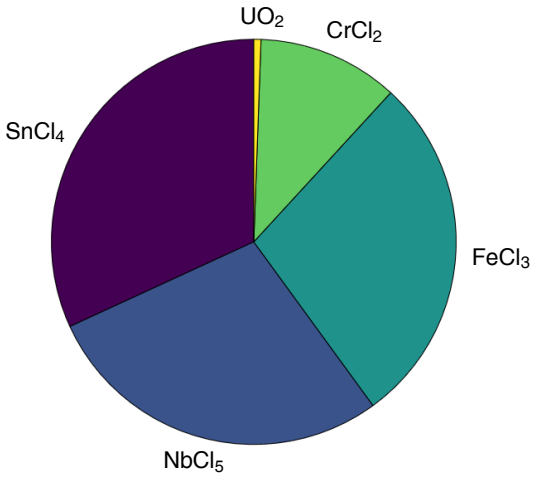

Figure 47: SC-4 feed: Additive composition with residual amounts of adhering or penetrated uranium dioxide from SNF-fuel material given in mol%.
Ref.: [15, 16]

The simulation results for the condensation in SC-4 show that chlorine together with possible small amounts of tin tetrachloride with 1E-02-mol% can be removed as vapour phase (see red bars shown on the right in Fig. (48) for chlorine and tin tetrachloride). Although zirconium tetrachloride does not have a liquid phase as a pure substance at 1 atm, there is no need to operate under higher pressures here until zirconium tetrachloride has to be separated, which is not the case here until distillation column DC 4 is investigated according to the process flow chart Fig. (32). However, the other predominant part of the tin tetrachloride is present in the liquid with a proportion of about 0.65-0.80-mol% (left blue bar of tin tetrachloride according to Fig. (48)). The other volatile chlorides, except for tin tetrachloride, then remain completely in the liquid or solid state of the settling tank S4 and do not enter the vapour phase under thermal equilibrium consideration (see blue bars shown on the left for each substance component in Fig. (48)). Because of the high vapour pressure values of tin tetrachloride at 298 K of 5.6170E-02 bar and at 270 K of 1.4446E-02 bar, a higher proportion of tin tetrachloride is present in the vapour phase. A more accurate separation of tin tetrachloride is not possible under these conditions,

even with the addition of several such separation stages, since the vapour pressure value remains relatively high and under lower temperatures other volatile chlorides can also partially condense out or sublime. Therefore, the chlorine gas separation of the excess chlorine is only possible with increased proportions of tin tetrachloride in the gas phase, which, however, does not contain any other impurities of other material components. The concentrated other components of the simulated liquid phase in S4 are fed to the SC-5 separation unit.

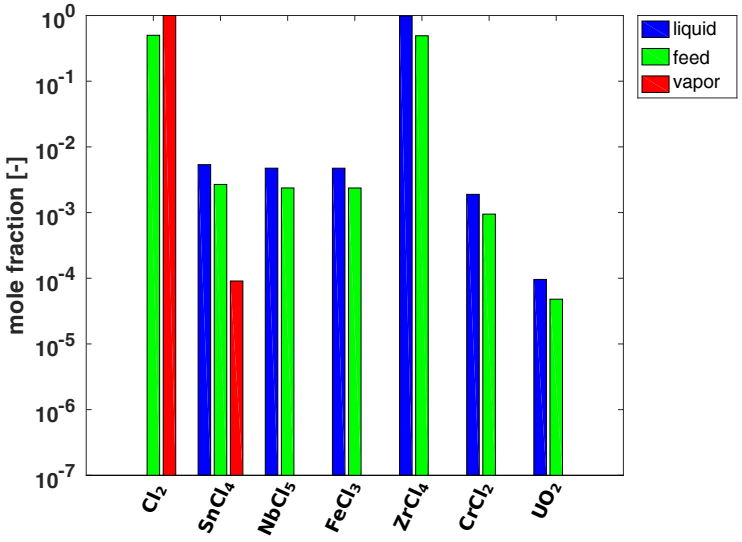

Figure 48: Flow-chart simulation for distillative zirconium alloy recycling of zirconium cladding material from fuel rods used for SNF material: SC-4, S4 results at 623 K and 1 atm

The simulation results for SC-5 shown in Fig. (49) at 725 K under 1 atm show a sharp separation of chromium dichloride and uranium dioxide from the other volatile chlorides (shown as blue bars in Fig. (49) of the two components). The volatility of chromium dichloride is very low compared to the other volatile chlorides and the volatility of uranium dioxide is practically negligible. Other volatile components are only present in the vapour phase (see red bars in Fig. (49) for each component). Chromium dichloride and uranium dioxide can then be fed into the main fuel reprocessing unit, in which these components are chlorinated with tetrachloromethane in PB-2 at 2000 K and higher pressures (see flowchart in Fig. (32)).

For the subsequent distillation, pressures above 23.36 bar must be set in C3 so that zirconium tetrachloride can have a liquid phase as a pure substance at all due to the position of the triple point. In a 24-stage separation column, the simulation results for the first steady-state total reflux column operating condition at 25 bar are shown in Fig. (50). Except for tin tetrachloride and iron(iii) chloride, the distillative separation task is analogous to the waste gas treatment of the DC-3 column for fine separation of the volatile chloride components without uranium tetrachloride.

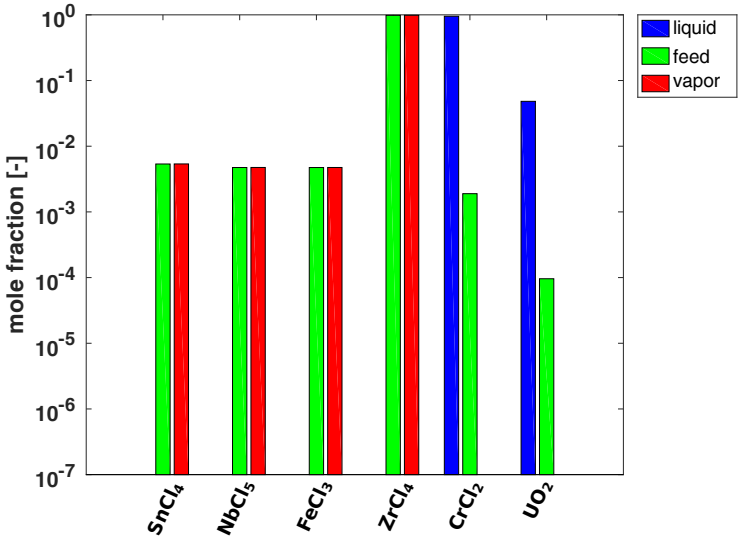

Figure 49: Flow-chart simulation for distillative zirconium alloy recycling of zirconium cladding material from fuel rods used for SNF material: SC-5 results at 725 K and 1 atm

According to the simulation results of the DC-4 column in Fig. (50), the zirconium tetrachloride light-boiling separation curve dominates in the first four separation stages in the first steady-state total reflux column condition (PPC 1). In the first stage tin tetrachloride is obtained as a high purity light boiling product and in the last stage high purity ferric chloride is obtained as a heavy boiling product with impurities in the ppm range. The temperature curve in the first total reflux state, as already shown in the waste gas treatment for the separation of zirconium tetrachloride from volatile components, qualitatively assumes such a curve progression from 538.5 K to 814.5 K (cf. Fig. (45) (upper figure)), including the curvature of the curve, in the column range 6-12, in which zirconium tetrachloride predominates as the material medium-boiling component. The light boiling component is then significantly depleted between the fifth and thirteenth stages and is considered to be completely separated after the fourteenth stage with a separation specification of 1E-04 mol%. The iron(iii) chloride separation curve, in which the formation of Fe_2Cl_6 has been neglected as a polymerised salt compound, increases from the fourth stage towards the column evaporator, with the greatest change in mole fraction observed between the fourth and fifteenth stages. In the macroscopic coarse separation, from the fifteenth stage onwards, the proportion of the medium boilers zirconium tetrachloride and niobium pentachloride decreases, so that the proportion of the high boiling component iron(iii) chloride increases accordingly. At the final separation stage, the iron(iii) chloride is then obtained in the evaporator just within the acceptable separation specification of 1E-04 mol% impurities for reuse, because iron is a very cheap metal. The separation curve for zirconium tetrachloride shows the maximum fraction of 98-99 mol% in the thirteenth stage, while the fractions of tin tetrachloride and ferric chloride together are relatively small, and in this stage these fractions become strongly minimal in total amounts. The maximum of the niobium pentachloride separation mole fraction curve is in the twelfth stage with a low proportion of only about 1 mol%. Beyond the maxima of the medium boiling separation curves (of zirconium tetrachloride and tin tetrachloride), the respective molar fraction values of these components decrease, as shown in

Fig. (50) (upper figure).

In PPC 2, the second stationary total-reflux column operating condition state according to Fig. (50) (lower figure), only the mentioned zirconium tetrachloride-niobium pentachloride mixture is then present, within which the zirconium tetrachloride component can only be slightly depleted by coarse separation in the direction of the evaporator, while the niobium tetrachloride component is increasingly enriched there. Accordingly, in the condenser for niobium pentachloride the lowest substance amount fraction of 3.3504E-04 is present, which is just below a separation accuracy of 4E-02-mol%, but still satisfactory in the non-nuclear application. However, there is still too much impurity of zirconium tetrachloride in the evaporator. Therefore, no pure bottom product is obtained. Since the transition point to the niobium pentachloride component is still reached in the last separation stage, the turning point of the temperature curve is present in the temperature profile in this stage, whereby otherwise between the temperatures 715 K and 736.1 K, the strictly monotonically increasing curve progression of the temperature profile shown in Fig. (50) .

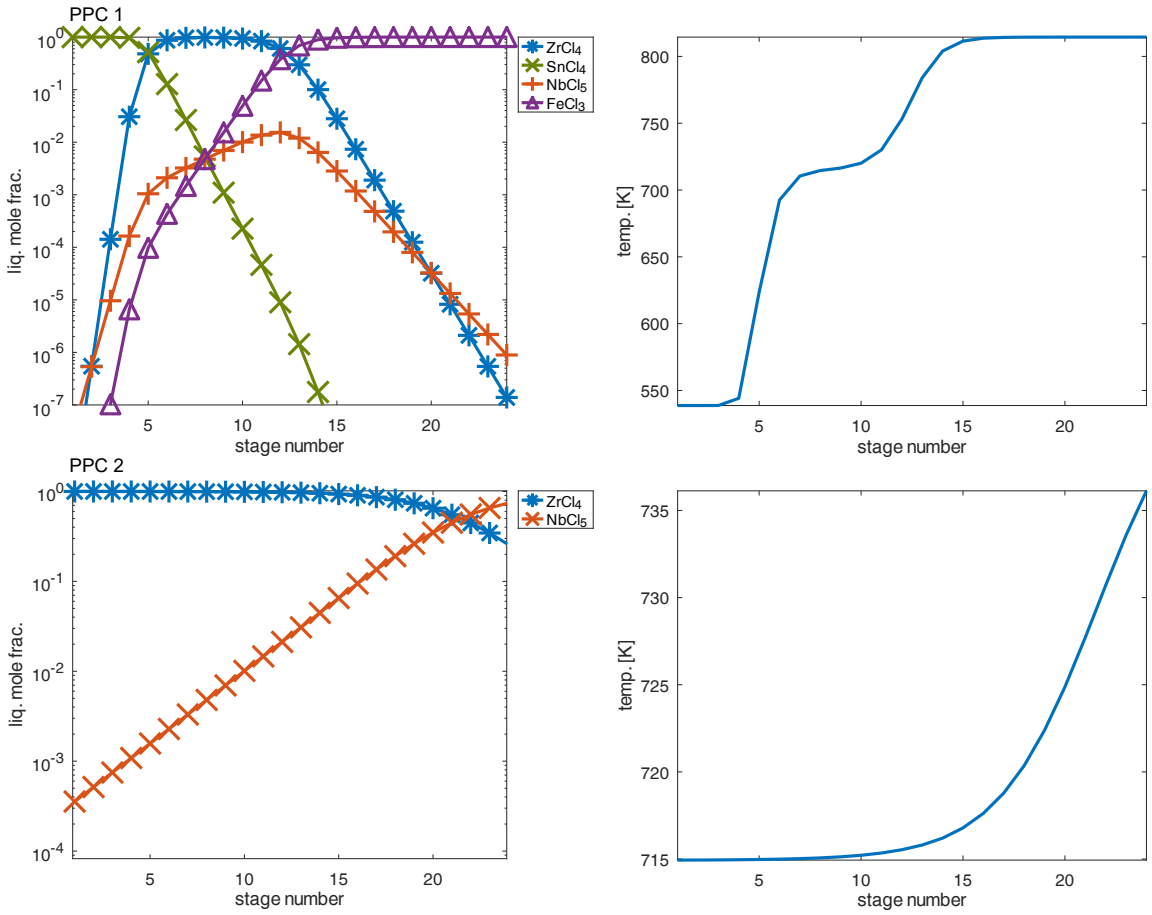

Figure 50: Flow-chart simulation for distillative zirconium alloy recycling of zirconium cladding material from fuel rods used for SNF material: DC-4 results of PPC 1 & PPC 2 at 25 bar

From the results shown in Fig. (50), it can be concluded for the recycling of zirconium cladding material in DC-4 that iron and tin components can be easily separated as chlorides by distillation, but zirconium only with minor impurities of niobium pentachloride with a maximum

content of 4E-02-mol%. With regard to technical recycling, the separation accuracy may not be sufficient for technical reuse of zirconium tetrachloride as a raw material in the nuclear sector. Since the zirconium tetrachloride content of 2-3 mol% is still too high in the last separation stage, it is recommended to carry out the distillation product removal in the last separation stage after the second total reflux column operation according to the principle of the discontinuous distillation column up to the maximum permitted content of niobium pentachloride. The remaining amount of niobium pentachloride and zirconium tetrachloride cannot then be further separated, but without bottom product removal under top product removal at the condenser, most of the zirconium in the form of zirconium tetrachloride can be recovered from the molten salt at the above separation specification of 4E-02-mol% (of residual niobium pentachloride). However, the niobium pentachloride itself cannot be recovered by distillation in this column modification at a reasonable cost. Due to the similarity of the separation problems with similar chloride components, feed compositions and a similar number of separation stages of the distillation columns DC-3 (distillation of volatile chlorides in waste gas treatment) and the DC-4 column considered here, the question of using the distillation in a single integrated distillation column may arise.

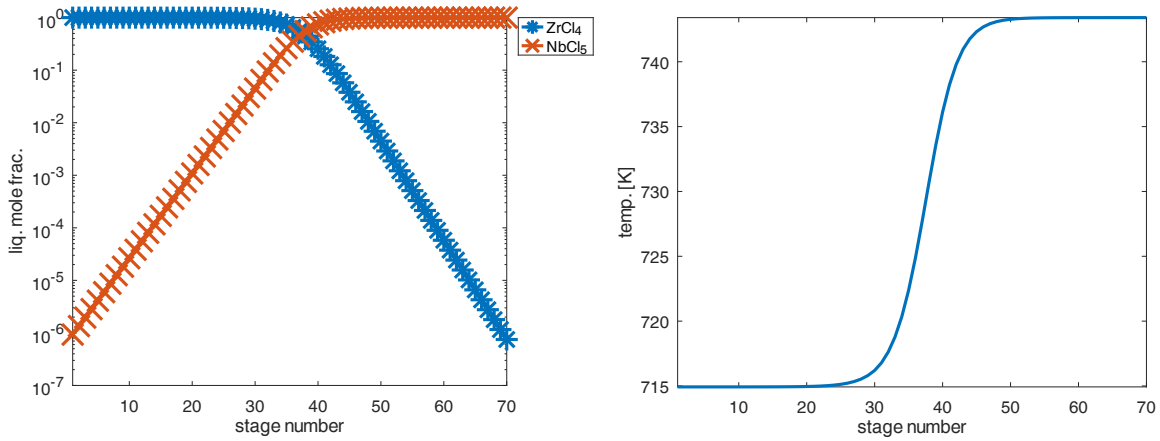

Figure 51: Flow-chart simulation for distillative zirconium alloy recycling of zirconium cladding material from fuel rods used for SNF material: Distillation application for the complete recovery of high-pure zirconium tetrachloride (Impurity content of 1E-04-mol% of niobium pentachloride) from chlorinated zirconium alloy

Alternatively, distillation with high separation accuracies in the range of 1E-04 mol% in a much longer column with significantly more stages is theoretically possible, but technically difficult to implement in order to recover both zirconium pentachloride and niobium pentachloride in high purity by distillation. Fig. (51) shows the simulation result of such a large total reflux column with 70 stages. High purity zirconium tetrachloride then accumulates in the first stage, and on the way to the evaporator the mixture becomes depleted in zirconium tetrachloride as the number of stages increases, while the mole fraction value of niobium pentachloride increases. High purity niobium pentachloride can then be obtained in the bottom product of the final column stage. The temperature profile shows the expected S-shaped strictly monotonic temperature curve with an inflection point centred near the middle of the column at about the fortieth stage. However, it is critical to question whether this separation effort is justified. This question depends in particular on the purity of the recycled product in relation to the separation

specifications, compared to the competing consideration of other alternative and possibly more cost effective separation processes. These statements apply only to zirconium recycling and not to fuel recycling by distillation.

7 Strategic elaboration on the complete utilization and depletion of national and worldwide SNF inventories

The idea of the following elaboration is to be able to use the Dual Fluid Reactor for the partial or complete depletion of national and global SNF waste inventories. As described in the introduction to Fig. (2), the possibility of recycling SNF material by distillative separation of the actinides and fission products and the subsequent use and consumption of these waste materials in the Dual Fluid Reactor. The subsequent cyclic process of utilization and distillative processing of the DFRm feedstock allows only short-lived fission products to be obtained at the end, so that these materials only need to be stored for a maximum of 500 years until the activity decays to natural ambient level. In this way, the waste inventories are completely used up and no new waste is produced for final disposal. The simulation results and the presentation of the applicability of distillative reprocessing of HLW and DFRm material are included in the section (C) (of the Appendix) and are not discussed in detail here. However, these results ensure that the overall strategy developed in this thesis can contribute to solving the repository problem.

A fundamentally elaborated strategy concept for the partial processing and utilization of SNF material concerns the possibilities of using distillation according to the following main options (for recalculation, the tables on SNF material according to Tab. 1 and the activity table according to Tab. 2 should be observed). The main strategy is to be understood in the following points:

1. A 50-vol% reduction of a repository for SNF material can already be achieved by applying distillation without having to use the Dual Fluid Reactor directly. In this case, only the most active components are separated by distillative treatment and procesing and the materials can be disposed of in a more space-saving manner, since the entire waste volume no longer has to be stored in an equally costly way. In addition the spearation volume will reduced to a factor of 1/2, referring to all the data of [29] activity and more. The waste is separated according to activity, with the greatest activity coming from a small number of fission products and actinide components.

2. If only the majority of the uranium from the spent nuclear fuel is used, the volume of the repository can be reduced to at least 90% by volume by using only uranium in the metallic version of the Dual Fluid Reactor, leaving the other 10% (in volume) part as waste. The calculations are based on the assumption that the Dual Fluid Reactor produces no further waste to be disposed of. The much smaller remaining volume of waste can then also be stored in the repository in a space-saving manner. The advantage of this is that, as shown in the process flow chart in Fig. (32) , the DC-2 column, which is the most complex in terms of process technology, is now completely removed from the SNF processing concept at this point, but the majority of the waste is successfully processed and reused. This is

also the case for the complete sistillation-based recovery of the DFRm melt, as can be seen from the simulation results in section (C.1.3) of the Appendix.

3. The almost complete recycling of the SNF material and the use of the Dual Fluid Reactor, as well as the avoidance of further fuel waste to be stored in the Dual Fluid Reactor concept or in other similar liquid fuel reactors (if these reaction concepts are available, integrable or will be available in the future), will provide a complete solution to the disposal problem, with no need for final storage in the future.

All calculated numbers for decreasing SNF waste are related to the separation accuracies of the simulation results here, to the total mass and subsequent total balance over time with inventory utilization and to the forecast made in [13]. In the second case, where only uranium tetrachloride is removed together with possible additional small amounts of neptunium tetrachloride, only 5 vol% of the repository volume needs to be stored. However, with the final increase in the intensity of the distillation application, the final storage volume can be reduced to only 1 vol%, but this estimate is based on maximum idealized assumptions and the most optimistic view of the simulation results. In the second and third options, the processing of radioactive waste by conversion, mainly of SNF material, including full recycling of cladding material, will lead to a fundamental change in the radioactive waste management strategy, which has not been taken into account in the estimation of waste volume reduction in this section.

The focus of the analysis now turns to the global temporal strategy for solving the waste problem of using up all SNF waste inventories in the short temporal period and not producing any new waste. With a global inventory of 370,000 tonnes of such waste, according to data from [13] and secondary from [29], it is possible to operate 6 such distillation plants with distillation separation together with feeding a fuel reactor such as the Dual Fluid Reactorr, each with a possible industrial reprocessing capacity of 1000 tonnes/year, for about 60 to 65 years, in order to significantly reduce the waste by the above-mentioned amounts of the second and third options. In this case, the reprocessing of spent fuel can be carried out continuously. For Germany alone, with a use of 19,000 tonnes/year, a single plant can operate for twenty years to completely reduce SNF waste. On a global scale, however, 6 plants will be needed to use up the fuel after 65 years and to solve the global disposal problem completely.

Part V
Conclusions and future perspectives

The results of this study impressively have demonstrated, under the best possible idealized conditions of ideal phase equilibria (according to equation (27) with $\gamma_i = 1$), the potential applicability of distillation-based separation processes for nuclear fuel reprocessing and further distillative recycling of zirconium cladding material. Under ideal phase equilibrium conditions, in the form of the most optimistic view of reprocessability, such an applicable distillation-based separation concept has been developed, as shown in Fig. (32). Here, the developed separation process from the simulation results impressively have demonstrated that the disposal problem can be solved by reprocessing of spent nuclear fuel and recycling of today's recovered nuclear-relevant waste materials in general. The overall thesis of this study is based on the idea of realising recycling in a meaningful way for the recovery of all nuclear waste and its reuse in suitable liquid fuel reactors, including the possibly necessary cyclic recovery of the reactor melt. In addition, from the simulation result of a total reflux column, an additional distillation column design has been conceptualised in this thesis, which is a safer closed separation principle close to cyclic usable total reflux principles, including product removal at the end of such process cycle, but even without significantly influencing the total reflux operation of the column. By applying this cyclic recycling process internally to each column operation and, more importantly, externally to each inventory charge processing until the world's entire waste inventory is depleted, only short-lived fission products will remain as waste, requiring only a few years of final storage. As a secondary benefit of this thesis, it will also provide cheap energy production, which will bring further prosperity to human civilisation. A suitable liquid fuel reactor for the reuse of such distillative recovered material has been selected in this thesis to be the so-called metallic Dual Fluid Reactor (DFRm). This reactor concept is a perfect example of such a cyclic separation process using the distillative separation plant designed here. This concept has an optimised utilization of two liquid cycles, a compositionally robust fuel cycle and a lead cooling melt cycle, where the fuel material can have different variations of feed compositions in terms of spent nuclear fuel waste, Dual Fluid fuel melt recovery, highly active waste material or even mixtures of these recycling examples, where the recovered melt can be directly reused by the Dual Fluid Reactor principle. Further results on the combination of the DFRm process in this thesis as well as simulation results have shown that not only the repository problem can be solved, but also the complete avoidance of new repository waste or any kind of waste inventory production due to the high separation accuracies after distillation shown by various distillation results in this thesis.

Since some material data were missing for theoretical work within this thesis, the best possible ideal phase equilibrium separation was assumed. More complex deviations from this behaviour would only increase the conceptual design in the ideal process units without changing the general design. Therefore, it is assumed that the developed design is the fundamental component for further development of such a realistic process design with much experimental and simulation work in the future. Therefore, in the following sections, the detailed conclusions are presented separately from the model ideas, model concepts, the simulation results and the conceptual design

development, including the idealized process flow chart simulation and possible deviations from the imaginable real phase equilibrium deviation behaviour . Simulation results from section (5) on the independently developed total reflux column model (model TRC-O/M according to chapter (III)) show a good agreement of the results with the corresponding total reflux column model of ChemSep Lite. This is shown by numerous results on exemplary test mixtures with ideal and real phase equilibrium behaviour . The comparison of the distillation of the feed stream of the titanium tetrachloride distillation according to [12] has also been simulated for the total reflux column principle. The comparison with the experimental results for the titanium tetrachloride distillation according to [12] shows reasonable separation results without contradictions despite the different operating principle between the experimental discontinuous operation with high reflux ratios within an experimental laboratory column compared to the simulated total reflux principle in this work. Furthermore, it shows even comparably good results for reflux ratios of 2.0 of the implemented pilot plant from the technical report of [12]. The simulation results of different distillation processes between two different simulation models, a self developed Octave/MATLAB model in this thesis and a freely available ChemSep Lite model, agree very well even for this more complex multi-component mixture as shown in Fig. (26), in that only slightly larger deviations can be observed in a few separation stages of the temperature profile and in the profiles of the mole flows. Based on the simulation results, such a cyclic working closed total reflux column design specialised for nuclear waste recycling is successfully developed in this thesis as mentioned above.

Among the simulation results of spent nuclear fuel material of the process design based on such a cyclic total reflux principle of this thesis, the following highlighted summarised distillable fractions have been obtained:

- Destillable light-boiling fractions:
    1. Uranium tetrachloride, which was originally present at 95 mol% in spent nuclear fuel material,
    2. Curium trichloride together with samarium trichloride impurities,
    3. Americium trichloride with cesium chloride, strontium dichloride and minor fraction values of samarium trichloride impurities.
- Destillable heavy-boiling fractions:
    1. Plutonium trichloride together with cerium trichloride, praseodymium trichloride and lanthanum trichloride,
    2. Neodymium trichloride together with barium dichloride.

Impurity means that the substance component does not occur elsewhere in any other end process stream of the conceptual design. Otherwise, a mixture of separation fractions is obtained by distillation. In addition, the results for the processing of zirconium cladding materials have shown that these material compounds are difficult to recycle due to the higher pressures required. However, antimony pentachloride, tin tetrachloride and tellurium dichloride can be separated by high-purity distillation, both in waste gas treatment and in distillative cladding material recovery.

Iron(III) chloride, which is only present in zirconium cladding material, can also be separated as a high purity distillation product in this total reflux column design separation mode.

In conclusion, this thesis has shown that the main actinide and fission products useful for the Dual Fluid Reactor can be provided by distillation as fuel under cyclic use of the closed cycle total reflux principle defined in this thesis and DFRm feed material separation by distillation until only short-lived fission products are available. Further results in the appendix show the integrability of the pyroprocessing separation unit even at mixing ratios of DFRm material to be recycled and even highly active HLW material, neglecting decay heat and ideal phase equilibrium relations. Thus, the applicability of the developed separation process coupled to the Dual Fluid Technology and the application of a pyroprocess separation plant for the purification of SNF and HLW fuel and the distillatively recovered Dual Fluid melt material under ideal conditions has been clearly demonstrated and presented. The assumption of deviations up to strong deviations from the real phase equilibria would probably only increase the number of separation stages required or, in the case of azeotropic mixtures, the number of columns required for each separation region resulting from a multi-component, dimensionally defined azeotropic boundary distillation region.

Possible follow-up studies resulting from this thesis Possible follow-up studies from the conceptual design of this thesis to a pilot plant include several steps to measure the phase equilibria and subsequent simulations with new models based on the theory of the UNIQUAC and LIQUAC models, which should be required in the future. After the design of a laboratory column, the first separation experiments can be carried out in this first closed total reflux column design. The following studies are recommended

1. Experimental measurement of vapour-liquid equilibria for the major binary inorganic salt mixtures with uranium tetrachloride first, in a closed chamber evaporator unit or other measuring device of a single stage distillation unit,

2. Development of new physical GE models for the description of nuclear salt mixtures in the vapour-liquid system,

3. Comparison of the results on the GE model with new experimental measurement data of the vapour-liquid systems and correction by suitable model equation parameters,

4. Simulations of distillation columns, which can reproduce the real phase equilibrium behaviour relatively accurately via the correspondingly developed GE models for the relevant molten salt mixtures,

5. Experimental research on the separation of the chloride components of simple and later of more complex spent fuel-relevant mixtures in laboratory distillation columns,

6. Development of a corrected real separation process based on the experimental separation results and simulations, as well as the basic separation design presented in this thesis,

7. Construction of single pilot separation plants for the distillative recovery of spent nuclear fuel.

Before the experimental phase can begin, calculations with complex GE models or modified UNIQUAC and LIQUAC models are required, whereby the Margules equation, exemplary shown in this thesis only corresponds to a simple correlation function and should only be applied at the beginning to estimate the non-ideal vapor-liquid equilibrium behaviour . In the UNIQUAC model, the repulsive interaction force of the parameters could be considered by the activation energy of interactions as well as for diffusion for the estimation of interaction force limits from a modelled chloride cell considered by the model. Here, also molecular dynamic simulation could be useful to determine the most important interaction parameters for the most important binary relevant mixtures for the realistic simulative solution for the distillation problem in the conceptual design. Here, after decomposing the fluid of such moving dynamic diffusion cells, the mean forces and the collision frequency C_0 could be determined to calculate the mean activation energy via an Arrhenius approach for example, such as

$$E_{A,ij} = -RT \ln\left(\frac{E_{D_{ij}}}{C_0}\right), \tag{101}$$
$$u_{ij} \approx E_{A,ij}.$$

The calculation should be done in such a way that a part of the quantity dissociates and another part remains covalently bound in the melt. This behaviour is to be quantified with the dissociation constant, which should be also measured, or derived from the ionic fraction φ_{ij} of the substance component i in chloride solvent j by suitable literature values. Therefore, a separation is made into an ionic fraction (with complete dissociation into chloride ions & metal cations) and a molecular-covalent fraction, each having a combinatorial and a residual fraction (see UNIUQAC/LIQUAC-GE models in the appendix of the section (2.2.3.3)). In each of the two residual parts, the diffusion activation energy is now taken into account as an energy parameter.

If molecular dynamic simulations are available from literature, the modelling can also be described alternatively as a modified UNIWUAC or LIQUAC model by considering the non-dissociated portion of the ion portion as a solvent in which the dissolved ions of the compounds with total ion portion φ are present. Using the example of the substance system UCl_4-LiCl-KCl according to [99, 103], the phase equilibrium could thus be estimated, if suitable information on the ion fraction or the dissociation constant is available. These phase equilibria can then be determined experimentally for representative mixtures in a simple laboratory closed distillation chamber unit.

After measuring the equilibria in a single distillation unit where thermodynamic equilibrium is reached, suitable GE models for VLE salt melts can be developed for the measured chloride vapour-liquid equilibrium systems. Discrepancies between experiment and model can be corrected by correlative fit parameter functions. Further experiments and improved modelling will allow the construction of a laboratory distillation column for experimental optimisation of the separation of chlorides in molten salt mixtures in a distillation column. Based on this, the realistic separation process and flowsheet development for a distillation-based SNF treatment plant will be successfully realised.

Prospects for using the proposed distillation-based separation installation As shown in the (7) section, there are opportunities to completely recycle the world's spent nuclear fuel inventories within 60-65 years and, as shown in the extended calculations in the Appendix in section (C), to completely consume other materials within such a distillation-based design to recover Dual Fluid Reactor melt and other highly active waste materials. This will revolutionise the use of nuclear energy through the cost-effective and sustainable processing of all relevant waste streams in this combination of Pyroprocessing Separation Unit (PPU) and Dual Fluid Technology (DFR) or even another suitable liquid fuel reactor capable of burning up the recovered material from the PPU.

Following the successful technical implementation of spent nuclear fuel processing and stream recycling in the Dual Fluid Reactor, there are other industrial applications for the use of high temperature distillation of molten salts for the recovery of valuable metallic and basic raw materials. For example, the following industrial and chemical applications are technically feasible with the distillation concept developed here, which could include example the following tasks:

- Raw material recovery from alloys, such as the distillative recovery of titanium from titanium alloys.
- Recovery of neodymium and lanthanides from NdFeB magnets (see also [70]) or generalised recovery of rare earths and their additional valuable constituents from these alloys using chlorine as a chlorination agent to volatilise the material, or even special glasses using carbine tetrachloride for chlorination to volatilise them.
- Recovery of lithium from lithium batteries, in alloys or from glasses and ceramics.
- Recycling of other valuable alloys.

NdFeB magnets in particular are contained in many electronic devices such as mobile phones and PCs as well as in almost all machines, in the automotive industry and in wind turbines and are thus indispensable as materials. The extraction of rare earths is relatively environmentally harmful in this respect. Recycling with distillative separation processes would already save resources enormously in this example of separating the rare earths from NdFeB magnets and does practically without additives. With regard to the consideration of resource conservation of metallic valuable materials, such as rare earths, lithium, titanium, but also refractory metals up to precious metals, the distillative separation process represents a decisive solution proposal for significant improvement. Since rare earths are thus elementarily important for the operation of wind power plants, the recycling of such raw materials will be indispensable in the future. However, without further energy input, a recycling process is not economically feasible. Only base-load capable and cost-effective energy generation without waste generation, such as the application of Dual Fluid technology, makes the economic recycling of such materials possible in the first place. This underlines the high importance of the application of the distillative separation technology of nuclear fuels and the application of the Dual Fluid technology and thus the enormous importance of the technical implementation of the distillation-based pyroprocessing separation unit developed in this thesis.

Part VI
Appendix

In this appendix, in addition to the list of references, extensive information on extended simulation results, calculations, but also on further partial aspects of the theoretical fundamentals are listed as follows. In the first part of the appendix, some extended aspects of the theoretical fundamentals from chapter (II) are explained, and in the following section, the state of the literature research for this current state of the work of the thesis is discussed in detail, with a focus on the pure property data for the use of the ChemSep and Octave/Matlab distillation models. In the next section, the discussed results on conceptual design, e.g. of HWL and DFRm fuel treatment problems, are extended by numerous simulations and integration analyses in the SNF conceptual design from chapter (IV) under other process conditions, as well as the detailed results on SNF, HWL and DFRm fuel treatment in a further subsection. Subsequently, the results on test mixtures from chapter (III) are presented and discussed in detail with regard to the comparison of the Margules approximated VLE with ideal phase equilibria. In addition, an exemplary investigation of possible heat effects as well as heat accumulation through decay heat within distillation columns of representative SNF-relevant reduced test mixtures containing active isotope elements is carried out and their estimation results are discussed. The last section explains the use of the ChemSep Lite models used for this thesis, as well as the requirements and inputs.

A Supplements to the theoretical background: Diffusion and modelling of vapor-liquid equilibria

Firstly, diffusion is fundamental to the description of mass transfer for chlorination and mass transfer between liquid and vapour. This is followed by the description of real phase equilibria for VLE systems and details of critical nucleation in suspension crystallisation.

A.1 Diffusion

Mass transport between the liquid and vapour phases and in chlorination is essentially dependent on diffusion. Diffusion is the main rate limiting step in almost all separation processes and even in solid reactions. In the appendix, the estimation of diffusion coefficients is important for some GE models and distillation or the expression of mass transfer between vapour and liquid in VLE systems, also for non-equilibrium distillation models.

A.1.1 Fick's first law

For a simple binary system with solvent B and diffusion of A in direction l, the first Fick's law applies in the presence of a concentration gradient in the same direction, which states that the diffusion flux is proportional to the concentration gradient but opposite to the diffusion direction [144, 78]. According to [78, 144] , the following applies to the diffusive flux under the assumption

that diffusion occurs only in direction l

$$J_A \Big|_{\text{in } l} = -D_{AB} \cdot \frac{dc_A}{dl} \,. \tag{102}$$

The expression in equation (102) for the diffusion flux can be easily extended via the differential mass balance in an infinitesimal Cartesian coordinate system for all spatial directions with

$$J_A = -D_{AB} \cdot \nabla c_A. \tag{103}$$

Here the proportionality factor D_{AB} is the diffusion coefficient of A in B, which can be determined or is given in literature databases for appropriately formulated diffusion problems, e.g. in the collective works [145, 146, 147] for numerous chlorides available as temperature-dependent substance data systems in a wide variety of solution media or in different diffusion atmospheres. Diffusion coefficients often tabulated in the literature are given for strong or infinite dilution. In the gaseous state, the mobility of the molecules for both components is considerably greater than in the solid or liquid state. The allowable range of binary diffusion coefficients in the gas phase is then generally between 10^{-5}–$10^{-4}\,\mathrm{m^2/}s$. Diffusion coefficients in liquids are 10^{-11}–$10^{-9}\,\mathrm{m^2/}s$, provided that both components are in the liquid state [76, 147]. For general diffusion in non-porous solids the upper limit of the diffusion coefficients is about $10^{-12}\,\mathrm{m^2/}s$ (see: [76, 51]). It should be noted that for binary systems $D_{AB} = D_{BA}$ always applies, so that if one of the substances diffuses, the other substance component will also diffuse in the opposite direction. However, this is not necessarily the case for multi-component systems and all interaction combinations of the systems must be considered. The following applies as a summation (for N $\geq$ 3)

$$J_A = -\sum_{j=1}^{\mathrm{N}-1} D_{Aj} \nabla c_j, \tag{104}$$

$$= -c_{A,\mathrm{tot}} \sum_{j=1}^{\mathrm{N}-1} D_{Aj} \nabla x_j. \tag{105}$$

For this purpose, $c_{A,\mathrm{tot}}$ is the total concentration of A in the mixture

A.1.2 Fick's second law

In [144, 88, 76], for binary diffusion in the l-direction via a time-dependent mass balance consideration through a time-constant, stationary cross-sectional area A. Using equation (1) without convection and a Fourier expansion, the so-called second Fick's law can be formulated, which provides a partial differential equation for the concentration dependence as follows

$$\frac{\partial c_A}{\partial t} = D_{AB} \left(\frac{\partial^2 c_A}{\partial l^2} + \frac{1}{A} \frac{\partial A}{\partial l} \frac{\partial c_A}{\partial l} \right). \tag{106}$$

The equation (106) can be simplified in many ways. One important simplification is that the cross-sectional area A is independent of the direction l, so that

$$\frac{\partial c_A}{\partial t} = D_{AB} \left(\frac{\partial^2 c_A}{\partial l^2} \right). \tag{107}$$

For diffusion in all three Cartesian spatial directions, analogous to the equation (107) for a substance increment balance, the expression follows (see: [76])

$$\frac{\partial c_A}{\partial t} = D_{AB} \triangle c_A. \tag{108}$$

In equation (108), $\triangle = \nabla^2$ is the Cartesian Laplace operator. In highly dilute fluids, diffusion has no flow relevant influence on the fluid. In the case of strong concentration gradients, however, convection flows can be excited by diffusion, which means that according to equation (1) the convection term cannot be neglected. In addition, suitable initial and, if necessary, boundary conditions must be formulated in relation to the induced flows, so that a mathematical solution of the partial differential equations also exists. In a differential increment and with insertion of convection according to equation (8) (for all three spatial directions), a suitable partial equation for the description of the diffusion problem can also be set up in an analogous procedure to the derivation of equation (108) [76]. After the mass balance in the increment and the Fourier expansion, the convection velocity vector $\vec{w}$ follows

$$\frac{\partial c_A}{\partial t} = -\nabla \left(\vec{w} c_A \right) + \nabla \left(D_{AB} \nabla c_A \right). \tag{109}$$

In many cases of more complex diffusion problems with further special features, such as chemical reactions, solutions of the differential equations are only possible numerically. However, simplified analytical approximate solutions can often be found for numerous diffusion problems.

A.1.3 Simplified diffusion models in vapor-liquid systems

To determine diffusion in VLE systems, it is necessary to determine or accurately estimate the diffusion coefficients. The methods are discussed below.

A.1.3.1 Estimation of diffusion coefficients in gas mixtures In gases, diffusion and thus the diffusion coefficients depend significantly on the mean free path length $\overline{\lambda}$ between the collisions of two gas molecule species (see [148] pp.113 for the theory of the mean free path length). Physically, in the common simplified type, particles collide elastically in a volume according to the principles of conservation of momentum, if these particles collapse with respect to a mean collision cross section σ^{col}. [149]. For the mean particle number density of the pure gas $N_A = \frac{n_A}{V_A}$

$$\lambda_A = \frac{V_A}{n_A \cdot \sigma_A^{\mathrm{col}}}. \tag{110}$$

In the approximation of spherical molecules it follows from the collision cross section in the monomaterial system that it must be directly proportional to the diameter of the molecule, which of course also applies to monatomic gases such as the noble gases. Consequently, a simplified correlative approach can also be set up with the correction term C^{col}

$$\sigma_A^{\mathrm{col}} |_{\mathrm{spherical}} = C^{\mathrm{col}} \pi \cdot d_{\mathrm{mol}}^2. \tag{111}$$

Furthermore, the following relation with the impact frequency Γ^{col} according to[148, 149] holds for the amount of the mean velocity of a moving molecule with Boltzmann constant $k_B \approx 1.38 \cdot 10^{-23}\,\mathrm{J/K}$ and mass of the single molecule m_A

$$\begin{aligned} \overline{w}_{A,\mathrm{mol}} &= \lambda_A \Gamma_A^{\mathrm{col}}, \\ &= \sqrt{3 k_B T / m}. \end{aligned} \tag{112}$$

If it is a matter of statistical, random particle movements in all three spatial directions, the correction factor $C^{\mathrm{col}} = \sqrt{2}$ follows according to [148] for the correction term. With $\lambda_A \propto 1/p$, the proportionality with the gas pressure applies to the mean free path length

$$\lambda_A = \frac{V_A}{\sqrt{2}\pi d_{\mathrm{mol}}^2 \cdot n_A}. \tag{113}$$

In the binary system with components A and B, the arithmetic averaging of the collision cross sections for both collision partners is often performed with $\sigma_{AB} = 1/2\,(\sigma_A + \sigma_B)$. Simplified, according to [88], the Chapman-Enskog theory for calculating the diffusion of spherical molecules applies to highly dilute solutions according to the following approach

$$D_{AB} = \frac{3}{16} \frac{\left(2\pi k_B T \cdot \left(\frac{1}{M_{w,A}} + \frac{1}{M_{w,B}}\right)\right)^{1/2}}{\pi \cdot f(p,T) \cdot (N_A + N_B) \left(\sigma_A^{\mathrm{col}} \mid_{\mathrm{spherical}}\right)^2 \Omega_{DI}(T)} C^{\mathrm{corr}}. \tag{114}$$

In equation (114), Ω_{DI} is the temperature-dependent collision integral, which is essentially represented by the Van-der-Waals interactions of the intermolecular forces when molecules collide [88]. In the most complex case, the calculation is carried out by molecular dynamic simulations. However, parameterised equations f are often derived in the literature, among others from molecular dynamic simulations, as partly described in for the calculation of the collision integrals. Often the evaluation leads via so-called Lennnard-Johnes potentials ϵ with $\Omega_{DI} = f\left(\frac{k_B T}{\epsilon}\right)$ with the parameters $\epsilon = \sqrt{\epsilon_1 \epsilon_2}$, as Lennard-Johnes force constants besides the averaged collision cross-sectional area $\sigma_A^{\mathrm{col}} \mid_{\mathrm{spherical}}$. (for the two diffusion partners involved) [78]. For this purpose, [78] provides a possible simplified approach for estimating the Lennard-Johnes parameters as a function of the critical temperature $T_{C,i}$ with the following correlative approach

$$\epsilon_i \approx \frac{k_B T}{1.30 \cdot \frac{T}{T_{C,i}}}. \tag{115}$$

As an estimate for the averaged collision cross-sectional area, however, gives the following c

$$\sigma_A^{\mathrm{col}} \mid_{\mathrm{spherical}} = 1.18 \cdot \left(v''\right)^{1/3}. \tag{116}$$

C^{corr} in the equation (114) is according to [88] a correction factor for the difference of the masses A and B. However, the pressure p is estimated more generally and in deviation from [88, 76] with the help of a correlative, linear, temperature-dependent calculation approach. Also of importance is the estimation of the diffusion coefficients in a multi-component mixture, where the following

mixing rule applies for the diffusion pair i in j with $i \neq j$ according to

$$D_i \approx \left(\sum_{j=1} \frac{x_i}{D_{ij}} \right)^{-1}. \tag{117}$$

Further details are given in [76, 88].

A.1.3.2 Estimation of diffusion coefficients in liquids The diffusion coefficients in liquids are 10^4 times smaller than in gases, which plays a considerable role due to the significantly stronger intermolecular interactions. The diffusion penetration depth is also significantly smaller, so that a significantly smaller diffusion distance is covered per time with $\Delta l = \sqrt{4D}\Delta t$ according to [76].

In contrast to collision as with gas molecules, there is constant interaction with other molecules in the liquid, so that only approximate equations are generally applicable [78]. Estimates of diffusion coefficients for slow, laminar flow and highly dilute solutions of substance to be diffused in solvent B is described using the Stokes-Einstein equation. In this, an approach for the temperature-dependent movement and the internal friction $f = 3\pi\eta_B d_A$ for suspended particles A to be diffused in solvent B is established according to [150]. This yields the following calculation approach with pressures below 10 bar for the diffusion coefficients

$$D_{AB} = \frac{k_B T}{3\pi\eta_B d_A^{\mathrm{mol}}}. \tag{118}$$

In reality, the diffusion coefficients are strongly dependent on the concentration and on fluid mechanical effects. Furthermore, for the applicability of equation (118) the following further simplifications apply

- Dilute solutions with no interactions between A and the solution molecules B,
- Slow, laminar flows,
- Spherical molecules,
- The continuum mechanics for the fluid is valid.

For more concentrated solutions, different mixing rules apply, as described in more detail in [76] and [88]. In addition, for liquids, due to the dominant phenomenon of intermolecular interactions, it is possible to estimate the diffusion coefficients from data on viscosity and surface tension. For mixtures in vapour-liquid systems, the correlation of the evaporation behaviour as a function of the vapour pressures of the pure substances p_i^{LV}, the activity coefficients γ_i and the viscosity must also be considered. These calculation approaches are also explained in detail in [88]. According to [78], the diffusion coefficients can be determined for molecules of approximately the same size according to an approach by Wilke & Chang as a function of the molar volume $v'' \coloneqq v(T = T'')$ at the dew point T'' of the mixture at a pressure of 1 atm and an additional parameter χ. The

calculation of the diffusion coefficients can then be done as follows

$$D_{AB}\left[\frac{\mathrm{cm}^2}{\mathrm{s}}\right] \approx \begin{cases} 7.4\cdot 10^{-10}\frac{T\left(\chi\cdot M_{w,B}\right)^{1/2}}{(x_A\eta_A+x_B\eta_B)(v'')^{0.6}}, & \text{small molecules containing only few atoms} \\ 1.05\cdot 10^{-9}\frac{T}{(x_A\eta_A+x_B\eta_B)(v'')^{1/3}}. & \text{large molecules like polymers} \end{cases} \tag{119}$$

All correlative calculation approaches and models are described in detail in [76, 88].

A.2 GE-models

In this section, the most important GE models for describing real phase equilibrium conditions, roughly simplified and modified for the use of molten salt SLE and VLE systems, are thematically considered and discussed below.

A.2.1 The Wilson model

The Wilson model as a very suitable rough model for simplified non dissociating salt molecules applies the local composition theory $\bar{x}_{kl}$ (related to molecule k, how many molecules l are compositionally present in the local environment) by calculating the activation energy required to overcome the internal interaction forces using the kinetic theory of gases. This describes the parameter matrix in which, analogous to the Arrhenius approach to calculating the activation energy with $k = k_{k,0}\exp\left(\frac{E_{A,kl}}{RT}\right)$ and the activation energy$E_A \rightarrow \Delta\lambda := \lambda_{kl} - \lambda_{ll}$ with the energetic interaction parameter \lambda and the impact parameter $k_{k,0} \rightarrow \frac{\bar{x}_{kl}}{\bar{x}_{ll}}$. Then it is

$$\Lambda_{kl} = \frac{\bar{x}_{kl}}{\bar{x}_{ll}}\exp\left(-\frac{\lambda_{kl}-\lambda_{ll}}{RT}\right). \tag{120}$$

The ratio of the local compositions corresponds to the ratio of the molar volumes of the pure substances as follows

$$\frac{\bar{x}_{kl}}{\bar{x}_{ll}} = \frac{v_{0k}}{v_{0l}}. \tag{121}$$

With the help of the parameters, the Gibbs free excess energy G^E can be determined analogously to the calculation of the equation (39) for the ideal mixture fraction, but corrected via the interaction parameters Λ_{kl} by $x_{i,real} = \sum_{l=1}^{N_{\mathrm{comp}}}\Lambda_{kl}x_l$. Thus, for G^E it is

$$-\frac{G^E}{RT} = \sum_{k=1}^{N_{\mathrm{comp}}} x_k \ln\left[\sum_{l=1}^{N_{\mathrm{comp}}}\Lambda_{kl}x_l\right]. \tag{122}$$

The description of the activity coefficients is then by applying equation (41) as follows

$$\ln\gamma_i = 1 - \ln\left(\sum_{l=1}^{N_{\mathrm{comp}}} x_l\Lambda_{il}\right) - \sum_{k=1}^{N_{\mathrm{comp}}}\frac{x_k\Lambda_{ki}}{\sum_{l=1}^{N_{\mathrm{comp}}}x_l\Lambda_{kl}}. \tag{123}$$

A.2.2 The NRTL model

The NRTL model also starts from the idea of local composition, but summarises the energy difference terms Δg_{kl} in comparison from the ideal to the real mixing fraction. The model can

generally be used for undissociated salt molecules or fully dissociated assumed salt molecules into ions. As a dimensionless interaction parameter, the expression $\frac{\tilde{g}^E}{RT} = \frac{\Delta g_{kl}}{RT}$ can be defined with $\tau_{kl} := \frac{\Delta g_{kl}}{RT}$ and the non-random additional parameter α_{kl}, so that the following total parameter approach applies

$$\ln G_{kl} = -\alpha_{kl}\tau_{kl}. \tag{124}$$

The equations for the GE calculation approach are then as follows

$$\begin{aligned} \frac{G^E}{RT} &= \sum_{k=1}^{N_{\text{comp}}} x_k \frac{S_k}{r_k}, \\ S_k &= \sum_{l=1}^{N_{\text{comp}}} x_l G_{kl}, \\ r_k &= \sum_{l=1}^{N_{\text{comp}}} x_l \tau_{kl} G_{kl}. \end{aligned} \tag{125}$$

The expressions for the activity coefficients then become

$$\ln \gamma_i = \frac{S_i}{r_i} + \sum_{l=1}^{N_{\text{comp}}} \frac{x_l G_{il}}{r_l} \left(\tau_{il} - \frac{S_l}{r_l} \right). \tag{126}$$

A.2.3 The UNIQUAC and the LIQUAC model

In the UNIQUAC model, the free Gibbs energy is composed of a combinatorial part $\left.\frac{G^E}{RT}\right|_C$, which includes the spatial expansion of the molten salt molecules without dissociation or within the complete system of conventional molecules and their dissociated ionic species. The remaining part is $\left.\frac{G^E}{RT}\right|_R$, in which the intermolecular forces are generally taken into account. In general, the superposition principle should apply to all physical dissociation or even electrochemical effects involved in the model, so that

$$\frac{G^E}{RT} = \left.\frac{G^E}{RT}\right|_C + \left.\frac{G^E}{RT}\right|_R + \sum_{a=1}^{N_{\text{other}}} \left.\frac{G^E}{RT}\right|_{\text{other},a}, \tag{127}$$

$$\ln \gamma_i = \ln \gamma_i|_C + \ln \gamma_i|_R + \sum_{a=1}^{N_{\text{other}}} \ln \gamma_i|_{\text{other},a}\,. \tag{128}$$

The greatest strength of the UNIQUAC model extended in this way is that it can be extended to include other physical effects. In the ordinary UNIQUAC model, however, only the purely combinatorial and residual part is available with $\frac{G^E}{RT} = \left.\frac{G^E}{RT}\right|_C + \left.\frac{G^E}{RT}\right|_R$, and respectively $\ln \gamma_i = \ln \gamma_i|_C + \ln \gamma_i|_R$.

The combinatorial fraction $\left.\frac{G^E}{RT}\right|_C$ is calculated exclusively from the substance-related relative Van Der Waals volumes $r_{V,i}$ and Van Der Waals surface areas q_i of the characteristic molecular diameters $r_{\text{mol}i}$ for each substance component i. For the combinatorial fraction, the evaluation is performed as a function of the average coordination number z, the characteristic volume fraction $V_i = \frac{r_{V,i}}{\sum_{i=1}^{N_{\text{comp}}} r_{V,l}}$ and the characteristic area fraction $F_i = \frac{q_i}{\sum_{i=1}^{N_{\text{comp}}} q_l}$ of the stable components in the mixture, the following calculation approach is used in the UNIQUAC model. Assuming no

dissociation as a simplification, it is

$$\left.\frac{G^E}{RT}\right|_C = \sum_{k=1}^{N_{\text{comp}}} x_k \ln\left(V_i\right) + \frac{1}{2} z q_i x_i \ln\left(\frac{F_i}{V_i}\right), \tag{129}$$

$$\ln\gamma_i|_C = \left(1 - V_i + \ln\left(V_i\right)\right) - \frac{1}{2} z q_i \left(1 - \frac{V_i}{F_i} + \ln\left(\frac{V_i}{F_i}\right)\right). \tag{130}$$

For the determination of $\ln\gamma_i|_C$ the equation (39) is used, which can be applied analogously to all GE parts. For liquids in the LLE and VLE systems of the general substance systems of non-dissociating molecules there is usually a coordination number of $z = 10$.

The calculation of the residual fraction $\left.\frac{G^E}{RT}\right|_R$ is done analogously to the model equations (120), (121) according to Wilson, but adapted to the UNIQUAC model of the van der Waals volume r_i with the parameter matrix $U := \Psi x$ of the intermolecular interactions u_{ij} by the following approach with $\tau_{kl} = \exp\left(-\frac{u_{kl}-u_{ll}}{RT}\right)$. So it is

$$\Psi_{kl} x_l := r_{V,l} \cdot \tau_{kl}. \tag{131}$$

Application of equation (122) analogous to the Wilson Model then provides the following calculation approach for the residual component

$$\left.\frac{G^E}{RT}\right|_R = -\sum_{k=1}^{N_{\text{comp}}} x_k q_k \ln\left(\sum_{l=1}^{N_{\text{comp}}} r_{V,l}\tau_{kl}\right), \tag{132}$$

$$\ln\gamma_i|_R = q_i \left(1 - \ln\left(\frac{\sum_{l=1}^{N_{\text{comp}}} q_l x_l \tau_{il}}{\sum_{l=1}^{N_{\text{comp}}} q_l x_l}\right) - \sum_{l=1}^{N_{\text{comp}}} \left(\frac{q_l x_l \tau_{il}}{\sum_{k=1}^{N_{\text{comp}}} q_k x_k \tau_{kl}}\right)\right). \tag{133}$$

For the extension to the model of a complete molten salt system with model convective (completely undissociated) and model completely dissociating ionised fractions, the evaluation could be carried out separately via the combination of the ion degree fractions ϕ, in which the combinatorial and residual fractions are applied separately to both partial fully ionic and fully covalent fractions and finally superposed within the ion degree fraction ϕ.

Another idea is to modify the LIQUAC model to assume that the molten salt itself is the solvent. The LIQUAC model is an extended model of the UNIQUAC model for the description of solid-liquid and vapour-liquid equilibria of dissolved salts in solutions, such as (e.g. aqueous) salt solutions. The extended model is described in detail in[103] and [92] and can be used for a wide range of salt solutions. In its present form, however, the model is not applicable to the description of molten salts, but could be suitably modified as mentioned.

A.3 Details on critical nucleation in suspension crystallization

In the case of homogeneous suspension crystallisation, where wall crystallisation is neglected, stable and mechanically separable solid particles of a certain size must be produced in the first crystallisation aspect. For example, the particles must be large enough to be mechanically separated, but more importantly, they must exceed a critical, minimum required nucleation size in

the crystallisation to have thermodynamically and then secondary stable crystallisation growth. For stable crystallisation of near ideal spherical solid particles, the critical nucleation radius for a material component to be crystallised must be exceeded as a necessary condition. Essentially, there are three crystallisation regions in primary nucleation: an unstable, a metastable and a stable region for the formation of solid particles, with the metastable region also referred to as the Ostwald-Miers region [151]. A possibility of crystallisation in the metastable region can be achieved by adding crystals of a certain size of the same or different material composition, as for example in the Czochralski process (see among others [84]). The Czochralski process is a crystallisation process for the production of single component or single crystal metallic materials in which nucleation is stimulated just below the melting temperature by the addition of seed crystals as auxiliary crystals. Often a rotating rod with a seed crystal at the tip is used in a melt, at the core of which the melt subsequently crystallises on cooling. The resulting material is obtained by various mechanical forming methods. The detailed process and methods are described in [151].

In the early stages of crystallisation, the width of the metastable region depends on various parameters such as stirring intensity, cooling temperature or cooling rate, but also on material properties such as solubility or viscosity. However, it is important to reach the stable nucleation region without auxiliary crystals. By calculating the SLE equilibria according to equation 20 and the corresponding composition of the liquid and solid phases at temperature T, it is generally shown for the mixture that a critical nucleation radius is required for the formation of stable nuclei and subsequent crystal growth. According to [83], nuclei form after the addition of elemental crystallisation components from the melt until a stable nucleus is formed to which further crystallisation products can attach to the solid matrix. The balancing and observation of the total energy difference ΔG during the process shows that, assuming spherical nuclei, a critical nucleation radius must be exceeded in order to obtain these stable nuclei for the subsequent crystallisation stages. According to [83], the formation of stable nuclei takes place after exceeding the local maximum of ΔG as a function of the crystallisation radius. For the total energy difference, the released crystallisation energy volume (difference) ΔG_V is related to the melt volume V with $\Delta G_V = V \frac{\rho_{\text{mix}}}{M_{w,\text{mix}}} \cdot \Delta\mu$ and the surface energy to be expended ΔG_A with$\Delta G_A = A \cdot \sigma_{\text{mix}}$. So the total energy differenceΔG is (with total energy difference ΔG and nucleation surface A)

$$\Delta G = \Delta G_V + \Delta G_A. \tag{134}$$

For spherical crystallisation nuclei from the liquid phase, the equation (134) is transformed into the following analytically calculable form

$$\Delta G(r,T) = {}^4\!/_3\pi r^3 \cdot \Delta\mu(T) - 4\pi r \cdot \sigma(T). \tag{135}$$

By evaluating $\frac{\partial \Delta G}{\partial r}$ an expression for calculating the thermodynamic critical nucleation radius can be obtained. The equation for the formation of the critical nucleus is then

$$r_{crit} = \frac{2\sigma_{\text{mix}} M_{\text{mix}}}{\rho_{\text{mix}} \Delta\mu}. \tag{136}$$

For simulation of crystallisation, the critical nucleation radius for stable nucleation must be

exceeded as a necessary condition. For the difference of the chemical potential to the phase change, (13) and (14) can be used from the simulation results of the mole fraction with $c_i = x_i \cdot c_{0,i}$ (at base concentration $c_{0,i}$) to determine the current critical nucleation radius r_{crit}. Evaluation of $\Delta G(r_{\text{crit}}, T_{\text{cooling}})$ shows that the nucleation work required for the crystallisation process is always 1/3 of the surface formation energy. Under the simplification that the melt is only a single component system and that the other non-crystallisable fractions in the melt are small and less active, the calculation approach $\Delta\mu_i = \Delta h_i^{SL} \cdot (T_{M,i} - T_{\text{cool}})$ applies for the estimation of the critical nucleation radius as an approximation for equation (136) by calculating the subcooling temperature T_{cooling}.

B Supplement: Section on the availability of required substance property data for modelling and simulations

In the following section, the availability of property data and the estimation of real phase equilibria based on literature data are listed and discussed as follows. Due to the lack of pure component property data and the poor availability of validated VLE data of representative substance systems, calculations with ideal phase equilibria were predominantly carried out in this thesis.

A realistic distillation simulation depends almost exclusively on the availability of validated property data. In general, the realistic representation of vapour-liquid equilibria (VLE) is crucial for the simulation of distillation processes, since already in simplified equilibrium relationships using the simpler gamma-phi concept for low pressures according to equation (27) the activity coefficients describe the physical behaviour of liquid molecules with respect to each other and their intermolecular interactions in the mixture. However, for the nuclear recycling relevant to the study of mixtures of actinides and fission product chlorides, practically no VLE data of representative binary mixtures exist, but only at low temperatures or SLE conditions in simple binary liquid systems with uranium tetrachloride and another metal chloride component.

B.1 Availability of substance property data

The substance data property data required for general simulation of distillation columns can be divided into the following five substance data classes:

1. Conventional data (1A): This includes pure substance property data, melting and boiling points, as well as temperature-independent data.

2. Data on the essential phase transformations of the pure substance, which are, however, independent of temperature (1B): At this point those pure substance property data are meant which characterise the most important phase transformation points in a p-T-diagram (pressure-temperature phase diagram to the pure substance); which thus essentially concern critical points or triple points of the pure substances involved. Furthermore, this also includes possible decomposition points of the pure substance.

3. Temperature-dependent substance data of the pure substances subdivided according to:

   (a) Ordinary phase change and thermochemical-temperature-dependent substance property data (2A): Includes all pure substance property data of vapour pressures or enthalpies of vaporisation, but also thermochemical data including heat capacities and free enthalpy or Gibbs energy of formation data.

   (b) Temperature-dependent substance property data of pure components relating to mass and heat transport (2B), such as essentially density, viscosity, thermal conductivity, surface tension or diffusion coefficients in certain media or solvents (including solution in melts).

4. Molecular properties of the pure substance components (3A), such as radius of gyration, van der Waals area & volume, binding properties, binding energy, binding angle and other molecular geometry properties, but also dissociation behaviour (with dissociation constant including) and ion sizes when the molecules tend to dissociate. The basic molecular geometric data on molecules can be used in many ChemSep models and in GE models as well, for example, in the estimation of model parameters in the combinatorial part of the UNIUQAC model.

5. Mixture property data and data on the activity of the pure substance components in the mixture as well as the corresponding intermolecular interaction parameters (3B) are required to describe realistic vapour-liquid equilibria or solid-liquid equilibria, so these interaction parameters are important parameters in the use of more complex GE models such as the UNIQUAC or LIQUAC model. Some rough available GE data of binary molten salt systems with uranium tetrachloride are given in section (3) of the main part of this thesis. However, realistic vapour-liquid equilibrium data of relevant mixtures for potentially realistic useability in this thesis can only be obtained experimentally, e.g. from single-stage closed chamber evaporators specialised for molten salts (see: [60, 109, 61]), from which complex models and the model parameters for simulations can be obtained. Mixture data often depend on temperature and composition, and possibly on pressure. The molecular interactions in the mixture could also include the dissociation behaviour in the mixture as a function of composition, temperature and pressure, including dissociation constants and a reaction network that may occur in the case of particularly chemically strong interactions in the mixture.

For each substance property data class, data from different databases available in the literature have been combined in terms of varying quality and availability. The availability and quality of these data are listed in the table (14). Such a tabulation has already been done in [29], but has been extended and updated in this work of the thesis. In the Dortmunder Stoffdatenbank as well as in the DECHEMA DETHERM database, many data sets are available on generally conventional, temperature-dependent substance data and model parameters for the theoretical description of mixtures. For solution equilibria, e.g. for many salts in aqueous solutions and organic solvents, much information on activity data can be found, as shown by the data from the LIQUAC development thesis from [92]. However, this changes for molten salt systems, where such activity data are rarely available, and are practically non-existent for nuclear relevant mixtures, such as those with uranium tetrachloride in vapour-liquid systems. Only for low temperatures

in the range of the melting temperature of the mixture with uranium tetrachloride are some GE data available, see [10, 120, 9, 121, 11] as well as indirectly given for the estimation of the mixing enthalpy in [152]. Only for conventional and temperature-dependent data, such as heat capacities, vapour pressure data and thermochemical substance data, some information can be found for the pure actinide and fission product chloride components, which are also less available in good quality, especially for the transplutonium actinide component chlorides. For this purpose, other databases are more suitable, such as the NEA database, which deals specifically with the thermochemical substance property data of specific actinide chlorides and other possible components, given in detail in the form of various series of books and publications. In the series of publications with the characteristic title "Chemical Thermodynamics of M" with e.g. M=U,Np,Am,Tc,Pu,.... the series deals with the thermochemical properties of these elements and their compounds, especially chlorides and many other compounds, see [153, 143, 154, 155, 156, 27, 157, 158, 159, 160]. The main advantage of this series is that the data is constantly updated and freely available in the public domain of the NEA database. In particular [161] provides well validated and high quality substance data. The disadvantage is that these publications mainly list conventional and thermochemical data of pure substances. In addition, the NIST databases [162] and the JANAF tables also provide mainly thermochemical properties of pure substances, but also vapour pressure data and sometimes other data on transport properties. Further compilations of vapour pressure and thermochemical data can be found in [24, 18, 14, 66]. However, critical data are almost completely missing, as well as suitable mixture data on VLE systems. For a wider range of property data, however, the book series "Gmelin's Handbook of Inorganic Chemistry" is suitable, in which each book also covers the property data of one element and its compounds, including critical data and transport properties [163]. For example, the critical temperature of 1598 K for the compound UCl_4 is given in [20, 163] as the only source, while extrapolation of the vapour pressure curves gives a critical pressure of 70.714 bar. However, these data urgently need to be validated and, if necessary, corrected in future experimental work, since uranium tetrachloride in particular is one of the most important elements for the investigation of nuclear distillation fields in the context of spent fuel reprocessing. Alternatively, it is also possible to estimate these data approximately by means of group contribution methods, e.g. according to [164, 165], as partially described in [88, 87]. However, the estimation of such substance data will not be pursued further here, as these are only very rough estimates. Information from the literature should always be preferred to estimates. Further sources for critical data, as well as data on molecular properties, temperature-dependent substance property data and transport properties of numerous fission product chlorides can be found in [166, 145].

Table 14: Availability of substance property data for actinide and fission product chlorides (DDB: Dortmunder Stoffdatenbank (updated from [29])

	Substance property class				
Substance property database	1A	1B	2A & AB	3A	3B
DDB(Dortmunder Stofffdatenbank) [167]	+/–	–	+/–	– –	–
DETHERM & DECHEMA[168]	+/–	– –	+/–	+/–	–
DIPPR(Design Institute for Physical Properties)[169]	+	– –	+	– –	– –
NIST & JANAF[162]	+	–	+	+/ –	–
OECD-NEA(Nuclear Energy Agency) database[170, 171]	+	–	++	– –	+/–
NTRL & NASA database[172, 173]	++	–	+/–	–	– –
Collections (e.g. Gmelin[163])	++	+	++	+	– –
Books and published tabled values	+	+/–	+	++	–
articles und publications	++	–	++	+	+
other databases	+/–	–	+/–	– –	–
++ Excellent quality, + good quality, +/– available data, – bad quality/lack of data, – – not available data					

The transport properties of pure substances for molten actinide chlorides are listed in numerous publications, such as in [174, 175, 176]. For fission products, most data on transport properties are given e.g. in [177, 146] or in [147, 166].

Based on the entire property data research and the evaluation of the availability of substance data according to Tab. (15), it becomes clear that particularly critical data and information about the activity of the substance component in a representative mixture are almost completely missing (see section (3)). Therefore, the simulations in this thesis are mainly performed under ideal phase equilibrium behaviour of equation (28) according to the Raoult and Dalton law, as already explained in the main part of the thesis.

B.2 Evaluation of the quality of substance property data

The quality of substance property data is assessed qualitatively and secondly quantitatively by linear error propagation on the basis of the deviations between data sets from different publications & sources, as well as information on their possibly given relative deviations within the publications. Using the vapour pressure data of uranium and thorium tetrachloride as an example, the deviation of substance data has already been discussed in more detail in [23, 178]. From these given data and deviations a linear error propagation analysis is performed for the evaluation of ideal phase equilibria according to the equation (27) with $\gamma_i = 1$ (summarised and estimatable broken down for the individual substance components as pure substance and in the mixture). The evaluation of the most important substance property data is listed in Tab. (15) together with the evaluation of quality of these shown data.

B.2.1 Qualitative analysis of substance property data quality

The qualitative assessment of the substance data corresponds to a rough classification in quality and availability into five assessment classes. The summary for the evaluation is given in Tab. (15) with the important actinide chlorides in the first table and the most important fission products in the second table, however, due to the avoidance of complexity without indication of molecular properties and mixture data. The assessment "+/-" is the standard case in which substance data are available at all, but cannot be assessed in more detail. This also includes the various data with limitations of the data approaches for small temperature ranges or with contradictory data. The notation "-" indicates that only one source with little or unreliable data is available in the literature. For the notation "- -" the substance data are completely missing. If several literature data are available, whose data qualitatively correspond, these data are to be valued at least with "+". If, in addition, the quantitative data from the literature sources agree well with each other, with small relative deviations of less than 10% for actinide chlorides and less than 5% for fission product chlorides, the availability of the substance under consideration is noted as "++" 'available in very good quality'. For temperature-dependent substance data, this means that these deviations must always be below this limit value in order to be assessed as "++".

Depending on the substance property data classes, the qualitative assessment of these data is available for each substance component according to Tab. (15) for actinide chlorides in the first table and for fission product chlorides in the second table. For actinide chlorides, the following can be summarised:

Conventional data for actinide chlorides: Conventional property data for actinide chlorides are mainly given in the literature on temperature dependent data and in [179], including data from the secondary literature. Sufficient information, such as boiling points, is still available for many chlorides. The data are particularly good and verified with very small relative deviations from the literature data for thorium tetrachloride, protactinium pentachloride and simple uranium chlorides, except for uranium pentachloride. For uranium pentachloride, plutonium trichloride, neptunium tri- and tetrachloride, some values, such as boiling points, show larger uncertainties (between literature data). On the other hand, the data situation for americium trichloride and curium trichloride is rather poor with "+/-" and for actinium trichloride, berkelium trichloride and californium trichloride even with "-".

Critical data for actinide chlorides: Critical data and triple point data values are almost completely missing for almost all actinide chlorides. Only for uranium tetrachloride, according to [20], is information given on the critical temperature of 1598 K and an indication of a valid extrapolation of the vapour pressure curve up to this critical point. According to [20], the triple point (the point where the solid, liquid and gas phases meet in the p-T diagram) for this component is 863.15 K and 0.026 bar. Furthermore, according to the group contribution method of [164], the critical data of the other simple uranium chlorides can also be estimated, so that in Tab. (15) these can be listed as available but of poor quality with "-". For all other actinide chlorides no critical data or triple point information is available. Therefore, there are also no group contribution data available for these

actinide chlorides for estimation by a group contribution method.

Simple temperature dependent data: Regarding the common temperature dependent property data, the most important of these are the vapour pressures of the pure components and the heat capacities in the following, numerous literature references are available, e.g. in [24, 14, 18, 161, 153, 48, 166]. Thermochemical property data thus also belong to the simple temperature-dependent property data. However, the measured vapour pressures are only available up to the boiling point. The small relative deviations between literature data are often given in the $\log p_i^{\mathrm{LV}}$ curve for the pure substance and increase with increasing temperature. This already applies to the vapour pressures of uranium tetrachloride and thorium tetrachloride in the internal comparison of different data and data of the vapour pressure in the error range according to [23, 178], despite the excellent quality of the data with "++" for uranium tetrachloride. In general, the data situation for uranium tetrachloride can be rated as very good with "++", due to the good agreement of the different data and the reasonably satisfactory extrapolation of the vapour pressure curves towards the critical point according to [20]. This is followed by thorium tetrachloride, protactinium pentachloride, uranium trichloride and uranium hexachloride with a "+" rating for actinide chloride components. Plutonium trichloride is also in this rating group at temperatures up to 1250 K, but unfortunately there is less reliable data above this temperature at high temperatures. Therefore the availability of this component is referred to the "+/- group". Below 1 atm the boiling point deviates and lies in the range 2000 K - 2044 K, depending on the evaporation curve at the boiling point with $\log p_i^{\mathrm{LV}} = 0$. Therefore the data for plutonium trichloride are only given as available with "+/-". The same applies to the neptunium chlorides up to the corresponding boiling points and to uranium pentachloride up to the thermal stability limit. For americium trichloride, according to [28], there is only one literature reference for the determination of vapour pressures up to the boiling point, where the correctness of the vapour pressures must be questioned due to large internal measurement deviations in the literature reference. The position of the boiling point of americium trichloride at 1526 K is also questionable, and there is no way of validating the data. More data are available for the heat capacities. Since the knowledge of the vapour pressures is of such central importance for the simulation of the distillation under ideal phase equilibria in this thesis, the qualitative evaluation of the simple temperature-dependent property data follows mainly via the qualitative availability and quality of the literature data to be compared. For the components actinium trichloride, thorium trichloride and curium trichloride, the extrapolation of some vapour pressure data is available, which allows a very rough estimation of the vapour pressures. For berkelium trichloride and californium trichloride, there is also no information on simple temperature-dependent data for this property class.

Transport properties of actinide chlorides: The main transport properties classically include the determination of liquid density, viscosity, surface tension and diffusion coefficients for self-diffusion or diffusion in a solvent or a mixture of other chlorides. Most of the transport property data are given in [177, 146, 147, 166, 180, 175, 176], among others, but also outdated and partly contradictory data on densities from Russian literature (e.g.

[175, 176]. If only the current and unambiguous literature data are used, the availability and quality of the describable data for uranium trichloride is excellent with "++". The data for thorium tetrachloride, uranium tetrachloride, neptunium trichloride, plutonium trichloride and americium trichloride can also be rated as good available with "+". Only for neptunium tetrachloride is there no reliable information on accuracy due to less available data.

Molecular properties: Molecular properties are mainly the geometric size of the molecule, with additional information on the geometry in the gas phase, but also on the bond length and the energetic state in the solid and liquid state given in the literature, e.g. in [145, 67]. For the actinide chlorides, protactinium pentachloride is the most suitable exemplar in terms of the ability to describe the molecular behaviour and geometric estimates according to [67]. Also available in good quality are data on the geometric extent and shape of the molecules, as well as data on bond lengths and angles for thorium tetrachloride, uranium tetrachloride, neptunium tetrachloride and plutonium trichloride. Little information is available for americium trichloride and actinium trichloride and for the other neptunium and uranium chlorides according to [67].

Mixing, activity coefficient data: The data on activity coefficients often refer only to LiCl-KCl melts or representative fission product chloride systems with uranium tetrachloride at lower temperatures, as indicated for example in[10] among others, of solid-liquid equilibrium systems or temperature near the melting point of the mixture. Also hardly available in the literature is information on critical data related to the actinide chloride pure components. Only for uranium tri- and uranium tetrachloride are critical data and mixing data available in relation to liquid systems, while for all other actinide chlorides no data are available or only individually at infinite dilution. Further specifics can be found in Tab. (15) . The estimation of representative vapour-liquid phase equilibrium data in this thesis, on the other hand, is only carried out using the Margules approach. More precise models will have to be developed in possible future work.

When considering the quality of the available substance property data in the second table of (15), it can be concluded that there is often significantly more information available for fission products than for actinide chlorides. Simple temperature-dependent substance property data available in very good quality are cesium chloride and cadmium dichloride. Very good quality of the data are given for strontium dichloride, cesium chloride and barium dichloride with a usually specified relative deviation value of 0.1% between the different literature data values. Conventional and critical data, however, are given less precisely in relation to the extrapolatable temperature-dependent substance property data, especially of vapor pressure data and liquid molar volume. Good data on available critical points are for cesium chloride and cadmium dichloride, but also for zirconium, tin, tellurium and antimony chloride. For selenium tetrachloride and silver chloride, some conflicting data are available, showing larger deviations compared to [166] and estimated values. For all other chlorides, there is also little critical data available. Molecular properties and data on mixture properties or activity coefficients are not presented in this second table of (15) for reasons of complexity. All other specifics in availability and quality of substance data

can be seen in (15) and an older version analysing the quality of substance data is available in [29].

Table 15: Availability and quality of substance property data for actinide chloride

Availability & quality	Conventional data	Critical data	Simple temp. dependent data	Transport properties	Molecular properties	Mixing, activity coefficient data
++	$ThCl_4$, $PaCl_5$, UCl_3, UCl_4, UCl_6		UCl_4	UCl_3	$PaCl_5$	
+	UCl_5, $NpCl_3$, $NpCl_4$, $PuCl_3$		$ThCl_4$, $PaCl_5$, UCl_3 UCl_6,	$ThCl_4$, UCl_4, $NpCl_3$, $PuCl_3$, $AmCl_3$	$ThCl_4$, UCl_4 , $NpCl_4$, $PuCl_3$	
+/–	$AmCl_3$, $CmCl_3$	UCl_4,	$NpCl_3$, $NpCl_4$, $AmCl_3$, UCl5, $PuCl_3$	$NpCl_4$	UCl_3, UCl_5, UCl_6, $NpCl_3$, $AmCl_3$, $AcCl_3$	UCl_4, UCl_3
–	$AcCl_3$, $BkCl_3$, $CfCl_3$	UCl_3 UCl_5, UCl_6	$AcCl_3$, $ThCl_3$, $CmCl_3$	$PaCl_5$, $CmCl_3$, UCl_6	$ThCl_3$	$ThCl_4$, $PaCl_5$, UCl_3, $NpCl_3$, $NpCl_4$, $PuCl_3$, $AmCl_3$, $CmCl_3$
– –		All others	$BkCl_3$, $CfCl_3$	$AcCl_3$, UCl_5, $BkCl_3$, $CfCl_3$, UCl_5, $ThCl_3$	$CmCl_3$, $BkCl_3$, $CfCl_3$	$ThCl_3$, UCl_5, UCl_6, $BkCl_3$, $CfCl_3$, $AcCl_3$
++ Excelent quality, + good guality, +/– available, – bad quality/lack of data, – – not available data						

Availability of actinide chlorides

Availability & quality	Conventional data	Critical data	Simple temp. dependent data	Transport properties
++			CsCl, $CdCl_2$	$SnCl_n$, CsCl, $BaCl_2$,
+	$ZrCl_n$, CsCl, $LaCl_3$, $CeCl_3$, $PrCl_3$, $NdCl_3$, RbCl, $CdCl_2$		$ZrCl_n$, $SnCl_n$, $BaCl_2$, $LaCl_3$, $CeCl_3$, $PrCl_3$, $NdCl_3$, RbCl, $SbCl_m$	$ZrCl_n$, RbCl. $CdCl_2$
+/–	$SrCl_2$, NbCl5, $SnCl_n$, $TeCl_n$, $SeCl_n$, $BaCl_2$, $SmCl_3$, $EuCl_3$, YCl_3, $PdCl_2$, $SbCl_m$, $GdCl_3$, MoCl5, AgCl	$ZrCl_n$, CsCl, $SnCl_n$, $TeCl_n$, $CdCl_2$, $SbCl_m$, $MoCl_5$, $SeCl_n$, AgCl	$NbCl_5$, $SmCl_3$, $EuCl_3$, YCl_3, AgCl, $GdCl_3$	$NbCl_5$, $TeCl_n$, $LaCl_3$, $CeCl_3$, $PrCl_3$, $NdCl_3$, AgCl, $SbCl_m$
–		$BaCl_2$, $PdCl_2$	$TeCl_n$, $PdCl_2$, $SeCl_n$, $MoCl_5$	$SmCl_3$, $EuCl_3$, $GdCl_3$, $SeCl_n$, $MoCl_5$
– –		All others		YCl_3, $PdCl_2$
++ Excelent quality, + good guality, +/– available, – bad quality/lack of data, – – not available data, n=2,4, m=3,5				

Availability of fission product chlorides

In summary, the qualitative evaluation of the availability of substance property data shows

that critical data are quite missing for actinide chlorides compared to fission products. In addition, practically all data and mixture properties required for the description of the activity coefficients are missing, so that simulations for distillation via vapour-liquid phase equilibria cannot be carried out as realistically as possible. The situation is much better for simple temperature dependent property data such as vapour pressures, heat capacities and transport properties. Thus, the simulation with ideal phase equilibria with the core components uranium tetrachloride, plutonium trichloride and cesium chloride is always possible and applicable, whereby some transplutonium chlorides can also be considered in the simulations, e.g. neptunium tetrachloride, americium trichloride and, with great simplifications, even curium trichloride. For the given list of available substance property data in Tab. (15), even modelling in non-equilibrium stage models and in rate-based simulation approaches for the simulation of distillation is possible with many data of transport properties such as densities, viscosities, surface tension, thermal heat of conductivity of the pure components in the liquid phase. Using simple mixing rule approaches as explained in [68] the estimation of these physical transport property data of the mixture can be estimated. However, it must be noted that for the actinide chloride components berkelium trichloride and californium trichloride, all the necessary substance property data for the simulation are missing and must therefore be completely neglected in the simulations of this thesis.

Another problem is that the property data of the molten salt mixture must also be determined by extrapolation of the temperature dependent data above the boiling point. This is particularly necessary for the data of the light boiling vapour pressure correlation component of the mixture, as in the boiling range of the mixture extrapolation of the data is required up to the heavy boiling component. Extrapolation also increases the relative error between the different literature data. The calculation of the increase in relative error without and with the critical point position is examined and discussed in more detail in a subsequent quantitative error analysis in the next section.

B.2.2 Quantitative error estimation for the simulation of a total-reflux distillation

When evaluating phase equilibria according to the equation (27), there are often larger deviations as a function of temperature due to deviating property data from the literature. Deviations from the ideal phase equilibria according to equation (28) result from deviations in the relative volatilities and hence the vapour pressure data. In the following, the resulting systematic deviations are estimated and graphically illustrated using binary mixture examples of UCl_4-CsCl und CsCl-$PuCl_3$ for the evaluation of $y_1 = f^{\mathrm{id}}_{\mathrm{VLE}}(x_1)$ via linear error propagation methodology.

For the ideal mixture assumption, extrapolation of the pure component vapour pressure data of uranium tetrachloride and cesium chloride above their pure component boiling points leads to increased significant deviations compared to various literature data. For uranium tetrachloride as a light-boiler component, the vapour pressure at the boiling point and the critical pressure at the critical temperature of uranium tetrachloride can be easily obtained by evaluating the Antoine equation. The same can be done for the mean critical point and boiling point data for cesium chloride.

The comparison of given literature data of the vapour pressures of these pure substances at an operating pressure of 1 atm are given in Fig. (52) for uranium tetrachloride and plutonium tetra-

chloride as examples (x-axis with 1/T and y-axis with $\log p_i^{LV}$). As can be seen for liquid uranium tetrachloride (left figure in Fig. (52)), the deviations of the correlative temperature-dependent vapour pressure data decrease towards higher temperatures. However, these deviations are still relatively small compared to the other components. Otherwise, for plutonium trichloride, the vapour pressure value is given exactly only up to 1250 K. Above 1250 K, two different trends of the vapour pressure curves occur, for which the literature data differ between the data of [24, 27] and [25, 28]). Since it is not clear which of the two trend curves for plutonium trichloride describes the vapour pressure curve better, because critical data for plutonium trichloride are not available either, this difference is assumed to be a large deviation value for the error propagation calculation.

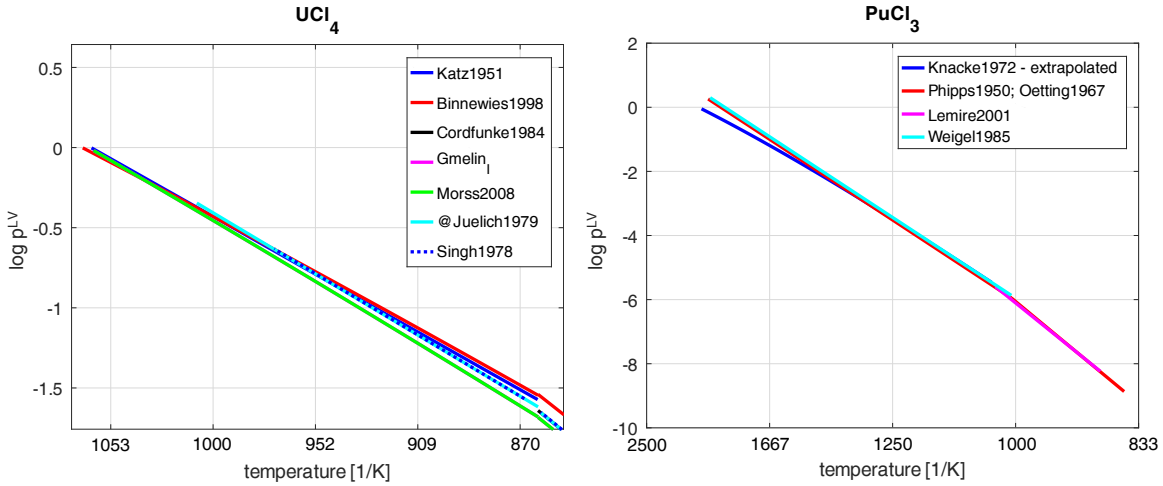

Figure 52: Some representative liquid vapour pressure data examples of uranium tetrachloride and plutonium trichloride

references: Katz1951:[17], Binnewies1998:[18], Cordfunke1984:[19], Gmelin-I:[20], Morss2008:[21], Jülich1979:[22], Singh1978:[23], Knacke1972:[24], Phipps1950:[25], Ötting1967:[26], Lemire2001:[27], Weigel1985:[28].

When extrapolating the vapour pressure data, it is to be expected for uranium tetrachloride, despite excellent vapour pressure data, that the error in the extrapolation increases significantly up to 1526 K and becomes much larger up to 2000 K than correspondingly for cesium chloride. This also means that for small composition values of the light-boiling substance component, due to the condition $p = \sum_i x_i p_i^{LV}(T)$, the boiling temperature of this mixture is also higher with the composition to higher plutonium trichloride proportions.

For the estimation of the systematic deviations in the evaluation of ideal phase equilibria, the following equilibrium condition ($x_2 = 1 - x_1$,$y_2 = 1 - y_1$ of the light-boiling component "1" and heavy-boiling component "2") first applies for the general determination of the composition of the vapour phase:

$$p = x_1 p_1^{LV}(T) + x_2 p_2^{LV}(T), \tag{137}$$

$$y_1 = \frac{x_1 p_1^{LV}(T)}{x_1 p_1^{LV}(T) + x_2 p_2^{LV}(T)}. \tag{138}$$

From the equation (138) the absolute deviationΔy_1 from the mean values$\bar{p}_1^{\mathrm{LV}}, \bar{p}_2^{\mathrm{LV}}$ and absolute measurement deviations Δp_1^{LV} and Δp_2^{LV} can be determined by linearized error propagation of the form:

$$\Delta y_1 = \left|\frac{\partial y_1}{\partial p_1^{\mathrm{LV}}}\right|_{\bar{p}_1^{\mathrm{LV}},\bar{p}_2^{\mathrm{LV}}} \Delta p_1^{\mathrm{LV}} + \left|\frac{\partial y_1}{\partial p_2^{\mathrm{LV}}}\right|_{\bar{p}_1^{\mathrm{LV}},\bar{p}_2^{\mathrm{LV}}} \Delta p_2^{\mathrm{LV}}, \tag{139}$$

$$= \left(\frac{x_1 x_2}{\left(x_1 p_1^{\mathrm{LV}} + x_2 p_2^{\mathrm{LV}}\right)^2}\right) \cdot \left(p_2^{\mathrm{LV}} \Delta p_1^{\mathrm{LV}} + p_1^{\mathrm{LV}} \Delta p_2^{\mathrm{LV}}\right). \tag{140}$$

Table 16: Some liquid vapour pressure data examples $\log p_i^{\mathrm{LV}} = \frac{C_1}{T} + C_2 + C_3 \log T + C_4 T + C_5 T^2 + C_{\mathrm{corr}}$ of UCl_4, CsCl and $PuCl_3$

(a) UCl_4

Reference	C_1	C_2	C_3	C_4	C_5	C_{corr}	Extrapolated T-range	
[17]	-7205	9.65	0	0	0	-2.8751	863	1063
[18]	-9720	29.332	-6.68	0	0	0	863	1068
[19]	-10443	10.46	0	0	0	0	863	1057
[21][20, 163]	-9950	28.96	-5.53	0	0	-2.8751	863	1062
[22]	-7627	7.22	0	0	0	0	863	1008
[23]	-7649±82	7.245±0.101	0	0	0	0	868	971

(b) CsCl

Reference	C_1	C_2	C_3	C_4	C_5	C_{corr}	Extrapolated T-range	
[166]	-2490.3	438.8475	-150.08	5.3499E-02	-7.3394E-06	-2.8751	1017.15	1573.15
[18]	-10800	17.33	-3.12	0	0	0	918	unsure
[163, 20]	-8460	8.29	0	0	0	-2.8751	1097.85	1577.15
[145, 67]	-8335.7	5.3205	0	0	0	0	919.15	1570.2

(c) $PuCl_3$

Reference	C_1	C_2	C_3	C_4	C_5	C_{corr}	Extrapolated T-range	
[24]	-15500.70201	28.95011	-6.46878	0	0	0	1041	2044
[27]	-12586	9.426	-0.94955	0	0	0	1041	2040
[25]	-12587	9.428	0	0	0	-2.8751	1007	1250
[28]	-12590	9.51	0	0	0	-2.8751	1007	1250

The systematic deviations can then be determined directly via the evaluation of $\frac{\Delta y_1}{\bar{y}_1}$ with the averages of the equations (137) and (138), which follows to the error propagation equation

$$\frac{\Delta y_1}{\bar{y}_1} = \frac{x_2}{x_1 p_1^{\mathrm{LV}} + x_2 p_2^{\mathrm{LV}}} \cdot \left(\frac{p_2^{\mathrm{LV}}}{p_1^{\mathrm{LV}}} \Delta p_1^{\mathrm{LV}} + \Delta p_2^{\mathrm{LV}}\right). \tag{141}$$

In the following, the systematic deviations in the simulation of a total reflux column are evaluated on the basis of the binary substance systems UCl_4-CsCl and CsCl-$PuCl_3$. An example mixture of UCl_4-CsCl with the feed composition $[0.96, 0.04]^T$ and a second example of $PuCl_3$ with the composition $[0.55, 0.45]^T$ are used. The simulation of a seven and a twelve stage total reflux distillation column is performed with the evaluation of the uncertainties based on the literature deviation base of the vapour pressure evaluated as a function of temperature for the evaluation of ideal phase equilibria.

Fig. (53) shows the error propagation results as uncertainties of the original relative deviations of the literature vapour pressure data for the total reflux distillation column of the mixture UCl_4-CsC with two different focal points in the observation of the mole fraction in a coarse separation (left figure of Fig. (53)) and a fine separation (right figure of Fig. (53)) with logarithmic y-axis for small mole fractions up to 1E-07. For the coarse separation (left part of the Fig. (53)) it is clear that the resulting uncertainties are relatively high, especially in the first three separation stages, which is due to the larger deviations of the vapour pressure data of the uranium tetrachloride component at higher volume fractions.

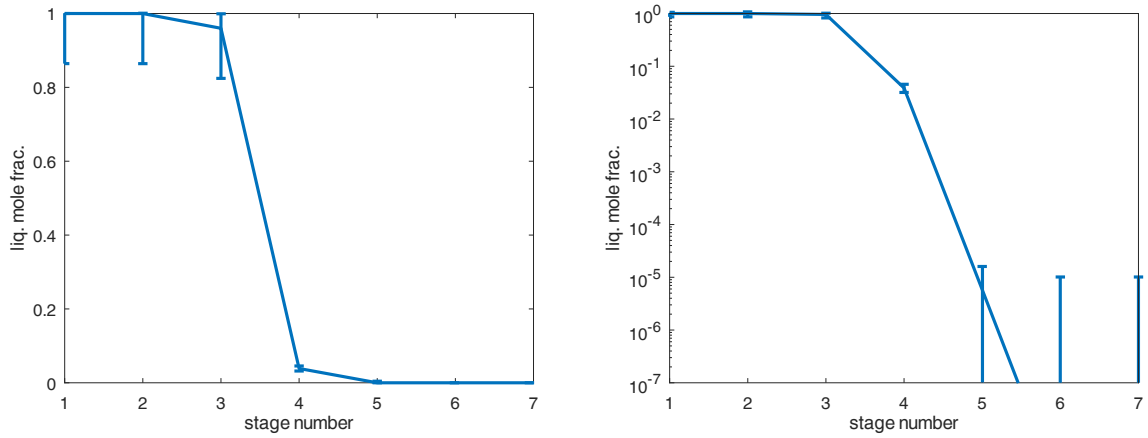

Figure 53: Simulation and error propagation of the distillation of the UCl_4-CsCl mixture within a total reflux column:
Shown on the left is the focused representation of the coarse separation, on the right that of the fine separation by logarithmic representation.

In this case, the uncertainties for the compositional results can increase to 14 mol%. However, for high cesium chloride contents the relative deviation is reduced to only 1E-03 mol%, which is a much smaller value than 14 mol%. Between the separation steps follow the mean values of the uncertainties resulting from the condition $p = \sum_i x_i p_i^{LV}(T)$ and subsequent normalisation. Thus, the best possible representation limit for the simulation of the seven-stage total reflux column is also 1E-03-mol% for this separation example.

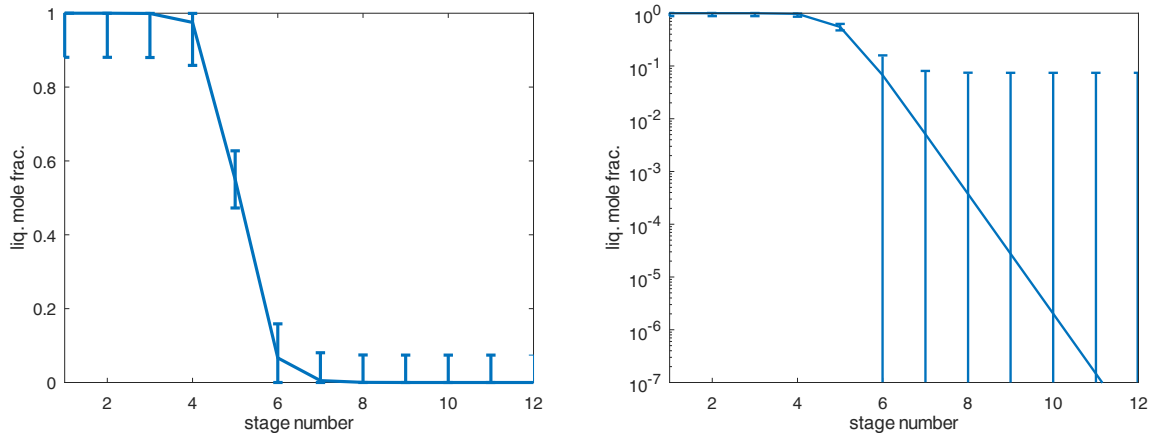

Figure 54: Simulation and error propagation of the distillation of the CsCl-$PuCl_3$ mixture within a total reflux column:
Shown on the left is the focused representation of the coarse separation, on the right that of the fine separation by logarithmic representation.

In the second simulation example according to Fig.(54), similar deviations as in the previous separation example of up to 14-mol% are also observed for high cesium chloride component as light boiler (see first separation stages according to the results from Fig. (54)). However, larger relative deviations are now present for the plutonium trichloride component as a heavy boiler, which can reach values up to a maximum of 8-mol% (rounded up). Furthermore, the condition $p = \sum_i x_i p_i^{LV}(T)$ at most only roughly 8-mol%. The reason for the poor approximability lies in the assumption of the error of the two trend curves of the vapour pressures towards 2000 K for the plutonium trichloride vapour pressure curve according to Fig. (52). This uncertainty range can be significantly reduced if more accurate and reliable data for vapour pressures of plutonium trichloride at temperatures up to 2000 K exist and at the boiling point is well-known under very small deviations. Similar orders of magnitude of relative deviations are to be expected for multi-component mixtures, as in the example of distillation of SNF preparation according to section (6.2.2).

C Supplement: Detailed simulation results for various feed material separation examples

In the main part of this thesis, the processing of SNF material, including the recycling of zirconium cladding material and waste gas treatment under idealized conditions of ideal phase equilibria (according to equation (28)), has been investigated in detail in chapter (IV) in order to obtain an overview of the separation problem and the associated technical process effort. The question of how the pyroprocessing separation unit (PPU) can be used in an integrated manner to close fuel cycles in a targeted manner and also to be able to make practically complete use of fuel inventories from SNF material is investigated and discussed in this section in a simulative manner. The same conceptual design from section (IV) Fig. (32) is used for the process simulations for these different feed materials.

C.1 Simulations for the reprocessing of DFR, HWL and SNF material

For the Dual Fluid Reactor, there are two main options for the feed material to be processed. It is important to know the basic mixture and the subsequent fission product composition, as well as the ratio of fission product fraction to basic molten fuel salt in the total feed material to be processed. In the case of the metallic DFRm variant, the base mixture is a eutectic U-Cr-Pu and the fission products are a spectrum for fast fissions of the main base mixture components. The technically less relevant salt variant is not considered further in this thesis. In addition to the DFRm feed material and the SNF material, the HLW material for the distillative treatment in the separation process is also examined in the following section according to chapter (IV) Fig. (32). Concepts of HLW partitioning ideas, formation and further information, as well as applicative reuse in thorium-based molten salts for transmutation can be found in[181]. Subsequently, mixtures of different feed streams of DFRm, SNF and HLW will also be investigated in more detail for distillation in the developed separation process, in order to demonstrate the robust application of such a designed distillation process. But

C.1.1 Feed composition and distillation examples

After chlorination of the SNF and HLW material in an equimolar mixing ratio of 1:1 fuel to carbon tetrachloride, inertization is performed with argon. For the DFRm material, chlorination of the metals is performed with excess elemental chlorine. This is the only exception to the flowchart modification to use pure chlorine instead, assuming a 100 mol% reaction yield to chlorides by neglecting the exact technical chlorination procedure. All chlorinated feed compositions are listed in Tab. (17). Using these feed compositions, simulations are carried out on the basic separation section flowchart as shown in Fig. (55). In the following it will be shown that this conceptualised distillation concept is applicable to all feed stream variants to be processed.

As can be seen from the tabular and graphical comparison of the composition according to Tab. (17), the feed streams differ fundamentally in the type of composition. While no excess chlorine is used for SNF and HLW recycling, the DFRm variant uses elemental chlorine with a large excess proportion without argon. The transplutonium elements have been neglected for the DFRm variant, as the corresponding proportions are relatively small. Since a eutectic U-Cr-Pu feed mixture is originally used as a basis for the DFRm and only small amounts of fissile material are produced overall, the material components uranium tetrachloride, chromium dichloride and plutonium trichloride are predominantly represented in the DFRm input.

Table 17: Overview of the main distillation feed cases in mol%

Component (proportion)	SNF	HLW	DFRm
Cl_2	–	–	9.7134e+01
Ar	3.3333e+01	3.3333e+01	–
CO_2	3.3333e+01	3.3333e+01	–
UCl_4	3.1413e+01	2.1624e-01	2.0731e+00
Cr, $CrCl_2$	–	–	5.6797e-01
$PuCl_3$	4.2285e-01	6.4323e-02	1.9879e-01
$NpCl_3$, $NpCl_4$ (0:1)	2.0097e-02	9.4384e-01	–
$AmCl_3$	4.7145e-02	1.1895e+00	–
$CmCl_3$	2.1413e-03	2.2820e-02	–
CsCl	1.0617e-01	4.0404e+00	2.0570e-03
$SrCl_2$	9.7788e-02	1.1281e+00	6.9411e-04
Tc	1.0465e-01	1.5289e+00	1.8147e-03
Ru	5.9953e-02	4.3636e+00	3.4566e-03
Rh	6.9970e-03	–	1.3798e-03
Mo	1.0466e-01	–	1.8151e-03
$BaCl_2$	1.0775e-01	–	1.7760e-03
$LaCl_3$	1.0777e-01	3.2054e+00	1.7803e-03
$CeCl_3$	1.9343e-01	3.2054e+00	2.9241e-03
$PrCl_3$	9.3419e-02	3.2054e+00	1.2567e-03
$NdCl_3$	1.3153e-01	3.2054e+00	1.9501e-03
$SmCl_2$	–	–	4.0131e-04
$SmCl_3$	9.6962e-03	3.2054e+00	3.2541e-04
$EuCl_3$	7.7001e-03	3.2054e+00	–
$ZrCl_4$	1.1096e-01	1.2067e-01	1.5068e-03
$NbCl_5$	1.1209e-01	1.2067e-01	1.5225e-03
$SnCl_2$, $SnCl_4$ (1:1)	–	1.2067e-01	–
$SbCl_3$, $SbCl_5$ (1:1)	4.4524e-04	1.2067e-01	–
$TeCl_2$, $TeCl_4$ (1:0)	7.2974e-02	1.2067e-01	1.5756e-03

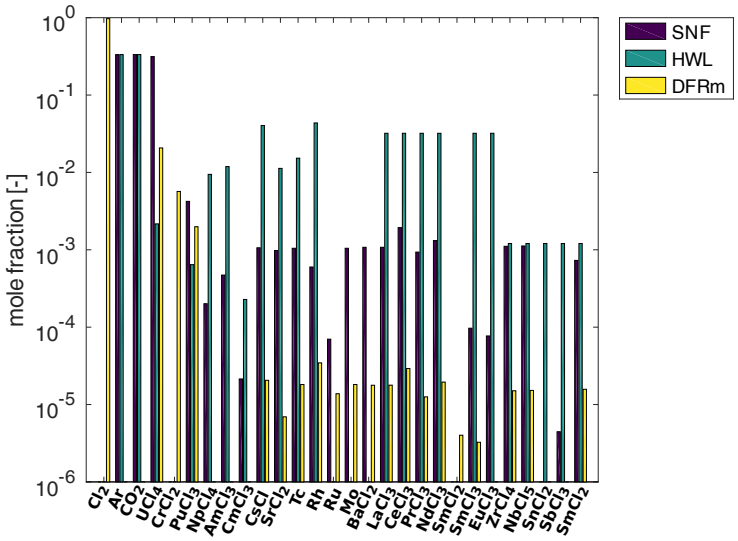

Figure 55: Overview of the main distillation feed cases in mol%

Regarding the difference in waste treatment between SNF and HLW, the feed composition differs essentially in the proportion of fission products present and less volatile high-level waste chlorides, the total proportion of which is significantly higher in the HLW example than in the SNF example. In the SNF material, uranium tetrachloride clearly predominates as a material component, which, according to the data from[139], is correspondingly only present to a minor extent in the HLW material. As the chlorination and inertization of SNF and HLW material is performed equally with carbon tetrachloride, the respective proportions of carbon dioxide and argon in the composition of the feed are very similar for both variants. Further values and differences between the variants can be found in Tab. (17). The following information is provided on the feed calculation for HLW and DFRm feed material, which differs from the feed calculation for SNF material.

Chlorination of DFRm material Chlorination of the metallic DFRm material via elemental chlorine should be operated with excess chlorine under similar chlorination conditions as for the chlorination of zirconium alloy cladding material according to [142]. 1/3 of the volume of the chlorination reactor should be occupied by the DFRm feed material and the remaining chlorine amount after chlorination. The molar flow is therefore made up of the excess chlorine $\dot{n}_{\mathrm{Cl_2}}^{\mathrm{excess}}$, the required stochiometric minimum chlorine amount $\dot{n}_{\mathrm{Cl_2,min}}$ and the composition of the DFRm feed material $\dot{n}_{\mathrm{DFRm}}$ of fully chlorinated basic fuel and the chlorinated fission products

$$\dot{n}_{F,\mathrm{tot}} = \dot{n}_{\mathrm{DFRm}} + \dot{n}_{\mathrm{Cl_{2,min}}} + \dot{n}_{\mathrm{Cl_2}}^{\mathrm{excess}}. \tag{142}$$

According to [39, 38], a U-Cr-Pu eutectic is used as the base mixture for the DFRm variant at a relatively low eutectic temperature of about 1000°C. The eutectic composition (excluding other components and fission products) is not known. Alternatively, a mixture of 73 mol% uranium, 20 mol% chromium and 7 mol% plutonium is chosen for the following simulation. Here, the fission product composition for fast reactions can be determined according to the DFRm feed example in [35] (in Fast Fission Yield) for 19 mol% with respect to U-238, 59 mol% for Pu-239

and 16 mol% for Pu-241. The remaining 6 mol% is interpolated from the Pu-241 and Pu-239 data for the fission of Pu-240. For the fission product fraction of the mixture, a fission product quantity of 1.1 t/a is assumed for the calculations from the total 120 t/a DFRm feed raw material, so that the total fission product fraction is 0.9167 mass %, just below 1 mass %. Then, assuming product conversions of 99 mol%, chlorination proceeds according to the following reduced chemical reactions. The chemical chlorination network of the basic fuel is

$$\begin{aligned} \mathrm{U}(s) + 2\mathrm{Cl}_2(g) &\rightarrow \mathrm{UCl}_4(g), \\ \mathrm{Cr}(s) + 1\mathrm{Cl}_2(g) &\rightarrow \mathrm{CrCl}_2(l/g), \\ \mathrm{Pu}(s) + {}^3\!/_2\mathrm{Cl}_2(g) &\rightarrow \mathrm{PuCl}_3(l/g). \end{aligned} \tag{143}$$

From the reaction scheme according to the reaction equations (143), the equimolar amount of chlorination required can be determined directly from the stoichiometric coefficients, and it applies in good approximation to the determination of the minimum amount of chlorine required (equimolar chlorine amount). It is therefore

$$\dot{n}_{\mathrm{Cl}_2,\mathrm{eq}} = (2x_{\mathrm{U}} + 1x_{\mathrm{Cr}} + {}^3\!/_2 x_{\mathrm{Pu}}) \cdot \dot{n}_{\mathrm{DFR}},\ \dot{n}_{\mathrm{DFRm}} \approx \frac{\dot{m}_{\mathrm{DFRm}}}{\sum_{i=1}^{N_{\mathrm{comp}}} x_i M_{w,i}}. \tag{144}$$

The excess chlorine quantity is derived from the specification that 1/3 of the volume in the chlorination reactor is to be used by the DFRm feed only, so that

$$\dot{n}_{Cl}^{\mathrm{excess}} = 2\frac{\dot{V}_0 \rho_{\mathrm{Cl}_2}}{M_{w,\mathrm{Cl}_2}}, \tag{145}$$

$$\dot{V}_0 = \left(\frac{w_{\mathrm{U}}}{\rho_{\mathrm{U}}} + \frac{w_{\mathrm{Cr}}}{\rho_{\mathrm{Cr}}} + \frac{w_{\mathrm{Pu}}}{\rho_{\mathrm{Pu}}}\right) \dot{m}_{\mathrm{DFRm}}. \tag{146}$$

The ratio between the molar flow of the excess and the required minimum amount of chlorine is relatively high with a calculated value of 18.201, which means that the resulting molar fraction has been used in the calculations of the total molar fractions of the feeds, the compositions of table Tab. (17).

C.1.2 Comparison of SNF and HLW recovery using the conceptual distillation design process

The developed distillative separation process for SNF treatment, as shown in Fig. (32), is used for the subsequent recovery of HLW material for reuse in suitable liquid fuel reactors, such as the Dual Fluid Reactor. The process temperatures are changed for separation, but the process pressures in the separation units remain largely the same. Only the zirconium material preparation process is of course not required here. The feed data of HLW material is available in Tab. (17).

The preprocessing and volatile chloride separation The following simulation results for the distillation-based processing of HLW material show, in that the separation can easily be

performed under the same process pressures as shown for the SNF recovery from Fig.(6.1). Due to the fact that the proportion of uranium tetrachloride in the PC-1 feed is much lower in the HLW recovery problem, but the proportion of less volatile chlorides from a volatility of cesium chloride is significantly higher, the separation efficiency with respect to uranium tetrachloride after the (first) SC-2 column increases significantly from 1E-01 mol% to well below 1E-03 mol% of involved components for impurifications. Uranium tetrachloride does not need to be distilled at high fractions, so separation is easier here than in the SNF process. All other components with decreasing volatility than uranium tetrachloride are separated from the SNF and HLW with a separation accuracy of 1E-04-mol%. The mole fraction of tin tetrachloride cannot be neglected for the HLW recovery problem.

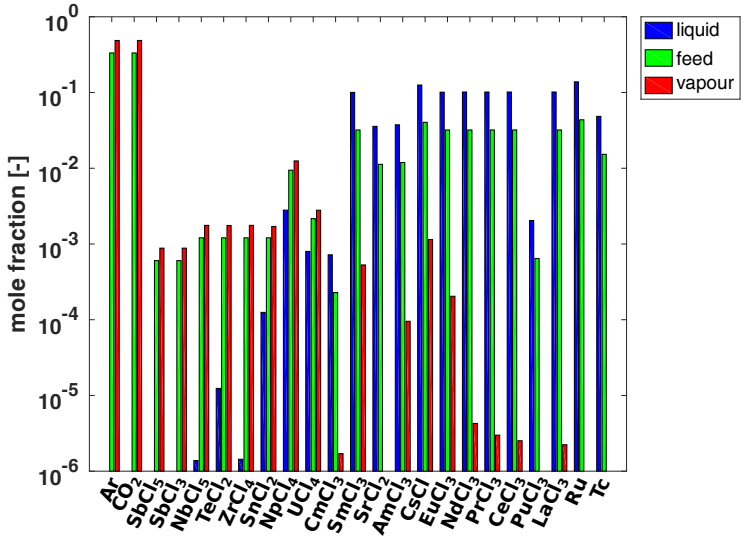

(a) SC-1 at 1135 K, 1 atm

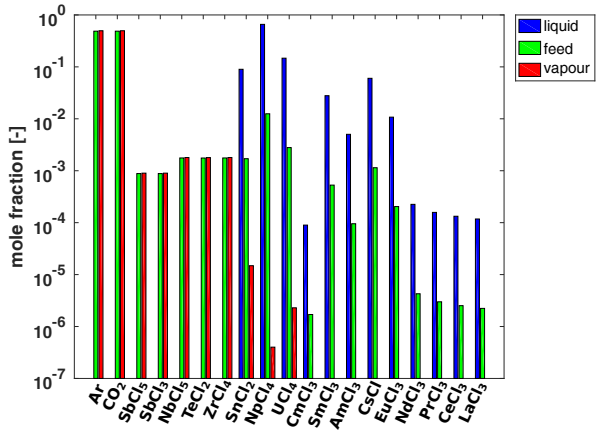

(b) SC-2 at 655 K, 1 atm

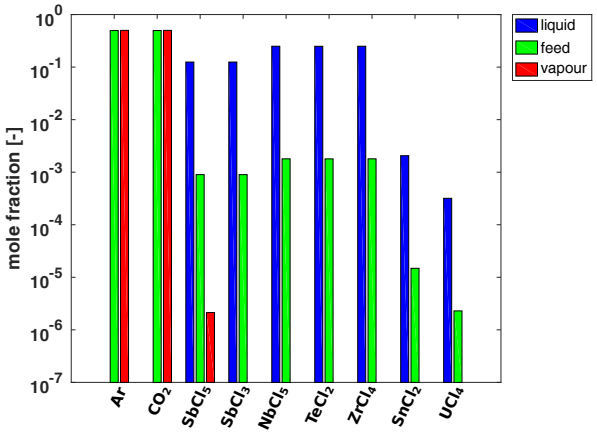

(c) SC-3 at 250-270 K, 1 atm

Figure 56: Flow-chart simulation of HLW distillation: Results for the separation of volatile chlorides

Since chlorination with chlorine results in chlorination to the less volatile tin dichloride is than preferred regarding chlorination equilibrium and the tin dichloride component is more difficult to separate as volatile chloride component than tit tetrachloride from melt at 725 K (at 1 atm).

The separation accuracy in the simulation results shown in Fig. (32) in SC-2 is slightly above 1E-03 mol% instead of the desired 1E-04 mol%. It also remains in the first phase separator in the liquid phase of PC 1. Due to exceeding the separation specifications for SNF treatment for uranium tetrachloride and tin dichloride in HLW recycling, a second separation step in SC-2 is required. The separation of all volatile chlorides from the remaining liquid phase material by the separation combination of evaporation and condensation according to PC-1 and SC-2 is otherwise equally good for SNF and HLW recycling.

In the final separation of the volatile chlorides from the vapour stream leaving the second SC-2 condensation column, all chlorides except antimony pentachloride (boiling point 79 °C as a highly volatile component) can be condensed in the SC-3 condensation as a residual fraction in the vapour phase with a separation accuracy in the range of 1E-04-1E-03 mol%. This is shown by the results in Fig. (56) (bottom) referring to HLW material. The reason for the higher residual fraction is, among other things, the significantly higher fraction value of the chloride component in the HLW material than in the SNF.

The simulation results of the final distilled volatiles of the HLW material in DC-3, simulated according to the total reflux distillation column principle mentioned in the main parts (III) and (IV) of the thesis, are shown in Fig. (45). In the first separation of the HLW distillation, higher temperatures of up to 1200 K have to be set in the evaporator instead of 850 K in the SNF processing.

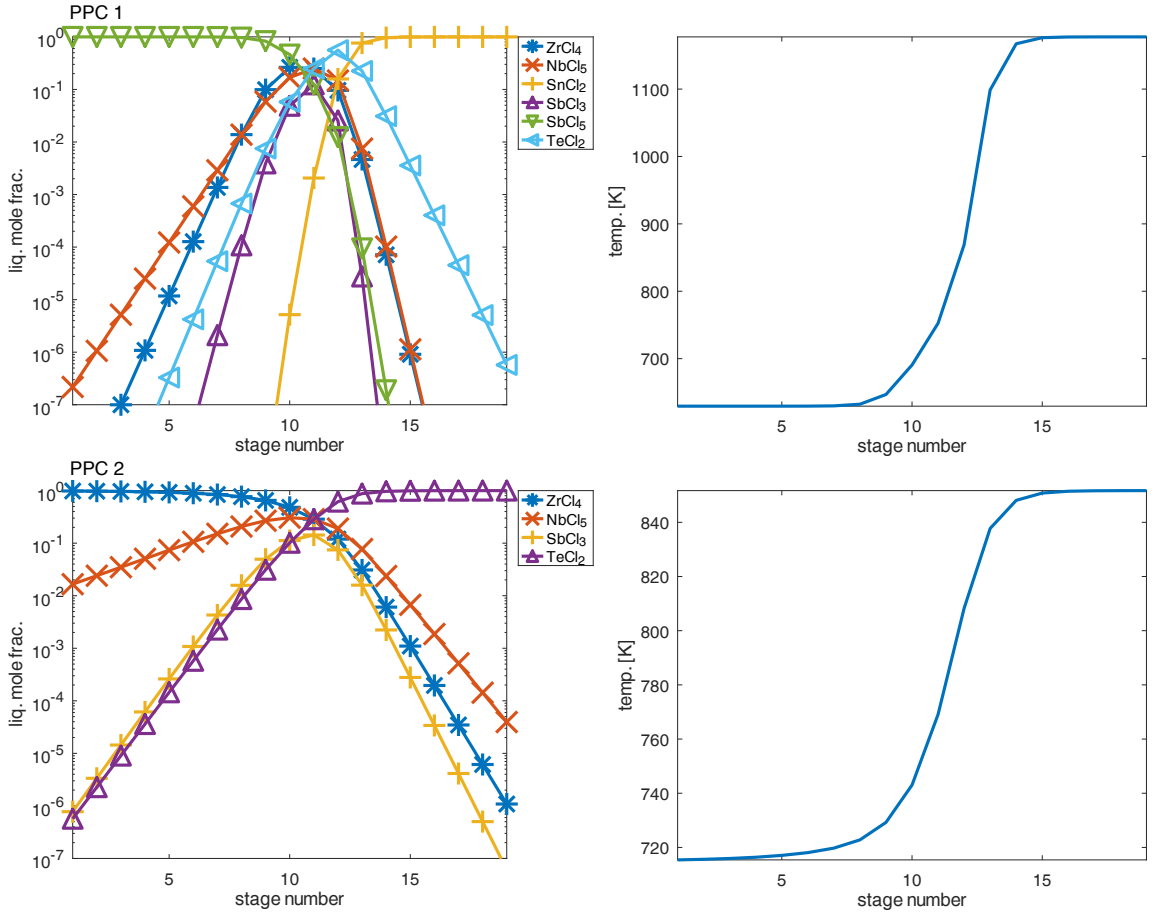

Figure 57: Flow-chart simulation of light volatile HLW distillation: DC-3 results of PPC 1 and PPC 2 at 25 bar

In a twenty stage distillation column at 25 bar, antimony pentachloride can be recovered as the light boiler component and tin dichloride as the heavy boiler component with impurities below 1E-04 mol% in the first stage of the total reflux distillation column. In the SNF recovery, tellurium dichloride is then recovered as the high purity material component in PPC 1 instead of tin dichloride in the first separation. In the HLW recovery example, tellurium dichloride is then recovered in PPC 2 as a less contaminated heavy boiler distillation product with small fractions of niobium pentachloride. This is the case for HLW recovery due to the now narrower temperature profile, as can also be seen from the narrower range of its pure boiling point components, in the PPC 2, which results in less separation effort of tellurium dichloride. Secondly, tellurium dichloride is not obtained as a high-purity chloride distillation product in these simulation results of the HLW recovery example, due to the reduced number of separation stages and the better separation results in the PPC 1.

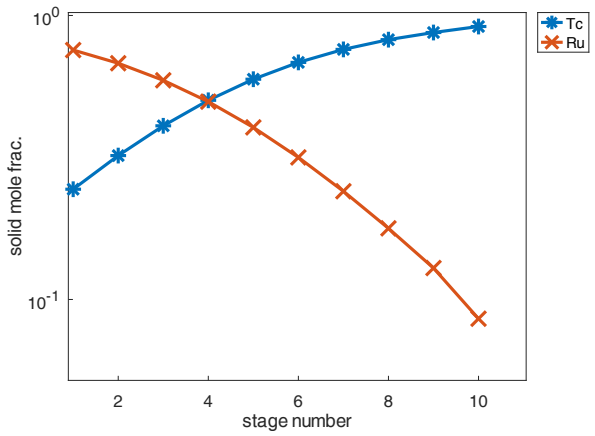

(a) SC-1 at 1135 K, 1 atm

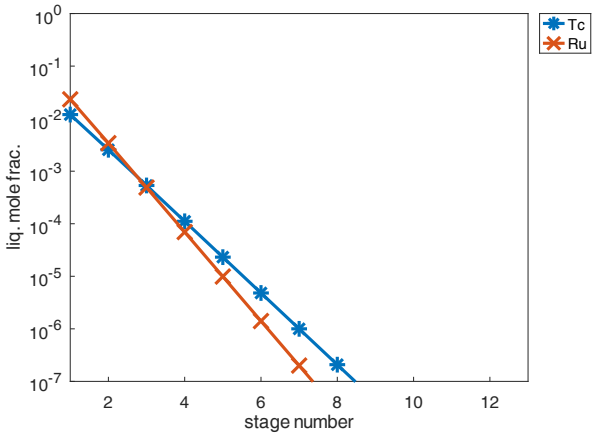

(b) SC-1 at 1135 K, 1 atm

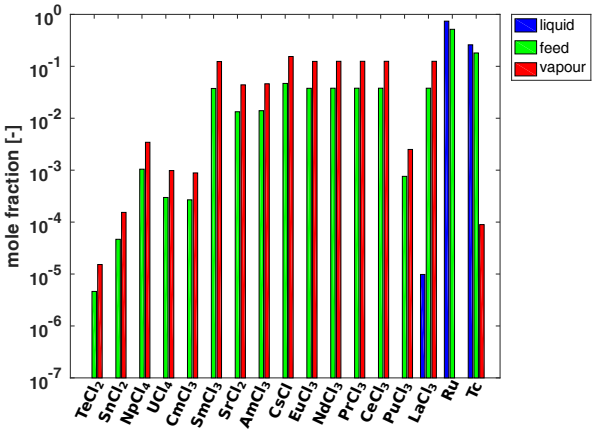

(c) E1 at 2000 K, 1 atm

Figure 58: Flow-chart simulation of HLW distillation: Results for the separation of non-solvable solid material

However, compared to SNF processing in PPC 2, there is a much stronger temperature gradient in the column height between stages 9-14 in the HLW recovery example. As a result, the zirconium tetrachloride content, which is now a light-boiling component of the PPC 2, decreases

much more rapidly. However, the separation accuracy for zirconium tetrachloride is not good either, comparable to the SNF processing example. Zirconium tetrachloride can be obtained from the simulation results shown in Fig. (57) with niobium pentachloride impurities between 0.5-2.0 mol%. As in SNF recycling, significantly more separation stages would be required to separate niobium pentachloride with an impurity content of 1E-04 mol-% from zirconium tetrachloride.

Except for the missing rhodium and molybdenum components in the feed, the separation of the solids is practically analogous with the same separation stages as separation repetitions as in the SNF preparation according to Fig. (39) and (40). The simulation results for the concentration and crystallisation of the precious metal components for the HLW separation example are summarised in Fig. (58). Based on the shown solid phase and also the depletion of the liquid phase results of the metallic components, it can be seen, especially for the HLW example, that technetium is somewhat more difficult to separate than ruthenium. Therefore, with increasing number of repetitions of solid separations, technetium accumulates more in the solid phase as it is the last component involved in the solid phase after repeated separations. After high purity separation of the solids after eight separation stages with residual impurities involved of 1E-04 mol% in S1 of the HLW recovery example.

The main distillation Due to the fact that significantly more fission products and other chlorides with very active elements are present in the distillation of the HLW variant than in the SNF preparation, significantly larger proportions of less volatile chlorides are removed with the vapour stream in the DF-1 fractionation column at 1064-1645 K and 1 atm. Therefore, a different type of DC-1 column is required for the purification of the uranium tetrachloride-neptunium tetrachloride fraction.

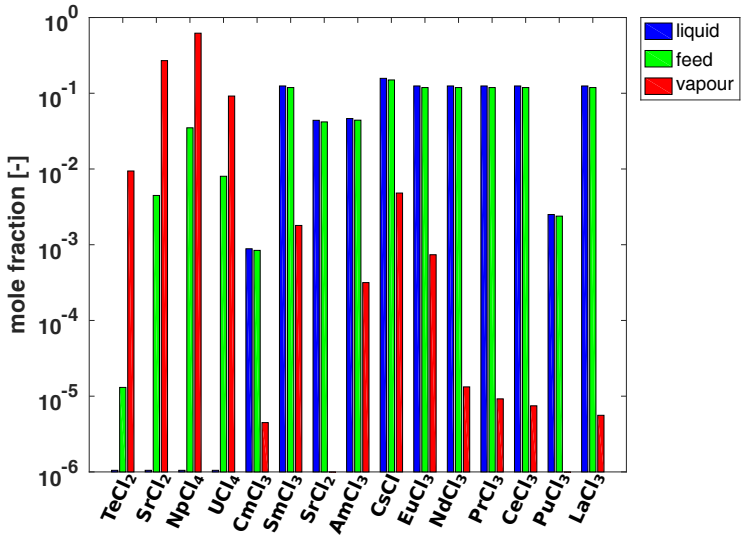

Figure 59: Flow-chart simulation of HLW distillation: Results of DF-1 at 1100-1640 K, 1 atm.

According to the simulation results of the distillation of DF-1 for HLW recycling shown in Fig. (59) , significantly higher proportions of less volatile fission product chlorides occur in the vapour phase. The less volatile components include samarium trichloride, europium trichloride, americium trichloride and cesium chloride with a molar fraction in the vapour phase of less than

1 mol% for each component. Other less volatile chlorides up to 1E-03 mol% are also present as heavy distillation product components, such as curium trichloride, neodymium trichloride, praseodymium trichloride, cerium trichloride and lanthanum trichloride. Strontium dichloride and plutonium trichloride are only present in the liquid phase at these separation limits of 1E-04 mol% for each component. One reason for the higher contamination of the vapour phase with less volatile chloride components compared to SNF recovery is the higher boiling temperature required and the narrower boiling behaviour of each component with more similar remaining less volatile components as in SNF recovery (temperature profile is not shown in this thesis).

In the DC-1 column, the simulation results of the whole reflux column (in PPCs) show a clear shift of the distillation separation areas to be expected due to the highly volatile and less volatile composed separable fractions. Based on the simulation results shown in Fig. (60), it can be seen that in the first PPC (PPC 1) in the evaporator, the residual portion of neodymium trichloride and the remaining volatile components are obtained as light-boilers before the uranium tetrachloride fraction follows. In contrast to the SNF separation example, the uranium tetrachloride fraction is less dominant as a contributing fraction here and is further not the first main separation fraction in SC 1. In PPC 2, the distillative enrichment of cesium chloride takes place in the evaporator and the heavy-boiling fraction is still present. In the last separation operation, the uranium tetrachloride fraction is separated from the samarium trichloride. The results in the example of distillation-based HLW processing thus show the high purity separability of all the fractions indicated, with otherwise high purity separation accuracies. In summary, for the SC 1 column, the light-boiling fraction of residual antimony, niobium, tin, selenium and tellurium chlorides is obtained as the light-boiling fraction, and finally the uranium tetrachloride fraction is obtained as a mixture with neptunium tetrachloride. The neodymium fraction, followed by the cesium chloride fraction and then the samarium trichloride fraction are obtained by distillation as the heavy-boiling product fractions.

After separation of the light-boiler volatile and uranium tetrachloride fractions in the DF-1 column, similar proportions of the remaining fission product chlorides and less volatile chlorides remain in the HLW material. As the simulation results for the DC-2 column, also simulated as a total reflux column with PPCs for the HLW material, from Fig. (61) show, the results for the separable fractions are similar to the SNF processing example (cf. Fig. (42)). Only the range of some mole fractions is slightly different. Here, only the fractions with americium trichloride and europium trichloride are slightly different in composition between the simulation results of the HLW and SNF processing examples (cf. Fig. (61) and Fig. (42)). The temperature fraction curve is also slightly different in the HLW distillation according to Fig. (61) of separation stages 2-10, as in the SNF preparation for comparison. All other differences can be seen in the simulation results presented in this section with the SNF results in Section (6.2.2) of chapter (IV).

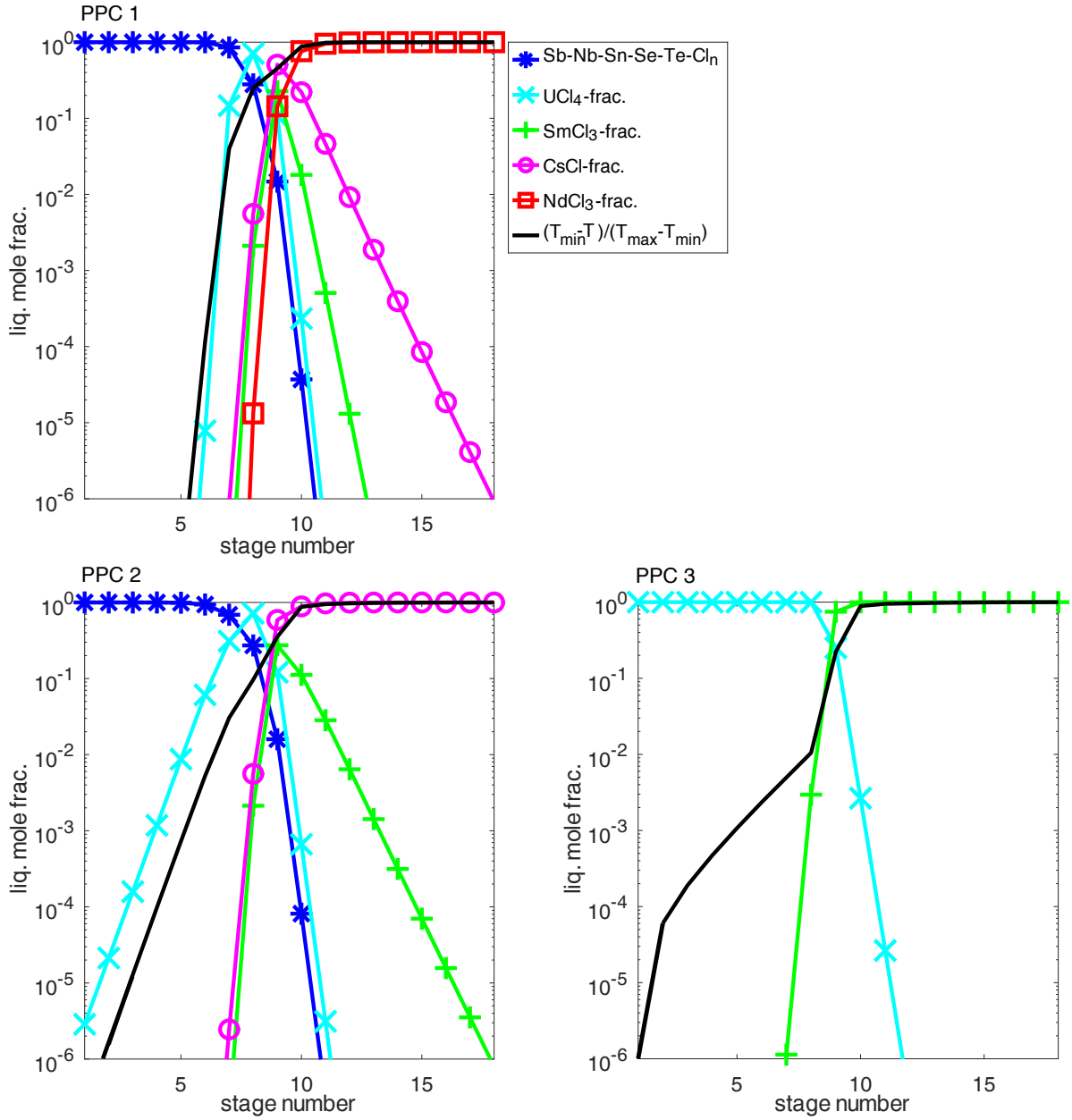

Figure 60: Flow-chart simulation of HLW distillation: DC-1 results of PPC 1, PPC2 & PPC 3***/**** at 593-1870 K, 1 atm **:
1*) Fraction of residual low volatiles (Sb-Nb-Sn-Se-Te-chloride system): Chlorides of antimony, niobium, tin, selenium and tellurium chlorides
2) Uranium tetrachloride fraction of mainly UCl_4 and $NpCl_4$ as mixture
3) $SmCl_3$-fraction: $SmCl_3$, $AmCl_3$
4*) CsCl.fraction: CsCl, $EuCl_3$
5*) $NdCl_3$-fraction: $BaCl_2$, NdCl3
*designated according to the largest proportion of the fraction present
**Separation accuracy: 1E-06
*** The choice of colors is intended to illustrate purely qualitatively the location of the respective substance component in relation to the temperature residence range of the component within the column: From dark blue with respect to cold temperatures in relation to the curium trichloride light-boiling fraction to red toward hot temperatures of the plutonium trichloride heavy-boiling fraction. Medium-boiling fractions are illustrated in mixed colors in relation to the temperatures
**** Detailed results each chloride component are available in the comparison of SNF and HLW recovery in section (C.2) .

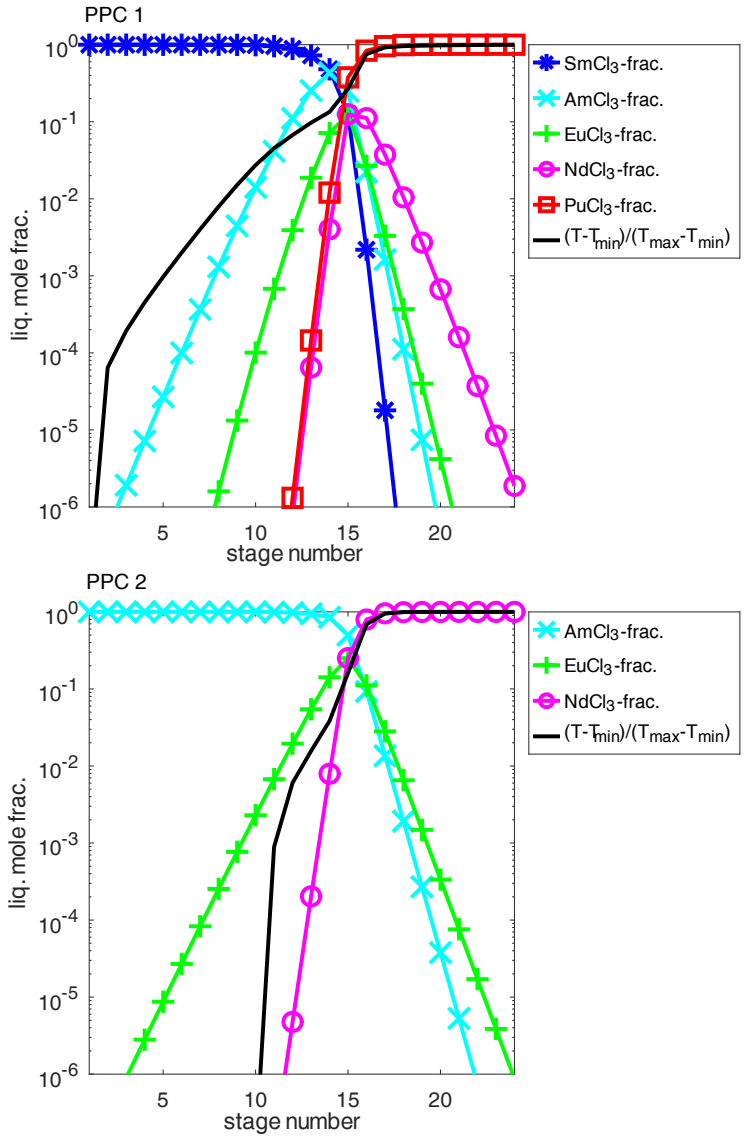

Figure 61: Flow-chart simulation of HLW distillation: DC-2 results of PPC 1 and PPC 2***/**** at 1409-2000 K, 1 atm **:
1*) $SmCl_3$-fraction/$CmCl_3$-fraction: $CmCl_3$, and $SmCl_3$
2*) $AmCl_3$-fraction: $AmCl_3$, $SrCl_2$, CsCl
3) $EuCl_3$-fraction: mainly $EuCl_3$, with impurities of CsCl and $SrCl_2$
4*) $NdCl_3$-fraction: $BaCl_2$, NdCl3
5) $PuCl_3$-fraction: $PrCl_3$, $CeCl_3$, $PuCl_3$, $LaCl_3$
*designated according to the largest proportion of the fraction present
**Separation accuracy: 1E-06
*** The choice of colors is intended to illustrate purely qualitatively the location of the respective substance component in relation to the temperature residence range of the component within the column: From dark blue with respect to cold temperatures in relation to the curium trichloride light-boiling fraction to red toward hot temperatures of the plutonium trichloride heavy-boiling fraction. Medium-boiling fractions are illustrated in mixed colors in relation to the temperatures
**** Detailed results each chloride component are available in the comparison of SNF and HLW recovery in section (C.2) .

C.1.3 Fuel recovery of DFRm feed material in a distillation-based conceptualized separation process

For closing the Dual Fluid Cycle after some reaction sequences in the Dual Fluid Reactor concept shown in Fig. (2), the accumulated fission products have to be separated by distillation as soon as a critical fission rate of a few percent is reached. Basic information on the material and composition of the Dual Fluid Reactor and the burn-up of actinides from spent fuel in the Dual Fluid Reactor is given in [39]. This corresponds to a very long operating life of decades before separation of the fission products becomes necessary. In the following, it is shown that separation can be operated with the same separation process developed after chlorination (see Fig. (32)) and even allows mixtures of SNF and DFRm material. In this case, of course, there is no need for the cladding material recovery step. First of all, pure DFRm fuel recycling is considered. The chlorination is performed with elemental chlorine as already described in section (C.1.1) with a high chlorine excess of 18.201 (chlorine to fuel material ratio) and analogous to the zirconium chlorination process according to [142, 16].

Compared to SNF and HLW material recycling, the DFRm recovery process differs in that no inert gases are used, but atmospheric oxygen and air are still completely excluded. Furthermore, the mixture to be distilled consists of only 0.917 mass % of fission products related to the fuel amount and the remaining fractions from the U-Cr-Pu eutectic DFRm feed composition under the simplification that the mole fraction remains unchanged after chlorination (see also section (C.1.1) for choice). In the DFRm material, the uranium tetrachloride, chromium dichloride and plutonium trichloride components dominate over all other fissile chloride components. Therefore, the main separation problem in material separation is to separate the DFRm feed mixture by distillation in DF-1 according to Fig. (32) in such a way that the fission products either pass into a UCl_4-$CrCl_2$ vapour phase separation fraction (see PC-1 in the flowchart according to Fig. (37)) or remain in the separate $CrCl_2$-$PuCl_3$ liquid phase. Based on the consideration of the mole fractions according to Tab. (17) and the boiling points of many components according to Fig. (37), the simulation results below show that practically all fission products enter the heavy-boiling column DC-2 (see flow chart in Fig. (32)). Chromium dichloride, as a relatively thermally unstable molecule, is present in both phases, while pure chromium remains in the liquid phase. For simplicity, chromium dichloride is assumed to be thermally stable, but it may be preferable if this is not the case to be able to better separate this component in a much larger concentration-crystallisation unit than elemental metallic chromium. However, for these simulations, chromium dichloride is assumed to be the only thermally stable chromium component in the separation process.

Prior to the main distillation, the solids, volatile chlorides and process gases must again be separated from the main stream in the pre-treatment unit before the main distillation in DF-1 and the separation in columns DC-1 and DC-2 can be applied. No off-gas cleaning is required in the pure distillation-based DFRm feed processing, as can be seen from the feed composition of the less important separable components so far in Tab. (17), with the exception of argon.

The preprocessing and volatile chloride separation The simulated separation process to the PPU for the specific example of DFRm feed processing is also analogous to the concep-

tualised PPU for SNF material recovery in Fig. (32), including all process temperatures and pressures. First, the volatile components are separated in the flash evaporation PC-1, which are much lower for the DFRm recycling material than for the SNF or HLW material. For this purpose, a chlorine atmosphere is used instead of noble gases such as argon. While the volatiles are completely transferred to the vapour phase, some other chlorides are also present in the vapour phase (at 1135 K below 1 atm) in higher mole fractions than in the SNF processing example. The simulation results of PC 1 show in Fig. (62) the most significant fractions in the vapour phase are uranium tetrachloride and chromium dichloride, which pass into the vapour phase. Other components of about 1E-03 mol% are cesium chloride and plutonium trichloride, including minimal residues of 2E-04 mol% of other components. The details of the data can be seen from the simulation results in Fig. (62).

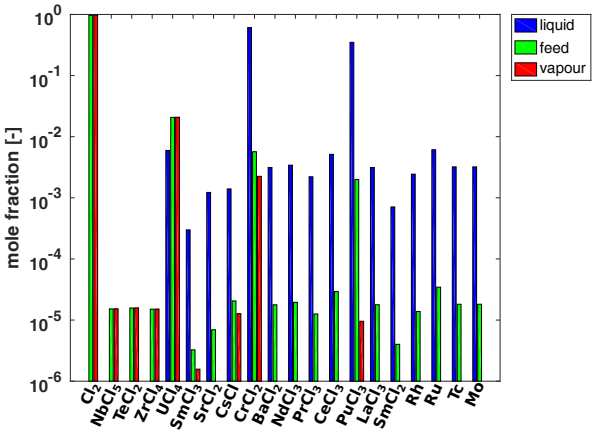

(a) PC-1 at 1135 K and 1 atm

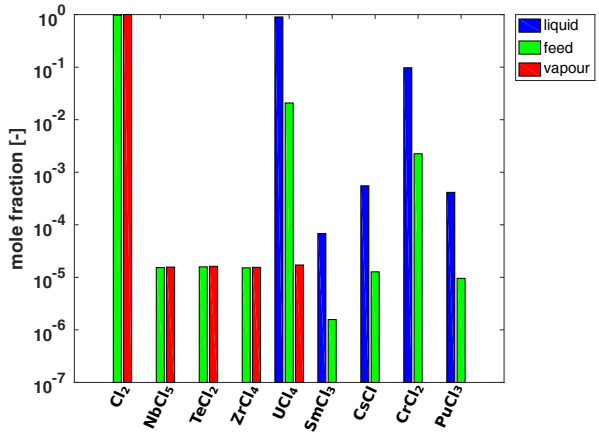

(b) SC-2 at 655 K and 1 atm

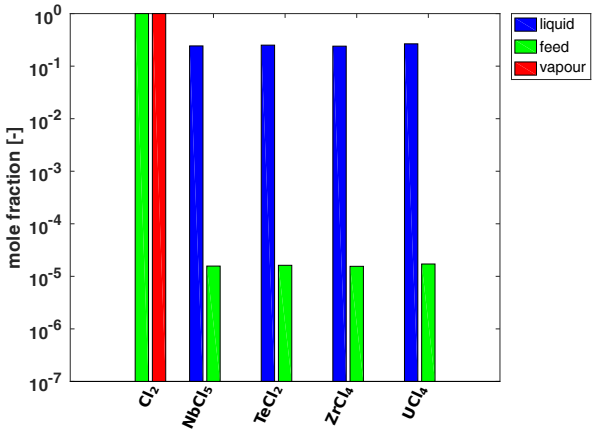

(c) SC-3 at 250-270 K and 1 atm

Figure 62: Flow-chart simulation of DFRm feed distillation: Results for the separation of volatile chlorides

The further separation steps follow analogously to the SNF and HLW substance separation, in the condensation of these less volatile chlorides from the vapour phase and the concentration and crystallisation of the non-volatile solids. The simulation results of the application of the single-stage condensation step in SC-2 shows from Fig. (62) for SC-2 that all chloride components except a remaining uranium tetrachloride fraction of 1E-03-mol% in the vapour stream can be

separated at 725 K. The components Samarium trichloride, cesium chloride, chromium dichloride and plutonium trichloride are completely condensed out. In the processing of the used DFRm feed material, a second separation stage will have to be operated at 625 K in order to separate also the remaining fractions of uranium tetrachloride with 1E-03-2E-03-mol% from the vapour phase in SC-2 which is feasible by further simulation resulting a value of near 2E-04 mol% of residual uranium tetrachloride in the vapour phase, which is slightly higher than in the SNF reprocessing, but quite acceptable for separation accuracy so far. With the condensation-crystallisation of the volatile chlorides at 250-270 K in the following condensation stage SC-3, only elemental chlorine will remain in the vapour phase. As the simulation results show only chlorine remains in the vapor phase, while all chloride components condensate out of the vapor phase into the liquid phase. Further off-gas treatment in column DF-2 (according to flow-chart Fig. (32)) is no longer necessary and the chlorine within the impurification level of less than 1E-04 mol% can be used again for chlorination.

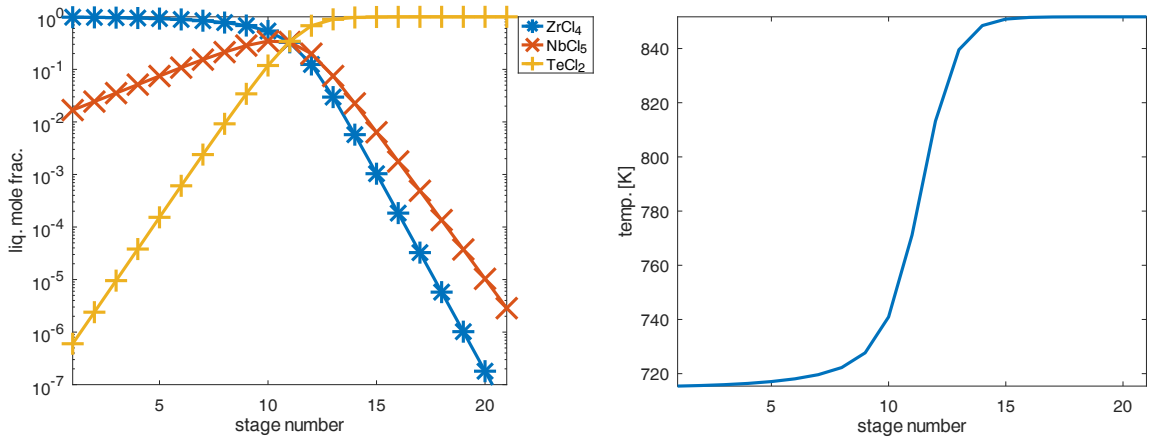

Figure 63: Flow-chart simulation of DFRm distillation: DC-3 at 25 bar

Due to the low proportions of volatile chlorides, intermediate storage is advisible in order to have a sufficiently large distillation volume available for the distillative purification of these volatile chlorides in a total reflux column of PPCs in DC-3, in order to realise the mass transport between vapour and liquid phase with a significant distillable total amount within the column. In DFRm processing, vessel tank B1 instead serves as an intermediate storage compared to SNF or HLW recycling where it is not required. Again, the simulation results in Fig. (63) show that in a 21-stage separation column at pressures of 25 bar and in the temperature range shown between 718 K and 850 K, a mixture of zirconium tetrachloride and niobium pentachloride can accumulate in the condenser, with the exception of tellurium dichloride, in which niobium pentachloride is present at 2 mol% as a medium-boiling impurity component. At the bottom of the column, tellurium dichloride with niobium pentachloride impurities of less than 2.5E-04-mol% can be obtained in the twenty-first separation stage as a residue in the evaporator by distillation at temperatures around 850 K. Niobium pentachloride cannot be separated pure in the PPC 1 separation stage. Twenty-five stages would be required to separate tellurium dichloride with high purity. Otherwise, the separation of the volatile chlorides is analogous to SNF and HLW recovery, but with less amount and components of the volatile chlorides.

The simulation results for the concentration, crystallisation of the solids in SC 1 and evaporation of the remaining concentrated chlorides in E1 are shown in Fig. (64). Analogous to the SNF processing, according to the simulation results in Fig. (64), the solids are depleted in the liquid phase in SC-1 in a series-connected multiple crystallisation procedure with concentration-crystallisation and sieving at each separation step, as they then accumulate in concentrated form in S1 under the same process conditions as previously described for the SNF processing according to chapter (IV). For molybdenum, the separation with an impurity level of 1E-04-mol% takes place already from the fourth separation stage. This is followed by the separation of ruthenium in the fifth stage with a separation accuracy of 1E-04 mol%, technetium in the sixth stage and rhodium in the seventh to eighth stages with the same separation accuracies.

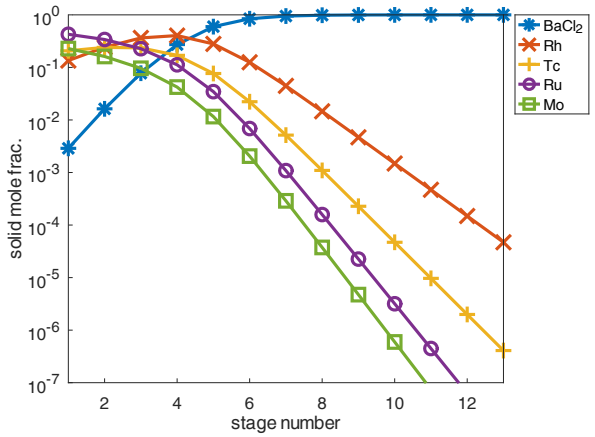

(a) SC-1 at 1135 K and 1 atm

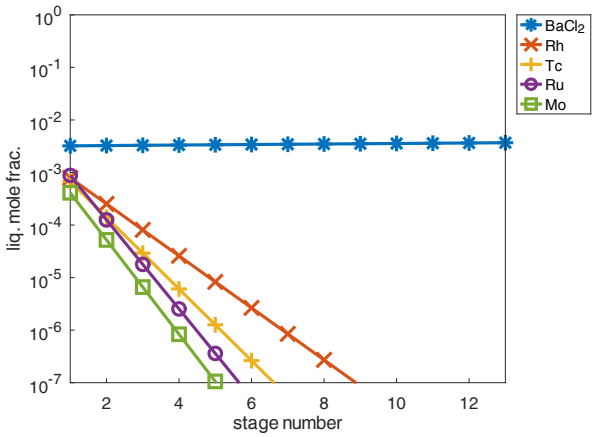

(b) SC-1 at 1135 K and 1 atm

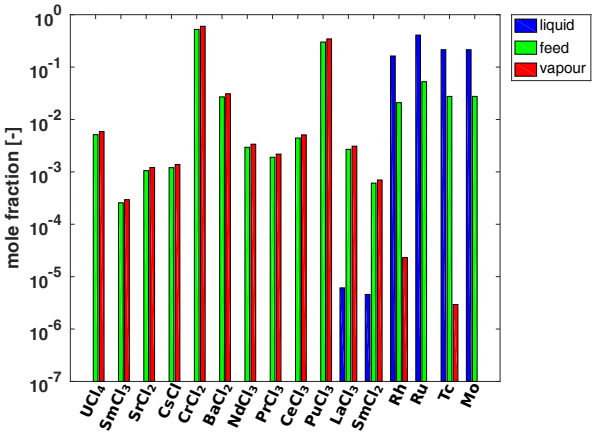

(c) E1 at 2000 K and 1 atm

Figure 64: Flow-chart simulation of DFRm feed distillation: Results for the separation of non-solvable solid material

Between the fifth and eighth stages, virtually only rhodium is removed from the liquid phase. As the metal components are reduced from the liquid phase, the proportion of barium dichloride in the solid phase increases continuously. From the ninth stage onwards, the separation of the metals can be considered complete in terms of separation accuracies below an impurity level of 1E-04 mol%, while the proportions in the solid phase can still show significantly higher proportions

of metallic components in the mode fraction results. This is because the total amount of solids is much smaller than that dissolved in the liquid phase. Nevertheless, in both the DFRm and SNF reprocessing cases, rhodium significantly determines the number of separation stages required to achieve the separation accuracies with a maximum impurity level of 1E-04 mol% of the final residual possibly dissolved solids (in terms of the modelling concept) in the liquid phase.

For the evaporation of the chlorides from the concentrated solid fraction, as described in the crystallisation for SNF recovery concept in section (32), it follows that negligible amounts of rhodium and technetium, with a maximum mole fraction of 3E-03 mol% each, also pass into the vapour phase. On the other hand, smaller impurity fractions of lanthanum trichloride and samarium dichloride remain in the liquid phase, as can be seen from the simulation results of E1 in Fig. (64). However, these fractions are only present in the ppm range and are negligible in the liquid phase. From a modelling point of view, it should be noted that in the case of crystallisation, these chlorides also remain in the liquid phase and not in the solid, so it can be assumed that these small impurity fractions are also evaporated as chlorides on the solid surface and not composed in higher proportions in the solid matrix.

All other separation details for all separation results according to Fig. (62) and Fig. (64) follow in the preprocessing analogous to the SNF recycling according to chapter (IV), as shown by the comparison of the separation curves and the separation product compositions per separation unit based on the simulation results shown for the preprocessing.

The main distillation The predominant 99.083-mol% relates to the original eutectic mixture of uranium, chromium and plutonium as a mixture of UCl_4-$CrCl_2$/Cr-$PuCl_3$ with about 73-mol% uranium tetrachloride, 20-mol% chromium dichloride and 7-mol% plutonium trichloride.

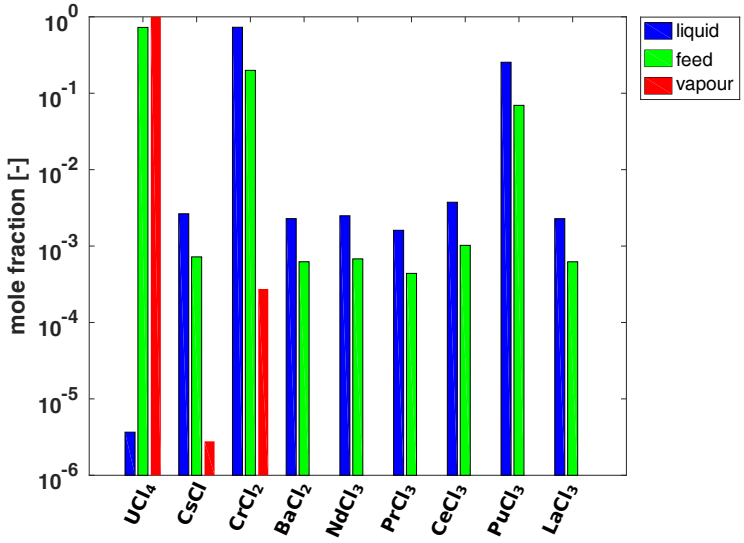

Figure 65: Flow-chart simulation of DFRm distillation: Results of DF-1 at 1100-1650 K and 1 atm

Fig. (65) shows the simulation results for the continuous fractionation column DF-1 according to the developed separation process of the flowchart in Fig. (32). The separation of uranium

tetrachloride as vapour phase together with chromium dichloride impurities and traces of cesium chloride with a fraction of 2-3E-04-mol% just above the separation specification limit of 1E-04-mol% in the condenser of this fractionation column can be clearly seen. All other chlorides, from barium dichloride to lanthanum trichloride, remain in the liquid phase in the DF-1 evaporator.

The chlorides are then separated from the vapour phase of DF-1 in the DC-1, neglecting the minimum cesium chloride impurity content. The simulation results of the following DC-1 as a five-stage total reflux column with PPCs show that the high-purity enrichment of uranium tetrachloride in the first separation stage as a light boiler and of chromium dichloride as a heavy boiler component in the fifth separation stage can be achieved far below the separation specifications of 1E-04 mol% of involved impurities. Due to the high relative volatility of uranium tetrachloride compared to chromium dichloride, only a five stage column is required to achieve the 1E-04 mol% separation specification. The temperature profile shows a large temperature change only from the third to the fifth stage, which is most pronounced between the third and fourth stages. In particular, the light-boiling component uranium tetrachloride dominates in the first to third stages and is replaced by chromium dichloride as the heavy boiling component between the third and fourth stages.

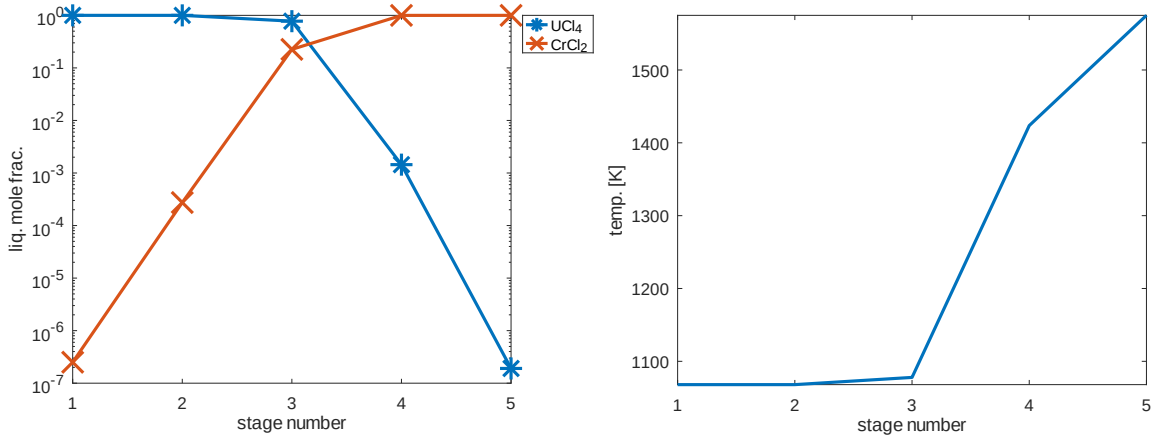

Figure 66: Flow-chart simulation of DFRm distillation: DC-1 results at 1068-1575 K, 1 atm

In order to reduce the large temperature change between stages three and four for technical reasons, two distillation columns are used, where the distillation in the first column is only carried out up to the temperature of the third stage. The strategy and simulation for this is explained in section (C.2.2) as an example.

Apart from plutonium trichloride, more than 80 mol% of the original DFRm feed with 1.1 t/a fissile material and 120 t/a original U-Cr-Pu mixture has already been separated in DF-1 and DC-1. The remaining portion of up to 20 mol% heavy salt material is processed in the DC-2 column. The simulation results for the DC-2 column are shown in Fig. (67) in only one required PPC of the specially designed total reflux column principle from chapters (III) and (IV). There, as can be seen from the simulation results in Fig. (67), chromium dichloride and cesium chloride can be enriched as a light-boiling fraction combined in the DC 2 total-reflux column with a separation accuracy of 1E-04 mol%.

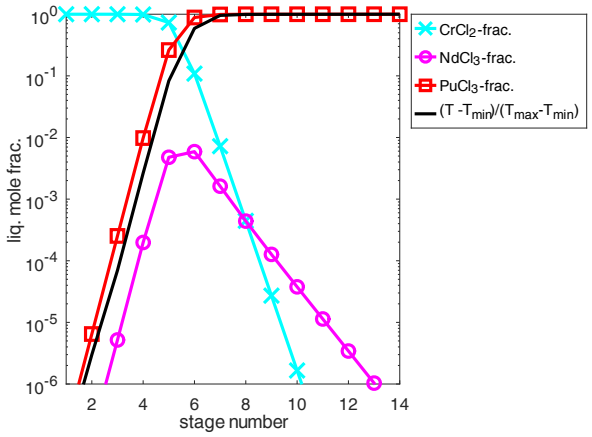

Figure 67: Flow-chart simulation of DFRm distillation: DC-2 results (PPC 1)***/**** at 1575-2005 K, 1 atm **:
1*) $CrCl_2$: $CrCl_2$, CsCl
2*) $NdCl_3$-fraction: $BaCl_2$, NdCl3
3) $PuCl_3$-fraction: $PrCl_3$, $CeCl_3$, $PuCl_3$, $LaCl_3$
*designated according to the largest proportion of the fraction present
**Separation accuracy: 1E-06
*** The choice of colors is intended to illustrate purely qualitatively the location of the respective substance component in relation to the temperature residence range of the component within the column: From light blue with respect to cold temperatures in relation to the chromium dichloride light-boiling fraction to red toward hot temperatures of the plutonium trichloride heavy-boiling fraction. Medium-boiling fractions are illustrated in mixed colors in relation to the temperatures
**** Detailed results each chloride component are available in section (C.2) .

Plutonium trichloride can be enriched in the plutonium trichloride fraction together with cerium trichloride, praseodymium trichloride and lanthanum trichloride in the final separation stage without the other separation fractions by distillation as a heavy boiling distillation product. The neodymium trichloride fraction remains in the column as a medium boiling fraction of the combined intermediate boiler chloride components, mainly neodymium trichloride and barium dichloride. Other components are negligible, as the simulation results have shown that these chloride components do not influence the curvature of the visible medium-boiling fraction. Consequently (according to the simulation results in Fig. (67)), the plutonium trichloride fraction is proportionally dominant down the column with increasing separation stages beginning from the sixth separation stage. Above lower separation stages than six, the uranium tetrachloride fraction slightly dominates inside the distillation column. Therefore, the temperature fraction curve $\theta = \frac{T-T_{\min}}{T_{\max}-T_{\min}}$ largely follows the plutonium trichloride fraction curve shown in Fig. (67) with $T_{\min}$ in the first and $T_{\max}$ in the last separation stage.

C.1.4 Recovery of SNF, HLW and DFRm mixtures in the conceptual distillation separation process

The simulation of different feed mixtures of SNF, HLW and DFRm material after completed chlorination from the previous sections has already shown the robust applicability of the designed distillation process under a wide range of feed compositions. While in the SNF feed material the major part (at least 95 mol%) is uranium tetrachloride, in the DFRm material to be recycled

mainly uranium tetrachloride, chromium dichloride and plutonium trichloride are present as a basic mixture with small proportions of fission products. It has therefore been demonstrated that the separation process shown in Figure (32) can be applied after chlorination under the same or similar process conditions as for a pure uranium tetrachloride-dominated SNF mixture with chlorinated fissile material. The simulation of the HLW material in the previous section has shown that even uranium tetrachloride or other higher chlorinated actinides do not have to be dominant in the chlorinated feed mixture for the developed separation process according to Fig. (32) to be applicable under consideration of idealized simulation results. Other significant differences are the amount of chlorine required, which also depends on the chlorination method, i.e. the use of elemental chlorine for the chlorination of metallic components and carbon tetrachloride or other hydrogen-free chlorocarbons for the chlorination of oxides. In addition, it is shown below that the separation concept developed and simulated under ideal phase equilibrium conditions for SNF recovery, as shown in Fig. (32), would also potentially allow the distillative recovery of mixture cases of simplified fully chlorinated SNF, HLW and DFRm feed materials to be processed. From a practical point of view, it is of course better to solve the separation problems separately, but simulation results of the mixture to be processed should demonstrate the robust use of a wide range of compositions in the application of the designed distillation process show.

In order to somehow reasonably combine these feed streams, a mixture of chlorinated SNF material with 1000 t/a and chlorinated DFRm material with 1001.1 t/a in a mass flow ratio of 1:1 was used here as an example for the process simulation. Furthermore, in addition to the SNF treatment case of 1000 t/a, HLW feed material of 20,874 t/a is added in the specified mass ratio of the total masses per year of HLW and SNF inventory according to information from [139].

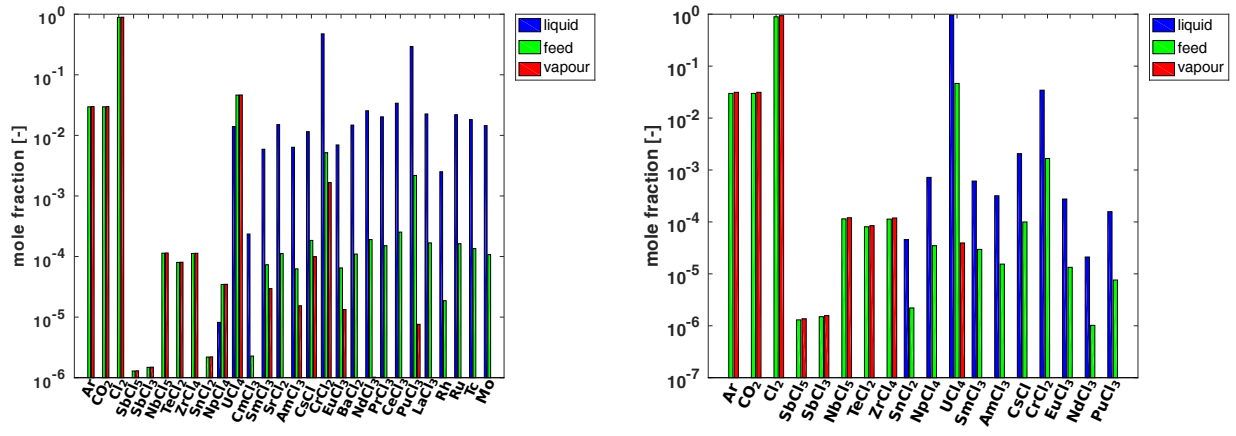

(a) PC-1 at 1135 K and 1 atm

(b) SC-2 at 625 K and 1 atm

Figure 68: Flow-chart simulation of mixed SNF, DFRm and HLW recycling: Results for the separation of volatile chlorides

As shown by the simulation results for flash evaporation in PC-1 in Fig. (68) (left part of figure), a simple separation at 1135 K is just as feasible as for all other pure SNF, HLW and DFRm feed examples already considered. Due to the condensation of the chlorides from the vapour phase in SC-2 (Fig. (68), right part of the figure), a residual amount of uranium tetrachloride remains also in the first separation process, as already shown in detail for the

simulation of the distillative purification of the pure SNF and DFRm feed material. A second condensation step is also required for the complete separation of uranium tetrachloride for the mixture of the above feed streams, with the first separation unit operating at 725 K and the second unit at 625 K. As the curium trichloride content is relatively small, it is neglected in the following calculations.

The concentration of the solids and crystallisation according to the simulation results in Fig. (69) of the mixture is also comparable to the DFRm feed and the SNF preprocessing example. The proportion of HLW recovery plays only a minor role here due to the significantly lower inventories of these materials. Between the fifth and eighth separation for the sequential concentration crystallisation, the removal of the metallic material components from the liquid phase takes place with residual fractions clearly below 1E-04-mol%, as shown in Fig. (69) of the liquid phase composition. Thus, in order, molybdenum and ruthenium are separated in the 5-6 separation stage and technetium and rhodium in the 7-8 separation stage. As rhodium and technetium are less separable than molybdenum and ruthenium and also have a lower melting point than the other metallic components, these metallic components are concentrated in the solid phase, similar to the DFRm simulation results. After practically complete separation of molybdenum and ruthenium, the residual components of technetium and rhodium are dominant and are separated in the subsequent separation stages. All detailed simulation results are shown in Fig. (69) and demonstrate the robust handling of solids as an example of varying mixture composition.

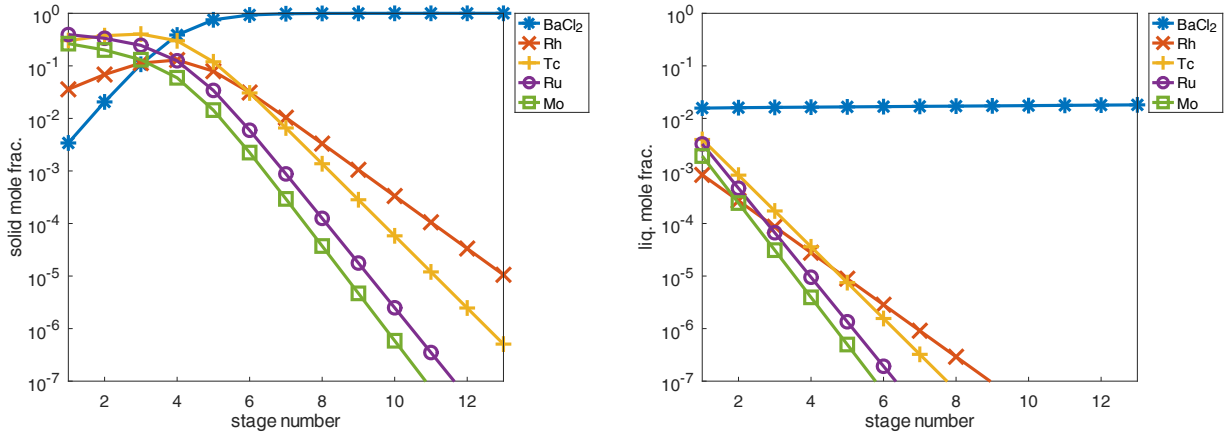

(a) SC-1 at 1135K and 1 atm

(b) SC-1 at 1135K and 1 atm

Figure 69: Flow-chart simulation of mixed SNF, DFRm and HLW recycling: Accumulation of solid material

After mixing the chlorides in M1 according to the flowchart in Fig. (32), the light-boiler components are distilled in the separation column DC-1 and the heavy-boiler components in DC-2.

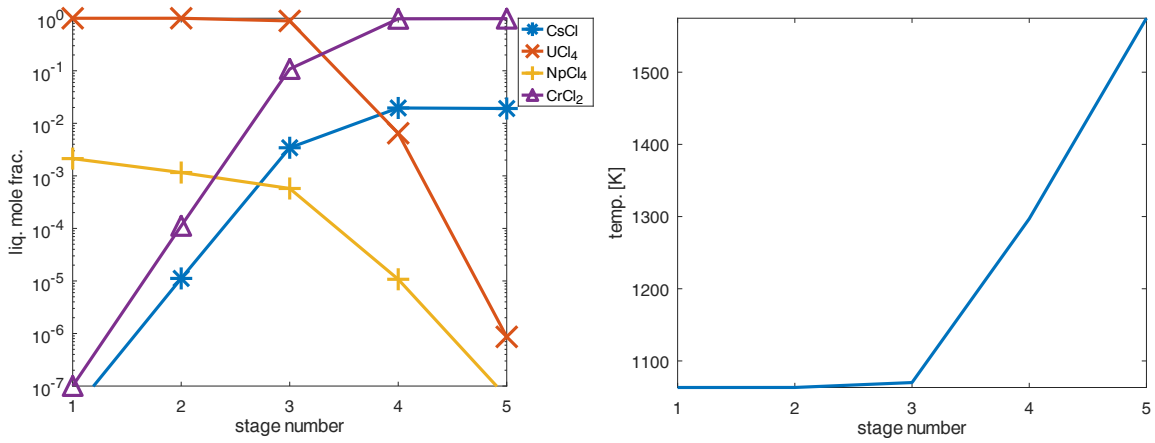

Figure 70: Flow-chart simulation of mixed SNF, DFRm and HLW recycling: DC-1 results at 1 atm

The simulation results of the DC-1 column shown in Fig. (70) now show the separation with cesium chloride, chromium dichloride but also neptunium tetrachloride components together with uranium tetrachloride. The separation of chromium dichloride is performed in five stages, similar to the DFRm feed example, in order to enrich a $CrCl_2$-CsCl mixture to high purity in the fifth stage in the condenser. Secondly, a high purity UCl_4-$NpCl_4$ mixture is obtained by distillation in the first stage. The separation curves do not show any local maxima or minima, so that no accumulation of other typical medium boiling components is expected in the mixed feed results compared to the pure HLW or DFRm recovery examples. All chlorides involved behave as either light or heavy boilers in the DC-1 column. The temperature profile shows that the heavy boilers chromium dichloride and cesium chloride dominate exclusively in the fifth separation stage, while the light boilers neptunium tetrachloride and uranium tetrachloride determine the separation behaviour in the total reflux column within the single PPC, with the exception of the fourth separation stage.

In the heavy-boiling column DC 2 according to the simulation results in Fig. (71) (a twenty-five stage total reflux column), the separation of the light-boiling components contained in the mixture is somewhat more difficult in terms of the separability of each separation fraction. Samarium trichloride is no longer separable with high purity in this mixture example. Therefore, in the first separation step, the combined samarium trichloride - ammonium trichloride fraction is obtained as the light boiling fraction. A plutonium trichloride fraction of lanthanum, praseodymium and cerium trichloride is again obtained as a high purity heavy boiler distillation product (impurities less than 1E-04 mol%). The influence of the HLW material is again negligible due to the higher proportion of SNF and DFRm in the feed material. The cesium chloride and europium trichloride fractions are present as intermediate boiling components between separation stages 10-14. In PPC 1 of the DC-2 column, the separation effort is increased, which makes the fine separation of the heavy boiling chlorides the most difficult compared to the treatment of the pure DFRm and SNF feed material simulation examples.

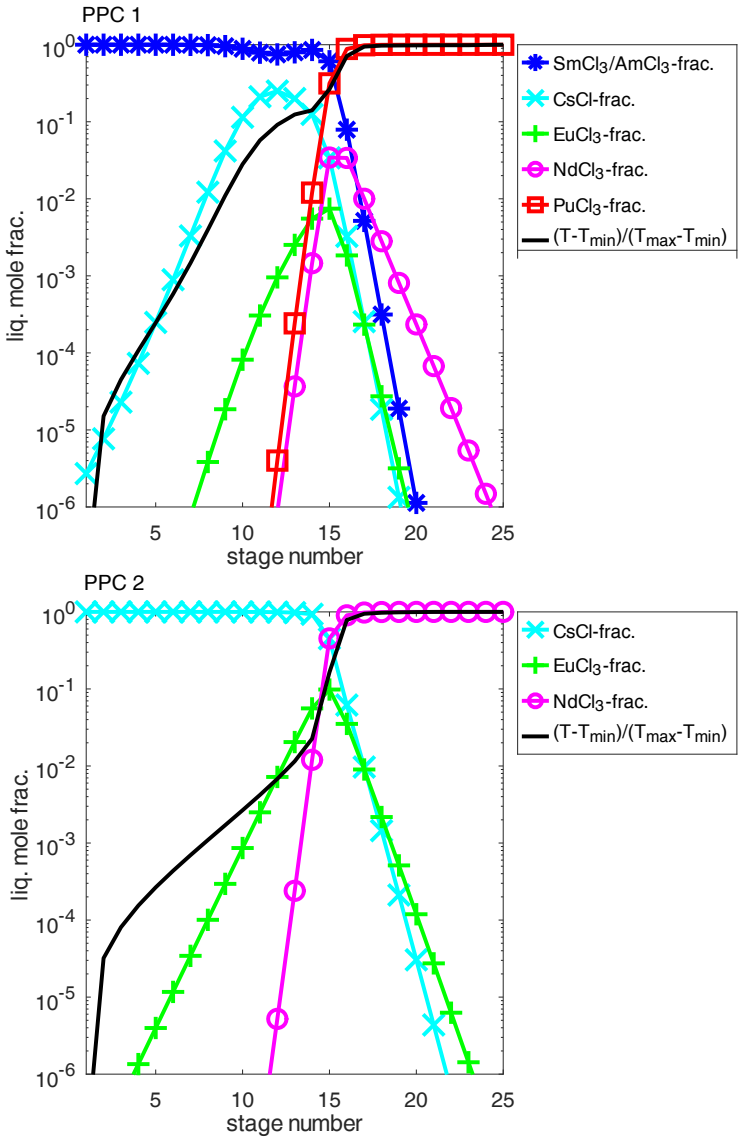

Figure 71: Flow-chart simulation of mixed SNF, DFRm and HLW recycling: DC-2 results PPC 1 & PPC 2***/**** at 1463-2016 K, 1 atm **:
1*) $SmCl_3/AmCl_3$-fraction: $SmCl_3$, $AmCl_3$, $SrCl_2$, and traces of CsCl
2*) $SrCl_2$/CsCl-fraction: $SrCl_2$, CsCl
3) $EuCl_3$-fraction: mainly $EuCl_3$, with very small impurities of CsCl and SrCl
4*) $NdCl_3$-fraction: $BaCl_2$, NdCl3
5) $PuCl_3$-fraction: $PrCl_3$, $CeCl_3$, $PuCl_3$, $LaCl_3$
*designated according to the largest proportion of the fraction present
**Separation accuracy: 1E-06
*** The choice of colors is intended to illustrate purely qualitatively the location of the respective substance component in relation to the temperature residence range of the component within the column: From dark blue with respect to cold temperatures in relation to the samarium trichloride light-boiling fraction to red toward hot temperatures of the plutonium trichloride heavy-boiling fraction. Medium-boiling fractions are illustrated in mixed colors in relation to the temperatures
**** Detailed results each chloride component are available in the comparison of SNF and HLW recovery in section (C.2) .

The separation results (Fig. (71), lower figure part) of the fractions in PPC 2 proceed under a slightly larger extended medium boiling fraction range of the europium trichloride fraction

separation curve in stages 4-23, in contrast to the separation range of stages 6-21 of the pure SNF separation example shown in Fig. (42) (for comparison). The cesium chloride fraction can be obtained by distillation as a light boiling fraction and the neodymium trichloride fraction as a heavy boiling fraction. The europium trichloride fraction remains highly contaminated as the last fraction in the column.

Finally, the simulation results show that mixtures from all feed examples can be separated with a reasonable separation effort. The separation effort increases only slightly and the number of separation stages does not need to be increased significantly for all CD columns. However, in the DC-2 column, the samarium trichloride fraction can only be separated together with larger americium trichloride fractions than in the distillation of the individual DFRm and SNF feed separation examples to be simulated.

C.2 Complete presentation of the simulation results for the total-reflux column in the conceptual design

This section shows the extension of the simulation results of the total reflux distillation column from all previously presented separate simulation results, which were previously grouped into single separation fraction by summing all components with similar separation behaviour and curves. In addition, omitted separation examples are shown, such as the extremely difficult distillation-based separation of neptunium tetrachloride from an $NpCl_4$-UCl_4 mixture as a separation option in a light boiling column of the SNF processing example.

C.2.1 Detailed simulation results for the distillation of SNF, HLW and DFRm feed materials

All the detailed mole fraction and temperature profile simulation results in this chapter for the separation in the total reflux distillation column with PPCs from the conceptual design chapter, such as those shown in Figs. (42),(60),(67), were originally grouped for components with the same separation curve behaviour and summarised as individual separation fractions for illustrative purposes.

Uranium tetrachloride - Neptunium tetrachloride purification First, the separation result for the DC-1 column in the SNF preparation for separating neptunium tetrachloride from uranium tetrachloride is shown with a required stage number of 32 separation stages according to Fig. (72)). Neptunium tetrachloride can be enriched to high purity under higher number of required separation stages with the separation specification of 1E-04-mol% of uranium tetrachloride impurities. A significant fraction of neptunium tetrachloride of about 0.1-mol% impurifies the heavy boiling uranium tetrachloride. Therefore, it is quite difficult to increase the separation accuracy for uranium tetrachloride distillation product. The temperature boiling range is relatively small in the range 1018-1068 K (see Fig. (72) right), so that many separation stages are needed for fine separation. The relative volatility of neptunium tetrachloride in relation to uranium tetrachloride is so similar and even small compared to other common actinide trichlorides that the approximation error in the determination of the substance composition of the thirty-second separation stage cannot be sharply resolved here using the Octave/Matlab code

for the total-reflux column in this single PPC of this distillation column. Since a mixture of uranium tetrachloride and neptunium tetrachloride still remains in the bottom, purification to pure uranium tetrachloride is even more difficult to realise in terms of separation technology, in which considerably more separation stages have to be practically used.

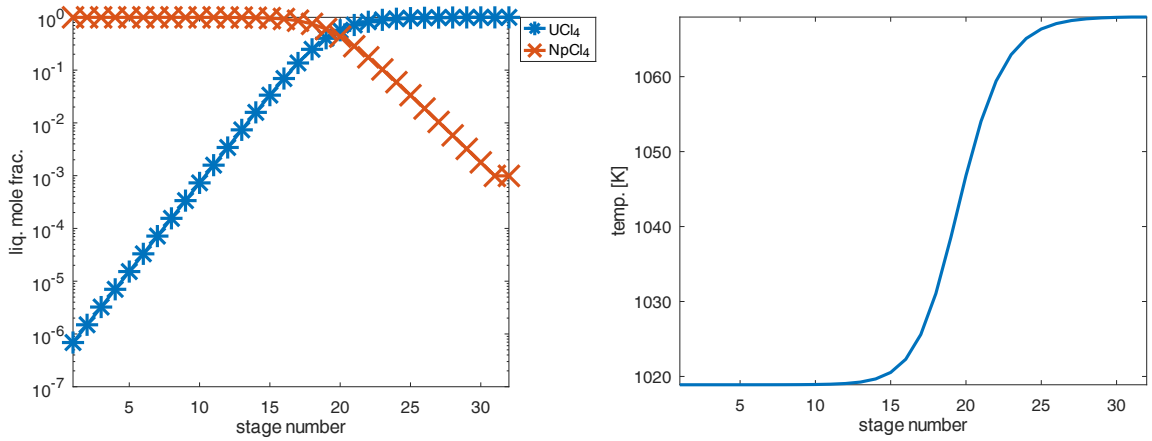

Figure 72: Detailed flow-chart simulation of SNF distillation: DC-1 results at 1 atm

DC 2 purification of SNF processing In the detailed results for the separation of the DC-2 column (see Fig. (73)) of the SNF processing, curium trichloride can be separated in the PPC 1 as a light boiler component together with very small proportions of samarium trichloride, so that according to Fig. (42) these separation curves were previously summarised as the samarium trichloride fraction in the simulation results. Subsequently, the strontium dichloride component dominates in stages 13-15. Therefore, in these stages the temperature profile takes the 'bulged shape' in Fig. (73) (first right). Then, from the fifteenth to the sixteenth separation stage, there is a temperature jump from about 1525 K to about 1900 K (according to Fig. (73) of the first and second separation operation). As this temperature jump is very large and leads to technical challenges in terms of material strength, the strategy could be to split the separation problem into two different separation operations or one separation in two subsequent separate distillation columns by setting either the 1525 K as the maximum evaporator temperature or the 1900 K as the minimum condenser temperature in the first separation. This will separate either the evaporator product or the condensate product of this first separation. The separation of this incompletely separated fraction is then carried out in the next separation step, effectively 'bypassing' the temperature jump. The proposed process is simulated in the subsection (C.2.2). A mixture of lanthanum trichloride, plutonium trichloride, cerium trichloride and praseodymium trichloride is distillatively concentrated as the heavy-boiling component in the final separation stage. These components are difficult to separate by distillation due to similar volatilities and pure boiling points, so these chlorides have been combined as the plutonium trichloride fraction as shown in Fig. (42). The temperature jump around the fifteenth separation stage of PPC 1 and PPC 2 is too large to be a potential problem for the column material strength. It is therefore necessary to split the column into two columns (see section (C.2.2)). At the beginning of the temperature jump in the first column, the evaporator temperature is practically set as the minimum temperature or, alternatively, the condenser temperature is set

as the maximum temperature for the first separation.

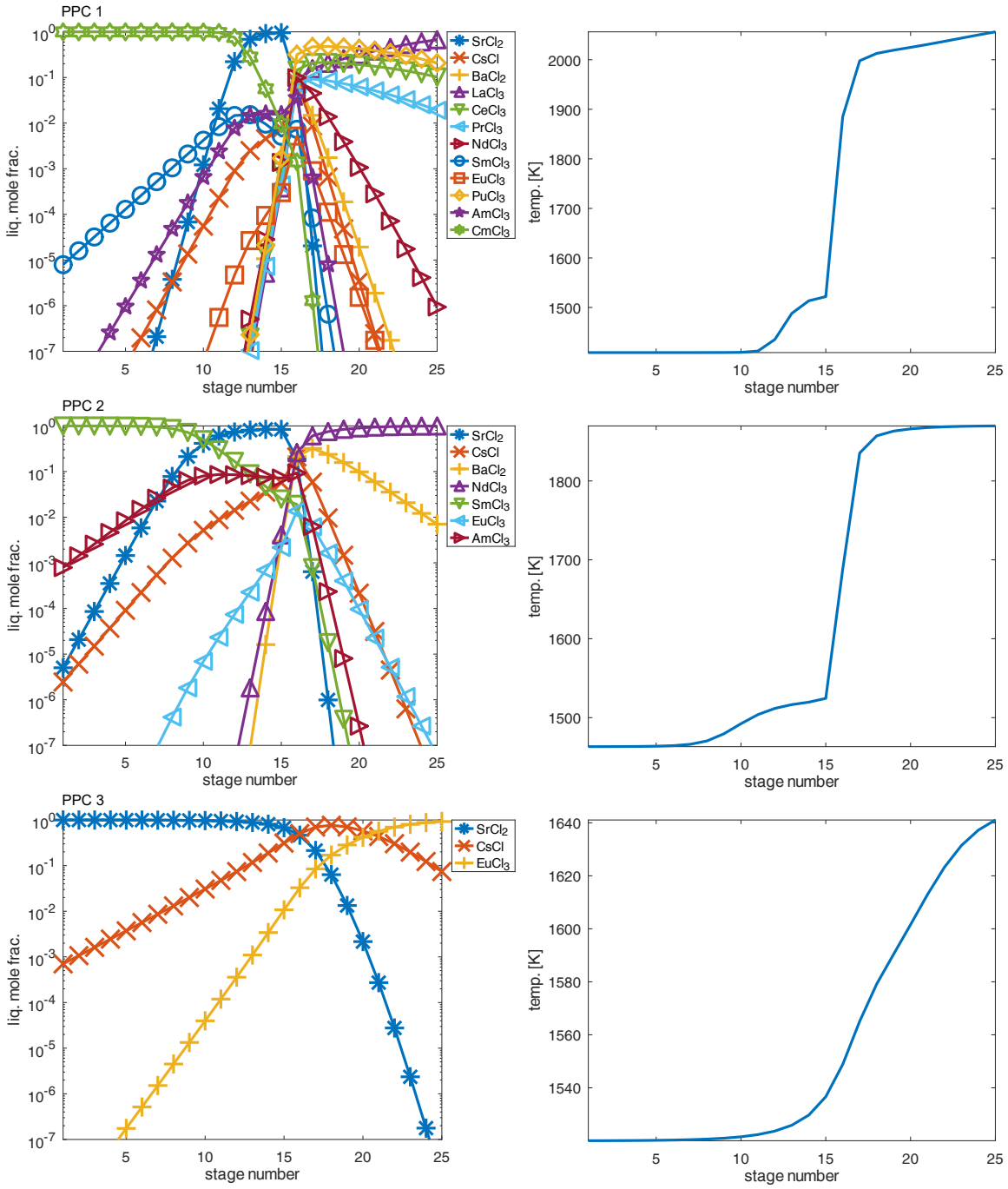

Figure 73: Detailed flow-chart simulation of SNF distillation: DC-2 results of PPC 1, PPC 2 & PPC 3 at 1 atm

DC 1 purification of HLW processing The simulation results for HLW processing in the DC 1 column with three PPCs are shown in Fig. (74)„ with respect to the molar composition on the left and the temperature profile on the right. In the DC 1 column of the HLW processing, high purity tellurium dichloride is obtained as a light boiler product in PPC 1 and high purity neodymium trichloride is also obtained as a high purity heavy boiler product with negligible impurities. The temperature curve shows a clear S-shaped temperature profile with

the temperature envelope of the 7-12 separation stage (ninth separation stage inflection point).

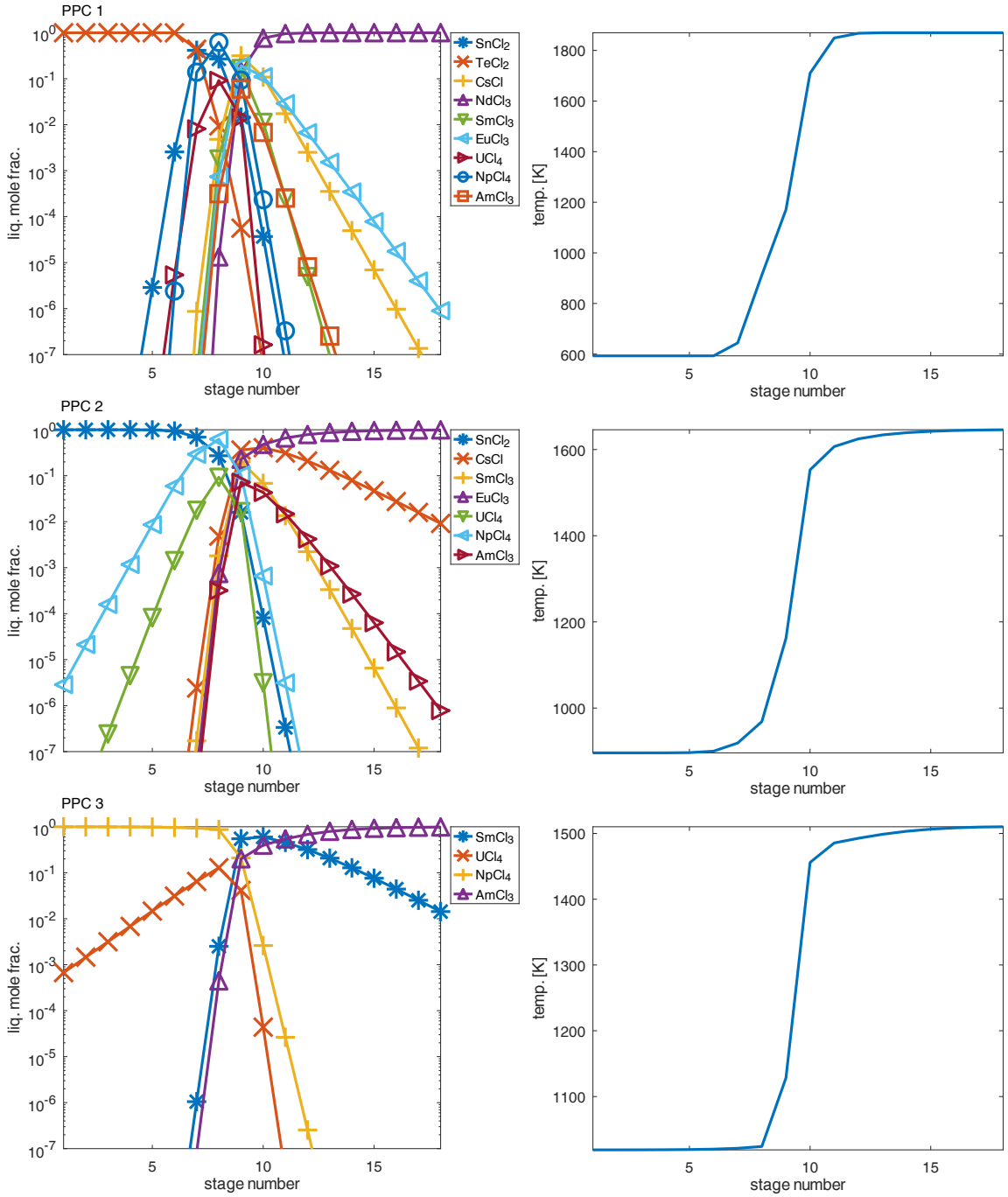

Figure 74: Detailed flow-chart simulation of HLW distillation: DC-1 results at 1 atm

In PPC 2 the low boiling product tin dichloride is slightly contaminated with neptunium tetrachloride. The heavy-boiling product, europium trichloride, is more heavily contaminated with cesium chloride. This means that no high purity distillation products can be obtained in the PPC 2 separation step, nor in PPC 3. In PPC 3, neptunium tetrachloride contaminated with uranium tetrachloride can then be obtained as a light boiler distillation product, and americium trichloride with a higher degree of impurity can correspondingly be obtained from samarium trichloride as a heavy boiler distillation product. As the PPC increases, the temperature range also decreases, with the temperature curve in the separation zones also changing slightly into the

visible separation stage range as shown in Fig. (74) (right). The temperature jump around the ninth stage is too large to be a potential problem for the column material strength. It is therefore necessary to split the column into two columns. At the beginning of the temperature jump in the first column, the evaporator temperature is practically set as the minimum temperature or, alternatively, the condenser temperature is set as the maximum temperature for the first separation (see section (C.2.2)).

DC 2 purification of HLW processing Two PPCs are required for separation in the DC-2 HLW distillation column. The detailed simulation results of the DC-2 column for HLW recycling are shown in Fig. (75). In PPC 1, the separation profiles of the curium trichloride and samarium trichloride fractions are obtained as light boiler fractions, with curium trichloride clearly dominating in the first separation stages.

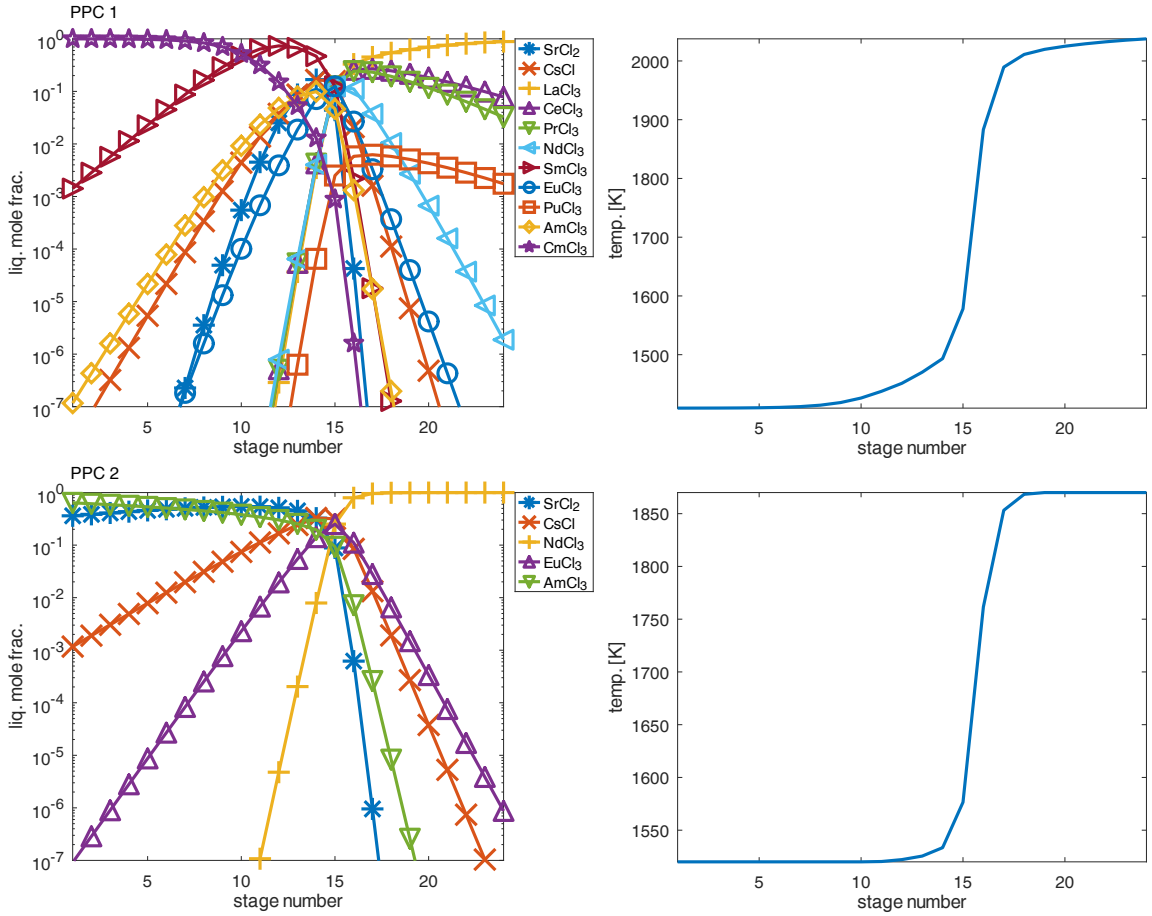

Figure 75: Detailed flow-chart simulation of HLW distillation: DC-2 results at 1 atm

The heavy boiler fraction consists of many components, summarised as the plutonium trichloride fraction with lanthanum trichloride, cerium trichloride, praesodym trichloride and plutonium trichloride. This composition will change over time until plutonium trichloride dominates as the heavy boiler distillation product, but is still contaminated with the other three distillation product co-components. However, the simulation results only show the total reflux condition point with the first higher fractions of lanthanum trichloride. In PPC 2, the americium trichloride fraction, consisting of americium trichloride, strontium dichloride and cesium chloride, is obtained

by distillation in the first separation stage as a light boiling product. Neodymium trichloride can be recovered as a high purity heavy boiling distillation product with negligible fractions of other chloride component impurities. In HLW recycling, the barium dichloride component does not exist, so that neodymium trichloride can be obtained as a high-purity substance component in the evaporator, the last separation stage of PPC 2 (in Fig. (75) (second figure on the left)). The residue obtained is a mixture of europium trichloride as the dominant component and any residual cesium chloride as the remaining intermediate boiler components.

The two temperature profiles shown in Fig. (75) (right) also show an almost abrupt rise in temperature from a certain separation stage, similar to the DC-1 column, but not as pronounced as for the DC-1 column. However, between the fifteenth and the sixteenth separation stage, the temperature rise is still abrupt with a temperature difference of 300 K, so that a division into two separation columns or columns should be carried out using the same strategy as for the DC-1 column in order to avoid the sudden high temperature jump inside the distillation column (see section (C.2.2)).

SC 2 purification of DFRm processing For the DFRm feed processing of the DC-2 column, the detailed simulation results are shown in Fig. (76). In this simulation example, only one PPC process step is required for this separation example. In this, chromium dichloride (which is assumed to be thermally stable) and cesium chloride can be recovered together as the light boiler fraction, while plutonium trichloride is obtained together with lanthanum trichloride, cerium trichloride and praseodymium trichloride as the heavy boiler fraction of the final separation stage. Neodymium trichloride then remains as the only medium boiling component in this distillation column.

Between the fifth and seventh separation stage a rapid temperature increase can be observed (see Fig. (76) (right)). This temperature rise may be too high for the structural column material, so that it may be necessary to use two different columns (see section (C.2.2)).

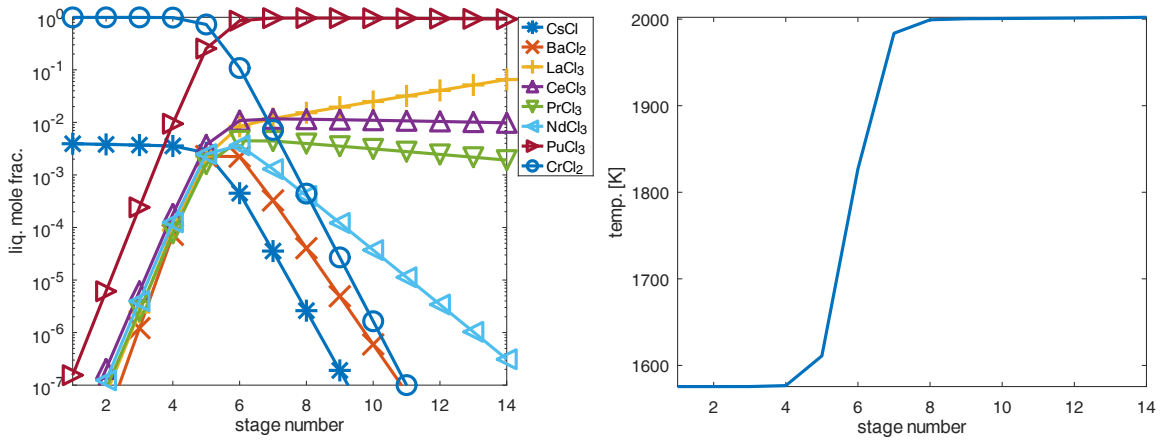

Figure 76: Detailed flow-chart simulation of DFRm distillation: DC-2 results at 1 atm

DC 2 purification for the mixed feed example In the separation of the fully chlorinated mixed SNF, HLW and DFRm feed example according to Fig. (77), it becomes clear in the simulation of the DC-2 column distillation, as already discussed in section (C.1.4), that more

separation stages are required, since in particular chromium dichloride and caesium chloride with high medium-boiling fractions increase the separation problem towards an unfavourable separation range. The comparison of the temperature profiles for SNF recycling according to Fig. (73) and for DFRm feed processing according to Fig.(76) shows for the light-boiling component that the temperature of the first separation stage lies between the boiling points of the light-boiling components of both separation cases. The condenser temperature is just above 1400 K for SNF processing and just below 1600 K for DFRm feed recovery. This is due to the fact that the temperature of the first separation stage is between the boiling points of the light boiling components of both PPCs. In addition, there is the effect of the dominant strontium dichloride component in the temperature profile of the SNF recovery, which is also weakly visible between stages 13-15 in the mixed case according to Fig. (77) for the first separation operation and also slightly increases the range of the separation curves of the medium boiling components.

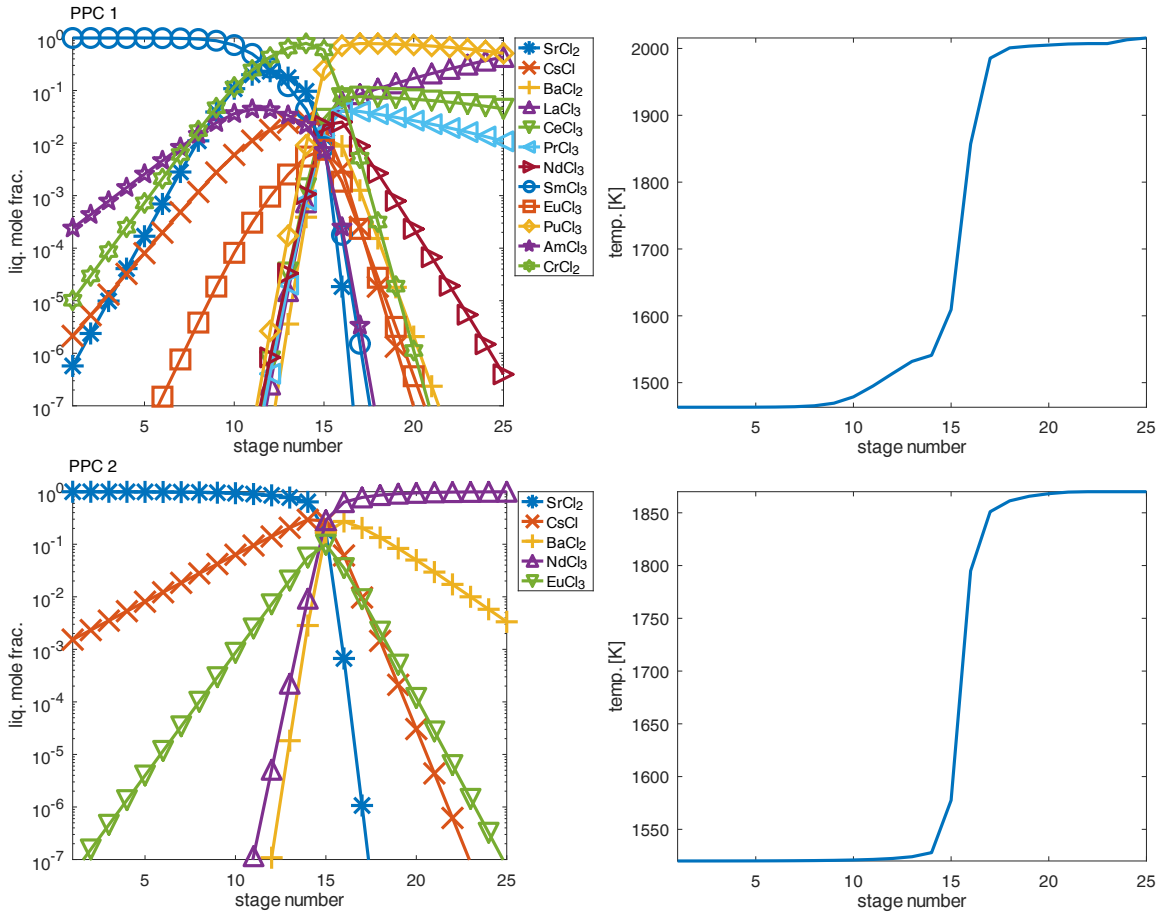

Figure 77: Detailed flow-chart simulation of distillation with mixed SNF, HLW and DFRm case of section (C.1.4): DC-2 results at 1 atm

As can be clearly seen in PPC 1 in Fig. (77), more contaminating components are present in the light-boiling component strontium dichloride fraction in separation stages 1-4 than in the consideration of the individual SNF and DFRm feed examples. On the other hand, the HLW fraction is negligibly small and plays only a minor role in the considered feed mixture. As a heavy boiler distillation product, a mixture of plutonium trichloride, lanthanum trichloride, cerium trichloride and praseodymium trichloride together with slightly negligible neodymium

trichloride impurities can be obtained in the last separation stage. In PPC 2, strontium dichloride contaminated with cesium chloride is distilled as a light boiler product, while neodymium trichloride contaminated with barium dichloride is obtained as a heavy boiler product. All details on the separation and temperature profiles can be taken from Fig. (77), analogous to the other pure SNF, HLW or DFRm feed material examples.

What should also be noted for both PPCs is the temperature jump from the fifteenth separation stage onwards: Here, it is probably necessary to separate the separation problem at this separation stage into two different separation columns in order not to stress the structural column material too much by the high temperature gradient in the column height direction. This strategy is more explained in the following section (section (C.2.2)) for a single representative separation example.

C.2.2 Strategies to avoid large temperature changes inside a total-reflux distillation column

As already shown in the temperature profiles of the simulation results under idealized phase equilibrium conditions according to Fig. (76), as well as in Fig. (73),(74) and (75), there are often abruptly increasing temperature changes between the separation stages when the composition of the mixture changes significantly between light and heavier boiling material components. Due to the high stress on the column material, the temperature gradient along the column height between these separation stages should not be too large. Therefore, temperature differences of more than 250 K between two or three separation stages should be definitely avoided. To achieve this, the separation is divided into two separation operations, either repeated in the same separation column in different separation operations or in a further secondary separate separation column. However, the following process steps are mandatory to avoid such pronounced temperature profiles:

1. Distillative separation in a separation column before the mentioned temperature difference or after (related to the separation stage number of the column) in two possible process options:

   - **Separation before the temperature change**: The light-boiler related separation concerns the high-purity separation of the light-boiler components and a mixed fraction is obtained as evaporator product, which must be further separated by distillation at higher temperatures in the second separation operation of the same column or other separate total reflux column.
   - **Separation after the temperature change**: The heavy-boiler separation refers to the high-purity separation of the heavy-boiler components and separation of a light-boiler mixed fraction, which must be further separated by distillation at lower temperatures in the second separation operation of the same column or other separate total reflux column.

2. In the second separation operation in the same separation column or in a further separation column, the corresponding mixed fraction which has not yet been separated to a high degree

of impurity is purified by distillation. The residual components are returned to the first separation operation or separation column.

For this purpose, the choice of light-boiler or heavy-boiler separation for the first separation process is based on strategic separation criteria and/or physical-thermochemical properties of the feed composition. Using the DFRm feed example from the previous section according to Fig. (75), it is shown by simulation that the component separation can be implemented without large temperature gradients by bypassing the necessary temperature jump in the column height somehow.

The general simulation result for distillative DFRm recycling without bypassing a temperature jump has already been discussed in detail in Fig. (75) in a total-reflux column under usual idealized phase equilibrium conditions. According to Fig. (75) (right figure), the temperature jump can be seen in the temperature profile between the fifth and seventh separation stages, which is greater than 300 K. The magnitude of the temperature change between these separation columns within the column must be significantly reduced in the path of the split in the two separation operations. For this purpose, the application of the fine separation of light boilers in the first separation operation is strategically chosen as suitable option in order to enrich the chromium dichloride- caesium chloride mixture as early as possible equimolar related to light and heavy boilers in the condenser (see heuristics for distillation in [72, 73]). The separation of the chloride components (assumed to be thermal stable as simplification) is otherwise carried out as usual with the corresponding separation operations in two process steps of a total-reflux enrichment and a subsequent product removal.

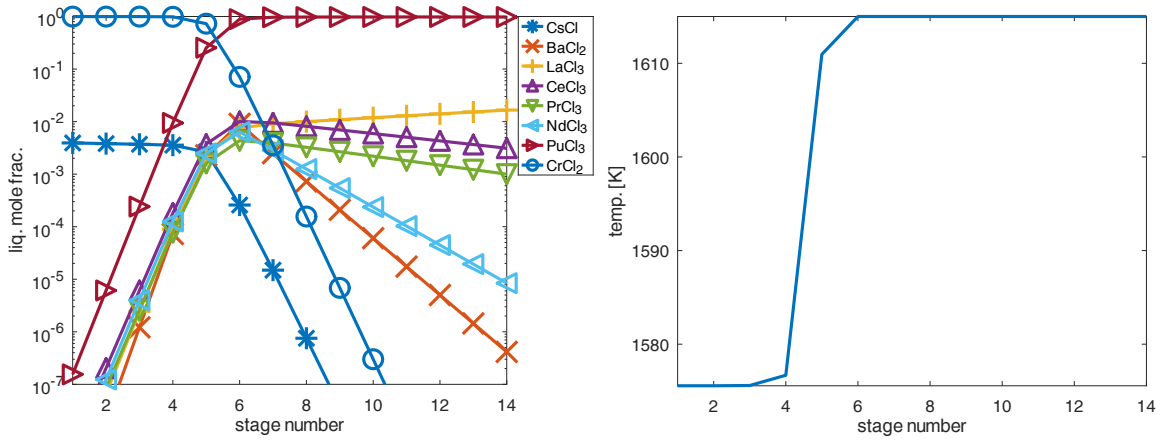

Figure 78: Detailed flow-chart simulation of the first modified DFRm distillation column: DC-2 results without hard temperature changes inside the column at 1 atm

The simulation results for the first separation with the same number of separation stages are shown in Fig. (78). Compared to the results in Fig. (76), the bottom product is now slightly more contaminated with neodymium trichloride in the first separation. In order to be able to separate neodymium trichloride from the plutonium trichloride fraction, the purification of the evaporator distillation product as a mixed heavy boiler fraction has to be carried out in a second separation process or in a separate separation column. Compared to the results in a single separation column shown in Fig. (76), the separation curves are otherwise analogous, except for

the weaker separation efficiency of the neodymium trichloride separation. The temperature jump has been significantly reduced in the context of the magnitude of the temperature difference and is now only 40 K instead of 300 K as before (see: Fig. (76) (right)). Due to the lower operating temperatures according to the simulation results in Fig. (76), the slope of the neodymium trichloride separation curve for the depletion between the seventh and fourteenth separation stage is also significantly reduced compared to the general results without temperature jump, so that higher impurities of neodymium trichloride are present at this first separation operating point.

In the case of high-purity separation (separation specification below 1E-04-mol% for the distillation product impurities) of the heavy-boiling fraction consisting of plutonium trichloride, lanthanum trichloride, cerium trichloride and praesodymium trichloride, this mixture is to be preferred first in the further separation operation as the option chosen here in the same separation column with the same number of stages.

In the application of this second separation operation for the purification of the bottom distillation product, the high purity separation of neodymium trichloride is aimed at in the same separation column with the same number of separation stages and after the complete removal of the other distillation products from the first separation operation. The simulation results are shown in Fig. (79). In this version, neodymium trichloride can be depleted very well in the liquid phase with increasing number of separation stages and with smooth temperature change of each column stage in total between 1870-2000 K. Towards the condenser, the mole fraction value of neodymium trichloride increases, while the mole fraction values of plutonium trichloride and lanthanum trichloride decrease slightly, but are always present in the mixture. The proportions of cerium trichloride and praseodymium trichloride remain almost in the same size of mole fraction values. This means that a composition with neodymium trichloride (but also depending on the other component) is obtained at the condenser. If possible, a column design with many more separation stages and a different temperature range than in Fig. (79), but in another separate total reflux column, would be necessary to obtain neodymium trichloride as a light boiling product by high purity distillation in the condenser here in the second operation.

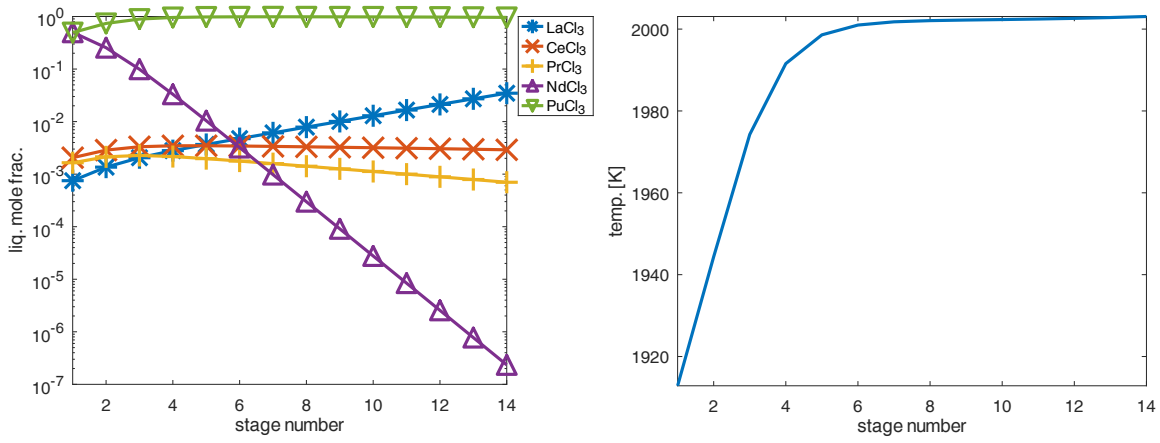

Figure 79: Detailed flow-chart simulation of the second modified DFRm distillation into the same column with the same number of separation stages: DC-2 results without hard temperature changes inside the column at 1 atm

The simulation results in Fig. (80) show the simulation results in a separate total reflux column with up to twenty-eight separation stages with a condensation temperature between 1870-1880 K. The temperature profile inside the column is also much smoother, between the temperature range of 1870-2000 K. Due to the higher number of separation stages, the temperature change between neighbouring separation stages is much smaller. When a stage temperature above 1900 K is reached with increasing separation stages, a significant depletion of the neodymium trichloride components can be observed from the fifteenth separation stage upwards towards the condenser (directly above the first separation stage), as could also be seen from the previous simulation results of the same distillation column as a second separation option. Neodymium trichloride can again be recovered as a light boiling product, but now in high purity in the first separation stage with negligible plutonium trichloride impurity below 1E-04 mol%. The remaining heavy-boiling chlorides are also recovered in the final separation stage as high purity distillation products with negligible impurity of neodymium trichloride impurity below 1E-04 mol%. The separation objective is therefore achieved for this selected separation option of two different columns.

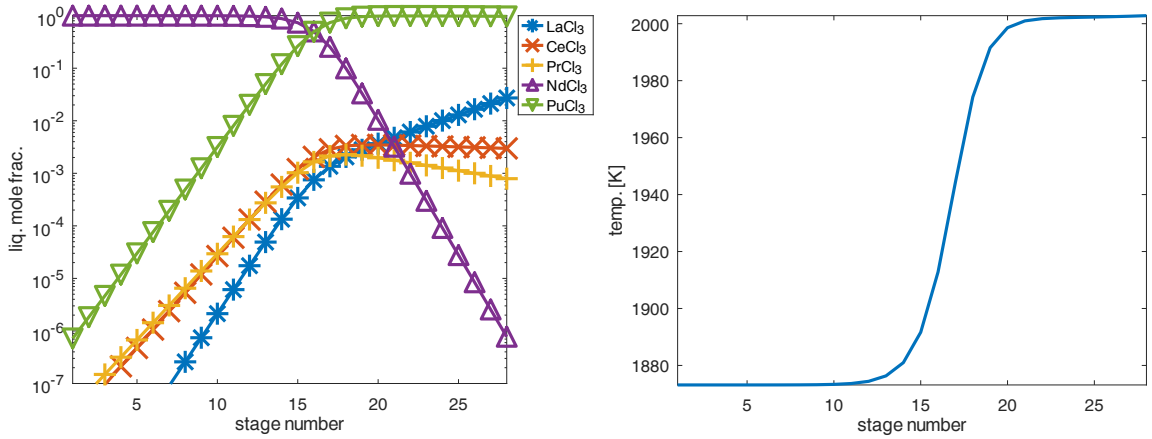

Figure 80: Detailed flow-chart simulation of the second modified DFRm distillation into another distillation column with more separation stages compared to the first column: DC-2 results without hard temperature changes inside the column at 1 atm

Simulations have shown that separation by two columns to avoid a strong temperature gradient inside a single column can be used to avoid significant temperature changes between a few adjacent separation stages, which would occur in a single operation in a single distillation column. Accordingly, an additional separation operation is required for each temperature jump. However, separation in the same column with the same number of stages means that in the second separation operation, if required, both distillation products cannot be obtained by high purity distillation in the condenser or evaporator. This means that the second top distillation product would have to be fed back to the first column, increasing the complexity of the separation handling. Therefore, it may be easier to choose the second option of having the second separation column outside as a simple serially connected separate distillation column to obtain two high purity distillation products at the top and bottom of the column.

In the case of non-ideal phase equilibrium behaviour and in the presence of azeotropes, it should also be noted that separation via the azeotrope still has to be carried out in pressure

swing column operation or other azeotropic separation options using chemical additives. Here, the problem of preventing significant temperature changes within the column could be integrated with the separation problem of azeotropic separation, if possible.

D Supplement: Extended simulation and estimation for the distillation of test mixtures

In this section, advanced simulations of test mixtures are performed to estimate the influence of decay heat under idealized phase equilibria and to estimate the deviation using Margules activity approximations compared to idealized phase equilibrium conditions (compare the basic VLE equations (27) and (28)). Secondly, the influence of decay heat accumulation within the column is roughly estimated, but under idealized phase equilibrium conditions (see: idealized VLE equation (28)) with a selection of few active isotope elements.

D.1 Simulations of UCl_4–MCl_n mixtures using purely hypothetical estimated VLE data

In this section, examples of feed test $UCl_4 - MCl_n, n = 1, \ldots, 4$ mixtures have been used for possible more realistic simulation of distillation columns using estimated VLE Margules data from the section (3.2), simplified from the data [11, 10, 9] of simplified non-evaporating molten salts and solid-liquid equilibrium data. Assumptions and simplifications for the determination can also be found in the section (3.2). All of the above VLE Margules estimates required for the more realistic distillation column simulation are used to estimate the activity coefficients using a polynomial approach. But, this simplified approach is purely illustrative of the phase equilibrium behaviour of certain binary chloride-based mixtures as they might occur and behave in reality. Nevertheless, the estimation with Margules from these poor GE literature data is still very rough, even though these GE data are additionally simplified for low temperature molten salt mixtures in the melting point region and not for VLEs. Therefore, the following results are really hypothetical and are only shown here to illustrate how the activity differs from the idealized case of $\gamma_i = 1$. To validate the VLE data, experimental measurements of VLEs would have to be made at least at the key composition points of the GE data from the literature. Unfortunately, these validation data are not available for the thesis and the results here are purely hypothetical and are only useful to describe if an azeotrope could form and if there is a great potential of high non-ideal deviation from the idealized phase equilibrium condition due to equation (28) with $\gamma_i = 1$. Using these representative simulation results presented below, deviations from Raoult's law could be discussed as to how large a possible deviation could be for the simulation results of various separation units to be simulated, especially for the DC columns in the conceptual design as shown in section (6.1) for the SNF recovery problem. This potentially deviating separation behaviour as a consequence of the non-ideal VLE behaviour of the binary substance system cases investigated here is qualitatively transferable to possible other complex substance systems and qualitatively comparable with regard to existing similarities of the degree of chlorination of each

chloride component in the mixture to the other chlorides and their degree of chlorination .[7]

The following simulation results using Margule's real estimated activity coefficient data according to section (3.2) are performed for different distillation column types of conceptual total reflux columns with a single PPC and continuous distillation columns with finite reflux ratios. A feed flow rate of 0.1 mol/s is used exemplarily. Here the feed composition is centred at $x_1 = 0.5$ for zeotropic mixtures and at the centre of the distillation range for azeotropic mixtures, with the interval limits of the achievable distillation limit compositions that can be obtained using a conventional distillation column. The following simplifications are made for the simulation. In the condenser, the mixture is assumed to condense only at the boiling temperature of the mixture, without supercooling the melt in the model. The separation purity of the distillation products as pure components must be 99.9999 mol%. Furthermore, all simplifications of the binary mixture models from section (4.4) of chapter (III) are used for further simulations. Therefore, all simulations performed with the Octave/Matlab model code will be referred to as "OML" and simulations performed with ChemSep will be referred to as "CSL". In ChemSep, the activity coefficients are given in the main ChemSep file under "thermodynamics"→"K-value:Gamma-Phi" and "Activity coefficient:Margules" with specification of the parameter values. The following conventions, labelled A, B and C, can be used to classify the type of approximate VLE estimated by the Margules approach from different methods of data preparation of these literature data.:

- A: Direct linear interpolation from the given experimental activity data with the equation (79),
- B: Approximated Margules functions by fitting to the x_1, γ_1 literature given data points, e.g. from Tab. (8) for binary mixtures of uranium tetrachloride with manganese dichloride or lanthanum trichloride,
- C: Approximated Margules functions from two given G^E-data points given in [11],
- D: Evaluation of idealized phase equilibria with $\gamma_i = 1$.

The following binary chloride substance systems are simulated and compared with the approximation approaches to the Margules approaches A-D below:

- UCl_4-$MnCl_2$ and UCl_4-$LaCl_3$ mixtures in a total reflux column at constant pressure of 1 atm with the VLE approximations from methods A, B and C,
- UCl_4-$ThCl_4$ and UCl_4-$CdCl_2$ in a total-reflux column at constant pressure of 1 atm (only for approximation method C),
- UCl_4-LiCl mixture to illustrate the results of an azeotropic VLE behaviour in a total reflux column at constant pressure of exemplary 0.1 bar,

[7] In the design of a distillation plant for the distillative reprocessing of spent nuclear fuel by means of simulations of ideal phase equilibria, qualitatively different statements can be estimated as a function of the degree of chlorination and, in part, also of the ion radii and ion potential ratios of the material components involved. However, qualitative assessments of the separation plant under rather pessimistically estimated real phase equilibrium behaviour with the Margules approach of the chloride components are also applicable here, in order to illustrate, with minor modifications of the separation design, that this separation concept is technically feasible in this designed form (see section (6.1) on the conceptual design of spent fuel reprocessing).

- Differences in the simulation of a finite reflux distillation column for a zeotropic mixture with an azeotropic mixture, representative of the mixture UCl_4-$CdCl_2$ at 1 atm compared to the mixture UCl_4-LiCl at 0.1 bar (with constant assumed column system pressures inside the distillation columns).

D.1.1 Deviations in total-reflux distillation column simulations between idealized and Margules approximated vapor-liquid equilibria

First, the simulation results for the mixtures UCl_4-$MnCl_2$ and UCl_4-$LaCl_3$ are examined by comparing the VLE approximation methods A, B and C via the Octave/Matlab model (OML). For the interpolative VLE approximation method A, only the validity range of the tabulated data given in Tab. (8), since beyond that only a very rough interpolative equilibrium line equation (79) can be evaluated. The results for the simulation of the mixtures UCl_4-$MnCl_2$ and UCl_4-$LaCl_3$ in a total reflux column at 1 atm are shown in Fig. (81) for a given product composition mole fraction separation accuracy of 99.9999 mol% of uranium tetrachloride.

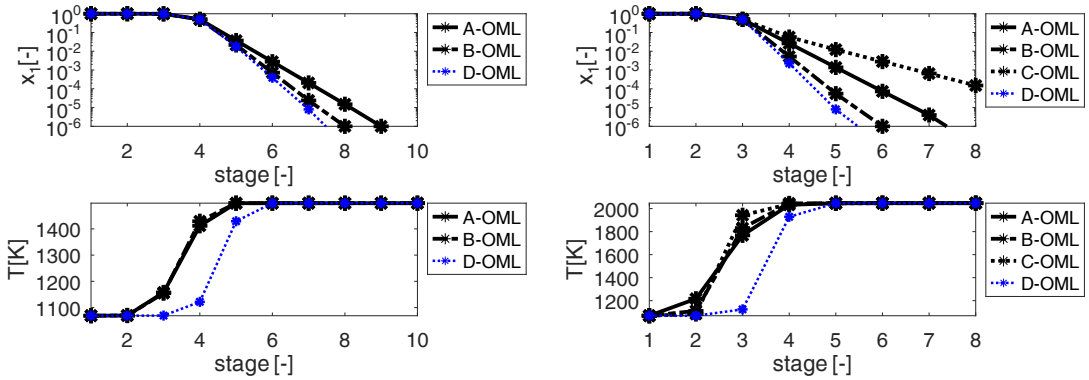

(a) Composition of UCl_4 for the UCl_4-$MnCl_2$-system(b) Composition of UCl_4 for the UCl_4-$LaCl_3$-system

Figure 81: Simulation of a total-reflux column using different VLE approximation methods and Octave/Matlab (OML) simulation model for the mixtures (a) UCl_4-$MnCl_2$ and (b) UCl_4-$LaCl_3$ at 1 atm

In the logarithmic plot of the simulation results in Fig. (81) on the y-axis, it can be observed that from the fourth separation stage for the manganese dichloride mixture example and from the third separation stage for the lanthanum trichloride case, the composition curves could be approximated by linear equations, depending only on the slope of the VLE approximation. The Margules approximation from tabulated VLE data is closest to the ideal composition curve of case D for each simulation example. The linear interpolation to the pure substances by a straight line equation of equilibrium results in a larger deviation of the simulation results between the interpolation mode according to case A and the Margules approximation according to case B for the VLE approximation. Only case C in the Margules approximation in the lanthanum trichloride example from two given G^E estimated data points leads the simulation result of the total reflux distillation column to a significantly larger deviation behaviour where the highest separation rate of all VLE approximation cases A, B, C and D is required to reach the separation value of 1E-04-mol% at the bottom of the column with respect to uranium tetrachloride. Due

to the small number of only two literature-given data points in [11] at only -50 mol% and 90 mol% of uranium tetrachloride, a narrower approximated VLE follows for uranium tetrachloride values, especially for small molar composition values. Here, the approximation accuracy of the VLEs is also particularly weak in relation to the missing activity relationship data between 0 and 50 mol% uranium tetrachloride in the mixture.

In terms of the total number of separation stages, in the case of the manganese dichloride separation example, the required number of separation stages is estimated to 4-7 under ideal phase equilibrium behaviour and 8-9 according to the VLE approximation method B. For the lanthanum trichloride mixture example, the variation of the required number of stages is larger due to larger deviations of cases A and B with respect to the VLE data compared to the manganese dichloride example. Case C in the lanthanum trichloride example, on the other hand, is significantly more deviant in the number of separation stages required, up to 12-13 total separation stages required. Ignoring case C, the number of separation stages required in the lanthanum trichloride example is between 5-8 under ideal phase equilibrium condition behaviour and 4-7 according to VLE approximation method B. With regard to the distillation of the substance mixture UCl_4-$MnCl_2$ within a total reflux column, it can be said that the simulated separation behaviour via the use of real-approximated VLEs differs only slightly from the ideal behaviour , apart from the temperature profile, despite the deviations mentioned in the less accurate interpolatively determined VLE approximation method according to case A. The temperature profiles of both exemplary shown simulated substance mixtures of uranium tetrachloride with manganese dichloride and lanthanum trichloride differ only slightly from the ideal behaviour . Secondly, the estimated temperature under the idealized phase equilibrium case is estimated to be lower compared to the real estimated VLE conditions for both mixture systems. In contrast, for the other cases of using real approximated VLEs, the deviations of the temperature curves are rather relatively small, as can be seen in the lower part of the Fig. (81). As a consequence, it can be simplified deduced that simulations with ideal phase equilibria of the type UCl_4-MCl_2, UCl_4-MCl_3 (with M for metals or transition metals, for example, further rare earths such as neodymium or plutonium up to transplutonium elements such as americium) are quite applicable for subsequent simulations in the conceptual design and the real VLE behaviour does not play a major role.

In the next simulation example of the simulation results of Fig. (82) (upper subfigure) show the separation behaviour of the mixtures UCl_4-$ThCl_4$ and UCl_4-$CdCl_2$. Fig. (82) (lower subfigure) shows the difference between the idealized and the Margules approximation results. Compared to the binary mixtures of uranium tetrachloride with manganese dichloride or lanthanum trichloride, the deviation behaviour between the ideally calculated and the actually approximated phase equilibrium according to evaluation method C is significantly more deviating with a difference of the required separation stages between 14 to 15-30 for the cadmium dichloride mixture and 15-23 for the thorium tetrachloride mixture example. Thus, in the VLE approximated by Margules, the mole fraction value of thorium tetrachloride decreases only slightly with a simultaneously higher boiling temperature compared to the ideal case as the shown number of separation stages increases (compare Fig. (82) (both mixture results). A similar observation can be made for the cadmium dichloride separation example. Although the simulation results of both mixture

examples behave zeotropically, the deviation behaviour between the ideal phase equilibrium behaviour and the real Margules approximated equilibrium according to approximation method C is relatively large. This result could be predicted, for example, in the conceptual design relevant mixture for the separation of $NpCl_4$ from UCl_4 according to section (6.1) with the same chlorination degree of the chlorides involved in the system UCl_4 - $ThCl_4$. Qualitative-heuristically, it can be determined that the number of stages from the ideal phase equilibrium calculations would have to be doubled for a realistic assessment of distillability, assuming that similar non-ideal behaviour would result for the mixture $NpCl_4$-UCl_4 (with neptunium tetrachloride as the low-boiling component) compared to the mixture UCl_4-$ThCl_4$.

Furthermore, the simulation results for the UCl_4-$CdCl_2$ mixture show that the OML and CSL models lead to the same simulation results, with negligible deviations between the two models used. This also shows the validity of the Octave/Matlab model, especially for simulations with binary mixtures, and its excellent applicability for the simulative description of real VLE approaches. In the following, further simulation examples will show that this agreement of simulation results leads to the same simulation results when either the ChemSep or the Octave/Matlab simulation code is used. Thus, it can be excluded that this is not a statistical coincidence that both models lead to the same simulation results.

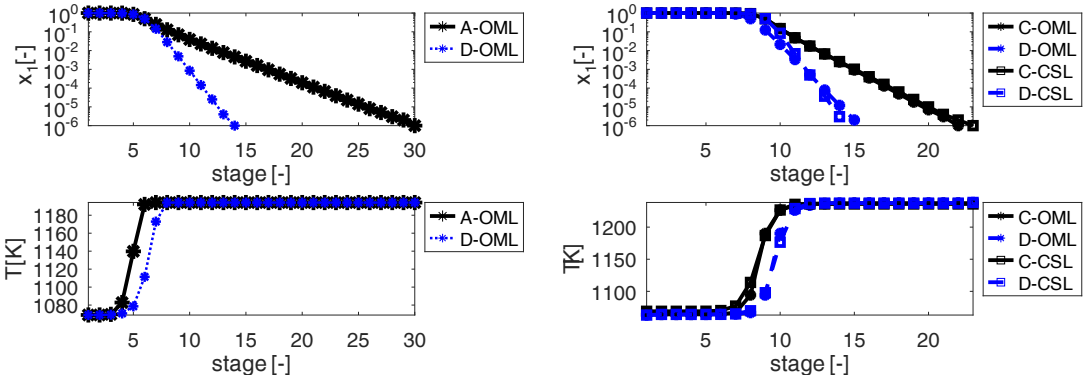

(a) UCl_4-$ThCl_4$ (b) UCl_4-$CdCl_2$

Figure 82: Simulation of a total-reflux column using different VLE approximation methods and simulation models with Octave/Matlab (OML) and ChemSep (CSL) for the mixtures (a) UCl_4-$ThCl_4$ and (b) UCl_4-$CdCl_2$ at 1 atm

For an azeotropically determined binary mixture of uranium tetrachloride and a monochloride, the example mixture UCl_4-LiCl is simulated at 0.1 bar operating pressure. As in this simulation example, the simulation results shown in Fig. (83) are so similar between the solution of the Octave model and the ChemSep model that no deviations can be detected. Thus, both simulation models lead to the same results, so that the Octave Model (OML) is also excellently suited for the simulation of binary zeotropic and azeotropic mixtures.

The details of the simulation results of the right side of the temperature-maximum azeotropic composition Fig. (83) (upper subfigure) and the left side Fig. (83) (lower subfigure) a suitable azeotropic separation behaviour can be seen with the separation of the light boiling uranium tetrachloride or light boiling lithium chloride component in two different distillation regions with respect to the initial feed composition positioning for a typically expected azeotropic binary

mixture (at least two distillation columns are required for azeotropic separation). For the right side of the distillation range from the azeotrope composition, the simulation results show a very high purity enrichment of uranium tetrachloride in the real approximated case according to evaluation method C.

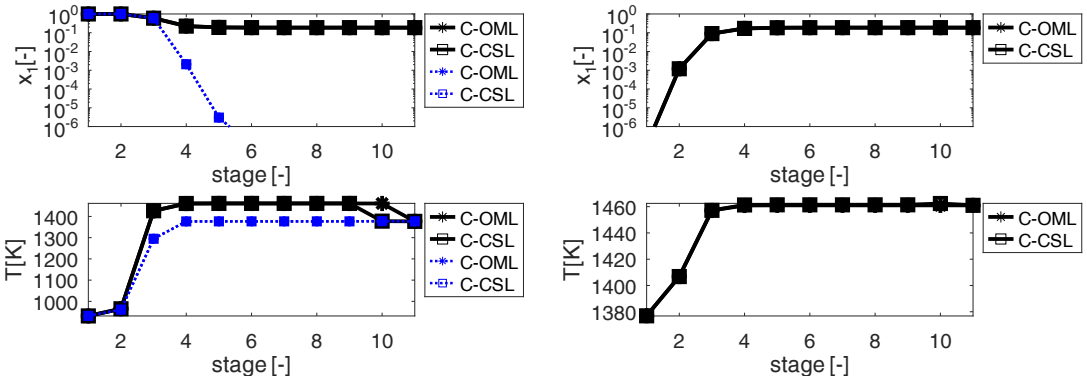

(a) UCl_4-LiCl for $x_1 > x_1^{az}$:
right side from the azeotropic composition

(b) UCl_4-LiCl for $x_1 < x_1^{az}$:
left side from the azeotropic composition

Figure 83: Simulation of a total-reflux column using different VLE approximation methods and simulation models with Octave/Matlab (OML) and ChemSep (CSL) for the azeotropic mixture UCl_4-LiCl at 0.1 bar

From the right side of the azeotropic composition, with only 5-6 stages required instead of 10-11, uranium tetrachloride is separable at 0.1 bar system pressure as a light boiling distillation product, while the azeotropic composition is reached at higher temperatures in the bottom of the column as a simplified assumed bottom distillation product pseudocomponent. The azeotropic composition of uranium tetrachloride is about 22.5-23 mol%, depending on the simulation model selected, between the OML and the CSL model, despite the surprising similarity of the simulation results between the simulation models selected. This separation behaviour is characteristic as the azeotropic composition is the limiting composition in distillation, so that this distillation barrier cannot be overcome by normal distillation. The simulation of the other distillation regions for the Margules approximated VLE, left of the azeotrope with lower uranium tetrachloride mole fraction values than the azeotropic composition, shows the high purity enrichment of lithium chloride as the light boiler component and again the azeotropic composition as the heavy boiler distillation product at the bottom of the total reflux column. The temperature profile follows the temperature maximum to the azeotropic composition to the bottom distillation product in both distillation regions (see: Fig. (83) for both distillation regions). All other details of the simulation result profiles can be seen in Fig. (83). [8]

The simulation result of the idealized assumed phase equilibrium behaviour shows a completely different separation behaviour , in which in a single distillation column only uranium

[8] Azeotropic composition pseudocomponent modelling of simulation of distillation columns: As an alternative to the simulation modelling idea, this azeotropic mixture could also be modelled as a kind of pseudo-boiling component for the azeotropic composition in a binary zeotropic substance system UCl_4-Az(UCl_4(az)-LiCl(az)) mixture, in which the composition of uranium tetrachloride and the azeotropic pseudo-component could be set for each separation stage in relation to the excess lithium chloride compared to the azeotropic composition case here.

tetrachloride can be obtained as light distillation product and lithium chloride as heavy distillation product in a net single distillation column with only 5-6 required separation stages, as can be seen in the results of Fig. (83) for the results marked by the blue dotted line. The maximum temperature interval in the ideal phase equilibrium behaviour ranges from the minimum boiling point of uranium tetrachloride to the maximum boiling point of lithium chloride, as shown by its S-shaped temperature profile.

Two different strategies are recommended to practically bypass the azeotropic composition point. The easiest way to reach the left distillation range of the azeotrope would be to add pure lithium chloride to the distilled bottom product, which is compositionally close to the azeotropic composition. The other chloride component would then be separated in a second distillation column under the same system pressure as a high purity light boiling distillation product. The heavy boiling azeotropic composition would be obtained again as heavy boiler distillation product, which would have to be fed back to the first distillation column. Alternatively, if this azeotropic composition point is significant enough and pressure dependent enough, separation by pressure swing methods between two used distillation columns can be used. Unfortunately, this cannot be investigated within the scope of these simulations, as pressure independence is already included as a simplifying model assumption of the Margules approximation.

D.1.2 Simulation of different continuous column operating modes from total-reflux through finite-reflux ratios

The deviation from total-reflux column operation via finite reflux ratios changes the column operation either via discontinuous distillation modification by obtaining distillation fractions separated in time or the setting as a continuous distillation column with a stationary feed at a fixed feed position and stationary compositions of the column stages within the distillation column. Using the estimated VLE data according to section (3.2), a clear summary of the main simulation results for the binary salt mixtures of uranium tetrachloride with cadmium dichloride and lithium chloride is presented.

Fig. (84) shows the simulation results with an optimised finite reflux ratio for which the number of separation stages becomes minimal. In the case study with cadmium dichloride, this reflux ratio is 21.188 and for lithium chloride 1.132 for mixtures with uranium tetrachloride, depending on the purely hypothetically estimated Margules VLE (Case C, defined for the last subsection). As can also be seen here, the very good agreement of both modelling variants of the Octave Model (OML) and the ChemSep Model (CSL) is clearly visible for both case studies with cadmium dichloride and lithium chloride in the case of total and finite reflux column operation (see simulation results of total reflux column in Figs. (82) (lower subfigure) for the UCl_4-$CdCl_2$ system at 1 atm and (83) for the UCl_4-LiCl system, and of finite reflux column for both substance systems in Fig. (84) with $v = 21,188$). However, the deviations in the cadmium dichloride case in temperature and composition, between ideal and estimated vapour-liquid behaviour , show a much larger deviation behaviour between the simulation results, especially for the azeotropic mixture case with lithium chloride at 0.1 bar, but also for the total reflux to finite reflux behaviour , as shown in the simulation results in Figs. (82) (upper figure) and the finite reflux operating case shown in Fig. (84) (upper figure) for continuous steady-state distillation column operation

and the set reflux ratios. This illustrates that the influence of the vapour-liquid behaviour has a much stronger effect in the simulations due to the additional mass and energy balance in the continuous case than in the total reflux operation. This should be taken into account in future simulations with directly measured VLE data when the simulation column is simulated continuously and possibly later used experimentally.

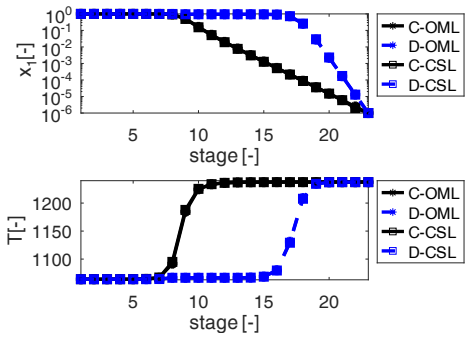

(a) UCl_4-$CdCl_2$ at 1 atm
with $v = 21, 188$ (stage number optimized) and the 9th stage as feed stage

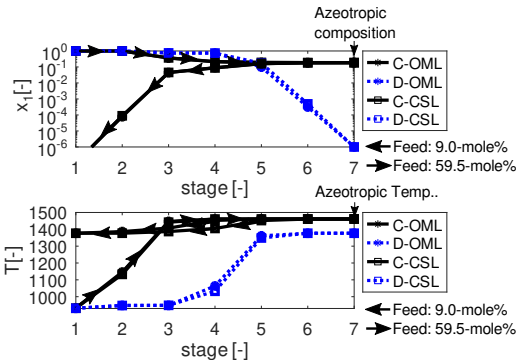

(b) UCl_4-LiCl at 0.1 bar:
First column marked with "→"-direction:
Reflux ratio: $v = 1.132$ (stage number optimized) and the 7th stage as feed stage
Second column marked with "←"direction:
Reflux ratio: $v = 1.998$ (stage number optimized) and the 7th stage as feed stage.

Figure 84: Simulation of a continuous finite-reflux column using different VLE approximation methods and simulation models with Octave/Matlab (OML) and ChemSep (CSL) for the mixtures (a) UCl_4-$CdCl_2$ and (b) UCl_4-LiCl

In the case study with lithium chloride for the continuous distillation column at the optimised reflux ratio of only $v = 1.132$ of the first column, the simulation results in Fig. (84) (lower figure) show the significantly large differences between the results with ideal phase equilibrium behaviour and the real-estimated case at a system pressure of 0.1 bar, since the azeotrope still has the decisive influence on the separation behaviour , as in total reflux operation. The same applies to the second column, although the ideal phase equilibrium case is not shown here, since the simulation results show that both uranium tetrachloride and lithium chloride can be separated with high purity. Here it is assumed that by adding lithium chloride or otherwise after separation of the azeotrope from the first column, the feed to the second column is e.g. about 9 mol% uranium tetrachloride. Theoretically, when lithium chloride is added, a small addition is sufficient to get behind the boundary azeotropic composition. However, for a more appropriate representation and simulation of the second column, a feed of 9 mol% uranium tetrachloride is assumed at the seventh separation stage, as in the first separation column. The arrows in Fig. (84) illustrate the separation directions in two different columns in the case of the estimated azeotropic UCl_4-LiCl mixture. Uranium tetrachloride can be obtained in high purity as a light-boiler condenser product from the first separation stage, and the heavy-boiler azeotrope is separated at the temperature maximum at the bottom. In the new feed with 9 mol% uranium tetrachloride after lithium chloride feed, the separation behaviour is reversed and the azeotrope is again obtained as a heavy boiling product, but now lithium chloride is obtained as

a light boiling distillation product in the condenser. It should also be noted that with a finite reflux ratio compared to a total reflux ratio, the number of separation stages increases by two column stages in order to separate lithium chloride and uranium tetrachloride with high purity, because the process deviates considerably from the more favourable case of a minimum number of stages with infinite reflux ratio $v \to \infty$ (with $v = \frac{\dot{n}_{\mathrm{R}}}{\dot{n}_{\mathrm{D,top}}}$), compared to total reflux operation. The increase in the number of separation stages required for finite reflux is also the case for the idealized vapour-liquid equilibrium behaviour . In the case of the Margules approximated VLE of the estimated temperature maximum azeotrope, this would play a minor role, since the azeotropic composition only needs to be approximately achieved by distillation in order to get to the other side of the azeotrope composition with a suitable azeotrope distillation process method. So the separation to the azeotropic composition at the bottom of the column does not need to be very accurate. All further differences of the separation curves simulation results related to uranium tetrachloride composition and the temperature profiles for the mixture examples of uranium tetrachloride with cadmium dichloride and lithium chloride are shown in the Figs. (82) (upper figure), (83) and (84). Considered in reverse order of the separation stage numbers from the bottom to the top of the column, light and heavy boiling product can be obtained in the simulation results of Fig. (85).

In the example of the separation problem for cadmium dichloride (Fig. (85) (upper subfigure)), high purity uranium tetrachloride can be obtained as a light boiling distillation product for $v = 2$ and v\rightarrow\infty as the total reflux column operation. This is only not possible for a feed composition of 9 mol% uranium tetrachloride at a reflux ratio of $v = 2$ because the uranium tetrachloride content is assumed to be too low to solve the mass balance. Therefore, both the molar flux and the composition in the rectifying section of the continuous separation column do not change from a separation stage above the nineteenth stage number. It can be assumed that the reflux is too low for the small proportion of uranium tetrachloride in the separation simulation example, so that the molar flow becomes too low because too much uranium tetrachloride is separated as a condensation product at the top of the column with a small feed value of 9 mol% uranium tetrachloride mole fraction. In addition, in the other feed composition examples, the uranium tetrachloride separation curve under total reflux column operation is always higher than that with finite reflux ratio. This is due to the fact that with the minimum-optimal separation effort in the total reflux column principle, the required number of separation stages becomes minimal (see Fig. (85) (upper sub-figure)).

For the mixture of uranium tetrachloride with lithium chloride, the simulation results show a completely different separation behaviour in Fig. (85), as already shown in the discussion of the different previous results on the separation ranges for this substance system of uranium tetrachloride with lithium chloride. The azeotropic composition causes a division of the simulation results for feed composition values below or above the azeotropic composition point. For feed compositions $x_{F,\mathrm{UCl_4}} < x^{az}_{\mathrm{UCl_4}}$ the light boiling distillation product obtained is lithium chloride, whereas for $x_{F,\mathrm{UCl_4}} = x^{az}_{\mathrm{UCl_4}}$ no change in substance would occur and for $x_{F,\mathrm{UCl_4}} > x^{az}_{\mathrm{UCl_4}}$ uranium tetrachloride is obtained as the light boiling distillation product. However, in all of the simulation cases shown for this mixture, the azeotropic composition is always obtained as a heavy boiler bottom distillation product. As mentioned before, the composition value in total-reflux

operation is closer to the azeotropic composition for $x_{F,\mathrm{UCl_4}} < x^{az}_{\mathrm{UCl_4}}$, whereafter operationally suitable distillability prevails in total-reflux operation, whereby the composition value of lithium chloride then increases more significantly towards the top of the column than in the finite reflux ratio case. For $x_{F,\mathrm{UCl_4}} > x^{az}_{\mathrm{UCl_4}}$ the relationship is reversed in the comparison of the separation curves and temperature profiles between total reflux and finite reflux column operation.

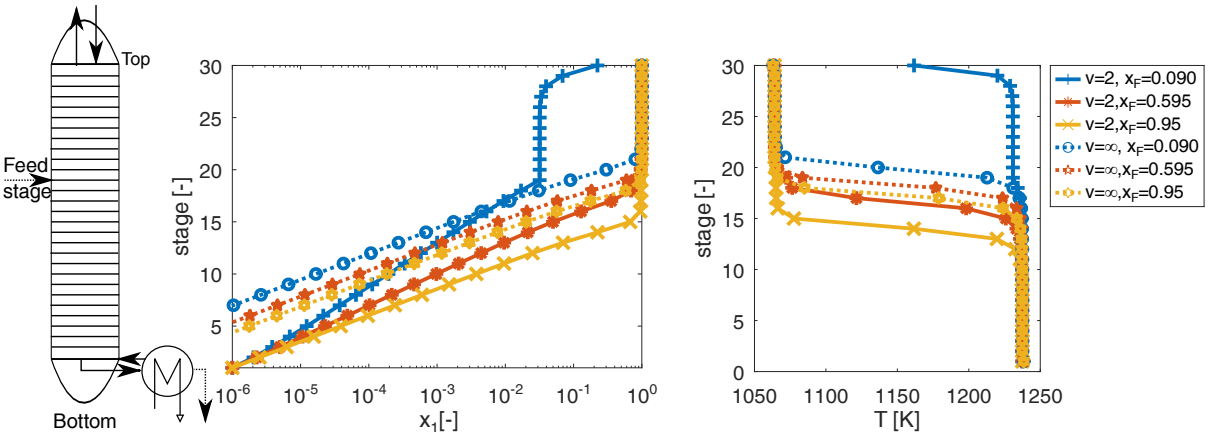

(a) UCl_4-$CdCl_2$ at 1 atm
with the 9th stage as feed stage (counting from the bottom)

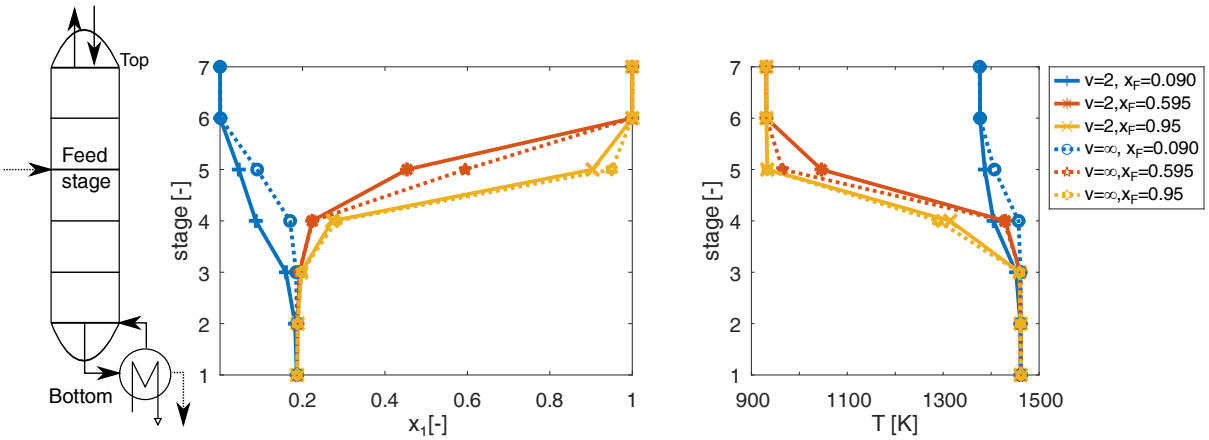

(b) UCl_4-LiCl at 0.1 bar
with the 3rd stage as feed stage (counting from the bottom)

Figure 85: Comparison of the simulation results between different feed compositions and use of continuous finite versus total-reflux column operations for the mixtures (a) UCl_4-$CdCl_2$ and (b) UCl_4-LiCl.

These effects must be considered when using significant finite reflux distillation column operations instead of total reflux column operations. All further details on the separation curves and temperature profiles can be seen from the simulation results in Fig. (85) (lower subfigure) for the binary mixtures of uranium tetrachloride with lithium chloride.

D.2 Estimation of decay heat effects in the distillation column

The heat production in distillation columns due to the decay heat of certain active isotope elements in chloride compounds is estimated from the simulation results of a total reflux distillation column with a suitable test mixture, carried out without simulating any decay heat effects. For

simplicity, only a single steady state PCC operating condition is considered in the specific total reflux operation referred to in chapter (III) section (5.2) and (4.3). In addition, active components (here generally meant and further defined as active elements bound in thermal stable compounds involved or as single elements) as active isotope elements within the chloride or elementary can only accumulate inside the column for simplicity, and the evaporation and condensation area is not considered for the accumulation of decay heat effects in order to study the decay heat effects only inside the inner column area. As a further assumption for a better worst case analysis, only one active isotope per chemical element should be considered in order to better discuss the results in terms of active isotope decay heat ratios. These active isotope elements are bound in chloride compounds. Since the heat supply and removal between evaporator and condenser can be controlled and adjusted, it is further assumed for simplification that the heat production by decay heat of the individual active chloride components there is reset in the estimation model to a value of the initial state heat production. As an upper bound, the proportion of active isotopes is still assumed to be maximised in the calculations. For simulations without decay heat analysis, the evaporator is added as a column stage, but is not analysed in the decay heat estimation.

For any of these decay heat calculations it is important to know or be able to roughly estimate the mean residence time of the active components accumulating discontinuously inside the inner part of the column and also in each separation stage. Strictly speaking, the type of column would be crucial for the estimation of the decay heat effects for the corresponding calculations. Therefore, a sieve tray column with a highly simplified constant liquid level high on the individual trays is considered here for the estimations. From an estimate of the mean residence time, the proportion of decay heat production can be simplified estimated by as follows as the similar accumulation time

$$\bar{t}^{\mathrm{L}}_{\mathrm{res},j} \approx \Delta t_j. \tag{147}$$

Within the inner part total reflux column, these decay heat effects are then to be calculated in the estimation model decoupled from the MESH equations (equations (55)–(58)) from the usual simulation results without heat production. Possible effects on the thematic equilibrium behaviour due to post-decay or decay heat processes are also neglected. This means that the simulation of the whole total reflux column without decay heat effects is done first, and then the estimation of the decay heat of the inner part of total reflux column only is performed from these simulation results. For further simplicity idealized phase equilibrium conditions referring to the validity of the Raoult's law is taken into account for the first required simulations of the total reflux column without decay heat effects. The assumptions not to consider the coupled heat of decay in the evaporator and condenser are not appropriate at this point. There are two reasons for this:

1. Only the effect of the decay heat within the column should be considered, since the condenser is used for cooling and the evaporator for heating and are the control parameters of the systems, and therefore the heat cannot accumulate without control engineering intervention in the condenser or evaporator.

2. From the perspective of the heat of decay estimation model idea, considering only the heat of decay between the inner column and the evaporator would lead to a coupled system of

differential equations, also coupled with the simulation of the total reflux column composition, which could somehow be solved within the scope of this thesis, but secondly would not mathematically reflect the significant separate accumulation effects within the total reflux column.

If the decay heat calculations show an increased heat production due to decay heat in the middle of the column, which would then have to be removed, then a temperature control within the internal separation stages of the column would have to be technically applied in order to avoid temperature hotspots inside the distillation column. Under certain circumstances, however, the decay heat also offers advantages in that the decay heat of the active isotope elements can be used as a(n) (addtional) heat supply in the evaporator. These effects will also be examined in more detail and the results discussed following the presentation of the calculation procedure.

D.2.1 Estimation procedure of heat production due to decay heat effects inside the distillation column

For a rough estimation of the mean residence time depending on the column type and mode of operation, only a total reflux sieve tray column with sharply separated vapour and liquid flows, as shown schematically in Fig. (3), is estimated from the simulation results for the following decay heat estimation. Since the decay heat effects are discontinuous and depend on the residence time behaviour , further simplifications have to be made for the accumulation range and behaviour of active isotopes and the resulting heating behaviour by decay heat accumulation. Thus, it can be assumed that in the estimation model for the decay heat evaluation, the value for the decay heat contribution for each active component is reset to the initial state after reaching the condenser and evaporator.

Additional simplifications required To estimate the heat accumulation, only a single tray column is considered, where the mean residence time per tray is estimated. For modelling simplifications, the liquid flows in a representative square column channel at each separation stage without interference with the vapour from a flow profile point of view. Furthermore, the liquid flows smoothly from the liquid inlet of each column stage to the opposite side of the inlet. The fluid dynamic continuity equation is valid for this net flow of vapour and liquid. Therefore, from a modelling point of view with all simplification still have been made, it can be further simplified to assume that the flow in the cross section is constant. The liquid passes to the next separation stage via a similarly square outlet shaft. Details of the geometric transition from the trough to the shaft are not required for the following calculations. Vertical to the liquid flow, the vapour rises to each separation stage without a simplified assumed liquid resistance in the calculation model and an idealized permeable tray for the vapour. This simplified model concept is used to roughly estimate the heat production by decay heat within each separation stage. In addition, the following further assumptions and simplifications must be made to estimate the decay heat of coupled column stages:

- The simplifications necessary to simulate the above total reflux columns with a single PPC under otherwise ideal phase equilibrium conditions are used.

- The isotopic composition remains more or less constant, and no other components of the substance are produced, added or changed in terms of mole fraction composition (either nuclear or chemical).
- In simple terms, it is assumed that each component of the system undergoes a phase change only once within the column in each circulation path or circulation round.
- The estimate of heat accumulation due to decay heat is derived from the simulation results and the estimated mean residence time of the liquid and vapour, where the temperature of the individual separation stages is not changed by the decay heat effects themselves.
- Estimation of the heat of decay of the active components via the active elements is performed as the undiluted component, regardless of the degree of chlorination of the compounds in the mixture.
- Time delays of the produced heat through decay heat to be transferred via the thermal conductivity properties of the fluids of liquid and vapour do not occur, since it is assumed that liquid and vapour are always ideally mixed in the model each phase and in each column stage, separately.
- There is no heat loss to the environment or heat transfer by conduction through the structured column material across the separation stages, or similar.
- Heat accumulation and decay heat production are also considered only within the inner part of the distillation column. As a further simplification, the decay heat accumulation in the condenser and evaporator is then set to zero by setting the average residence time required there for the active isotopes at each column stage.
- The HETP value of each separation stage should be set approximately to the HETP values of titanium tetrachloride distillation given in [12] (with$\mathrm{HETP}_{\mathrm{min}}$ = 16 inch) as a rough simplification.
- The cross sectional area of the column is determined from the gas kinetic energy of the first separation stage with $E = \rho^G/2w_G^2$, where the vapour is treated as an ideal gas and no liquid is present or entrained. This then allows the simplified approach of calculating the flow velocity of the gas via the F-factor according to equation (70).
- The liquid flows down the column stage shaft of each separation stage assuming frictionless free fall according to the shaft height z ($z_{\mathrm{shaft}} \approx$ HETP) with

$$z(t) = 1/2gt^2. \tag{148}$$

- The values of the specific decay heat per active isotope element are given in Tab. (18) and are taken from approximated values from [29] under all necessary simplification assumptions made in [29] for their calculations.

The calculation procedure The estimation of heat production by decay heat within the column is based on the molar heat output per chemically bound decay isotope and the determination of the average residence time per separation stage under the above simplifications & assumptions. It should be noted that the bound chlorine atoms do not produce any decay heat. Therefore, the decay heat balance must be made using the molar heat portion q_i per bound isotope in the ratio of the mixture to the molar flow and the mean residence times $\bar{t}_{\mathrm{res}}$ for both phases. The produced heat between the separation stages $\Delta\dot{Q}$ is therefore initially equal to the heat portion supplied in the following separation stages. For each separation stage separately, the following applies to the calculation of the additional heat production with initial timet_0:

$$\Delta\dot{Q}_j^L = \sum_{i=1}^{N_{\mathrm{comp}}} (x_i q_i)\, \Delta n_j^L \cdot \left(\bar{t}_{\mathrm{res}}^L - t_0\right), \tag{149}$$

$$\Delta\dot{Q}_j^V = \sum_{i=1}^{N_{\mathrm{comp}}} (y_i q_i)\, \Delta n_j^V \cdot \left(\bar{t}_{\mathrm{res}}^V - t_0\right). \tag{150}$$

For this purpose, the mean residence time $\bar{t}_{res}$ must be estimated, which is done in different ways for the two fluid phases. The velocity of the fluids corresponds to the mean residence time per distance travelled in each column. In this case, the vapour must travel a distance above the HETP value defined for each separation stage, while the liquid must flow across the column stage and down the drainage shaft of the tray column stage. According to Phytagoras' theorem, the distance from the inlet to the outlet is approximately equal to $d_{\mathrm{col}}/\sqrt{2}$ (a comparison with a circular column cross-section). The mean residence time of the two phases for a single separation stage is approximately as follows

$$\bar{t}_{\mathrm{res},j}^V \approx \frac{\mathrm{HETP}}{w^G}, \tag{151}$$

$$\bar{t}_{\mathrm{res},j}^L \approx \frac{d_{\mathrm{col}}/\sqrt{2}}{w^L} + t_{\mathrm{shaft},j}, \tag{152}$$

$$t_{\mathrm{shaft},j} \approx \sqrt{\frac{2 \cdot \mathrm{HETP}}{g}}. \tag{153}$$

The gas velocity is calculated via the F-factor according to the equation (70). The active cross sectional area $A_q = \frac{\dot{V}^G}{w^G}$ (as the simple continuity flow equation) of each column stage must be calculated for the design of the inner part of the total reflux column with a single PPC.

For the liquid phase, the mean residence time is the sum of the mean residence time in the drainage shaft and the mean residence time in the cross-flow of the separation stage. The flow through the drainage shaft follows the law of free fall according to equation (153). Therefore, the following summation is used to estimate the mean residence time of the liquid:

$$\bar{t}_{\mathrm{res},j+1}^L \approx \phi_L \cdot \frac{V_{\mathrm{stage}}}{\dot{V}_{j+1}^L} + t_{\mathrm{shaft}}. \tag{154}$$

The fraction of liquid flow can be calculated from the difference of the flow rates of a separation

stage with

$$\phi_L = \frac{\dot{V}^L}{\dot{V}^L + \dot{V}^V} \tag{155}$$

It should be noted that for the calculation the density of the liquid of the mixture must be determinable at this constant column stage temperature. For this purpose, the so-called mole-specific Amagat law, i.e. the calculation of the liquid density from the pure substances, is to be followed

$$\rho^{\mathrm{L}}_{\mathrm{molar,mix},j}(x_j, T_j) = \left(\sum_{i=1}^{N_{\mathrm{comp}}} \frac{x_{ij}}{\rho^{\mathrm{L}}_{\mathrm{molar},i,j}(T_j)} \right)^{-1}, \; x_j = [x_1, \ldots, x_{N_{\mathrm{comp}}}]^T, N_{\mathrm{comp}} \geq 2. \tag{156}$$

The calculation procedure for estimating the mean residence time, including the coupling of the column stages, is as follows. Initially, only the column diameter and the vapour velocity in the first separation stage need to be determined. The vapour velocity is approximated by specifying the F-factors according to equation (70). The continuity condition $\dot{V}^V = w^G A$ can be used to calculate the cross-sectional area of an assumed circular column. This column diameter is assumed to be constant in the calculations. The calculations for the liquid phase then follow.

Table 18: Activity and calculation of mole specific decay heat, Ref.: [29](p.19,Tab. 3.1 (german version))

Compound	mass [kg]	Half-life time [a]	activity [Bq]	Specific heat [kW/t]	q [W/mol]
^{90}Sr	1830	29.1	9.34E+18	928	73.55
^{137}Cs	4577	30.0	1.46E+19	428	50.44
^{238}Pu	2088	87.8	1.32E+18	567	5.53
^{241}Am	23290	433	2.95E18	112	39.14
^{244}Cm	101	18.1	3.01E+17	2828	1000.39

$^{90}SrCl_2$: q=928 W/kg · 158.52 g/mol · 1kg/1000g x 0.5* = 86.08 W/mol***
^{137}CsCl: q=428 W/kg · 168.35 g/mol · 1kg/1000g x 0.7*= 50.44 W/mol***
$^{238}PuCl_3$: q=(0.019* · 567 W/kg + 5** W/kg) · 350.45 g/mol= 5.53 W/mol***
$^{241}AmCl_3$: q=112 W/kg · 349.45 g/mol · 1kg/1000g= 39.14 W/mol***
$^{244}CmCl_3$: q=2828 W/kg · 354.45 g/mol · 1kg/1000g= 1002.39 W/mol***
*including stable isotopes each MCln, n=1,2,3 and **existence of other active isotopes, *** without dilution

q: Mole specific decay heat of compound

The mean residence time from the previous stage increases with each additional separation stage. However, there are two possibilities for the component, either to remain in the phase or to change once to the other phase. For each separation stage, these two paths (or circular paths for intermediate boiling components) can be followed. Since the component can only pass through a phase once, the case studies can simply be added up and then averaged. The desired heat accumulation within the separation column as a function of column height (or column stage at discrete intervals) is then obtained by simply summing the heat production up to that column stage. This procedure is numerical because a single flux input required to estimate the heat

accumulation is unknown for each phase and column stage and is updated at each following stage until the last values can be updated at the end, as the column is in mass and energy balance. So the idea is basically similar to the tears stream procedure explained in section (2.2.4.2) of chapter (II) or in section (4.4) of chapter (4).

D.2.2 Analysis of the decay heat effects inside the distillation column

For the estimation of the decay heat in a total reflux distillation column using the estimation method described in the previous subsection, two test mixtures are selected which are typically representative of decay heat production and are also representative of the spent fuel composition. The first example is the test mixture of UCl_4-$CdCl_2$-CsCl with the composition $[0,960, 0,016, 0,024]^T$, where for simplicity it is assumed that caesium-137 is the active isotope in Tab. (18). For simplicity, it is assumed that no other isotopes of caesium-137 are present here for maximum heat estimation. In the second example of a test mixture, a representative mixture of UCl_4-$SrCl_2$-$PuCl_3$ with the composition $[0.500, 0.200, 0.300]^T$ is selected and simulated. In the first step, a liquid mole flow rate of 0.1 mol/s is set for all required simulations without decay heat consideration. In the second spent of the estimation of heat production resulted from decay heat effects, only the isotopes listed in Tab. (18) should be present in the chloride compounds in order to estimate the heat production in the maximum case for both test mixtures. Apart from the isotopes, the second example of a test mixture corresponds to a typical representative simplified separation problem for the processing of nuclear fuel after separation of uranium tetrachloride, in that in this second example of a test mixture two active components are present, but of different elements and not isotopes of the same element. In the first example, however, the only active element is caesium-137.

For the primary simulation results without decay heat, representative results from the ChemSep model TRC-C/S ChemSep are used, as TRC-C/S additionally provides further useful information on possible mixture properties in the simulation results as well as on possible heat transport. In the fist stage a liquid mole flow rate of 0.1 mol/s is set for all primary required simulations without decay heat view.

Results for the study of heat accumulation through decay heat effects The basic simulation results of both test mixtures without the decay heat view are shown in Fig. (24) (after section (5.2)) and (87), which are necessary for the estimation of the decay heat, with the final results shown in Fig. (86) and (88) for different F-factor values. For normal pressures of 1 atm, a common F-factor of 2 is selectable according to [73, 72].

The results of the decay heat estimation are shown in figures (86) and (88). The first result example of the first test mixture UCl_4-$CdCl_2$-CsCl already illustrates that the heat generated by decay processes within the column is significantly high and should not be neglected, although the estimate is maximised for the active isotope element caesium-137 involved in the active CsCl component of the mixture. This is already the case for a low mole flow of 0.1 mol/s in the first separation step for both calculation examples. As can be seen from Fig. (86), the heat production in the liquid phase increases significantly more than in the vapour phase as the number of stages increases from the fifth stage onwards. This is mainly due to the higher mean residence time

of the active cesium chloride component in the liquid phase compared to the vapour phase. In addition, the mean residence time of the high-boiling component in the final stages of separation from the evaporator is negligible for the very small molar fractions of active CsCl. In the middle of the column, the heat production is mainly caused by the mass transfer (of cesium chloride) from the liquid to the vapour phase, which is significantly observed in stages 6-12. In the eighth separation stage there is a maximum heat production of only 9 W for the vapour phase at $F = 2$, while in the twelfth separation stage a much higher value of 3.103 kW is reached in the liquid phase. All other F-factor examples assume similarly large comparable values, which do not differ significantly. The heat accumulation in the vapour phase is therefore negligibly small, and the formation of temperature hotspots later in practice due to the low heat input from the vapour phase can therefore be considered very unlikely in this example only for the vapour phase view.

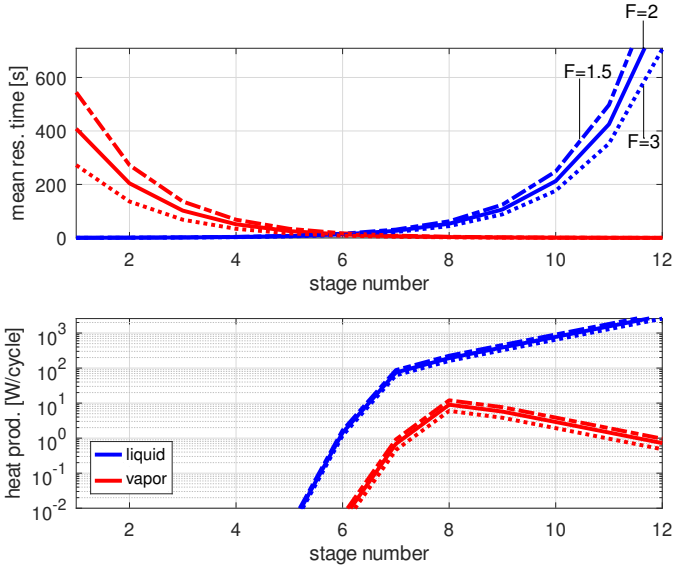

Figure 86: Decay heat estimation for the UCl_4-$CdCl_2$-CsCl system at 1 atm

Since heat production only occurs near the evaporator, it is possible to use the caesium chloride component as a heat production source for the evaporator. For this purpose, a total of 6.107 kW of heat output is available for each separation stage at $F = 2$ when the total available heat production from decay heat of the entire column is added up. With a determined evaporator performance of required 14.120 kW, this corresponds to almost half of the necessary heat demand for the evaporator. In the case of $F = 1.5$, even more than half of the evaporator performance can be used with 7.148 kW. However, as the F-factor increases, the share of heat output via decay heat decreases, since the mean residence time in each separation stage decreases. Thus, for $F = 3$ only a total value of only 5.066 kW is achieved. As the case for $F = 2$ exemplifies, 3.103 kW of heat has been generated in the last separation stage, but this corresponds to only half of the total available heat output of 6.107 kW. For this reason, heat integration stages should be considered for the upper separation stages for this separation example.

Cesium chloride in the test mixture example UCl_4-$CdCl_2$-CsCl, as a high-boiling component, does not circulate in the column like the medium-boiling components, so the composition profiles follow a strictly monotonous decreasing curve from the first separation stage to the evaporator. The circulation effect plays a much greater role in the second SNF relevant separation example

of the text mixture system CsCl-$SrCl_2$-$PuCl_3$. In this example, active strontium-90 is involved in the active intermediate-boiling strontium dichloride component, together with a second active element, plutonium 238, as the heavy-boiling plutonium trichloride component. Here caesium should be assumed to be a non-active isotope.

For the primary evaluation of the decay heat, the primary simulation results without decay heat as shown in Fig. (87) for the second test mixture example are considered first. Cesium chloride and strontium dichloride are accumulated as distillation products, where cesium chloride is an intermediate boiler component and strontium dichloride is a light boiler component. Both components are obtained in the first column of a twelve stage total reflux column of single PPC. Plutonium trichloride accumulates at the bottom as a very high purity separable heavy-boiler distillation product, requiring only a few separation stages to achieve the 99.9999 mol% purity. While the molar flow is maximum at the first column stage with a value of 0.1 mol/s, the other values are always lower, with an overall minimum value of 1.37E-02 mol/s in the sixth separation stage. In general, the lower the molar flux, the lower the total potential heat generation, so that the heat accumulation of the liquid phase in the sixth separation stage can only be high if particularly active isotopes bound in the chloride accumulate preferentially in higher mole fractions in this separation stage. Considering the example of the composition of the mixture CsCl-$SrCl_2$-$PuCl_3$, the value of caesium chloride with a molar fraction of 0.5 is particularly high and caesium-137 with $q = 50.44\,\mathrm{W/mol}$ is present as the second most active element. In this separation example, the activities of the bound active isotopes also decrease in the order of decreasing volatilities, so that the effect of the formation of strong global maxima or minima is only weakened by the decay heat profile depending on the stage number.

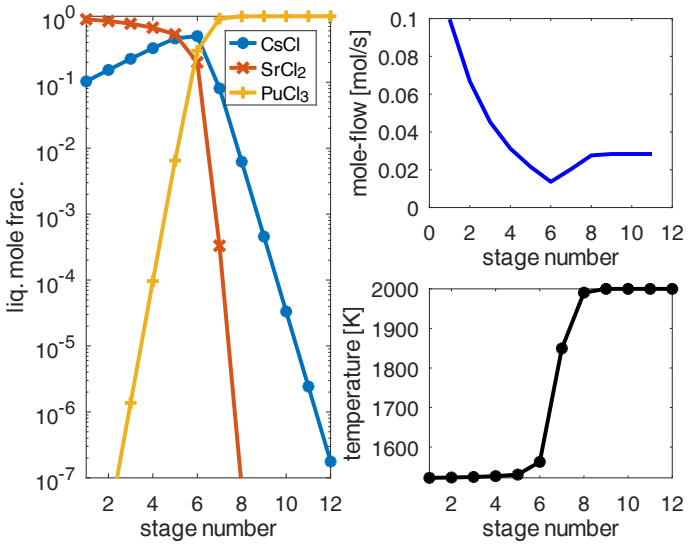

Figure 87: Simulation results of the CsCl-$SrCl_2$-$PuCl_3$ system at 1 atm

The results for the decay heat in the second evaluation step are shown in Fig. (88). In contrast to the previous separation example, the heat production is distributed over the entire separation column, but in this case with larger fractions in the vapour phase for the lower column stages. In the liquid phase, the heat production value due to decay heat is higher in the direction of the evaporator, where the active plutonium-238 chloride component accumulates

more. As the most active isotope elements are now present as a light boiler component compared to the previous separation example, despite the low mean residence times of the vapour, the heat accumulation in the vapour phase inside the column now additionally increases significantly in the condenser region of the column with preferred lower separation stage numbers and reaches a maximum value in the first column stage. While the mean vapour residence time is high above the sixth separation stage, the heat production values also increase significantly in the direction of the condenser, so that heat accumulation in the vapour phase predominates. Below the sixth separation stage, the mean residence time value of the active components involved in the liquid phase increases, so that from the seventh separation stage, the heat accumulation in the liquid phase is dominated by the plutonium trichloride component. Thus, the heat production in the vapour and liquid phases related to the separation stage is lowest in the sixth to eighth separation stages because the mean residence times and the total amount in both phases are still relatively small. In this separation example, the summed heat accumulation in the liquid is much lower than in the summarized vapour phase heat accumulation over all separation stages. For example, from the twelfth stage onwards, the maximum heat production value in the liquid is only 158 W, compared to 2,142 kW in the vapour phase in the first stage, with a still significantly higher value.

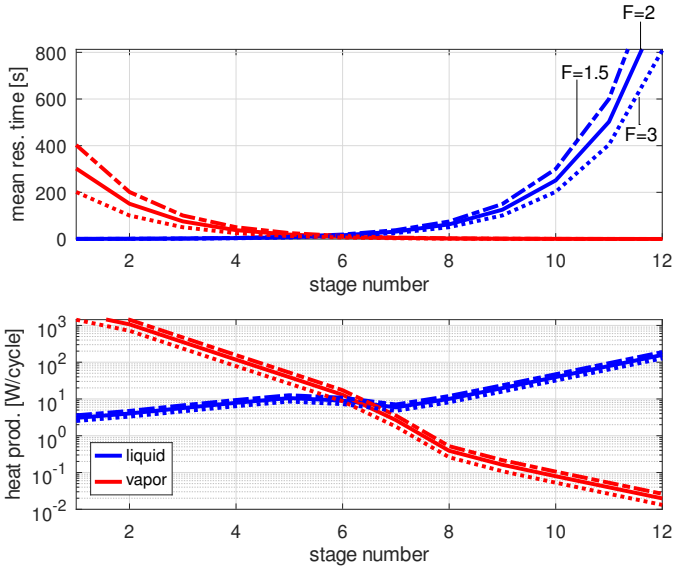

Figure 88: Decay heat estimation for the CsCl-$SrCl_2$-$PuCl_3$ system at 1 atm

Due to the high heat production and heat accumulation in the vapour phase, heat must be removed at each separation stage where it is significant. Therefore, for the second test mixture, compared to the first mixture example, there is a risk of the theoretical temperature hotspot formation within the column when considering the results for the decay heat contribution. As the value of the heat generation power in the evaporator is now relatively low, a large proportion of the heat power cannot be used to supply heat as part of the evaporator performance. In addition, more effort must be expended on separate stage cooling to remove the additional heat from the separation stages and phases, particularly in the vapour phase in the second separation example, which would ultimately make the separation problem of such a distillation column more complex as a practical application for this separation example. In the first separation example,

however, the decay heat is practically advantageous as part of the heat supply.

Comparison of results for evaluating the impact of decay heat effects Fig. (89) summarises the comparison of the two decay heat estimation results. For this,(89) compares the absolute heat production within the separation stages of the two separation examples. In the case of the first UCl_4-$CdCl_2$-CsCl mixture example, the predominant heat production in absolute terms is observed in the evaporator region of the total reflux distillation column, especially significant from the eighth separation stage with a significantly high increasing contribution. Furthermore, further up in the direction of the condenser, the remaining heat production contribution is negligible and disappears, since the active caesium chloride component has previously been distillatively depleted from the liquid phase and this component with the active isotope Cs-137 in ^{137}CsCl accumulates in the first separation stages. However, compared to the first separation example, the absolute value of the heat production in the second example for the CsCl-$SrCl_2$-$PuCl_3$ system is lower because caesium is assumed to be the non-active isotope. In the second example, the heat production and subsequent heat accumulation takes place mainly in the vapour part of the upper separation stages 1-4, while further down the column the heat production values are significantly lower. The heat in the second separation example is therefore much more difficult to remove from the separation stages, whereas in the first separation example the decay heat can even be actively used for evaporator performance. As the temperature in the general operating distillation column principle should increase from top to bottom of the column, the greater contribution to heat accumulation in the upper part of the column in the second separation example is counterproductive to the separation of the substances, with the risk of possible temperature hotspot formation due to heat accumulation in the vapour phase with insufficient cooling within the separation stages. In practice, this could require additional complex cooling of these separation stages. In addition, due to the lower thermal conductivity of the vapour, it is difficult to remove this heat quickly enough by cooling in the column area to fulfil the distillation process. All other summarised absolute values for the heat production of both exemplary separation examples can be taken from Fig. (89).

In summary, the investigation of the decay heat, in addition to the measurement of the phase equilibria, is of fundamental importance for both experimental investigations in distillation columns of such test salt mixtures. It may also be an important factor for more realistic simulations in the future.

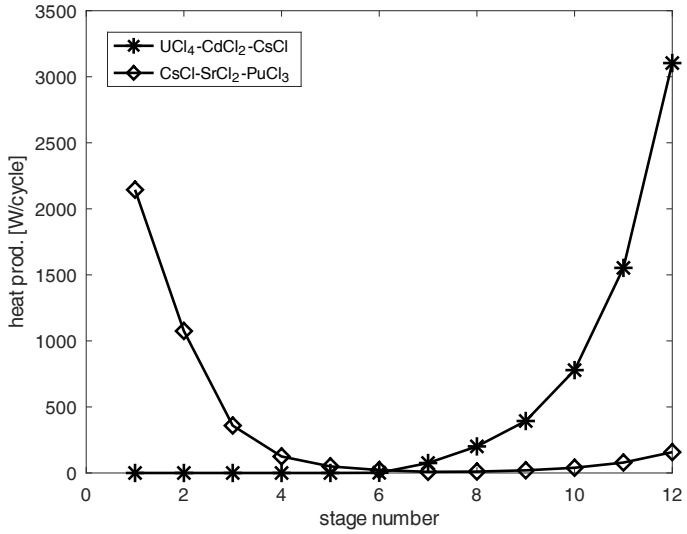

Figure 89: Comparison of total stage decay heat each stage $\left(\dot{Q}_j^L + \dot{Q}_j^V\right)$ of the substance system UCl_4-$CdCl_2$-CsCl and CsCl-$SrCl_2$-$PuCl_3$ at 1 atm

E Use of ChemSep Lite software

The ChemSep models described in [68] are used in this thesis to compare and validate the Octave/MATLAB equilibrium stage models with respect to single and multi-stage distillation processes. The single-stage implemented Octave models are validated for single-stage distillation and isothermal flash evaporation, as well as for a condensation or evaporation unit. The Octave/MATLAB isothermal flash evaporator is simulated in the ChemSep Lite software with a simple flash model at constant temperature and pressure in the feed and flash chamber. In addition, by defining the thermal state of the feed under "Selection", a condensation stage can also be simulated by defining the feed as saturated liquid or an evaporation stage by definition as saturated vapour. Multi-stage distillation processes include the validation of the total reflux distillation column according to the ChemSep "total reflux" model and the continuous distillation column with finite reflux according to the "simple distillation" model. The main models to be validated are listed in the Tab. (10).

The application of the software for this thesis is done in the ChemSep Main File (Sep-file). From the Pure Component substance property database file (Pcd-file) substances can be selected within their specific pure substance properties of conventional, molecular and temperature dependent properties. The defined substance data classes of the pure substance components include critical data, molecular properties and common temperature dependent substance data ("T_correlations"). In addition, there are group data and mixture properties, which play a minor role for the simulation in this thesis. However, for the application of the ChemSep distillation models, at least the following pure substance data must be known for a reasonable simulability of the separation problem under ideal phase equilibrium conditions: conventional data (e.g. melting and boiling points), including critical and/or triple point data, vapour pressure data, densities, heat capacities, heat conductivities, enthalpy of evaporation, enthalpy of fusion and, if applicable, surface tension. The internal estimation of molecular properties requires the simpli-

fied calculation of molecular size via bond lengths & angles, atomic radii, ionic radii and other properties describing the geometric extent of the molecules.

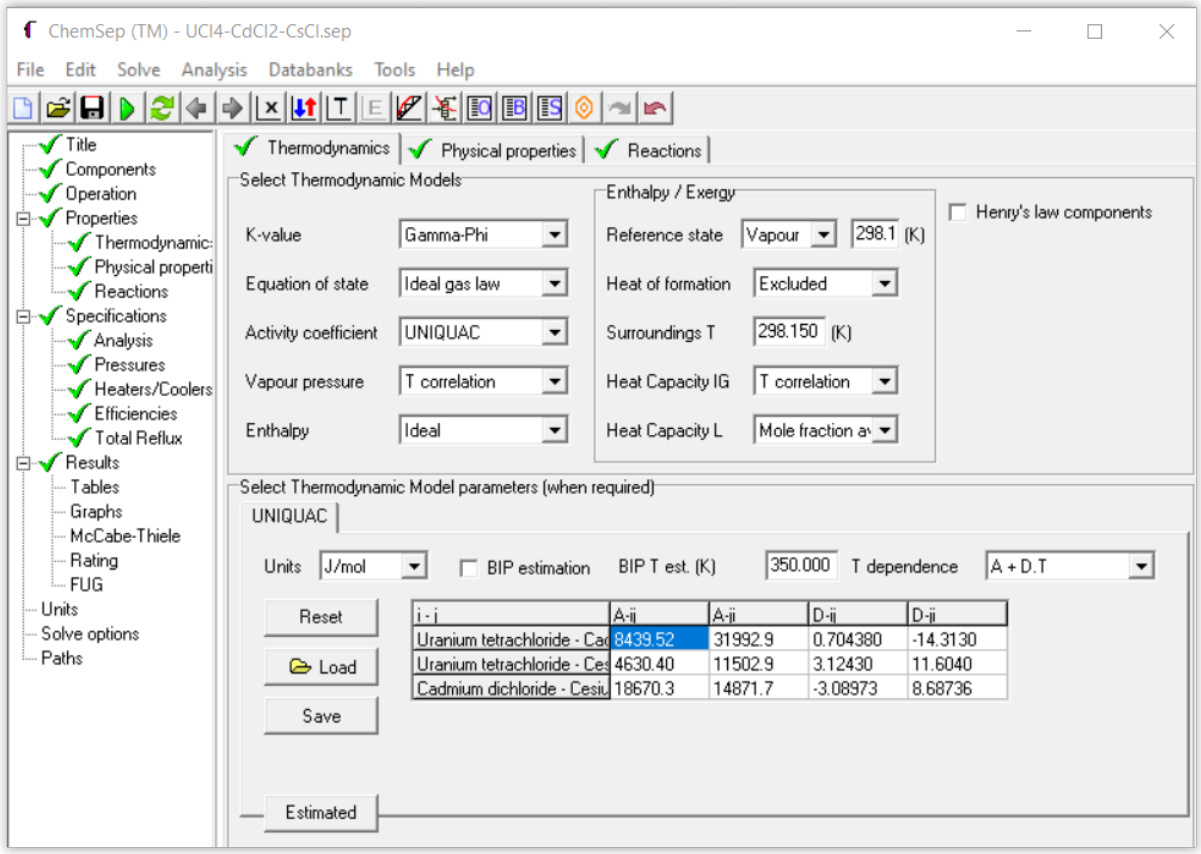

Component	A_{ij}	A_{ji}	D_{ij}	D_{ji}
UCl_4	8439.52	31992.9	0.704380	-14.3130
$CdCl_2$	4630.40	11502.9	3.12430	11.6040
CsCl	18670.3	14871.7	-3.08973	8.68736

Figure 90: Thermodynamic equilibrium settings in the Sep-file:
The data were fitted to a UNIQUAC model as an example in two parts of a fully dissociated system and a fully undissociated system, with an assumed dissociation fraction of only 0.1 mol%, without any validation on experimental VLE behaviour .

In the Sep file it is also possible to select different calculation methods with activity coefficients via temperature dependent correlation fit functions. Examples of input are given in Fig. (90). These data have been approximated in Octave/MAtlab code for example for simple estimated UNIQUAC model parameters for the system UCl_4-$CdCl_2$-CsCl:

1. Simplified estimation of the combinatorial part assuming the molecular size estimated with the molecular geometry and bond angles, ionic radii, characteristic and bond lengths to be able to estimate the model-part required Van der Waals area and surfaces.

2. Estimation of the residual part of each involved component to be required for the estimation of the interaction energy by enabling diffusion through a chlorine shielding region by overcomming the activation energy in combination with the ionic potential of the ionic cation which is assumed to be fully dissociated. For this purpose, a fixed ionic fraction was

set, e.g. an ionic fraction value of $\varphi = 0.001$, where all chloride components are assumed to be completely dissociated and the other fraction is assumed to be completely undissociated.

These data are not physically validated, but could be used as a simplified model idea just to understand the use of ChemSep Lite software. These UNIQUAC model parameters can be inserted into the Sep file by selecting "Properties"->"Thermodynamics"->"K-values"="Gamma_Phi"->"Activity Coefficient"="UNIQUAC". The example values are shown in Fig. (90). A linear temperature dependence was also calculated in order to estimate the change of the parameters at different temperatures as a correlative fit function. For this purpose the calculation was performed separately for ionic and covalent fractions to the combinatorial and residual fractions according to the UNIQUAC/LIQUAC model with a fixed assumed ionic fraction of $\varphi = 0.001$ as an example and the estimation of the activation energy simplified by diffusion and repulsion with ionic potentials for each ionic component. Van der Waals covalent interactions are neglected in the estimation. However, the interaction parameters obtained cannot be validated in more detail and also give questionable results in the representation of many ternary phase diagrams. Further work on model development with UNIQUAC/LIQUAC models may help to improve simulation in the future. However, further experimental work is needed to do this and to even improve this simple UNIQUAC model.

F Bibliography and References

All relevant author activities in terms of publications, journal papers, conference proceeding papers and published conference contribution activities relevant to this topic of the thesis are listed below. A distinction is made between the most directly relevant author's publications, which cover the main topic of this thesis, and those which also consider related recycling problems in a more distant thematic context (under 'Other publications by author').

Author's publications

The most important publications on the subject of the simulation and modelling of test mixtures are presented (listed in priority for this thesis):

- D. Böhm, A. Huke, D. Weissbach, G. Ruprecht, S. Gottlieb, K. Czerski, and R. Macian-Juan. *Partitioning of Nuclear Waste by Fractionated Distillation,* 150153 NuDest, technical report, report number 150153 NuDest, 2019:
  This publication is one of the largest and most important monographic publication focusing on the initial separation ideas and design concepts for the processing of spent nuclear fuel and its application in the Dual Fluid Reactor as a fuel melt. The main concepts in this publication deal with the fundamental aspects of distillation and also with the research of substance property data, but it does not include the process simulation results and deals with weak estimation or simulation models for estimating the separation accuracy of the separation by distillation. These points have been much better developed in this thesis, such as the substance property data research (see section (B) in the appendix), the simulation and modelling with test mixtures (see chapter (III)), and the conceptual design with process simulations for spent nuclear fuel including cladding material recycling and waste gas treatment for noble gas recovery (see chapter (IV)), as well as other separation tasks to be solved with this separation design, such as the processing of metallic Dual Fluid Reactor melts (see section (C) in the appendix). On this basis, the general assessment of the feasibility of the separation will be carried out in this thesis.

- D. Böhm, K. Czerski, A. Huke, J.C. Lewitz, D. Weißbach, S. Gottlieb, and G. Ruprecht. *New methods for nuclear waste treatment of the Dual Fluid Reactor concept*, Acta Physica Polonica B, 51:893, 2020:
  The first publication, which primarily presents a compact overview of the idea of a distillation-based conceptual separation design for the recovery of spent nuclear fuel (see chapter (IV)) within first simulation results, is presented here.

- D. Böhm, K. Czerski, D. Weißbach; S. Gottlieb, A. Huke, and G. Ruprecht. *Renewable distillation of spent nuclear fuel*, Annals of Nuclear Energy, 202x, x (To be published):
  This publication summarises the main results of the conceptual design of the complete distillation-based separation process (see chapter (IV)) and the total reflux column principle with developed PPCs (Progressing Process Cycle) (see section (5.2), chapter (III)). It will be published soon.

- A. Huke, D. Boehm, D. Weißbach, G. Ruprecht, S. Gottlieb, K. Czerski, R. Macian-Juan, J.C. Lewitz. *A novel P and T-Schema based on the Dual Fluid Reactor Technology,* 50th Annual Meeting on Nuclear Technology, AMNT, CD (KTG und Kerntechnik Deutschland e. V. (KernD)), INFORUM Verlags- und Verwaltungsgesellschaft mbH, 2019:
  This was the first publication of the conference proceedings, which included the first presentation of distillation-based recovery to the most relevant reprocessing test mixture examples with uranium as tetrachloride (see chapter (III)), as well as the idea for use plus integration in Dual Fluid technology.

- D. Böhm, K. Czerski, D. Weißbach, J.C. Lewitz, A. Huke, G. Ruprecht, R. Kaesemann and S. Gottlieb. *Processing design for a pyrochemical-distillative recovery alternative in nuclear waste recycling - Distillation-based concepts for making nuclear energy more sustainable,* International Conference on Radioactive Waste Management: Solutions for a Sustainable Future (IAEA-CN--294): Management of Radioactive wastes, and non-radioactive wastes from nuclear facilities, IAEA, 2021:
  This conference article deals with the theoretical overall view of the fulfilment of the disposal problem on the assessment of the separation success of the developed separation concept (see Chapter (IV) with the focus on section (7)). From these simulation results of the conceptual design of distillation-based spent fuel recovery, possible options for reuse of the fuel in liquid fuel reactors, such as the Dual Fluid Reactor, are discussed.

- D. Böhm, K. Czerski, S. Gottlieb, A. Huke, and G. Ruprecht. *Recovery of rare earth elements from NdFeB magnets by chlorination and distillation*, Processes, 11(2):577, 2023:
  This publication shows the separation design for the consideration of the distillative recycling of NdFeB magnets by chlorination and subsequent distillation, simplified with used total reflux columns for simulations and under ideal phase equilibrium conditions (thermodynamic). This also includes an analogous investigation of the separation problem of rare earths as a common heavy earth fraction in the conceptual design of this thesis (see Chapter (IV)) as well as following aspects on the use for further recycling technology, such as discussed in this thesis in chapter (I) (introduction) and(V) (conclusions and future perspectives) of this thesis.

Publications which also relate to the distillation problem relevant to this thesis, but from a more distant point of view than that discussed in this thesis, are listed below (in order of priority for this thesis):

- D. Böhm, D. Weißbach, S. Gottlieb, G. Ruprecht, and A. Huke. *Destillation als recyclingmethode für metallische Rohstoffe* (in german language, only), Poster Konferenzband zur 16. Recy & DepoTech Konferenz, pages 355–360. Lehrstuhl für Abfallverwertungstechnik und Abfallwirtschaft der Montanuniversität Leoben, Recy & Depotech, November 2022.
  This conference article is mainly focused on the distillability of common industrial components of the alloys. Various concepts and design ideas have been developed using simulations, such as the recycling of lithium from electrode material, rare earths and many other examples of closed-loop raw material cycles. The provision of low-cost energy is also crucial, such as the use of nuclear liquid fuel reactor concepts, which also rely sustainably

on distillation to recycle these fuels. However, this is of secondary importance and the general application of industrial alloy recycling is the analogous focus to the spent nuclear waste recycling problem to the concept developed in this thesis.

- Böhm, D. & Czerski, K. The Applicability of Distillation as an Alternative Nuclear Reprocessing Method, International Journal of Nuclear and Quantum Engineering, 2021, 15, 137-142.
  This publication in the series of the conference of the same name, at which this paper was also presented, examines the distillability of ternary test mixtures of uranium tetrachloride-cesium chloride-plutonium trichloride and thorium tetrachloride-sodium chloride-plutonium trichloride, which are representative of liquid fuel reactors such as MSR or thorium-based reactors. Unfortunately, the author has published this paper with the now undesired publisher World Academy of Science, Engineering and Technology, which is known as a predatory publisher and is on the Beall's list[182].

Summary of author's conference oral presentations or partly leading discussions

Conferences with most important oral presentations and slides have been hold on the following topics:

- Actinide Separations 44th annual conference, 18–21 May 2021, (USA, online conference) with the oral presentation (within the same abstract name, required for the active contribution to this conference) *Distillation as an industrial separation alternative for actinides.*

Other conference and workshops with oral presentations:

- PhD4 Gen High-Temperature Summer School, 01–05 June 2020, NCBJ (Warsaw, Poland, online conference) with the oral presentation *Decay heat estimation in the design of distillation columns.*
- 5th edition National Scientific Conference "e-factory of Science", 10–11 April 2021, Poznan, but mainly online conference, with a short oral presentation *The applicability of Distillation as an alternative in nuclear fuel reprocessing*, including abstract of the same name.
- Participation in the 5th national Virtual Festival of Life and Earth Science in Poznan (Poland) in 26–31 October 2021, Virtual video presentation of 10 minutes: Contribution of the Dual Fluid Reactor in combination with distillation-based separation processes towards environmentally friendly, CO2-free industrial development and abstract with the name *Method of finding new innovative industrial processes for closing the global „industrial carbon and raw material cycle" on earth.*

Conferences and workshops with partly leading discussions

- BfE Status Conference on Nuclear Waste Disposal for Germany (BfE Statuskonferenz für nukleare Endlagerung), 14-15 November 2019 (Berlin, Germany), with partly leading discussion and brainstorming on whether disposal is necessary at all to solve the nuclear waste problem, and on distillation as a potential recovery method for spent nuclear fuel and further reuse in liquid fuel reactors such as the Dual Fluid Reactor.

Summary of author's conference poster presentations

Conferences and workshops with poster presentations have been hold on the following topics, which are most relevant to this thesis:

- XXXVI Mazurian Lake Conference on Physics, 01–07 September 2019 (Piaski, Poland) on the topic *New Methods for Nuclear Waste Treatment of the Dual Fluid Reactor Concept: The Pyroprocessing unit* (including abstract *New Methods for Nuclear Waste Treatment of the Dual Fluid Reactor Concept*).
- IAEA International Conference on Radioactive Waste Management: Solutions for a Sustainable Future, 01-05 November 2021 (Vienna, Austria and as well additional available including as online conference) on the topic *Processing design for a pyrochemical distillative recovery alternative in nuclear waste recycling* (Including abstract and video abstract as a short presentation of the separation problem).
- Recy & DepoTech, 2022 (Leoben, Austria) on the topic together with the abstract(in English language) *Distillation as a recycling method for metallic raw materials*, Poster Konferenzband zur 16. Recy & DepoTech Konferenz, page 444.
- Dual Fluid Reactor workshop, 25–27 April 2019, University of Szczecin (Poland) on the topic *Distillative separation processes as an alternative to the PUREX process.*

References

[1] A. Huke, G. Ruprecht, D. Weißbach, S. Gottlieb, A. Hussein, and K. Czerski. The dual fluid reactor – a novel concept for a fast nuclear reactor of high efficiency. *Annals of Nuclear Energy*, 80:225–235, jun 2015.

[2] P. M. F. Valerio. *Archaeometallurgical study of pre and protohistoric production remains andartefacts from Southern Portugal.* PhD thesis, Faculdade de Ciencias e Tecnologia, March 2012.

[3] H. Okamoto. Cr-u (chromium-uranium). *Journal of Phase Equilibria and Diffusion*, 33(6):495–495, jul 2012.

[4] J. Gmehling. *Azeotropic data.* VCH, Weinheim New York, 1994.

[5] H. C. Ko, A. Landsberg, and J.L. Henry. The vapor-liquid equilibria of the aluminum chloride-ferric chloride system. *Metallurgical Transactions B*, 14(2):301–303, jun 1983.

[6] H. C. Ko and A. Landsberg. The vapor-liquid equilibria of the aluminum chloride-titanium tetrachloride system. *Metallurgical Transactions B*, 17(3):609–610, sep 1986.

[7] A. Landsberg and H. C. Ko. On the separation of TiCl4 from AlCl3. *Metallurgical Transactions B*, 17(1):232–234, jan 1986.

[8] M. R. Zaghloul, D. K. Sze, and A. R. Raffray. Thermo-physical properties and equilibrium vapor-composition of lithium fluoride-beryllium fluoride (2Lif/Bef2) molten salt. *Fusion Science and Technology*, 44(2):344–350, sep 2003.

[9] G. Gaweł and A. Górniak. Phase diagram and thermodynamic properties of the system MnCl2–UCl4, prediction and investigation results. *Journal of Nuclear Materials*, 340(1):64–68, apr 2005.

[10] W. Gaweł. Phase diagram and thermodynamic properties of the system lanthanum(iii) chloride - uranium(iv) chloride. *Polish Journal of Chemistry - Roczniki Chemii*, 61:69 – 72, 1987.

[11] W. Gaweł. Regularities of phase equilibria in the binary uranium tetrachloride systems and their thermodynamic interpretation. *Journal of Nuclear Materials*, 247:301–303, aug 1997.

[12] C. K. Stoddard and E. Pietz. Pilot-plant distillation and purification of titanium tetrachloride (report of investigations). techreport, 1947.

[13] D. Böhm, K. Czerski, D. Weissbach, J.C. Lewitz, A. Huke, G. Ruprecht, R. Kaesemann, and S. Gottlieb. Processing design for a pyrochemical-distillative recovery alternative in nuclear waste recycling - distillation-based concepts for making nuclear energy more sustainable. In *International Conference on Radioactive Waste Management: Solutions for a Sustainable Future (IAEA-CN–294): Management of Radioactive wastes, and non-radioactive wastes from nuclear facilities*. IAEA, 2021.

[14] I. Barin and G. Platzki. *2 Volume Set, Thermochemical Data of Pure Substances, 3rd Edition*. Wiley-VCH, 1997.

[15] S. Suzuki. De 600 14 577 t2, mitsubishi heavy industries, ltd., tokio/tokyo, jp and hoffmann & eitle, 81925 muinch, 2005.

[16] B. Arnold. *Zirkon, Zirkonium, Zirkonia - aehnliche Namen, verschiedene Materialien*. Springer Berlin Heidelberg, 2019.

[17] J Katz and E Rabinowitch. CHEMISTRY OF URANIUM. collected papers. Technical report, jan 1958.

[18] M. Binnewies and E. Milke, editors. *Thermochemical Data of Elements and Compounds*. Wiley-VCH Verlag GmbH, dec 1998.

[19] E.H.P. Cordfunke, W. Ouweltjes, and G. Prins. Standard enthalpies of formation of uranium compounds VIII. UCl3, UCl5, and UCl6. *The Journal of Chemical Thermodynamics*, 14(5):495–502, may 1982.

[20] R. Keim, C. Keller, and D. Brown. *Handbuch der anorganischen Chemie (Gmelin Handbook of Inorganic and Organometallic Chemistry). System-Nr. 55. Uranium Suppl. Vol. C.9.: Compounds with Chlorine, Bromine, Iodine.* Springer, 8 edition, 1979.

[21] N. M. Edelstein, J. Fuger, and L. R. Morss. *The chemistry of the actinide and transactinide elements*, volume 1. Springer, 3 edition, 2006.

[22] Thermodynamics of nuclear materials. Symposium presentation, Juelich, 1979.

[23] Z. Singh, R. Prasad, V. Venugopal, and D.D. Sood. The vaporization thermodynamics of uranium tetrachloride. *The Journal of Chemical Thermodynamics*, 10(2):129–134, feb 1978.

[24] I. Barin. *Thermochemical properties of inorganic substances.* Springer-Verlag Verlag Stahleisen, Berlin New York Duesseldorf, 1991.

[25] T. E. Phipps, G. W. Sears, R. L. Seifert, and O. C. Simpson. The vapor pressure of plutonium halides. *The Journal of Chemical Physics*, 18(5):713–723, may 1950.

[26] F. L. Oetting. The chemical thermodynamic properties of plutonium compounds. *Chemical Reviews*, 67(3):261–297, jun 1967.

[27] R. Lemire. *Chemical Thermodynamics of Neptunium and Plutonium*, volume 4. Elsevier Science, 2001.

[28] F Weigel and W Schuster. The vapor pressure of americium(III) chloride: An ultramicro apparatus for the determination of saturation vapor pressures of actinide halides. *Journal of the Less Common Metals*, 113(1):157–176, nov 1985.

[29] D. Böhm, A. Huke, D. Weissbach, G. Ruprecht, S. Gottlieb, K. Czerski, and R. Macian-Juan. Partitioning of nuclear waste by fractionated distillation, 150153 nudest report. technical report 150153 NuDest, 2019.

[30] D. Weissbach, G. Ruprecht, A. Huke, K. Czerski, S. Gottlieb, and A. Hussein. Energy intensities, EROIs (energy returned on invested), and energy payback times of electricity generating power plants. *Energy*, 52:210–221, apr 2013.

[31] F. Marscheider-Weidemann, S. Langkau, T. Hummen, and L.T. Espinoza. *DERA Rohstoffinformation, Rohstoffe fÃŒrZukunftstechnologien.* Frauenhofer, 2016.

[32] R.E. Masterson. *Introduction to Nuclear Reactor Physics.* Taylor and Francis Ltd., 2017.

[33] M.B. Chadwick and et.al. ENDF/b-VII.1 nuclear data for science and technology: Cross sections, covariances, fission product yields and decay data. *Nuclear Data Sheets*, 112(12):2887–2996, dec 2011.

[34] D.A. Brown and et.al. ENDF/b-VIII.0: The 8 th major release of the nuclear reaction data library with CIELO-project cross sections, new standards and thermal scattering data. *Nuclear Data Sheets*, 148:1–142, feb 2018.

[35] IAEA. Cumulative fission yields c3 table, international atomic energy agency - nuclear data section p.o. box 100, wagramer strasse 5, a-1400 vienna, austria, https://www-nds.iaea.org/sgnucdat/c3.htm, 2006.

[36] A. Huke, G. Ruprecht, D. Weissbach, K. Czerski, S. Gottlieb, A. Hussein, and F. Herrmann. Dual-fluid reactor. In *Molten Salt Reactors and Thorium Energy*, pages 619–633. Elsevier, 2017.

[37] A. Huke, D. öand D. Weissbach, G. Ruprecht, S. Gottlieb, K.Czerski, R. Macian-Juan, and J.C. Lewitz. A novel p & t-schema based onthe dual fluid reactor technology. In *50th Annual Meeting on Nuclear Technology (AMNT 2019) CD (KTG und Kerntechnik Deutschland e. V. (KernD))*. INFORUM Verlags- und Verwaltungsgesellschaft mbH, Berlin, Deutschland, 2019.

[38] J. Sierchuła, D. Weissbach, A. Huke, G. Ruprecht, K. onrad Czerski, and M. P. Dąbrowski. Determination of the liquid eutectic metal fuel dual fluid reactor (DFRm) design – steady state calculations. *International Journal of Energy Research*, 43(8):3692–3701, apr 2019.

[39] D. Weissbach, J. Sierchuła, M. P. Dąbrowski, K. Czerski, and G. Ruprecht. Dual fluid reactor as a long-term burner of actinides in spent nuclear fuel. *International Journal of Energy Research*, 45(8):11589–11597, mar 2021.

[40] A. Huke, G. Ruprecht, A. Hussein, K. Czerski, and S. Gottlieb. Wo2013041085a3, dual fluid reaktor, May 2013.

[41] A. Huke, G. Ruprecht, D. Weißbach, S. Gottlieb, A. Hussein, and K. Czerski. The dual fluid reactor -a new concept for a highly effective fast reactor. In *The 19th Pacific Basin Nuclear conference (PBNC 2104)*. IAEA, 2014.

[42] J. Sierchuła, M. P. Dąbrowski, and K. Czerski. Negative temperature coefficients of reactivity for metallic fuel dual fluid reactor. *Progress in Nuclear Energy*, 146:104126, apr 2022.

[43] Tomasz Hanusek and Rafael Macian-Juan. Analyses of the shutdown system and transients scenarios for the dual fluid reactor concept with metallic molten fuel. *International Journal of Energy Research*, 46(12):17230–17246, jul 2022.

[44] X. Wang and R. Macian-Juan. Steady-state reactor physics of the dual fluid reactor concept. *International Journal of Energy Research*, 42(14):4313–4334, aug 2018.

[45] X. Wang, C. Liu, and R. Macian-Juan. Preliminary hydraulic analysis of the distribution zone in the dual fluid reactor concept. *Progress in Nuclear Energy*, 110:364–373, jan 2019.

[46] M. Wang, X. He, R. Macian-Juan, and X. Wang. One-dimensional transient analysis of the dual-fluid reactor system. *Annals of Nuclear Energy*, 162:108481, nov 2021.

[47] D. Böhm, K. Czerski, A. Huke, J.C. Lewitz, D. Weissbach, S. Gottlieb, and G. Ruprecht. New methods for nuclear waste treatment of the dual fluid reactor concept. *Acta Physica Polonica B*, 51:893, 2020.

[48] A. P. Paiva and P. Malik. Recent advances on the chemistry of solvent extraction applied to the reprocessing of spent nuclear fuels and radioactive wastes. *Journal of Radioanalytical and Nuclear Chemistry*, 261(2):485–496, 2004.

[49] G. Modolo, A. Wilden, A. Geist, D. Magnusson, and R. Malmbeck. A review of the demonstration of innovative solvent extraction processes for the recovery of trivalent minor actinides from PUREX raffinate. *Radiochimica Acta*, 100(8-9):715–725, aug 2012.

[50] W.L. Carter, R.B. Lindauer, and L.E. McNeese. Design on an engineering-scale, vacuum distillation experiment for molten-salt reactor fuel. ORNL-report ORNL TM-2213, 1968.

[51] D.W. Green and R.H. Perry. *Perry's Chemical Engineers Handbook 7th, Section 13 : Distillation; Distillation perry's chemical engineering.* McGraw-Hill, 7 edition, New York, 1997.

[52] H. C. Eun, Y. Z. Cho, H. S. Park, I. T. Kim, and H. S. Lee. Study on a separation method of radionuclides (ba, sr) from LiCl salt wastes generated from the electroreduction process of spent nuclear fuel. *Journal of Radioanalytical and Nuclear Chemistry*, 292(2):531–535, sep 2011.

[53] H. C. Eun, J. H. Choi, I. H. Cho, T. K. Lee, T. J. Kim, J. S. Shin, H. S. Park, and D. H. Ahn. Purification of LiCl–KCl eutectic waste salt containing rare earth chlorides delivered from the pyrochemical process of used nuclear fuel using a reactive distillation process. *Journal of Radioanalytical and Nuclear Chemistry*, 307(2):1419–1427, jun 2015.

[54] I. S. Kim, S. C. Oh, H. S. Im, J. M. Hur, and H. S. Lee. Distillation of LiCl from the LiCl–Li2O molten salt of the electrolytic reduction process. *Journal of Radioanalytical and Nuclear Chemistry*, 295(2):1413–1417, jul 2012.

[55] J.H. Lee, J.H. Kang, S.C. Hwang, J.B. Shim, B.G. Ahn, E.H. im, and S.W. Park. Electrodeposition characteristics of uranium in molten LiCl-KCl eutectic and its salt distillation behavior. *Journal of Nuclear Science and Technology*, 43(3):263–269, mar 2006.

[56] S. B. Park, D. W. Cho, M. S. Woo, S. C. Hwang, Y. H. Kang, J. G. Kim, and H. Lee. Investigation of the evaporation of rare earth chlorides in a LiCl–KCl molten salt. *Journal of Radioanalytical and Nuclear Chemistry*, 287(2):603–608, aug 2010.

[57] I. H. Yang, H.C. Yang, and H.J. Kim. The effect of menisci on kinetic analysis of evaporation for molten alkali metal salts (CsNO3, CsCl, LiCl, and NaCl) in small cylindrical containers. *Journal of Chemistry*, 2018:1–10, 2018.

[58] L. Cassayre, P. Souček, E. Mendes, R. Malmbeck, C. Nourry, R. Eloirdi, and J.-P. Glatz. Recovery of actinides from actinide–aluminium alloys by chlorination: Part i. *Journal of Nuclear Materials*, 414(1):12–18, jul 2011.

[59] P. S., L. Cassayre, R. Eloirdi, R. Malmbeck, R. Meier, C. Nourry, B. Claux, and J.-P. Glatz. Recovery of actinides from actinide–aluminium alloys by chlorination: Part II. *Journal of Nuclear Materials*, 447(1-3):38–45, apr 2014.

[60] H.-C. Yang, H.C. Eun, H.S. Lee, and Y.J. Cho. Closed chamber salt distillation system for an enhanced recovery of evaporated pure salt. *Journal of Nuclear Science and Technology*, 47(11):973–976, nov 2010.

[61] H. C. Eun, Y. Z. Cho, T. K. Lee, I. T. Kim, G. I. Park, and H. S. Lee. An improvement study on the closed chamber distillation system for recovery of renewable salts from salt wastes containing radioactive rare earth compounds. *Journal of Radioanalytical and Nuclear Chemistry*, 295(1):345–350, may 2012.

[62] Y. Mochizuki, N. Tsubouchi, and K. Sugawara. Selective recovery of rare earth elements from dy containing NdFeB magnets by chlorination. *ACS Sustainable Chemistry & Engineering*, 1(6):655–662, apr 2013.

[63] Kuniaki Murase, Tetsuya Ozaki, Ken ichi Machida, and Gin ya Adachi. Extraction and mutual separation of rare earths from concentrates and crude oxides using chemical vapor transport. *Journal of Alloys and Compounds*, 233(1-2):96–106, jan 1996.

[64] D. Gaede. Chlorination and selective vaporization of rare earth elements. mathesis, Montana Tech of the University of Montana, 2016.

[65] Joachim Eckert. Niobium and niobium compounds. *International Journal of Refractory Metals and Hard Materials*, jun 2000.

[66] I. Barin, O. Knacke, and O. Kubaschewski. Thermochemical properties of inorganic substances. 1977.

[67] J. Rumble. *CRC Handbook of Chemistry and Physics: 99th edition.* American Chemical Society (ACS), Boca Raton, 2018.

[68] H. Kooijman and R. Taylor. *ChemSep Tutorial: Simple (Multicomponent) Distillation, http://www.chemsep.com*, 2020.

[69] P. A. Baisden and G. R. Choppin. Nuclear waste management and the nuclear fuel cycle. *Radiochemistry and nuclear chemistry*, 2007.

[70] D. Böhm, K. Czerski, S. Gottlieb, A. Huke, and G. Ruprecht. Recovery of rare earth elements from NdFeB magnets by chlorination and distillation. *Processes*, 11(2):577, feb 2023.

[71] M. Reimer, H. Schenk-Mathes, M. Hoffmann, and T. Elwert. Recycling decisions in 2020, 2030, and 2040 — when can substantial NdFeB extraction be expected in the EU? *Metals*, 8(11):867, oct 2018.

[72] C. R. Branan. *Rules of thumb for chemical engineers.* Gulf Publishing Company, Houston, Texas, 2 edition, 1998.

[73] D.R. Woods. *Rules of Thumb in Engineering Practice.* Wiley-VCH, 2007.

[74] J. Steimel, M. Harrmann, G. Schembecker, and S. Engell. Model-based conceptual design and optimization tool support for the early stage development of chemical processes under uncertainty. *Computers & Chemical Engineering*, 59:63–73, dec 2013.

[75] J. Steimel, M. Harrmann, G. Schembecker, and S. Engell. A framework for the modeling and optimization of process superstructures under uncertainty. *Chemical Engineering Science*, 115:225–237, aug 2014.

[76] E.L. Cussler. *Diffusion : mass transfer in fluid systems.* Cambridge University Press, New York, 1997.

[77] H. Kister. *Distillation design.* McGraw-Hill, New York, 1992.

[78] M. Baerns, A. Behr, A. Brehm, J. Gmehling, and H. Hofmann. *Technische Chemie.* Wiley VCH Verlag GmbH, 2013.

[79] A. Górak and Z. Olujic. *Distillation: Equipment and Processes (Handbooks in Separation Science).* Academic Press, 2014.

[80] A. Górak and E. Sorensen. *Distillation: Fundamentals and Principles (Handbooks in Separation Science).* Academic Press, 2014.

[81] J. Mackowiak. *Fluiddynamik von Fuellkoerpern und Packungen.* Springer Berlin Heidelberg, 2012.

[82] H. Mori, C. Ito, A. Oda, and T. Aragaki. Total reflux simulation of packed column distillation. *Journal of chemical engineering of Japan*, 32(1):69–75, 1999.

[83] A. Mersmann, M. Kind, and J. Stichlmair. *Thermische Verfahrenstechnik*, volume 2. Springer-Verlag GmbH, 2005.

[84] Czochralski method (https://www.sciencedirect.com/topics/physics-and-astronomy/czochralski-method). ScienceDirect overview on publications, 2023.

[85] B.R. Westphal, D. Vaden S. X. Li, G.L. Fredrickson, and R.D. Mariani. Fate of noble metals during the pyroprocessing of spent nuclear fuel. techreport, Ohio National laboratory INL/CON-08-15187, Global 2009, 2009.

[86] O. Levenspiel. *Chemical reaction engineering.* Wiley, Hoboken, NJ, 1999.

[87] D. Ralf. *Berechnung von Phasengleichgewichten.* Vieweg+Teubner Verlag, 2013.

[88] B. Poling. *The properties of gases and liquids.* McGraw-Hill, New York, 2001.

[89] G. M. Kontogeorgis and G. K. Folas. *Thermodynamic Models for Industrial Applications: From Classical and Advanced Mixing Rules to Association Theories.* WILEY, March 2010.

[90] D.Y. Peng. Extending the van laar model to multicomponent systems. *The Open Thermodynamics Journal*, 4(1):129–140, jan 2010.

[91] H.C. Carlson and A.P. Colburn. Vapor-liquid equilibria of nonideal solutions. *Industrial and Engineering Chemistry*, 34(5):581–589, may 1942.

[92] A. Mohs. *Weiterentwicklung eines auf der LIQUAC- und LIFAC-Methode basierenden Modells zur Berechnung von Salzloeslichkeiten in Loesungsmittelgemischen.* phdthesis, Institut fuer Reine und Angewandte Chemie der Carl von Ossietzky Universitaet Oldenburg, 2011.

[93] W. H. Press, S. A. Teukolsky, W. T. Vetterling, and B. P. Flannery. *Numerical Recipes in C, The Art of Scientific Computing.* Cambridge University Press, New York, 2 edition, 1992.

[94] J.P. Leinroth and D.M. Watt. Building a multicomponent distillation computer program. *Chemical engineering education CEE*, 6(2):80–83, 1972.

[95] T.J. Ho, C.T. Huang, L.S. Lee, and C.T. Chen. Extended ponchon-savarit method for graphically analyzing and designing internally heat-integrated distillation columns. *Industrial & Engineering Chemistry Research*, 49(1):350–358, nov 2009.

[96] R. Goedecke. *Fluidverfahrenstechnik : Grundlagen, Methodik, Technik, Praxis.* Wiley-VCH, Weinheim, 2006.

[97] S. Cotton. *Lanthanide and actinide chemistry.* Wiley, 2006.

[98] Y. Okamoto, F. Kobayashi, and T. Ogawa. Structure and dynamic properties of molten uranium trichloride. *Journal of Alloys and Compounds*, 271-273:355–358, jun 1998.

[99] T. Jiang, N. Wang, S. Peng, and L. Yan. Structural and transport characteristics of UCl3 in molten LiCl-KCl mixture: a molecular dynamics simulation study. *Chemical Research in Chinese Universities*, 31(2):281–287, mar 2015.

[100] R. D. Mariani and D.E. Vaden. Modeled salt density for nuclear material estimation in the treatment of spent nuclear fuel. *Journal of Nuclear Materials*, 404(1):25–32, sep 2010.

[101] X. Li, J. Song, S. Shi, L. Yan, Z. Zhang, T. Jiang, and S. Peng. Dynamic fluctuation of ucl3 coordination structure in the molten LiCl–KCl eutectic via first principles molecular dynamics simulations. *The Journal of Physical Chemistry A*, 121(3):571–578, jan 2017.

[102] S. Barnert et al. *Lexikon der Physik: Salzschmelzen.* Spektrum-Verlag, 1998.

[103] M.-Y. Li, L.-S. Wang, B. Jiang, and J. Gmehling. Generalized LIQUAC model for the single- and mixed-solvent strong electrolyte systems. *AIChE Journal*, 57(9):2535–2546, nov 2010.

[104] G. T. Fukuda. *Vapor Liquid Equilibria of the ternary lithium fluoride-sodium fluoride-beryllium fluoride system.* phdthesis, University of California, Berkeley, 2006.

[105] V. N. Prusakov and V. K. Ezhov. Physicochemical properties of mixtures of heavy metal fluorides i. liquid-vapor phase equilibrium of the system uranium hexafluoride-tungsten hexafluoride. *Soviet Atomic Energy*, 25 (1)(1):771–774, 1968.

[106] V.N. Prusakov, V.K. Ezhov, and E.A. Efremov. Liquid-vapor equilibrium in systems with dilute solutions of metal fluorides in uranium hexafluoride. *Soviet Atomic Energy*, 41 (2)(2):711–714, 1976.

[107] J.F. Ellis and KI.D.B. Johnson. The fluorides of uranium-i: Liquid-vapour equilibria in the systems uranium hexafluoride-chlorine trifluoride and uranium hexafluoride-bromine pentafluoride. *Elsevier: Journal of inorganic and nuclear chemistry*, 6(3)(3):194–198, 1958.

[108] R.C. Limatainen and B. S. Swanson. Vapor-liquid equilibrium in the system bromine pentafluoride-uranium hexafluoride. *American Institute of Chemical Engineers (AIChE)*, 10(6)(6):860–863, 1964.

[109] J.X. Geng, Y.Y., H.Y. Fu, Y. Luo, Q. Dou, and Q.N. Li. Process optimization of a closed-chamber distillation system for the recovery of FLiNaK molten salt. *Nuclear Science and Techniques*, 32(1), jan 2021.

[110] J. R. Hightower and L. E. NcNeese. Low-pressure distillation of molten mixtures of lithium fluoride, beryllium fluoride, and zirconium fluoride for removal of rare-earth fission products. *Industrial and Engineering Chemistry Process Design and Development*, 12(3):232–236, jul 1973.

[111] R.O. Ivins. The distillation of uranium hexafluoride and bromine pentafluoride in a 0.5-inch diameter packed column. Technical report, Chemical engineering devision, University of Chicago, may 1962.

[112] T. Ishihara, K. Hirano, and T. Honda. Processing of uranium dioxide fuel by chloride fractional distillation. *Journal of the Atomic Energy Society of Japan / Atomic Energy Society of Japan*, 4(4):231–239, 1962.

[113] J.F. Ellis, L.H. Brooks, and K.D.B. Johnson. The fluorides of uranium—II. *Journal of Inorganic and Nuclear Chemistry*, 6(3):199–206, jun 1958.

[114] A.N. Shubin, V. D. Michurov, V. K. Mustafaev, and V. K. Ezhov. Separation of enriched uranium hexafluoride on a protoype commercial rectification facility. *Atomic Energy*, 103(3):706–709, sep 2007.

[115] W. Mears, R. Townend, R. Broadley, A. D. Turissini, and R. Stahl. Removal of some volatile impurities from uranium hexafluoride. *Industrial and Engineering Chemistry*, 50(12):1771–1773, dec 1958.

[116] W. Zhou and J. Zhang. Direct calculation of concentration-dependent activity coefficient of UCl3in molten LiCl-KCl. *Journal of The Electrochemical Society*, 162(10):E199–E204, 2015.

[117] S. Noh, D. Kwak, J. Lee, J. Kang, and B. Han. First-principles calculations of the thermodynamic properties of transuranium elements in a molten salt medium. *Journal of the Korean Physical Society*, 64(6):806–812, mar 2014.

[118] B. Li, S. Dai, and D. Jiang. First-principles molecular dynamics simulations of UCln NaCl n=3,4 molten salts. *ACS Applied Energy Materials*, 2(3):2122–2128, feb 2019.

[119] T.B. Bechtel and T.S. Storvick. Activity coefficients of actinide and rare-earth chlorides in molten LiCl/KCl eutectic salt. *Industrial & Engineering Chemistry Research*, 38:1723–1728, feb 1999.

[120] W. Gaweł. Phase equilibrium diagram for the system indium(i) chloride - uranium(iv) chloride. *Polish Journal of Chemistry - Roczniki Chemii*, 65:1219 – 1225, 1991.

[121] W. Gaweł. Phase equilibria in the mercury(ii) chloride - uranium(iv) chloride system. *Polish Journal of Chemistry - Roczniki Chemii*, 57:391–394, 1983.

[122] G. De Cordoba, A. Laplace, J. Lacquement, and C. Caravaca. Electrochemical behavior of np in the molten LiCl–KCl eutectic. *Journal of The Electrochemical Society*, 154(1):F16, 2007.

[123] L. Cassayre, J. Serp, P. Soucek, R. Malmbeck, J. Rebizant, and J.P. Glatz. Electrochemistry of thorium in LiCl–KCl eutectic melts. *Electrochimica Acta*, 52(26):7432–7437, sep 2007.

[124] O. Beneš and R.J.M. Konings. Thermodynamic evaluation of the NaCl–MgCl2–UCl3–PuCl3 system. *Journal of Nuclear Materials*, 375:202–208, apr 2008.

[125] W. Zhou and J. Zhang. Thermodynamic evaluation of LiCl-KCl-PuCl3 system. *Journal of Alloys and Compounds*, 695:2306–2313, feb 2017.

[126] E.M. Foltyn, R.N.R. Mulford, K.M. Axler, J.M. Espinoza, and A.M. Murray. Thermodynamic modeling and experimental investigations of the CsCl-CaCl-PuCl3 system. *Journal of Nuclear Materials*, 178(1):93–98, jan 1991.

[127] Y.S. Yang, Y.H. Kang, and H.K. Lee. Estimation of optimum experimental parameters in chlorination of UO2 with cl2 gas and carbon for UCl4. *Materials Chemistry and Physics*, 50(3):243–247, oct 1997.

[128] J. Serp, P. Chamelot, S. Fourcaudot, R.J.M. Konings, R. Malmbeck, C. Pernel, J.C. Poignet, J. Rebizant, and J.-P. Glatz. Electrochemical behaviour of americium ions in LiCl–KCl eutectic melt. *Electrochimica Acta*, 51(19):4024–4032, may 2006.

[129] D. Lambertin, J. Lacquement, S. Sanchez, and G. S. Picard. Americium chemical properties in molten LiCl–KCl eutectic at 743 k. *Plasmas & Ions*, 3(1-4):65–72, jan 2000.

[130] P. Masset, R.J.M. Konings, R. Malmbeck, J. Serp, and J.P. Glatz. Thermochemical properties of lanthanides (ln=la,nd) and actinides (an=u,np,pu,am) in the molten LiCl–KCl eutectic. *Journal of Nuclear Materials*, 344(1-3):173–179, sep 2005.

[131] P. I. Masset, C. Apostolidis, R. Malmbeck, J. Rebizant, J. Serp, and J.P. Glatz. Assessment of the thermochemical properties of actinides in molten chlorides. *Zeitschrift fÃŒr Naturforschung A*, 63(1-2):107–113, feb 2008.

[132] J. J. Roy, L. F. Grantham, D. L. Grimmett, S. P. Fusselman, C. L. Krueger, T. S. Storvick, T. Inoue, Y. Sakamura, and N. Takahashi. Thermodynamic properties of u, np, pu, and am in molten LiCl-KCl eutectic and liquid cadmium. *Journal of The Electrochemical Society*, 143(8):2487–2492, aug 1996.

[133] L. Martinot, G. Duyckaerts, J.C. Spirlet, and W. Mueller. Thermodynamic properties of dilute solutions of PaCl4 in (li-k)cl eutectic. *Inorganic and Nuclear Chemistry Letters*, 16(4):177–183, 1980.

[134] H. Shibata, H. Hayashi, and T. Koyama. Evaluation of apparent standard potentials of curium in LiCl-KCl eutectic melt. *Electrochemistry*, 83(7):532–536, 2015.

[135] A. Osipenko, A. Maershin, V. Smolenski, A. Novoselova, M. Kormilitsyn, and A. Bychkov. Electrochemistry of oxygen-free curium compounds in fused NaCl–2cscl eutectic. *Journal of Nuclear Materials*, 396(1):102–106, jan 2010.

[136] H. Hayashi, M. Takano, H. Otobe, and T. Koyama. Syntheses and thermal analyses of curium trichloride. *Journal of Radioanalytical and Nuclear Chemistry*, 297(1):139–144, jan 2013.

[137] R. Agrawal, D.W. Woodward, and T.F. Yee. Argon production from air distillation: Use of a heat pump in a ternary distillation with a side rectifier. *Gas Separation and Purification*, 8:37–43, jan 1994.

[138] A. Koning. *The JEFF-3.1 nuclear data library: JEFF report 21.* OECD Nuclear Energy Agency, France, Paris, 2006.

[139] A. Schwenk-Ferrero. German spent nuclear fuel legacy: Characteristics and high-level waste management issues, article id 293792. *Science and Technology of Nuclear Installations*, 2013:1–11, 2013.

[140] S. Kitawaki, T. Nagai, and N. Sato. Chlorination of uranium oxides with CCl4 using a mechanochemical method. *Journal of Nuclear Materials*, 439(1-3):212–216, aug 2013.

[141] E.H.P. Cordfunke and G. Prins. Equilibria involving volatile UO2cl2. *Journal of Inorganic and Nuclear Chemistry*, 36(6):1291–1293, jun 1974.

[142] E.D. Collins, G.D. DelCul, B.B. Spencer, R.R. Brunson, J.A. Johnson, D.S. Terekhov, and N.V. Emmanuel. Process development studies for zirconium recovery/recycle from used nuclear fuel cladding. *Procedia Chemistry*, 7:72–76, 2012.

[143] P.L. Brown. *Chemical Thermodynamics of Zirconium.* OECD Publishing, 2005.

[144] A. Fick. Ueber diffusion. *Annalen der Physik und Chemie*, 170(1):59–86, 1855.

[145] D.R. Lide. *CRC Handbook of Chemistry and Physics, 84th Edition.* American Chemical Society (ACS), feb 2004.

[146] G. J. Janz and N. P. Bansal. Molten salts data: Diffusion coefficients in single and multicomponent salt systems. *Journal of Physical and Chemical Reference Data*, 11(3):505–693, jul 1982.

[147] C. Yaws. *Transport properties of chemicals and hydrocarbons : viscosity, thermal conductivity, and diffusivity of C1 to C100 organics and Ac to Zr inorganics.* William Andrew, Norwich, NY, 2009.

[148] H. Breuer. *Dtv-Atlas zur Physik.* Dt. Taschenbuch Verl, Munich(Germany), 1987.

[149] J. Zierep and K. Bühler. *Strömungsmechanik.* Springer-Verlag GmbH, 2013.

[150] A. Einstein. Über die von der molekularkinetischen theorie der wärme geforderte bewegung von in ruhenden flüssigkeiten suspendierten teilchen. *Annalen der Physik*, 322(8):549–560, 1905.

[151] H. J. Scheel. Historical aspects of crystal growth technology. *Journal of Crystal Growth*, 211(1-4):1–12, apr 2000.

[152] L. Rycerz. Termochemia halogenków lantanowców i związków tworzących się w układach halogenki lantanowców-halogenki litowców, nr 68/35. Technical Report 68/35, Prace Naukowe Instytutu Chemii Nieorganiczneji Metalurgii Pierwiastków Rzadkich Politechniki Wrocławskiej, 2004.

[153] R. Guillaumont. *Update on the chemical thermodynamics of Uranium, Neptunium, Plutonium, Americium and Technetium.* OECD Publishing, 2003.

[154] H. Gamsjaeger. *Chemical Thermodynamics of Tin – Volume 12.* OECD Publishing, dec 2012.

[155] I. Grenthe. *Chemical thermodynamics of Uranium.* OECD Publishing, 2004.

[156] W. Hummel. *Chemical Thermodynamics of Compounds and Complexes of U,Np,Pu,Am,Tc,Se,Ni and Zr with selected organic ligands.* OECD Publishing, 2004.

[157] A. Olin. *Chemical Thermodynamics of Selenium.* OECD Publishing, 2004.

[158] M. Rand. *Chemical Thermodynamics of Thorium.* OECD Publishing, dec 2008.

[159] J. A. Rard. *Chemical Thermodynamics of Technetium*, volume 3. Elsevier, 1999.

[160] R. Silva. *Chemical Thermodynamics of Americium.* Elsevier, 1995.

[161] I. Grenthe, editor. *Second update on the Chemical Thermodynamics of Uranium, Neptunium, Plutonium, Americium And Technetium, Volume 14.* OECD, jan 2021.

[162] Nist chemistry webbook, national institute of standards and technology, standard reference database number standard reference database number 69, doi: https://doi.org/10.18434/t4d303. (online), 2022.

[163] Gmelins handbook of inorganic chemistry. In 8th, editor, *database of inorganic compounds*. Springer-Verlag, 1924 – 1998.

[164] G. R. Somayajulu. Estimation procedures for critical constants. *Journal of Chemical & Engineering Data*, 34(1):106–120, jan 1989.

[165] B.I. Lee and M. G. Kesler. A generalized thermodynamic correlation based on three-parameter corresponding states. *AIChE Journal*, 21(3):510–527, may 1975.

[166] C. Yaws. *Chemical Properties Handbook: Physical, Thermodynamics, Engironmental Transport, Safety & Health Related Properties for Organic & Inorganic Chemical*. McGraw-Hill Education, 1998.

[167] Dortmunder stoffdatenbank, http://www.ddbst.com/. (online), 2022.

[168] U. Westhaus. Detherm(https://dechema.de/medien/datenbanken/detherm.html). (online), 2022.

[169] Design Institute for Physical Properties. *DIPPR 801- database - Sponsor and Public version https://www.aiche.org/dippr/events-products/801-database, Design Institute for Physical Properties*, 2019.

[170] Nuclear energy agency. *TDB Project Publications - Chemical Thermodynamics Series, NEA(Nuclear energy agency), https://www.oecd-nea.org*, 2020.

[171] A. Koning. Jeff-3.1 joint evaluated fission and fusion file, incident-neutron data. techreport, OECD/NEA, 2006.

[172] Nasa headquarters library databases, https://www.nasa.gov/centers/hq/library/find/databases, 2021.

[173] National technical reports library, https://ntrl.ntis.gov/ntrl/. (online), 2014.

[174] J.Y. Kim, S.B. Bae, D.H. Kim, Y.S. Choi, J.W. Yeon, and K. Song. High-temperature viscosity measurement of LiCl-KCl molten salts comprising actinides and lanthanides. *Bulletin of the Korean Chemical Society*, 33(11):3871–3874, nov 2012.

[175] V. N. Desyatnik, S. F. Katyshev, S. P. Raspopin, and Yu. F. Chervinskii. Density, surface tension, and viscosity of uranium trichloride-sodium chloride melts. *Soviet Atomic Energy*, 39(1):649–651, jul 1975.

[176] V. N. Desyatnik, S. F. Katyshev, S. P. Raspopin, and Yu. F. Chervinskii. Density, surface tension, and viscosity of melts of uranium trichloride with rubidium and cesium chlorides. *Soviet Atomic Energy*, 42(3):246–248, mar 1977.

[177] G. J. Janz, R. P. T. Tomkins, C. B. Allen, J. R. Downey, G. L. Garner, U. Krebs, and S. K. Singer. Molten salts: Volume 4, part 2, chlorides and mixtures—electrical conductance, density, viscosity, and surface tension data. *Journal of Physical and Chemical Reference Data*, 4(4):871–1178, oct 1975.

[178] Z. Singh, R. Prasad, V Venugopal, K.N Roy, and D.D Sood. Thermodynamics of the vaporisation of thorium tetrachloride. *The Journal of Chemical Thermodynamics*, 11(1):31–36, jan 1979.

[179] P. Patnaik. *Handbook of Inorganic Chemicals*. McGraw-Hill Professional, 2002.

[180] Nist-janaf tables, periodic table of compounds by element https://janaf.nist.gov/janaf4pdf.html, national institute of.

[181] H. Katasuta. Liquid target-fuel and associated fuel cycle technologies (iaea-tecdoc–985) p. 17 – 22. techreport, Japan Atomic Energy Research Institute, International Atomic Energy Agency (IAEA), 1997.

[182] J. Beall. List of standalone journals: Potential, possible, or probable predatory scholarly open-access journals, 2017.